CIVIL ENGINEERING STUDIES
Illinois Center for Transportation Series No. 13-015
UILU-ENG-2013-2019
ISSN: 0197-9191

SEISMIC PERFORMANCE OF QUASI-ISOLATED HIGHWAY BRIDGES IN ILLINOIS

Prepared By
James LaFave
Larry Fahnestock
Douglas Foutch
Joshua Steelman
Jessica Revell
Evgueni Filipov
University of Illinois at Urbana-Champaign

Jerome Hajjar
Northeastern University

Research Report No. FHWA-ICT-13-015

A report of the findings of
ICT-R27-070
Calibration and Refinement of Illinois' Earthquake Resisting System Bridge Design Methodology

Illinois Center for Transportation

June 2013

Technical Report Documentation Page

1. Report No.	2. Government Accession No.	3. Recipient's Catalog No.
FHWA-ICT-13-015		

4. Title and Subtitle	5. Report Date
Seismic Performance of Quasi-Isolated Highway Bridges in Illinois	June 2013
	6. Performing Organization Code

7. Author(s)	8. Performing Organization Report No.
James LaFave, Larry Fahnestock, Douglas Foutch, Joshua Steelman, Jessica Revell, Evgueni Filipov & Jerome Hajjar	ICT-13-015 UILU-ENG-2013-2019

9. Performing Organization Name and Address	10. Work Unit No. (TRAIS)
Illinois Center for Transportation Department of Civil and Environmental Engineering University of Illinois at Urbana-Champaign 205 N. Mathews, MC 250 Urbana, IL 61801	11. Contract or Grant No. R27-70

12. Sponsoring Agency Name and Address	13. Type of Report and Period Covered
Illinois Department of Transportation Bureau of Materials and Physical Research 126 East Ash St. Springfield, IL 62704	14. Sponsoring Agency Code

15. Supplementary Notes
Volume 2 of 2 submitted for Project ICT-R27-70

16. Abstract

The Illinois Department of Transportation (IDOT) commonly uses elastomeric bearings to accommodate thermal deformations in bridges, and these bearings have potential utility in seismic events. IDOT has developed an Earthquake Resisting System (ERS) using the displacement capacity of typical bearings to achieve a structural response similar to isolation. Project R27-70 was conducted to validate and calibrate the quasi-isolated ERS based on full-scale laboratory tests of bearings and computational models capturing full-bridge seismic response. The overall report is divided into two volumes. Volume 1 discussed the experimental program. This second volume focuses on the analytical program but also contains retainer design recommendations. Results from the experimental testing program were used to develop constitutive bearing models, which were incorporated into the finite element model of a three-span bridge with simply supported abutments and fixed bearings at one pier. A suite of 48 bridges was created to represent the most common highway bridge configurations in Illinois. Variables included superstructure type, pier type, pier height, elastomeric bearing type, and foundation flexibility. Two sets of ten synthetic ground motions from the New Madrid Seismic Zone were scaled to match the AASHTO seismic design spectra for Cairo, Illinois, and applied in the longitudinal and transverse directions. A total of 12,000 nonlinear dynamic analyses were conducted in OpenSees at six scale factors from 0.5 to 1.75 and used to create coarse incremental dynamic analyses. On the basis of the findings of the parametric study, most bridges in Illinois would not experience severe damage during a 75-year design life, and bearing unseating or span loss are not likely to occur in regions with moderate seismic hazard. Piers with fixed bearings commonly yielded for small earthquakes, but future calibration of fuse capacities may improve this behavior.

17. Key Words	18. Distribution Statement
Seismic isolation, quasi-isolation, highway bridges, bridge bearings, bearing retainers, earthquake response history analysis	No restrictions. This document is available to the public through the National Technical Information Service, Springfield, Virginia 22161

19. Security Classif. (of this report)	20. Security Classif. (of this page)	21. No. of Pages	22. Price
Unclassified	Unclassified	65 plus appendices	

Form DOT F 1700.7 (8-72) Reproduction of completed page authorized

ACKNOWLEDGMENT AND DISCLAIMER

This paper is based on the results of ICT R27-70, **Calibration and Refinement of Illinois' Earthquake Resisting System Bridge Design Methodology**. ICT R27-70 was conducted in cooperation with the Illinois Center for Transportation; the Illinois Department of Transportation, Division of Highways; and the U.S. Department of Transportation, Federal Highway Administration (FHWA). The authors would like to thank the members of the project Technical Review Panel, chaired by D. H. Tobias, for their valuable assistance with this research. Grid resources from the Texas Advanced Computing Center (TACC) at The University of Texas at Austin were used to generate research results reported within this paper.

Members of the Technical Review Panel were the following:

Daniel Tobias, IDOT (Chair)

Mark Shaffer, IDOT (Co-Chair)

Dan Brydl, FHWA

John Ciccone, IDOT

Patrik Claussen, IDOT

Chad Hodel, WHKS

William Kramer, IDOT

Carl Puzey, IDOT

Kevin Riechers, IDOT

EXECUTIVE SUMMARY

The 2009 AASHTO seismic provisions increased the design earthquake return period from 500 to 1000 years, leading to higher bridge design and construction costs. Such code updates have been guided primarily by the seismic practices in the western United States and have focused on bridge configurations where energy will be dissipated by either plastic deformation of the piers or by a specially designed and constructed seismic isolation device placed between the superstructure and substructure.

The Illinois Department of Transportation (IDOT) has identified the potential to adapt concepts underpinning this second “classical isolation” approach to formulate a cost-effective “quasi-isolation” alternative targeted to the seismic hazard and typical bridge configurations in Illinois. The quasi-isolated Earthquake Resisting System uses conventional elastomeric bearing elements but deviates from conventional seismic design requirements by allowing bearing anchorages to fracture during a design earthquake and relies on the subsequent bearing deformation and sliding to accommodate seismic demands. Sufficient seat width is provided to allow bearing sliding, and as an extra level of redundancy, the piers can be used to dissipate additional energy.

The objective of Project R27-070 was to facilitate full implementation of the quasi-isolated seismic design concept through a combined experimental and analytical program at the University of Illinois at Urbana-Champaign. As discussed in Volume 1 of this report, IDOT Type I and II elastomeric bearings were tested in the laboratory along with retainers and fixed bearings. This second volume presents final retainer design recommendations based on the results discussed in Volume 1, but the focus of Volume 2 is the analytical program, wherein nonlinear numerical bearing models were developed based on the experimental data and then incorporated into 3D finite element bridge models to explore the system-level response of typical IDOT bridges.

A three-span bridge with no skew, simply supported abutments, fixed bearings at one pier, and H-pile foundations was used for system analyses. From this base model, a suite of 48 bridges was created to represent the most common highway bridge configurations in Illinois. Variations included steel superstructures with 50- or 120-ft center spans, a concrete superstructure with 60-ft spans, column or wall piers either 15 or 40 ft tall, Type I or Type II elastomeric bearings, and fixed or flexible foundation conditions. A range of seismic hazards was represented using two sets of ten synthetic ground motions—one set to represent shallow soil/rock and another for deep soil conditions in the southern Illinois region of the New Madrid Seismic Zone. The ground motions were scaled to match the AASHTO seismic design spectra for Cairo, Illinois, and then linearly scaled to six factors from 0.5 up to 1.75, (with 1.0 representing the design earthquake) and applied in the longitudinal and transverse directions. Roughly 12,000 nonlinear transient dynamic analyses were executed in OpenSees, an open-source earthquake engineering software package. Force and displacement data were recorded at each time step and used to identify what limit states occurred.

On the basis of the findings of the parametric study, most bridges in Illinois would not experience severe damage during a 75-year design life, and bearing unseating or span loss is not likely for regions with moderate seismic hazard. Type I IDOT bearings did not unseat at the design earthquake and are appropriate for use with all seismic hazard levels and all soil types in Illinois. Type II IDOT bearings were prone to unseating, particularly in the transverse direction, and should either be limited to regions of low or moderate seismicity or redesigned with a larger bearing surface. Additionally, it is recommended that seat width

requirements be redefined based on bearing unseating rather than girder unseating. Transverse displacements were roughly 36% higher than longitudinal displacements and increased more severely with earthquake intensity. This difference arises because, after the retainers and fixed bearings have failed, there is no active restraint of the system in the transverse direction, whereas the backwall and backfill continue to provide resistance in the longitudinal direction. Thus, independent calibration of longitudinal and transverse seat width requirements could be economical. The piers with fixed bearings commonly yielded for small earthquakes, a non-ideal response that often precluded the intended bearing fusing. This behavior can be improved, but identification of acceptable substructure damage at the design earthquake is essential to fully define the earthquake resisting system and to effectively calibrate fuse capacities in future research.

In the transverse direction, retainers are the restraining element with the greatest potential for calibration. Test results presented in Volume 1 showed that retainer force capacities consistently exceeded those predicted by the IDOT Bridge Manual. Additionally, nonlinear response characteristics varied significantly with retainer geometry. Volume 2 presents a design methodology to achieve anchor rupture prior to severe concrete crushing at the retainer toe, thus providing a more predictable force capacity and hysteretic response.

CONTENTS

CHAPTER 1 BACKGROUND

1.1 MOTIVATION FOR RESEARCH PROJECT

In 2008 and 2009, the American Association of State Highway and Transportation Officials (AASHTO) published modernized standards for the design of highway bridges under earthquake loading. The methods and soil parameters used to determine design earthquake response spectra, along with numerous other aspects of seismic bridge design philosophy, were modified. Most significantly, the design earthquake, previously characterized by a 500-year return period, is now based on a 1000-year return period. These changes have increased the complexity of seismic design and the cost of construction, as well as substantially increasing the population of structures in Illinois requiring seismic design.

In an effort to reduce design and construction costs, while still ensuring structural safety during seismic events, the Illinois Department of Transportation (IDOT) developed an innovative Earthquake Resisting System (ERS) strategy tailored specifically to common bridge configurations and typical earthquake hazards in Illinois. The IDOT ERS is an extension of the seismic isolation bridge design methodology employed in higher seismic regions of the United States, where the substructure and superstructure ideally remain elastic and a fusing mechanism is provided at the interface between the two. Historically, the fusing mechanism has been a seismic isolation device, such as a lead-rubber bearing. These classical isolation systems have typically been used in high seismic regions (such as the West Coast of the United States, as well as Japan and New Zealand), where the additional design and construction costs are justifiable when balanced against the seismic hazard. For bridges outside of high seismic areas, however, some commonly employed structural components, such as steel-reinforced elastomeric bearings, may inherently possess properties suitable for an isolation system.

As a result, the concept of quasi-isolation has emerged as an innovative, yet pragmatic, design philosophy for bridges in moderate seismic regions. Typical bridge bearing systems can be designed and detailed to act as fuses, providing the benefit of reduced force demands for the superstructure and substructure, so long as the structural system can be designed to accommodate the concomitant increase in displacements. The IDOT ERS features three distinct levels of fusing and redundancy, namely: Level 1—permit damage and failure of the bearing components to allow quasi-isolation; Level 2—provide sufficient seat widths to accommodate the sliding of the bearings; and Level 3—permit some damage to the substructure, so long as there is no span loss. The overall intent is to provide a cost-effective bridge, with an ERS that limits damage for small seismic events and still prevents span loss during a strong event in the New Madrid Seismic Zone (NMSZ).

Although the Illinois ERS strategy is described in the IDOT Bridge Manual and supported by a Seismic Design Guide (with examples), the theoretical methods used in its development have lacked systematic experimental testing to verify or calibrate some of the fundamental design assumptions. There is also concern that, without refined and improved guidance, designers who are less experienced with seismic design principles could exercise unnecessary conservatism, leading to more expensive designs, or they might inadvertently develop designs that are not conservative enough for seismic load effects.

To facilitate full implementation of quasi-isolated seismic design, IDOT and the Illinois Center for Transportation (ICT) sponsored a combined experimental and computational research program at the University of Illinois. The overall research program comprised five primary components, summarized as follows:

1. Conducting full-scale tests of typical bridge bearings used in Illinois, to study how bearings not designed for seismic demands behave when subjected to large displacement demands.
2. Developing numerical models of bridge bearings, validated against test results.
3. Developing numerical models of full bridge systems, which capture all important aspects of nonlinear behavior when a bridge is subjected to an earthquake.
4. Conducting parametric studies, using the numerical bridge models, to explore system-level seismic response for a range of representative Illinois bridges.
5. Developing recommendations for seismic design of bridges using the quasi-isolation philosophy.

The research presented in this report should assist IDOT in further developing a consistent bridge design approach that can best balance the requisite structural safety with design methodologies and construction practices appropriate for the state of Illinois.

1.2 REPORT ORGANIZATION

The primary goal of this research was to investigate, validate, and calibrate the IDOT ERS strategy, focusing on the specific seismic hazard and bridge structural characteristics appropriate for Illinois. This report presents the results of laboratory testing of standard bridge bearings and computational modeling of typical IDOT bridge configurations, conducted from 2009 through 2012 in the Department of Civil & Environmental Engineering at the University of Illinois at Urbana-Champaign. The report is divided into two volumes, with the first addressing the experimental program, and this second volume describing the computational bridge modeling. Following is a brief summary of the contents of Volume 2.

Chapter 1 discusses the motivation for the research and provides an overview of the state of practice for the design of bridge bearings and bridge seismic design.

Chapter 2 explains the development of computational models for both bearing components and bridge systems; the methodology of the parametric study, including selection and scaling of ground motions, is also presented.

Chapter 3 presents detailed results from the dynamic analysis of one representative bridge model.

Chapter 4 presents overall results from the dynamic analysis of all 48 bridge models developed in Chapter 2.

Chapter 5 expands on the discussion in Volume 1 of retainer response and presents suggested revisions to the current retainer design procedure.

Chapter 6 summarizes the key results from the project and provides design recommendations, based on both the experimental and analytical research programs; recommendations for continued research are also presented.

1.3 STATE-OF-PRACTICE REVIEW

1.3.1 Bridge Bearings

In conventional (i.e., thermal expansion) applications, steel-reinforced elastomeric bearings must be designed to resist loads and accommodate movement at the service and strength limit states. Failure of the bearing is generally due to gradual deterioration over

many cycles rather than sudden failure under a single load, and the AASHTO specifications are written with an eye to controlling compressive stress, uplift, buckling, and fatigue over the design life of the bearing (Roeder and Stanton 1991).

The AASHTO specifications allow two distinct methods for elastomeric bearing design. Both methods require bearings to be checked at limit states governed by compression stress, combined compression and rotation, buckling stability, shear, and stress on the internal reinforcing. Method A is the older, simpler, and more conservative method. This design approach allows shear modulus to be approximated from hardness measurements. Method B, by comparison, requires laboratory testing to verify shear modulus, but it compensates for the additional material testing with less stringent stress and deformation limits (AASHTO 2008). This method is the more rigorous of the two and requires significantly more effort on the part of the designer, but it may result in a bearing that uses less material.

The criteria employed by IDOT for elastomeric bearings are summarized below and generally align with AASHTO Method A (IDOT 2009).

- The total elastomer height must be at least twice the total movement for a Type I bearing and equal to the total movement for a Type II bearing, effectively limiting shear strain to roughly 50% in order to control bearing fatigue.
- The width of the bearing parallel to the direction of movement must be at least three times the total elastomer height, in order to ensure stability of the bearing under service loads.
- The average compression stress from dead load must be between 200 and 500 psi.
- The average compression stress from dead load and live load (without impact) must be between 200 and 800 psi. This is more conservative than the AASHTO criteria, which would allow up to 1250 psi average compression stress.

IDOT has augmented these provisions with tabular and graphical design aids that incorporate the design parameters and limitations and simplify the elastomeric bearing selection process for ordinary highway bridges.

1.3.2 Seismic Design

In bridge seismic design, the ERS controls the seismic displacements and provides the load path for transmitting seismically induced forces down into the ground. In the AASHTO Guide Specifications for LRFD Seismic Bridge Design, there are three recognized ERS categories (AASHTO 2009):

- Type I—A ductile substructure with essentially elastic superstructure. This is the conventional seismic design approach, and it is representative of the way that many IDOT bridges are currently designed for seismic effects.
- Type II—An essentially elastic substructure with ductile superstructure. This less common approach applies only to steel superstructures with specially detailed ductile cross-frames.
- Type III—An elastic superstructure and substructure with a fusing mechanism in between. This approach is characteristic of traditional seismic isolation, and is also generally representative of the philosophy IDOT is targeting with the quasi-

isolated ERS concept (perhaps with some limited substructure damage also permitted).

A Type I ERS generally employs a capacity design approach, wherein the substructure is specially detailed for a ductile response, and the foundation and superstructure are provided with sufficient strength to remain essentially elastic while plastic hinges form in the substructure. In high seismic zones, this requires designers to complete involved analyses, and the labor-intensive detailing requirements can inflate construction costs.

Bridges designed with traditional seismic isolation utilize a Type III ERS, and a vertical load-carrying component that also functions as a seismic isolator is placed between the superstructure and substructure. This isolation device is designed to carry the bulk of the seismic displacement and provides sufficient lateral flexibility to lengthen the period of the system. This period elongation can significantly reduce seismic forces, but there is generally a concomitant reduction in stiffness that leads to increased displacements, as illustrated conceptually in Figure 1.1 and Figure 1.2 (Buckle et al. 2006). To limit displacements to practical magnitudes, it is necessary to introduce additional energy dissipation into the isolation system by way of hysteretic or viscous damping. The isolation system should also have some means of ensuring lateral rigidity under service loads such as wind and truck-braking.

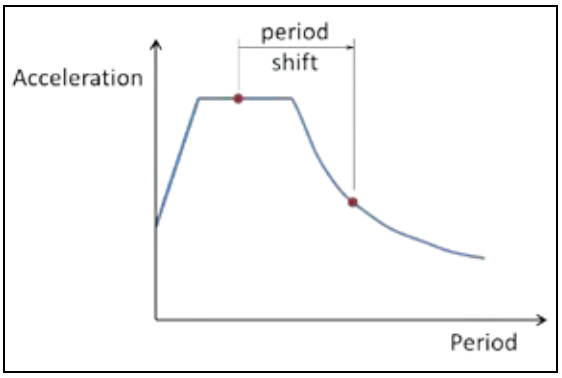

Figure 1.1. Effect of period shift on acceleration.

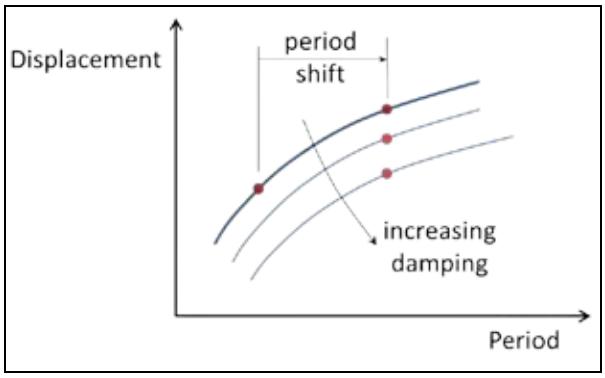

Figure 1.2. Effect of period shift and damping on displacement response.

CHAPTER 2 ANALYTICAL RESEARCH PROGRAM

2.1 OVERVIEW OF BRIDGE MODELS

The first objective of the analytical study was to develop numerical models of Type I and Type II elastomeric bearings, low-profile fixed bearings, and retainers. These component-level models were developed to accurately match experimental results and intended to be implemented in finite element software. The second objective was to investigate how the quasi-isolated design philosophy impacts overall bridge system behavior. Global system models were developed and analyzed using the open source, nonlinear seismic analysis program Open System for Earthquake Engineering Simulation (OpenSees; McKenna, Mazzoni, and Fenves 2011). A prototype bridge model was developed with the ability to capture a variety of nonlinear behaviors potentially encountered under earthquake loading. Variations of the model were then developed to envelop a range of bridge systems encountered in practice. This suite of bridges, 48 in total, was analyzed as part of a parametric study; the results are presented in Chapter 4.

2.1.1 Prototype Bridge Model

The prototype bridge, shown in Figure 2.1, is a three-span, continuous steel I-girder superstructure supported on multi-column concrete piers and stub abutments. All components were proportioned in accordance with the IDOT Bridge Manual. The 42-ft superstructure width accommodates two lanes of traffic and consists of six W27x84 girders composite with an 8-in. cast-in-place concrete deck. All superstructure elements, including diaphragm elements, were modeled as linear with appropriate elastic stiffness.

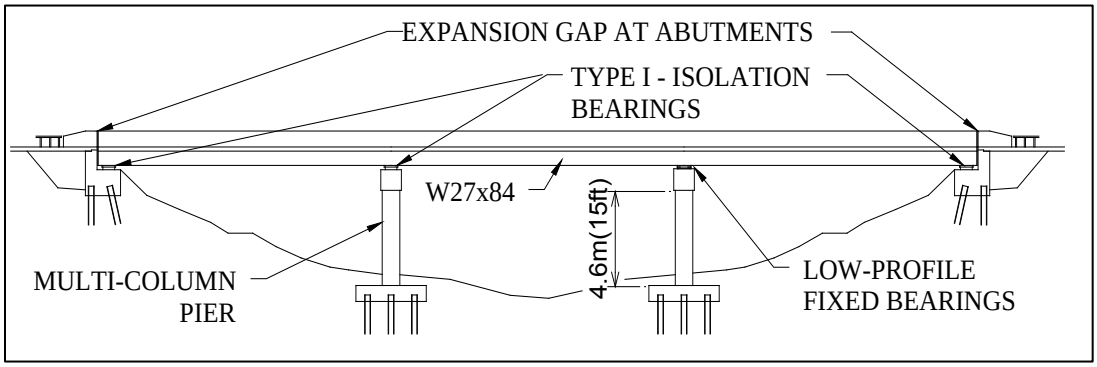

Figure 2.3. Elevation view of prototype bridge model.

The multi-column piers have a 15-ft clear height and were modeled using beam-column elements with plastic hinges and fiber sections that capture material nonlinearities in the concrete and reinforcement. The prototype bridge foundations were modeled as a fixed base, representing a foundation bearing on rock. Behavior of the abutment backwalls was modeled with a 2-in. gap to simulate an expansion joint and a hyperbolic material to capture nonlinear backfill behavior. Low-profile fixed bearings were installed at the second pier (Pier 2), while Type I elastomeric expansion bearings were used at the other pier and abutment locations. Stiffness and mass proportional damping of 5% was used in the first longitudinal and transverse modes, and additional damping occurred from hysteretic behavior of the nonlinear elements.

2.1.2 Parametric Variations

The parametric variations studied in this paper were based on the current bridge stock in Illinois as defined in Bignell, LaFave, and Hawkins (2005), as well as current trends of bridge design in Illinois in which elastomeric bearings are the preferred type of expansion bearing. At the time of the study, 75% of the bridges had three spans with lengths ranging from 110 to 270 ft, consisting of 86% steel girders and 14% concrete girders with composite decks. Sixty-seven percent had multi-column piers, and 32% had wall piers. Pier heights ranged from 9 to 46 ft. Site conditions ranged from Class B to E soils, foundations consisted primarily of piles (86%), and 33% of bridges had elastomeric bearings (Bignell, LaFave, and Hawkins 2005).

The research focused on continuous steel and concrete superstructures that were simply supported at the abutments. Both IDOT Type I and Type II bearings, which differ in coefficient of friction and response mechanism, were modeled. Substructure variations included multi-column piers and wall piers of two different heights. All substructures were founded on H-piles, and two different soil stiffnesses were considered. The components of each bridge variant were proportioned in accordance with the IDOT Bridge Manual.

Integral abutment bridges, bridges with skew or curvature, and bridges with flexible foundation types such as spread footings were not considered. Although the quasi-isolation system may be applicable to those bridge configurations, these bridge types were not included in the present study because they require more detailed seismic modeling.

Table 2.1. Summary of the 48 Bridge Variations Used in the Parametric Study

		Bridge Type 1 Steel - Short				**Bridge Type 2 Steel - Long**				**Bridge Type 3 Concrete - Short**			
Parameter	**Alternatives**	1	2	3	4	5	6	7	8	9	10	11	12
Span Length	50' - 50' - 50'	*	*	*	*								
	60' - 60' - 60'									*	*	*	*
	80' - 120' - 80'					*	*	*	*				
Pier Type	Continuous Wall	*	*			*	*			*	*		
	Multi Column Pier			*	*			*	*			*	*
Pier Height	Short - 15'	*		*		*		*		*		*	
	Tall - 40'		*		*		*		*		*		*
Movement Bearings	Type I Elastomeric	All (12) of the above bridges are modeled with											
	Type II Elastomeric	Elastomeric Type I and Type II Bearings											
Foundations	Fixed Foundation	All (24) of the above bridges are modeled with											
	Flexible Foundation	Fixed and Flexible Foundations											

Bridge model variations are named with a series of letters and numbers indicating what parameters were used. The first two letters of the model name indicate the superstructure type (Ss—steel short; Sl—steel long; Cs—concrete short). The third letter and the following two numbers designate the pier type (C—column pier; W—wall pier) and height in feet (15 ft; 40 ft). The next letter and number indicate the bearing type used (T1—Type I IDOT bearing; T2—Type II IDOT bearing). The final letter indicates the foundation boundary condition flexibility (F—fixed/rock; S—flexible foundation boundary condition). The flexible boundary condition simulates a group pile foundation in soft soils, while fixed foundations represent rock. This foundation condition defines the equivalent springs used to

represent the foundation in the model and is independent from the ground motion site class subsequently defined in Section 2.4. As an example of this naming convention, the prototype bridge is designated SsC15T2F—short steel superstructure with 15-ft column piers, Type II bearings, and fixed foundations.

Using the permutations indicated in Table 2.1, the selected parametric variations resulted in 48 distinct bridges for analysis. The basic parameters for the bridge models created in OpenSees are summarized in Table 2.2.

Table 2.2. Basic Design Information for the Parametric Study Bridges

Superstructure	Steel Short (Ss)		Steel Long (Sl)		Concrete Short (Cs)	
Girder Size	W27x84		W40x183		36" PCC I-Girder	
Span Lengths	50 - 50 - 50 ft		80 - 120 - 80 ft		60 - 60 - 60 ft	
Superstructure Wt.	6.28 kip/ft		6.85 kip/ft		8.17 kip/ft	
Abutment Bearings						
Type I	9-b		15-e		9-c	
Type II	7-b		9-b		9-a	
Retainer Bolt Dia	0.625 in		0.75 in		0.75 in	
Pier Bearings						
Type I	11-a		15-b		13-a	
Type II	11-a		15-b		13-a	
Retainer Bolt Dia	1.0 in		1.5 in		1.25 in	
Fixed Bearing Bolt Dia	0.75 in		1.25 in		1.00 in	
Column Piers						
Column Clear Height	15 ft	40 ft	15 ft	40 ft	15 ft	40 ft
Column Diameter	3 ft	3 ft	3 ft	3 ft	3 ft	3 ft
Reinforcement	#9 tot 11	#9 tot 11	#9 tot 15	#9 tot 15	#9 tot 15	#9 tot 15
Reinforcement Ratio	1.07%	1.07%	1.46%	1.46%	1.46%	1.46%
Wall Piers						
Wall Clear Height	15 ft	40 ft	15 ft	40 ft	15 ft	40 ft
Wall Width	35 ft	35 ft	35 ft	35 ft	35 ft	35 ft
Wall Thickness	3 ft	3 ft	3 ft	3 ft	3 ft	3 ft
Reinforcement	#7@12	#7@12	#7@12	#8@12	#7@12	#8@12
Reinforcement Ratio	0.28%	0.28%	0.28%	0.37%	0.28%	0.37%

2.2 GLOBAL BRIDGE MODEL FORMULATION

A visualization of the prototype bridge as modeled in OpenSees is shown in Figure 2.2. To draw meaningful conclusions about global bridge behavior, each component of the bridge needed to be carefully modeled. Elements were modeled with varying levels of complexity depending on predicted response, and whenever possible, the model formulation was validated using experimental results taken from published literature.

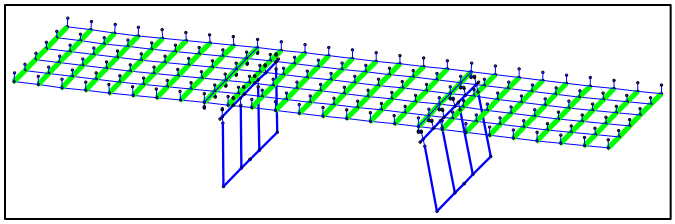

Figure 2.4. Prototype bridge as modeled with OpenSees (foundation springs not shown).

2.2.1 Superstructure

Several modeling approaches were considered for the bridge superstructure in an effort to find the simplest formulation that captured important behavior. Ultimately, the grid model shown in Figure 2.3 was selected (Chang and White 2008; Barth and Wu 2006). This is a more rigorous approach than a lumped parameter beam but still far less computationally expensive than a full shell model. A key advantage of the grid model over a lumped parameter beam was the ability to represent the transverse and vertical mass distributions that affect breakaway behavior of the bearings.

The grid model distributed mass in the plane of the deck and captured superstructure stiffness in three dimensions. Six longitudinal elements represented composite stiffness of the steel girders and concrete deck. Transverse elements were added to represent the deck stiffness in this direction, linking the girders for torsional stiffness and out-of-plane deformation. Parapet stiffness was neglected, and the gross moments of inertia about the x and y axes were multiplied by 0.75 and 0.35, respectively, to account for cracking. The model was validated by loading the deck in the vertical and lateral directions, with good correlation observed between computed deformations and theoretical deformations (Filipov 2012).

Note that no nonlinear behavior was modeled in the superstructure. The deck, girder, and diaphragm components were modeled with linear elastic elements because the quasi-isolated ERS concept features an essentially elastic superstructure. A parallel internal study showed that the diaphragms of many bridges in Illinois might not be fully elastic for transverse seismic loading. Diaphragm performance is beyond the scope of this study, but it is recommended that future designs ensure elastic diaphragm behavior.

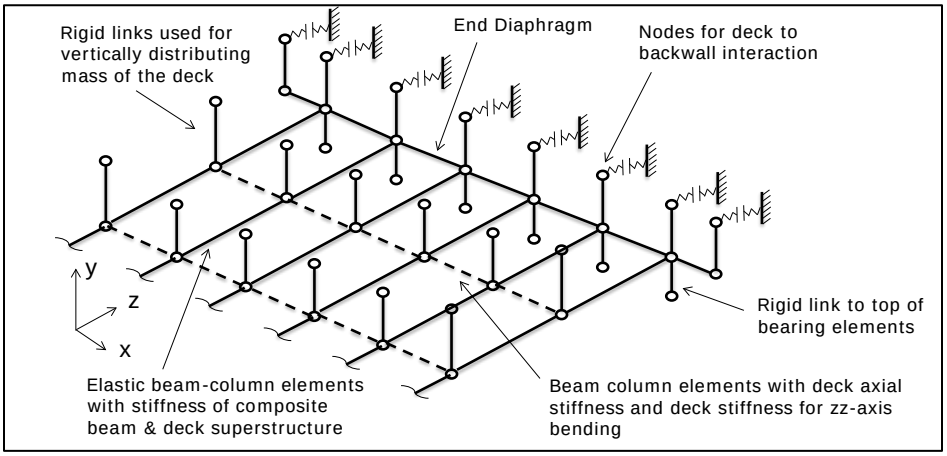

Figure 2.5. Grid model used to represent the superstructure.

2.2.2 Bearing Elements

The bearing elements are the primary connection between the superstructure and substructure, and they are expected to have significant influence on the global behavior of the bridge structure. The bearings and retainers were modeled with zero-length elements (ZLE) formulated to capture three-dimensional and nonlinear behavior. Figure 2.4 illustrates how rigid links were used to connect these zero-length elements to the bridge girders and pier cap with appropriate vertical spacing.

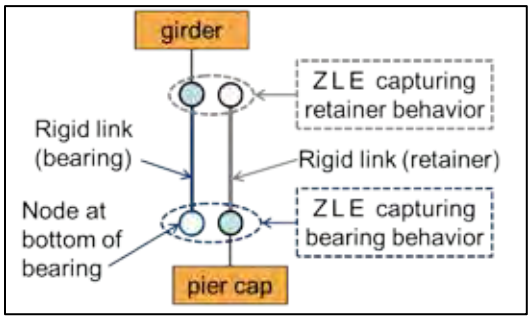

Figure 2.6. Implementation of bearing and retainer models.

Bearing systems modeled with uncoupled, uniaxial elements are considered unreliable for multi-directional seismic analysis. For example, friction pendulum isolators modeled with uncoupled elements resulted in overestimation of forces and underestimation of system displacements when compared with bi-directional coupled models and experimental data (Becker and Mahin 2011; Mosqueda, Whittaker, and Fenves 2004). Although friction pendulum bearings were not considered in this study, the findings are applicable to other types of isolation systems. Thus, an orthogonally coupled, bi-directional model was developed in OpenSees to model the bearings, and data from the experimental program were used to determine what behaviors should be captured. Further discussion of bearing element formulation, validation, and calibration is included in Section 2.3.

2.2.3 Seat Width

Pier caps and abutment seats were dimensioned based on the IDOT Bridge Manual (IDOT 2009) and the AASHTO seismic hazard for Cairo, Illinois. The seat widths calculated by Equation 2-1 are given in Table 2.3; the calculated *N* applies to both the abutments and piers in the longitudinal and transverse directions. An illustration of the seat width, *N*, is provided in Figure 2.5.

For the 1000-year event, the required support width, *N*, in inches, is calculated as

$$N = \left[3.94 + 0.0204L + 0.084H + 1.087\sqrt{H}\sqrt{1 + 2\left(\frac{B}{L}\right)^2}\right]\frac{1 + 1.25F_v S_1}{\cos\alpha} \qquad \text{(Eq. 2-1)}$$

where

L = Typical length between expansion joints (ft)
H = Height of tallest substructure unit between expansion joints
B = Out-to-out width of the superstructure (ft)
α = Skew angle (°)

F_vS_1 = 1-second period spectral response coefficient modified for site class
B/L = Not to be taken greater than 3/8
N = In this study, the distance between the centerline of bearing and the edge of support in both longitudinal and transverse directions. AASHTO measures it as the distance from the back edge of the girder to the edge of the support.

Table 2.3. Calculated Seat Width (in.) by Superstructure Type

	Steel Short (Ss)	Steel Long (Sl)	Concrete Short (Cs)
15-ft columns	23	27	24
40-ft columns	32	36	33

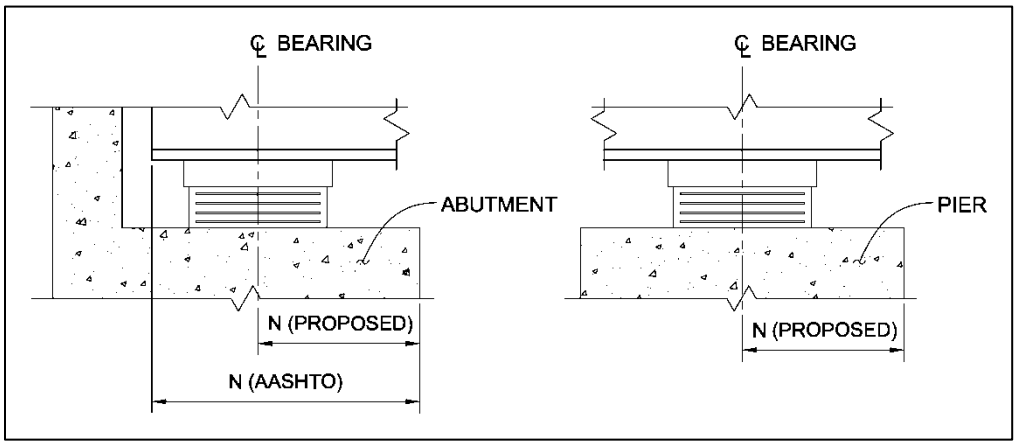

Figure 2.7. Explanation of the seat width definition proposed for this study.

2.2.4 Piers

Multi-column and wall piers were the two types of intermediate substructures considered in the parametric bridge study. Each substructure variation was studied with two different clear heights, 15 ft for short and 40 ft for tall structures, measured from the top of the foundation pile cap to the bottom of the pier cap. The reinforced concrete substructures were designed per the IDOT Bridge Manual (IDOT 2009) and the American Concrete Institute's code (ACI 318 2008). The pier cap and foundation pile cap are significantly stiffer than the columns and walls and were therefore modeled as linear elastic.

2.2.4.1 Multi-Column Piers

The columns can experience nonlinear phenomena such as cracking followed by flexural and shear yielding when subjected to high lateral loads, and it was important to model the columns in a way that could capture this nonlinearity. The distributed plasticity model proposed by Scott and Fenves (2006) was used because it captures the curvature in the plastic hinge regions, shows good correlation with experimental results, and is available for implementation in OpenSees. A fiber section (Figure 2.6, Figure 2.7) was used to model the nonlinear material behavior in the plastic hinge regions of the column, capturing cracking and yielding behaviors for the column member. Outside of the plastic hinge regions, the column was modeled by an elastic beam-column element, with a gross moment of inertia

about both axes multiplied by 0.7 to account for initial cracking. Sufficient transverse confining reinforcement was assumed present, such that the full moment capacity of the pier could be developed without bar buckling or shear failure of the column. The distributed plasticity model was validated against three sets of experimental data available in the published literature (Filipov 2012).

All column piers featured four 36-in. diameter columns spaced at 10-ft on center. The prototype bridge and all short steel parametric variations used columns with 3500-psi normal-weight concrete and 11 #9 longitudinal bars with 2-in. clear cover. The long steel and short concrete bridge parametric variations used 15 #9 longitudinal bars with 2-in. clear cover, as indicated by the higher reinforcing ratio in Table 2.2. Longitudinal steel was modeled with the OpenSees Steel02 material, assuming 67 ksi yield strength and 1% strain hardening. It was important to define the limit states reached by the concrete piers, so cracking, and more importantly, steel yielding effects were monitored. Figure 2.8 demonstrates this capability in the force-displacement hysteresis for a prototype bridge column in single curvature.

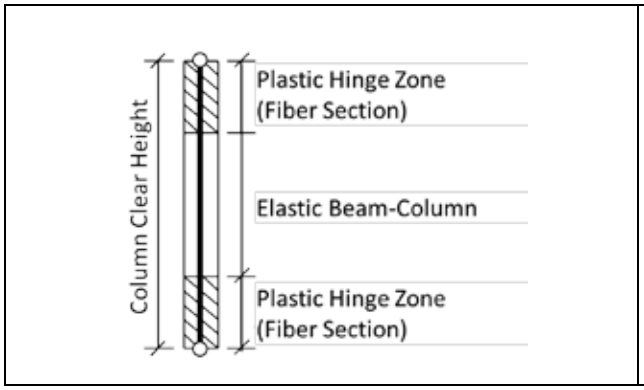

Figure 2.8. Beam-column with hinges.

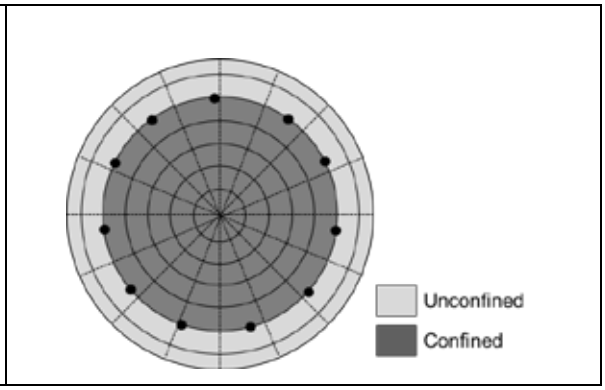

Figure 2.9. Fiber section.

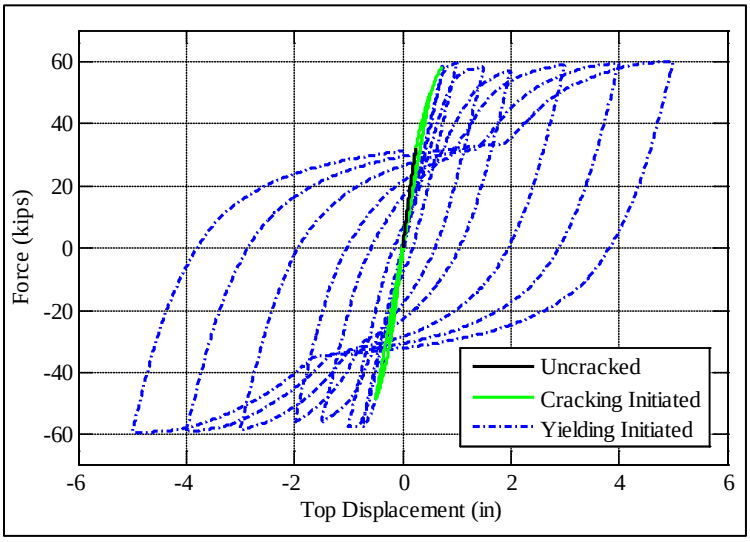

Figure 2.10. Prototype bridge column in single curvature.

2.2.4.2 Wall Piers

A reinforced concrete wall, 35 ft wide and 3 ft thick, was used for all parametric study bridges with wall substructures. Most bridges used #7 longitudinal reinforcement placed at 12 in. on center with 2.5-in. clear cover, but in tall wall variations, the Steel Long and Concrete Short bridges increased to #8 at 12 in. on center. The resulting reinforcing ratios are indicated in Table 2.2. Longitudinal steel was modeled with the OpenSees Steel02 material, assuming 62 ksi yield strength and 4% strain hardening.

Basic calculations were performed to determine what limit states were important to consider. For lateral loading in the strong axis, the wall was expected to remain linear elastic because both flexural and shear capacity significantly exceeded the anticipated bearing fuse force. For lateral loading in the weak axis, however, flexural yielding may occur. To capture this nonlinearity, the reinforcement and concrete were modeled in the same fashion as the circular column, and the same distributed plasticity model was used to represent plastic hinge formation. The fiber section used in the plastic hinge zones is shown in Figure 2.9. In the linear elastic region between plastic hinges, the gross moment of inertia about both the major and minor axis was multiplied by 0.7 to account for initial cracking. Shear deformations were determined to be negligible for loading in both directions and were therefore not considered in the final model. The wall pier model was validated against two sets of experimental data available in the published literature (Filipov 2012).

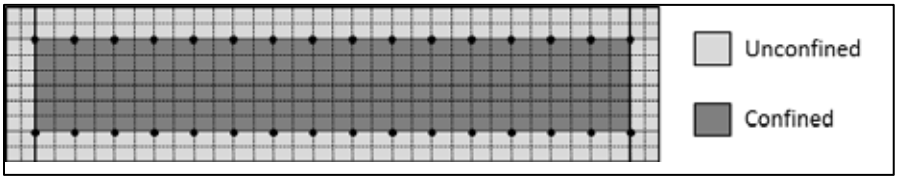

Figure 2.11. Fiber section for wall piers used with the prototype bridge.

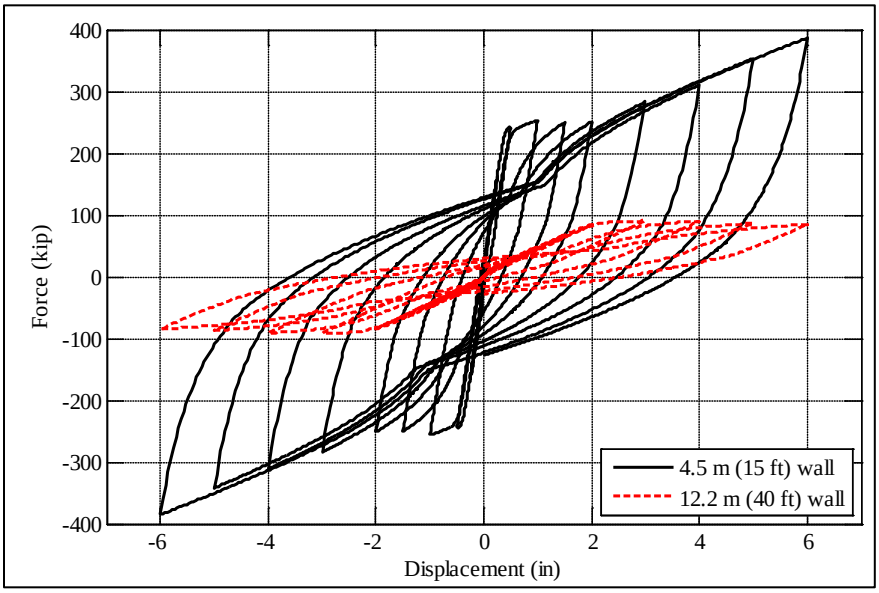

Figure 2.12. Out-of-plane pushover for wall piers used with the prototype bridge.

2.2.5 Abutment Backwall

In the parametric study, abutment backwalls were positioned to provide a 2-in. longitudinal expansion joint gap from the end of the bridge deck. The gap is expected to accommodate service-level thermal movements, but under seismic excitation, superstructure displacements will be large enough to close this 2-in. gap. When the superstructure contacts the backwall, there will be a nonlinear response from both the backwall and the backfill that may substantially impact overall bridge response (Wilson and Elgamal 2010). Important aspects of backwall-deck interaction are shown schematically in Figure 2.11. The superstructure-backwall-backfill interaction is most prominent for longitudinal excitation, but it should also be considered for transverse excitation because twisting of the deck can cause the corners of the deck to interact with the backwall.

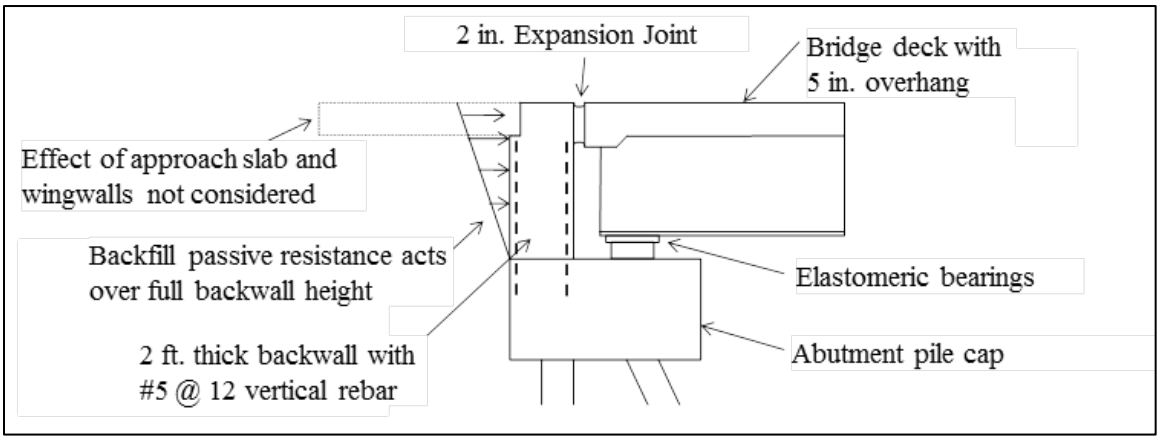

Figure 2.13. Aspects of superstructure-backwall-backfill interaction.

While the AASHTO seismic guide specifications consider only the passive resistance of the backfill (AASHTO 2009), effectively treating the backwall as sacrificial, typical IDOT backwalls were found to have significant force capacity. This can be beneficial in reducing longitudinal bridge deck movement, but it is also likely to induce large base shears in the abutments, potentially damaging foundation elements. It was therefore considered important to incorporate the structural capacity of the backwall into the model. Calculations for the prototype bridge indicated the shear friction capacity at the cold joint between backwall and pile cap significantly exceeded flexural capacity. Thus, the contribution of the backwall was captured through a rotational plastic hinge in the bridge model, as shown in Figure 2.12. All the bridge models in the parametric study used the same rotational plastic hinge capacity at the bottom of the backwall.

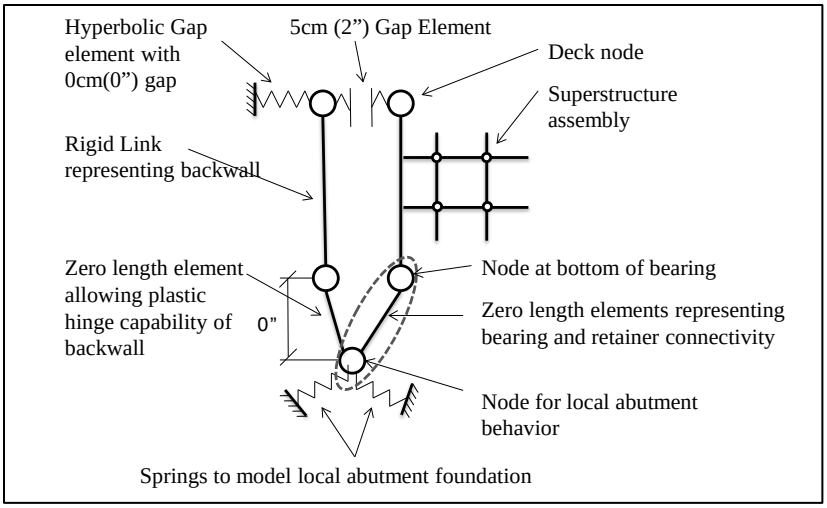

Figure 2.14. Representation of backwall and backfill in bridge models.

Nonlinear soil behavior was defined per Shamsabadi, Rollins, and Kapuskar (2007) and modeled using the OpenSees hyperbolic gap material (McKenna, Mazzoni, and Fenves 2011). This material traces a hyperbolic force-displacement relationship for the backfill, up to a user-defined peak passive resistance. The material model can also be set to reflect an initial gap, but this configuration would preclude backwall modeling, and the bridge models in this study were specifically formulated to capture backwall response. Accordingly, the "gap" in the hyperbolic gap material was set to zero, and a separate, conventional gap element was defined, as indicated in Figure 2.12. Input parameters for the hyperbolic material model were based on data from a centrifuge test of a seat-type abutment in dense Nevada sand (Shamsabadi, Rollins, and Kapuskar 2007). In the parametric study, backfill stiffness and strength depended on the backwall height, which was different for each of the three superstructure types considered. For the prototype bridge, the estimated ultimate passive resistance was 10.8 kips per linear foot of backwall, and the estimated stiffness was 440 kips/in.

2.2.6 Foundations

The abutment foundation was defined as 11 HP12x63 piles driven to a depth of 45 ft, with a 4 x 6 x 42-ft concrete pile cap. The row of four toe piles was battered at 3:1, the five heel piles were vertical, and two additional vertical piles were placed in the wingwalls. The typical foundation for an intermediate substructure was defined as three rows of four vertical HP12x63 piles driven to a depth of 45 ft, with a 2.5 x 12 x 35-ft pile cap.

Representative soil types were (1) stiff rocky soil, modeled as a fixed base and (2) soft clay or loamy soil, modeled with a shear strength of 300 to 500 psf. The soil-foundation interactions were represented with force-displacement curves calculated using a geotechnical pile group analysis program, GROUP 7.0, provided by Ensoft Inc. (2010). The foundations were then simulated in OpenSees as a single restraint at the bottom of each substructure, using springs to represent equivalent lateral and rotational stiffness.

2.3 BEARING ELEMENT FORMULATION

Bearing component formulations were developed for implementation in OpenSees. Key aspects of the formulations are discussed here, and more detailed documentation is available in Filipov (2012). The parametric study bearing models are described here to

ensure clear understanding of the OpenSees models (refer to Volume I of this report for recommendations on quantifying bearing response in practice).

2.3.1 Calibration of the Bi-Directional Sliding Bearing Elements

A zero-length bi-directional model similar to that of Constantinou, Mokha, and Reinhorn (1990) was created specifically to model the friction stick-slip behavior exhibited by Type I and Type II IDOT bearings. The model, shown schematically in Figure 2.13, is capable of capturing an initial static friction break-off force, a kinetic friction force, and a post-slip friction break-off force. Different coefficients of friction were specified for each condition, and the formulation also accounted for variable axial load on the bearing. Properties of the parametric study bearing models (summarized in Table 2.4) were based on the experimental results presented in Volume I of this report, and a sample validation of the bearing model is shown in Figure 2.14. Additionally, bearing stiffness, *K*, was calculated by Equation 2-2.

Table 2.4. Modeled Properties for Type I and II Bearings

	Property	Type I	Type II
G	Shear modulus	85 psi	85 psi
μ_{SI}	Initial static coefficient of friction	0.60	0.16
μ_K	Kinetic coefficient of friction	0.45	0.15
μ_{SP}	Stick-slip coefficient of friction	0.50	0.15

$$K = \frac{\text{G *Area}}{\text{Effective Rubber Thickness}} \qquad \text{(Eq. 2-2)}$$

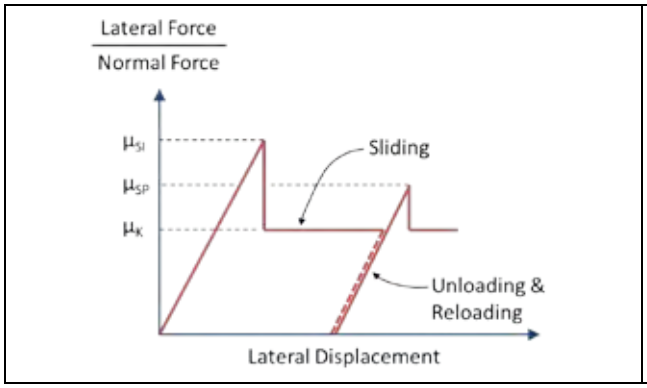

Figure 2.15. Schematic representation of sliding bearing model.

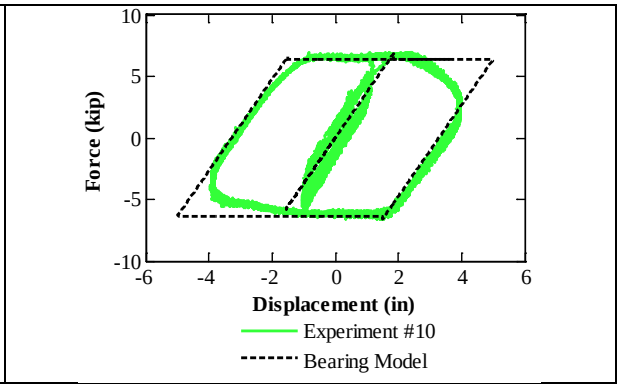

Figure 2.16. Validation of sliding bearing model with Test #10 experimental data.

2.3.2 Calibration of the Uni-Directional Retainer Elements

In experimental testing, the transverse retainers exhibited roughly elasto-plastic behavior, and failure was characterized by localized concrete crushing (primarily for larger anchor bolts) followed by anchor bolt tensile-shear failure. For modeling purposes, the overall retainer assembly behavior was based only on anchor bolt properties and was calibrated to experimental data from single retainer tests. The nonlinear uni-axial model, illustrated in Figure 2.15, featured an initial gap followed by elasto-plastic response and

failure at an ultimate displacement; Figure 2.16 provides a sample validation of the retainer model.

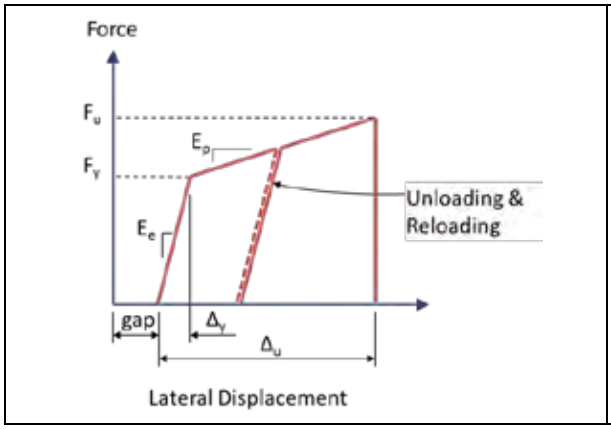

Figure 2.17. Schematic representation of retainer model

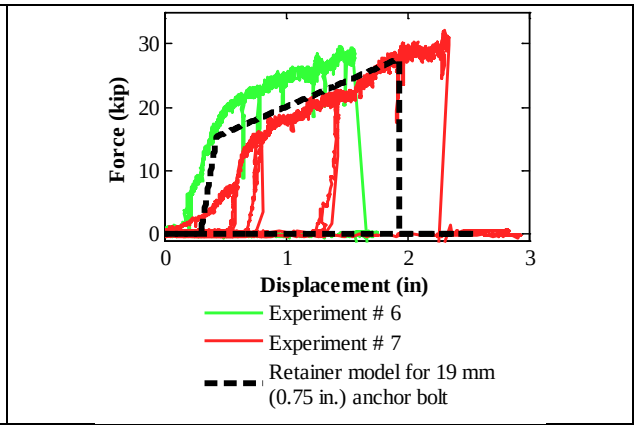

Figure 2.18. Experimental and model pushover behavior of retainers with 0.75-in. anchor bolts.

Retainer material properties and gap were based on experimental results, and Table 2.5 summarizes the values chosen for the parametric study. An additional 0.3 in. was added to the IDOT specified installation gap of 0.125 in. because testing demonstrated that the oversized bolt hole in the retainer left space for the retainer to slide before actually developing force. In an effort to represent bearing systems encountered in practice, anchor bolt sizes for the parametric study were determined using Section 3.7.3.1 of the IDOT Bridge Manual (IDOT 2009), with ultimate anchor bolt capacity estimated by Equation 2-3, below. However, experimental testing showed poor correlation with this equation; thus, in the model, elasto-plastic retainer behavior was instead defined using Equations 2-4 and 2-5.

Table 2.5. Retainer Properties for Parametric Study

Property	Value
Retainer gap	0.425 in
F_u	60 ksi
$E_{elastic}$	115 kip/in
$E_{plastic}$	8.2 kip/in

$$F_{ult} = \phi 0.48\, A_{bolt}\, f_u \quad \phi = 0.75 \qquad \text{(Eq. 2-3)}$$

$$F_{ult} = \phi 0.80\, A_{bolt}\, f_u \quad \phi = 1.00 \qquad \text{(Eq. 2-4)}$$

$$F_{yield} = \frac{F_{ult}}{1.8} \qquad \text{(Eq. 2-5)}$$

2.3.3 Calibration of the Bi-Directional Fixed Bearing Elements

On IDOT highway bridges, low-profile fixed steel bearings are often installed at one of the intermediate substructures to prevent global movements of the bridge deck caused by service-level loads. These bearings are normally placed on a 0.125-in. elastomeric

neoprene leveling pad and attached to the substructure using anchor bolts. While in theory, either an anchor bolt or pintle failure mode is plausible, only the anchor bolt failure mode was modeled. This was considered reasonable because the minimum pintle diameter of 1.25-in. was always larger than the modeled anchor bolt diameter; thus, the anchor bolt was the critical component.

A new bi-directional element was created to simulate the elasto-plastic yielding and fracture of the anchor bolts. This element was coupled with the sliding bearing element to capture friction between the bearing component and the substructure. A schematic of the model in Figure 2.17 shows a peak-oriented model based on Ibarra, Medina, and Krawinkler (2005) with variable pinching that follows a pre-defined elasto-plastic envelope capable of fracturing at a predefined displacement.

The model was initially developed based on existing literature for experiments with hysteretic behavior similar to that expected from the low-profile fixed bearings (Mander et al. 1996; Klinger, Mendonca, and Malik 1982; Gomez et al. 2009) and has since been validated against experimental results for the actual fixed bearings, as shown Figure 2.18. Table 2.6 summarizes the properties used to define the fixed bearings in the parametric study.

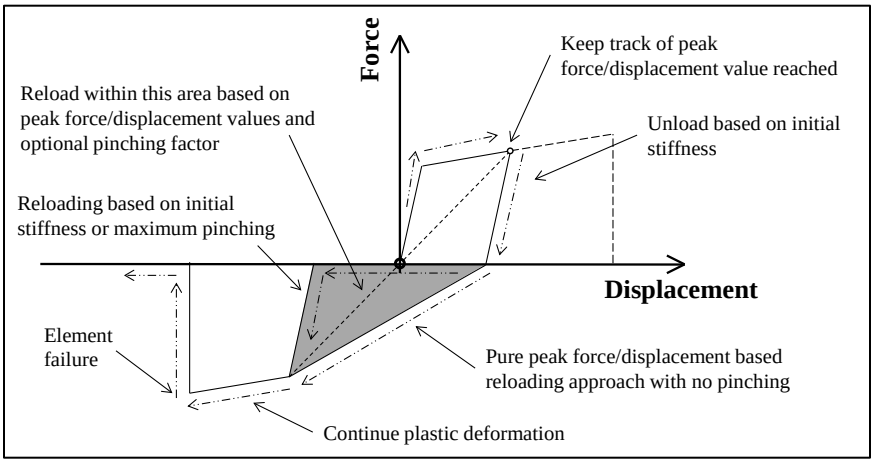

Figure 2.19. Schematic representation of fixed bearing model.

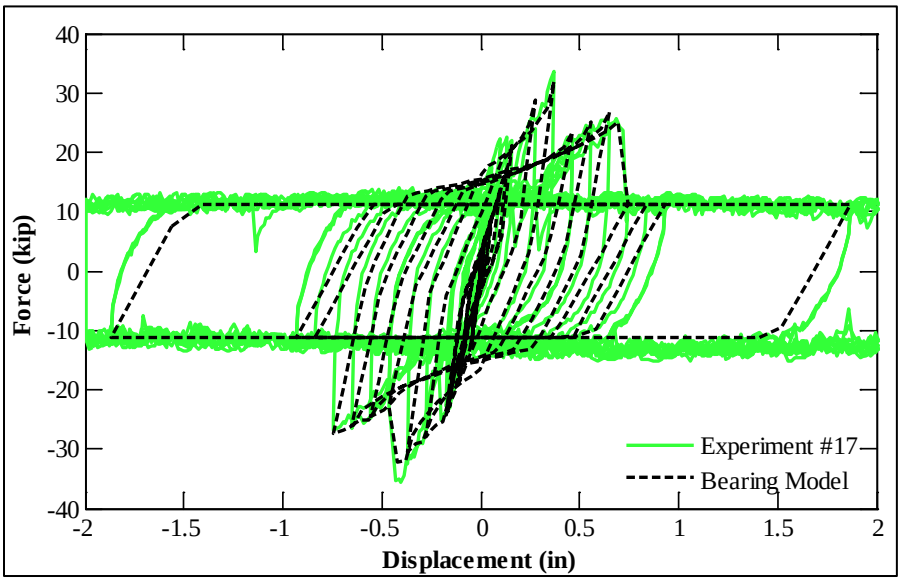

Figure 2.20. Experimental and model cyclic behavior for Test #17.

Table 2.6. Fixed Bearing Properties for Parametric Study

Elastomeric Pad		Anchor Bolts	
E	40 k/in	f_y	36 ksi
μ_{SI}	0.31	f_u	60 ksi
μ_K	0.30	P_y	2*Abolt*0.48*fy
μ_{SP}	0.305	Δ_y	0.1*Bolt Diameter
		P_u	2*Abolt*0.6*0.8*fu
		Δ_u	1.0*Bolt Diameter

2.4 GROUND MOTIONS FOR TIME-HISTORY ANALYSES

The bridges in the parametric study were subjected to response history analyses with different ground motions to assess the impact of several important parameters, including the characteristics of the seismic hazard, the intensity of earthquake excitation, and the different directions of shaking.

2.4.1 Ground Motion Selection

On the basis of studies of the New Madrid Seismic Zone (NMSZ), researchers have developed various synthetic records that are capable of modeling different soil characteristics in the Mississippi embayment (Fernandez and Rix 2008). The Cape Girardeau, Missouri records (CG), based on a 10-m soil column, were selected to represent the rock condition. The Paducah, Kentucky records (Pa), based on a 120-m soil column, were selected for the soil case. Each location supplied a set of ten synthetic records that modeled a risk of 7% in 75 years (1000-year event). The current research does not include the effects of vertical acceleration for two reasons. First, recent research (Zandieh and Pezeshk 2011) indicates that horizontal-to-vertical component spectral ratios for the region are relatively high, with values between 2 and 4 in the low-frequency range (frequency ≤ 5 Hz). Second, the project is focused on bridges in southern Illinois, north of the New Madrid fault zone. Vertical accelerations are primarily a near-field phenomenon, attenuating quickly from the source, and are therefore not expected to be significant for the region of interest.

2.4.2 Ground Motion Scaling

The parametric suite contains bridges with elastic first-mode natural periods varying from 0.2 seconds to more than 1 second; periods can increase significantly when nonlinearities appear during analysis. Thus, ground motions were normalized based on a technique used by Somerville et al. (1997), which uses a least-squares approach to normalize ground motions to a specific target spectrum. The methodology was used to fit the synthetic ground motions to a 1000-year recurrence design spectrum for Cairo, Illinois, as defined by AASHTO (2009). The CG rock records were normalized to a Site Class B hazard, while the Pa soil records were normalized to Site Class D.

Figure 2.19 shows the ground motion spectra normalized to the respective design spectra. The ground motions as shown are considered to be at a scale factor (SF) of 1.0

and constitute the baseline hazard for this research. The parametric study used six distinct scale factors (0.5; 0.75; 1.0 = design; 1.25; 1.5; 1.75) to encompass different hazard levels and create a coarse incremental dynamic analysis (Vamvatsikos and Cornell 2002). The SF = 1.0 ground motions were linearly scaled up and down to provide relative estimates of structural performance for different hazard levels. The Cairo location has one of the highest hazards for the state and a reasonably high hazard within the overall NMSZ. Other locations in Illinois would typically have lower hazards. As an example, the design hazard in Carbondale can be approximated by scaling the baseline ground motions with a factor of 0.5. The spectral acceleration of actual earthquake events increases logarithmically for higher magnitude hazards, so the linear scaling used herein does not correspond directly to particular higher hazard levels. However, the maximum considered earthquake (MCE) hazard (2% in 50-year risk) for the Cairo location can be approximated to be between the 1.5 and 1.75 linearly scaled ground motion levels.

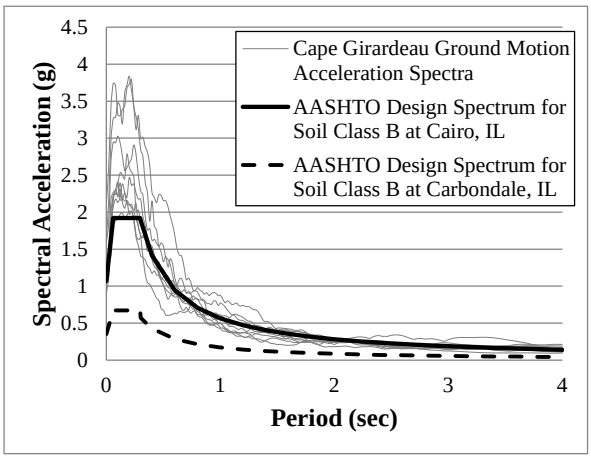

(a) Acceleration spectra for Cape Girardeau normalized to Cairo Soil Class B.

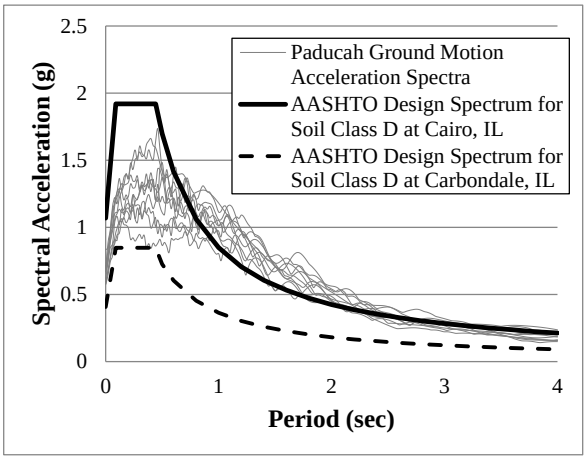

(b) Acceleration spectra for Paducah normalized to Cairo Soil Class D.

Figure 2.21. Acceleration spectra for the parametric study baseline hazard (1000-year event).

2.4.3 Ground Motion Directionality

Current design provisions (AASHTO 2009) recommend that designers simultaneously apply the full demand in the direction of interest and 30% of the demand in the perpendicular direction in order to account for the directional uncertainty of earthquake motions. Recent research (Mackie, Cronin, and Nielson 2011) used nonlinear multi-degree of freedom (MDOF) analyses of symmetric multi-span highway bridges within a stochastic framework to show that the incidence angle is typically negligible in the bridge response. However, other work (Bisadi and Head 2010) showed that there might be significant variance caused by the incidence angle. Only uni-directional ground motions are available for the geographic region of interest, and the current research focused primarily on orthogonal application of ground motions. Sample studies were carried out with non-orthogonal (45° incident angle) excitation for the SsC15T2S bridge variation, and the findings are presented in Section 5.1.1. For the very regular bridges in the parametric study, non-orthogonal seismic excitation was generally found to be as critical as or less critical than uni-directional ground motion application.

2.5 MODAL RESPONSE OF PROTOTYPE BRIDGE

Modal analysis was performed in OpenSees for 48 bridge variants, and periods of vibration were recorded for the first eight modes. The eigenvectors were used to plot the deformed bridge shape in each mode and used for visual identification of the fundamental longitudinal and transverse modes.

Two distinct modeling cases were considered for the modal analysis. The elastic case used the elastic response of all bearings, including the fixed bearings, along with the elastic response of the retainers in the transverse direction. This represents the initial elastic response of the bridge. By comparison, in the fused case, the fixed bearings and retainers were removed, and only the elastomeric bearings remained at the superstructure-substructure interface. This fused case represents the response of the bridge later in the earthquake record, when retainers and fixed bearings have fused and when the elastomeric bearings are in a static configuration but can deform elastically. Note that if all bearings were to slide simultaneously, the effective period would be infinite.

Table 2.7. Periods of Vibration for Short Steel (Ss) Superstructure Variants

			Longitudinal Period (s)				Transverse Period (s)			
			Short (15 ft)		Tall (40 ft)		Short (15 ft)		Tall (40 ft)	
			Elast.	Fused	Elast.	Fused	Elast.	Fused	Elast.	Fused
Column Pier	Type I Bearings	Fixed base	0.65	0.73	1.32	1.32	0.24	0.80	0.33	0.96
		Soft soil	0.73	0.80	1.35	1.35	0.33	0.82	0.41	1.01
	Type II Bearings	Fixed base	0.63	0.70	1.19	1.20	0.24	0.73	0.33	0.91
		Soft soil	0.71	0.76	1.22	1.22	0.33	0.75	0.41	0.95
Wall Pier	Type I Bearings	Fixed base	0.37	0.58	0.93	0.95	0.19	0.78	0.19	0.78
		Soft soil	0.58	0.69	1.07	1.08	0.33	0.81	0.41	0.82
	Type II Bearings	Fixed base	0.37	0.57	0.89	0.90	0.19	0.71	0.19	0.71
		Soft soil	0.57	0.66	1.01	1.02	0.33	0.74	0.41	0.75

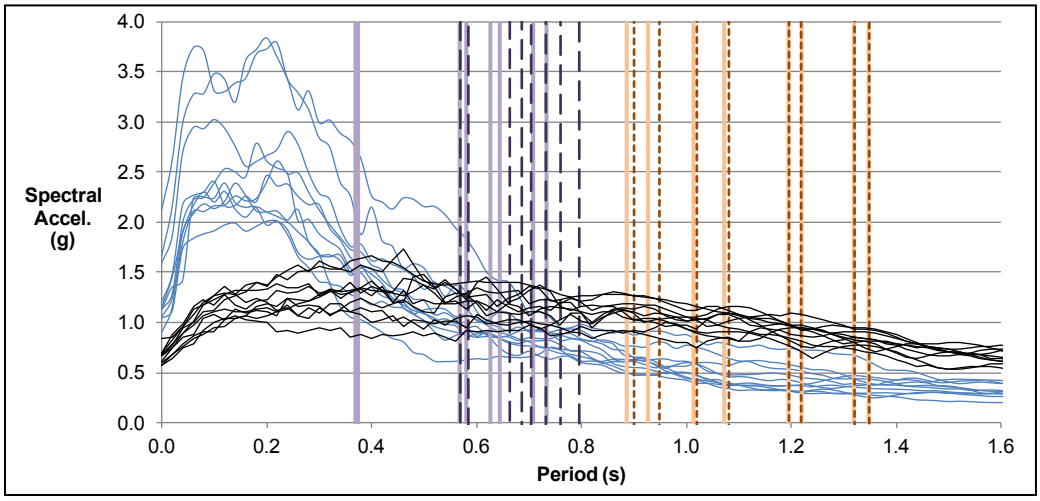

(a) Longitudinal modes

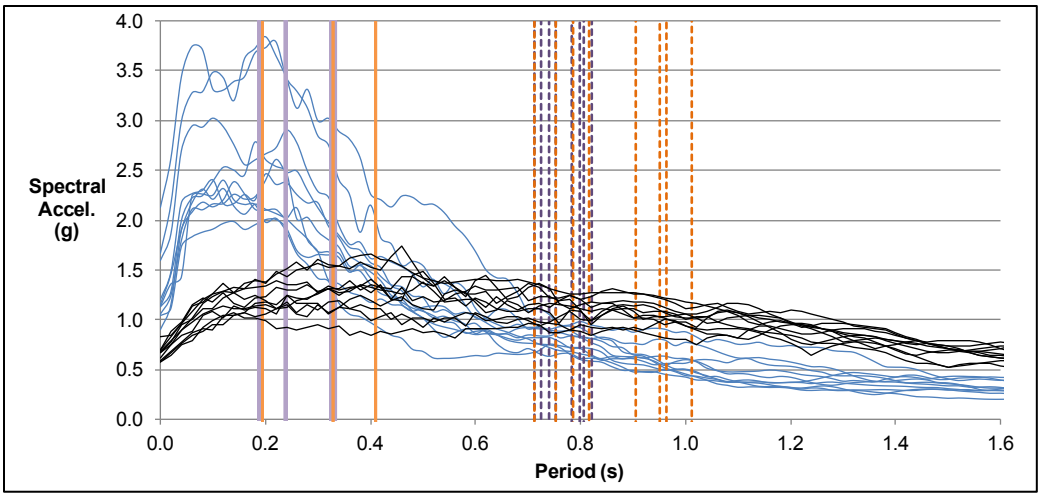

(b) Transverse modes

Legend

CG Response Spectra
Pa Response Spectra
Elastic Mode w/ 15ft Piers
Elastic Mode w/ 40ft Piers
Fused Mode w/ 15ft Piers
Fused Mode w/ 40ft Piers

Figure 2.22. Fundamental periods of vibration.

Table 2.7 summarizes the fundamental longitudinal and transverse periods of vibration for the short steel superstructure variants. A visualization of the period shift that occurs from the elastic case to the fused case is provided in Figure 2.20. In the longitudinal direction, tall bridge variants had noticeably longer periods than short pier variants, but the elastic and fused cases produced similar modal responses. The opposite was true in the transverse direction, where the fused bridges had longer periods than the elastic bridges and pier height was not particularly influential. Figure 2.20 also overlays the periods of vibration on the Pa and CG response spectra scaled to SF = 1.0. Modal response data for all 48 bridge variants are included in Appendix A.

CHAPTER 3 DYNAMIC ANALYSIS OF QUASI-ISOLATED SYSTEM

Transient dynamic analyses were performed for the parametric study bridges using the open source nonlinear seismic analysis program, Open System for Earthquake Engineering Simulation (OpenSees). A single analysis "run" was uniquely defined by the bridge model, the ground motion, the direction of application of that ground motion, and the scale factor (SF) applied to the accelerogram. This resulted in a total of nearly 12,000 dynamic analysis runs.

In all analysis runs, stiffness and mass-proportional viscous damping of 5% was used for the first (elastic) mode, and additional energy was dissipated through nonlinear hysteretic behavior of components in the model. Force and displacement data were recorded for all elements of the bridge model at each time step in a run, resulting in an enormous amount of data for evaluation. In this chapter, the short steel bridge, SsC15T2S, is used to present detailed samples of dynamic behavior. This bridge model was chosen to illustrate several interesting nonlinearities and a sequence of damage that is not ideal for the proposed quasi-isolated ERS. An overall summary of bridge performance findings, based on the full suite of dynamic analysis runs, is also provided in this chapter. Detailed research results are reported in the appendices.

3.1 LIMIT STATES

A list of typical limit states is shown in Table 3.1, and hereafter the abbreviations in this table will often be used as a shorthand reference to the limit states. Nonlinear limit states include retainer failure, elastomeric bearing sliding, and fixed bearing failure, as well as yielding of the backwalls and piers. Hysteretic force-displacement curves for the various bridge components were used to determine whether these limit states had been reached. By comparison, the unseating limit states were defined in terms of maximum acceptable displacements. These allowable displacements, indicated schematically in Figure 3.1, were set based on a combination of modeling capability and engineering judgment.

Table 3.8. Typical Limit States Observed in Parametric Study

Acceptable for quasi-isolation		**Acceptable as secondary fuse**	
EA	Elastomeric bearings slide at abutment	P1	Pier 1 yields
EP	Elastomeric bearings slide at Pier 1	P2	Pier 2 yields
RA	Retainer failure at abutment		
RP	Retainer failure at Pier 1	**Discouraged for quasi-isolation**	
Fb	Fixed (low-profile) bearing anchorage failure	UA	Unseating of bearing at abutment
Bw	Backwall yielding	UP	Unseating of bearing at pier

3.1.1 Bearing Unseating Limit States

Type I bearing unseating was assumed to occur when the leading edge of the bearing moved to the edge of the support with seat width (N) calculated by the IDOT equation presented in Section 2.2.3. This unseating definition is quite conservative when compared with the allowable seat widths defined by AASHTO and IDOT, which focus on the

girder moving to the edge of support rather than to the leading edge of the bearing. The leading edge was chosen for this research because when the bearing reaches the edge of support, the bearing model can no longer accurately capture bearing response; furthermore, the system is likely to shift toward increasingly unstable configurations, potentially resulting in span loss. Similarly, Type II bearings were shown experimentally to exhibit unstable and highly nonlinear behavior when the contact area between the top plate and bottom plate was reduced. Unseating was therefore assumed to occur when the contact distance (smallest dimension of rectangular contact area) became less than 3 in. For example, for Type II 7b bearings used at the abutments of short steel structures, it was assumed that unseating began at a longitudinal displacement of 4 in.

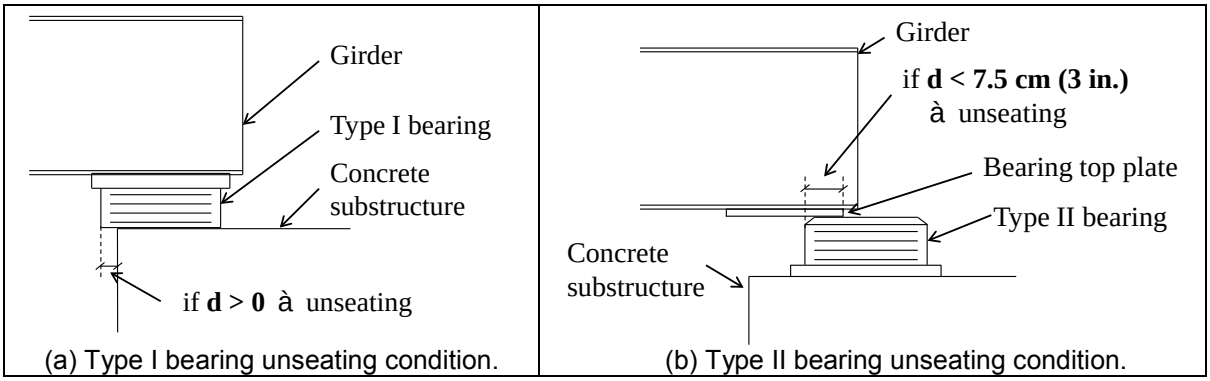

Figure 3.23. Schematic representation of bearing unseating condition.

Unseating of the bearings has the potential to cause extensive damage to the superstructure and diaphragm elements and might lead to local or global collapse of the girders. Additionally, as discussed above, the validity of the computational models is questionable once bearing unseating occurs. Thus, although bearing unseating is not explicitly unacceptable based on current IDOT ERS philosophy, it is considered a critical limit state in these analyses, and bridges that experienced unseating by this definition were not considered successfully quasi-isolated.

3.1.2 Pier Yielding Limit States

As indicated in Table 3.1, yielding of the piers is not desired for quasi-isolation but is nevertheless allowed to function as a secondary structural fuse after the bearings have fused. Thus, a bridge with a sequence of damage where the bearings fuse and then the piers yield could still be considered quasi-isolated. A bridge where pier yielding dominates the inelastic response, preventing the bearings from fusing or resulting in severe damage to the substructure, would not be considered quasi-isolated. To help make this distinction, drift ratios were used to assess substructure damage. Pier drift ratios (peak substructure displacement divided by the substructure clear height of 15 or 40 ft) between 2% and 4% were correlated with moderate damage, and ratios in excess of 4% were considered to represent severe substructure damage (Building Seismic Safety Council 2000).

3.1.3 Foundation Limit States

Although the foundations were modeled with nonlinear elements, no significant nonlinearity was ever encountered in the foundation elements; thus, no foundation limit states appear in Table 3.1. Note, however, that the performance of the steel H-pile foundations used for the parametric study bridges is likely better than would be expected of

some other foundations types used in Illinois. Base shear data from this study could be used to determine whether other foundation systems are also appropriate for use with quasi-isolated bridges. The foundation springs in the bridge models were based on analysis of an H-pile group out to 3 in. of lateral displacement, which enveloped recorded foundation displacements for most parametric study bridges. The tall wall pier bridge variants (XxW40XXS) had transverse foundation displacements of 4 to 7 in. at the design earthquake, and the force-displacement relationship was extrapolated from available data.

3.2 QUANTIFYING BRIDGE PERFORMANCE

Incremental Dynamic Analysis (IDA) was an important tool for studying the overall system-level behavior of each bridge when subjected to a suite of ground motions. An IDA represents the average response variable (in this case, displacement or force at a point in the structure) under a set of ground motions scaled to several levels of intensity (Vamvatsikos and Cornell 2002). Examples are shown in Figure 3.3, with similar plots provided in Appendix B for each bridge in the study. A scale factor (SF) of 1.0 corresponds to the design seismic hazard, as discussed in Section 4.4. Scale factors up to 1.75 were considered in an effort to capture behavior of bridges where all bearings had fused, as well as to provide context for the results at SF = 1.0. Similarly, some of the lower scale factors may provide insight into bridge performance in regions with a lower seismic hazard than the design location of Cairo, Illinois.

Note that while the dynamic analysis models incorporated extensive nonlinear behaviors, the models were not necessarily always able to identify when a collapse limit state was reached. At high scale factors, some of the IDAs may represent structures with unrealistically high levels of damage or unattainable deformed configurations. This is of particular note for bridges that experience pier yielding, where, after multiple cycles to large drifts, damage to the plastic hinge zone may result in the loss of gravity load-carrying capacity. The same is true for unseating of the bearing(s) at the abutments and Pier 1, though for these limit states a dashed line was added to the IDAs at the unseating displacement to indicate that a critical limit state had been reached.

3.3 SAMPLE BRIDGE SUBJECTED TO LONGITUDINAL EXCITATION

The SsC15T2S bridge model was subjected to pure longitudinal ground shaking from one of the stiff soil (Pa) ground motions, with scale factors of 0.5 and 1.5. Longitudinal hysteretic response of the bearings, backwalls, and piers is shown in Figure 3.2, where the maximum recorded forces are marked with an X and peak relative displacements marked with a square. The relative pier displacement was calculated by taking the top of pier displacement and subtracting the contribution from foundation translation and base rotation, thereby providing a force-displacement behavior that is comparable across different foundations and different pier heights. In Figure 3.2, bearing displacements include elastic deformation, but backwall displacements do not include the 2-in. expansion joint gap.

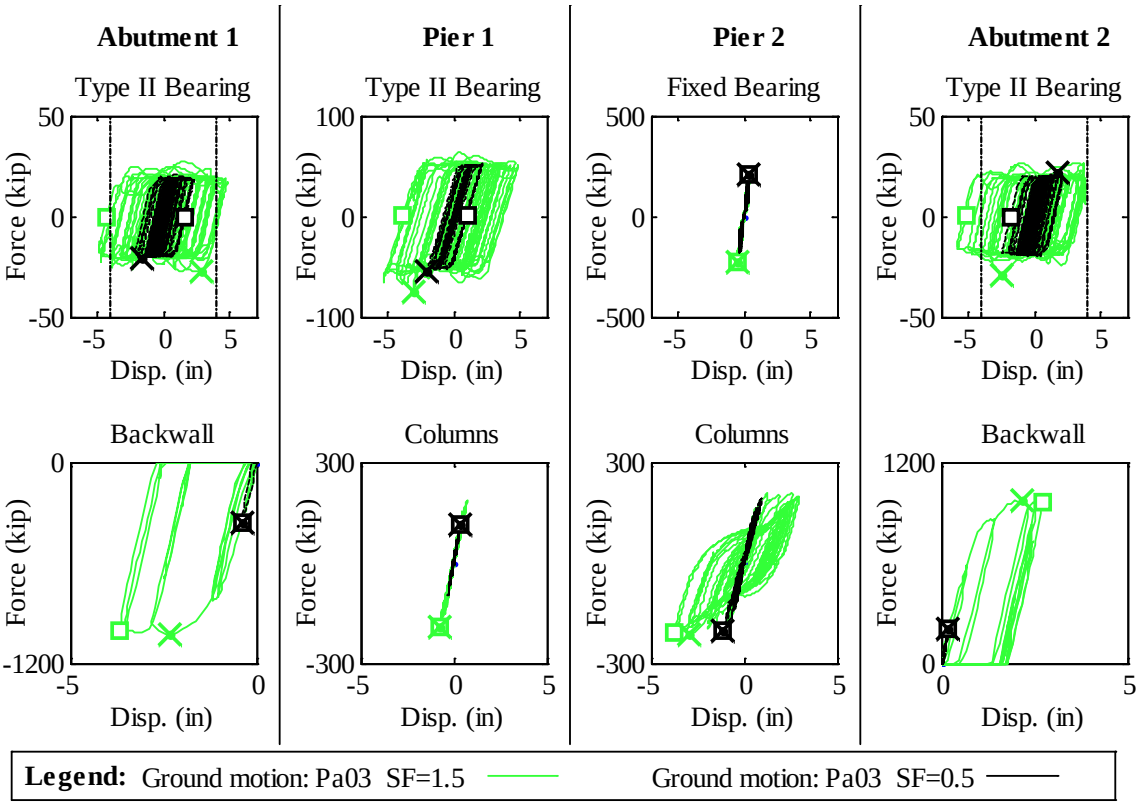

Figure 3.24. Longitudinal dynamic behavior of the SsC15T2S bridge, subjected to pure longitudinal excitation. Maximum response is indicated with a square for relative displacement and an X for force.

Figure 3.2 shows the occurrence of several interesting nonlinear behaviors. The ground motion applied at SF = 0.5 results only in elastic deformation of the column piers and slight contact with the backwalls. In contrast, when the SF = 1.5 motion is applied, columns at Pier 2 yield, the backwalls are engaged and experience nonlinear deformations, and the bearings slide much more, reaching unseating at the abutments, where the UA limit state is indicated by the vertical dash-dot lines. Yielding occurred in Pier 2 because excessive strength of the fixed bearing anchor bolts prevented fusing of the bearing. Yielding of Pier 2 prior to fusing of the fixed bearings was observed for longitudinal excitation of most parametric study bridges at SF 1.0 and higher.

Results similar to those presented above can provide detailed insight into behavior of a component over the course of a single record, but they are less helpful in developing a broad understanding of expected system performance. To capture bridge behavior for the entire suite of ground motions and for varying earthquake intensity, the force and displacement response were plotted against the earthquake scale factor, resulting in an IDA curve for bridge response. The plots use a circle to show the average response to the suite of ten Paducah ground motions at a given scale factor, and horizontal bars indicate the standard deviation of the dataset. To illustrate the connection between the force-displacement plots for a single run and the IDAs for a bridge, the X and square markers indicating maximum forces and relative displacements for the runs (shown in Figure 3.2) have been transferred onto Figure 3.3. Note that while the force-displacement plots included

elastic bearing deformation, in the IDA plots elastic deformation has been removed, and relative bearing displacements can be interpreted as bearing sliding displacements.

The IDA curves in Figure 3.3 also show the incremental behavior for the SsC15T2S bridge subjected to non-orthogonal shaking at a 45° incident angle. The fixed bearing behavior at Pier 2 is the most notable difference in the response of this bridge to pure longitudinal versus non-orthogonal shaking. The force-displacement plots in Figure 3.2 show that for the pure longitudinal case, Pier 2 experienced yielding, but the fixed bearings deformed only elastically. The non-orthogonal shaking, by comparison, generated coupled longitudinal and transverse forces that exceeded fixed bearing capacity, causing the fixed bearing component to fracture and slide at SF = 1.0. Finally, these IDA plots show that, with the exception of the fixed bearing displacements at Pier 2, force and displacement responses were greater for pure longitudinal excitation than for non-orthogonal.

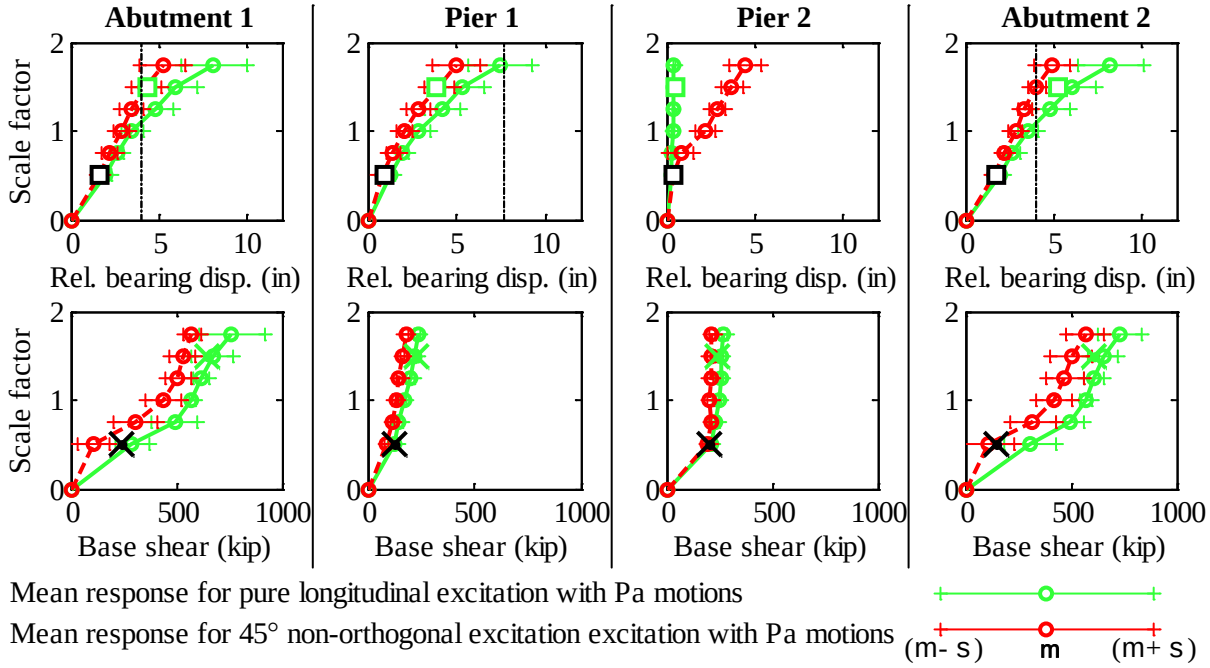

Figure 3.25. Maximum longitudinal response of the SsC15T2S bridge for incremental hazard.

The IDA plots are a tool to assess overall system behavior and the sequence of damage when different limit states occur in different analyses. In the pure longitudinal case, the elastomeric bearings at the abutments and Pier 1 began sliding by SF = 0.5, but the fixed bearings remained elastic even at SF = 1.75. At the abutments, the increase in base shear beginning at SF = 0.5 correlated with backwall interaction. This is corroborated by Figure 3.2, where, as previously discussed, there was nonlinear backwall-backfill response beyond SF = 0.5. Note that the IDA abutment base shear forces were lower than the backwall force in Figure 3.2 because the base shear did not include force transferred into the backfill. At Pier 2, the base shear was limited to roughly 270 kips as a result of the yielding of the column pier at that substructure. Finally, dashed lines added to the IDAs for bearing displacement indicate that bearing unseating occurred at the abutments around SF = 1.0.

The information from the IDAs and force-displacement plots was used to determine which limit states were reached at which scale factors (i.e., the sequence of damage). The sequence of damage for the SsC15T2S bridge subjected to longitudinal Pa (stiff soil) ground motions is shown in Figure 3.4(a). This bridge experienced yielding of Pier 2 before the design-level earthquake and unseating of abutment bearings at the design earthquake (SF = 1.0). Bearing unseating is discouraged for a quasi-isolated system, and pier yielding, while acceptable in some situations, is not ideal.

A preferred longitudinal sequence of damage for a quasi-isolated system would begin with “inexpensive” bearing sliding limit states (EA and EP) for small earthquakes, followed by fixed bearing and backwall limit states (Fb and Bw) for design-level earthquakes. Finally, it would permit some damage to substructure elements (P1 and P2) so long as there was no unseating of the bearings. Figure 3.4(a) shows the sequence of damage for SsC15T2S, while Figure 3.4(b) shows a sample preferred sequence of damage. Figure 3.4(c) provides a visualization of both. Note that the exact sequence of damage does not need to follow any particular pattern as long as limit states do not enter the dark orange shading indicated in Figure 3.4(c). The light blue shading indicates limit states that are acceptable but not ideal.

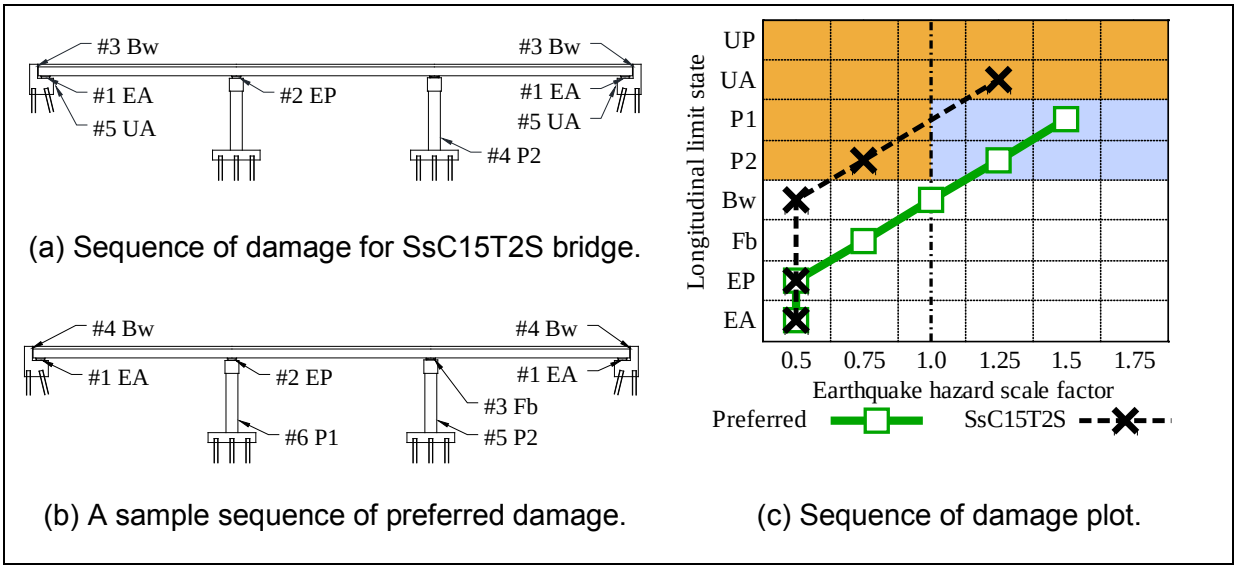

Figure 3.26. Sequence of damage representation for incremental longitudinal hazard.

3.4 SAMPLE BRIDGE SUBJECTED TO TRANSVERSE EXCITATION

The SsC15T2S bridge model was subjected to pure transverse ground shaking from one of the stiff soil (Pa) ground motions, with scale factors of 0.5 and 1.5. Transverse hysteretic responses of the retainers, bearings, and foundations are shown in Figure 3.5, where the maximum recorded forces are marked with an X and peak relative displacements marked with a square. As shown in the force-displacement plots, the bearings primarily began to slide after the retainers failed. In Figure 3.6, the maximum absolute response values are transferred onto IDA curves that show the response means and standard deviations of the SsC15T2S bridge for pure transverse and non-orthogonal excitations. The abutment base shears roughly corresponded to the maximum combined retainer and bearing sliding forces recorded earlier, while base shears at the piers tended to increase even after bearing and retainer failure because the mass of the piers can lead to additional

seismic force for higher levels of ground acceleration. With regard to failure sequence of fuse components, the abutment retainers and low-profile fixed bearings failed and permitted sliding at a hazard level of roughly SF = 0.75, and the Pier 1 retainers fused last, at SF = 1.25. After the fuse components failed, displacements began to increase significantly, resulting in both abutment and pier bearings unseating by SF = 1.5. Pure transverse excitation again resulted in much larger base shears and displacements than from the non-orthogonal excitation.

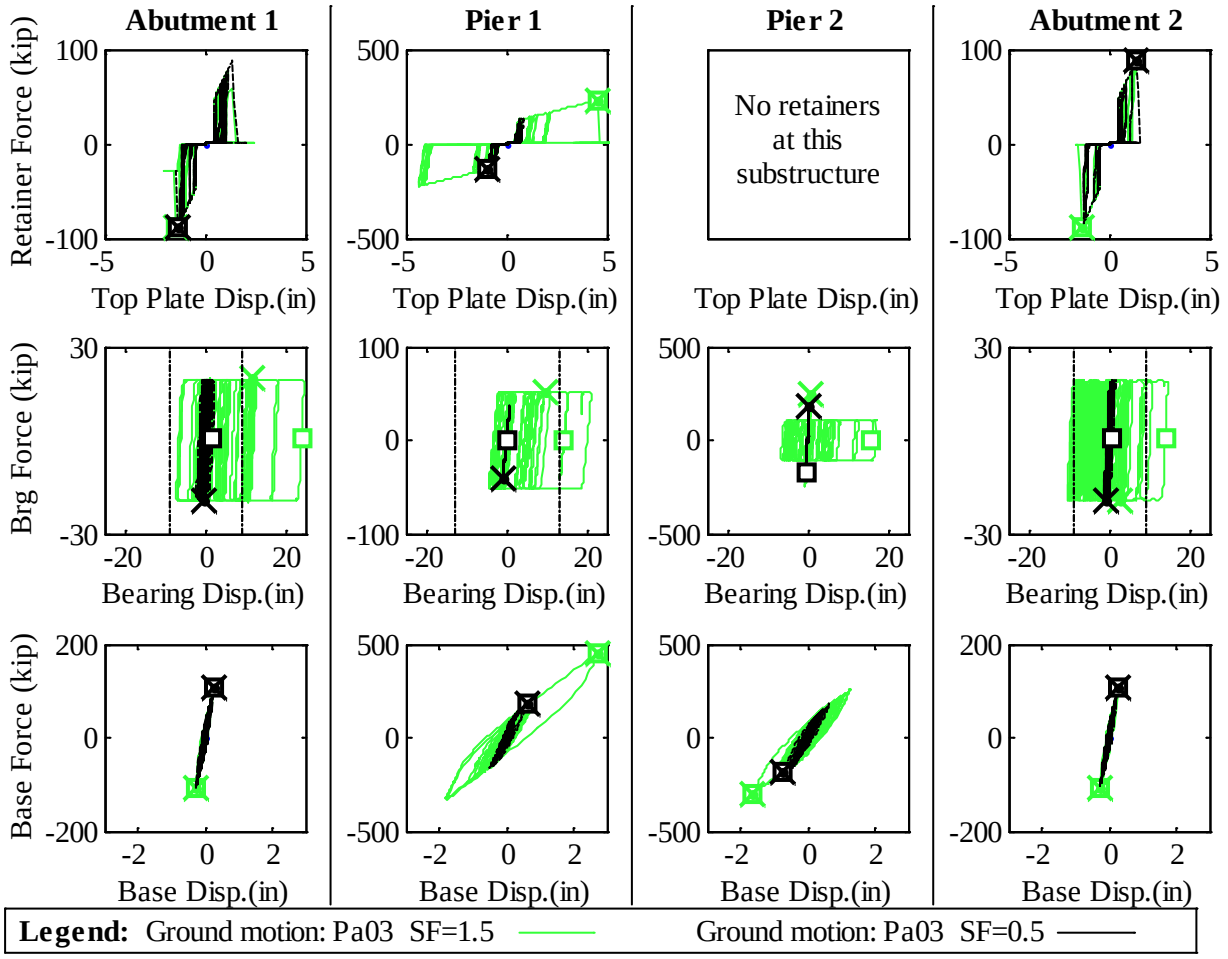

Figure 3.27. Transverse dynamic behavior of the SsC15T2S bridge subjected to pure transverse excitation. Maximum response is indicated with a square for relative displacement and a cross for force.

The transverse sequence of damage for the SsC15T2S structure, as shown in Figure 3.7, matched that desired for quasi-isolated performance, with the exception of the unseating behavior close to the MCE hazard level. A preferred sequence of damage for the system, outlined in Figure 3.7(b), permits retainer damage (RA and RP) and fixed bearing damage (Fb), as well as some column pier yielding (P1 and P2) for larger than design-level earthquakes.

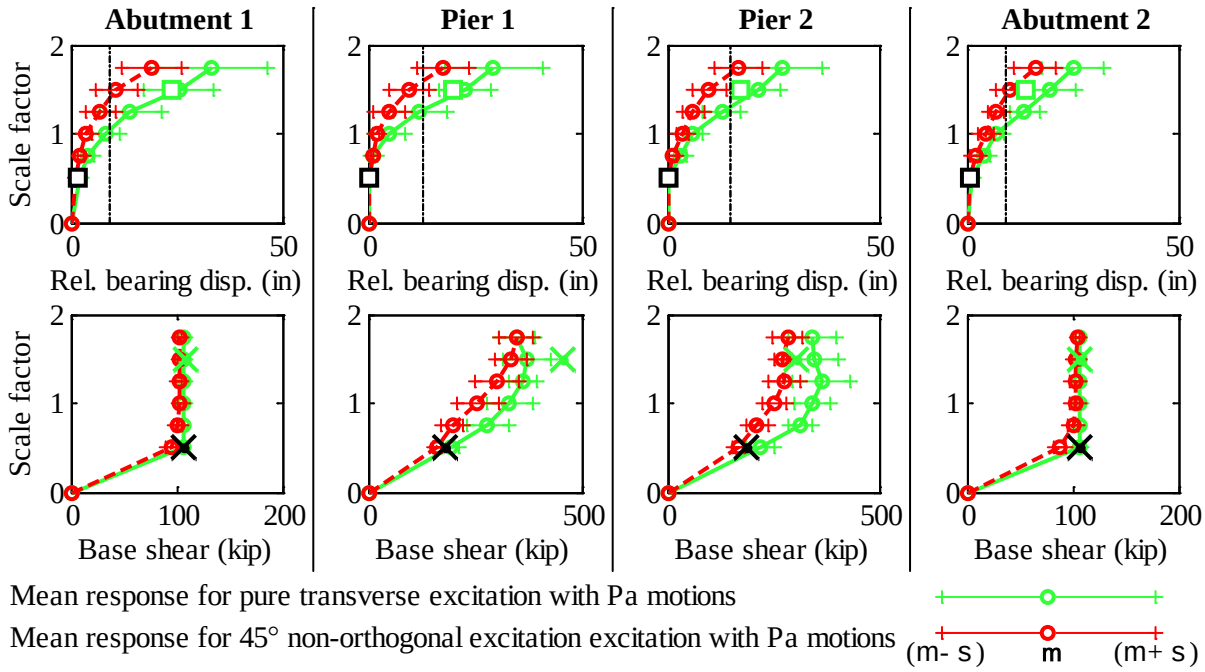

Figure 3.28. Maximum transverse response of the SsC15T2S bridge for incremental hazard.

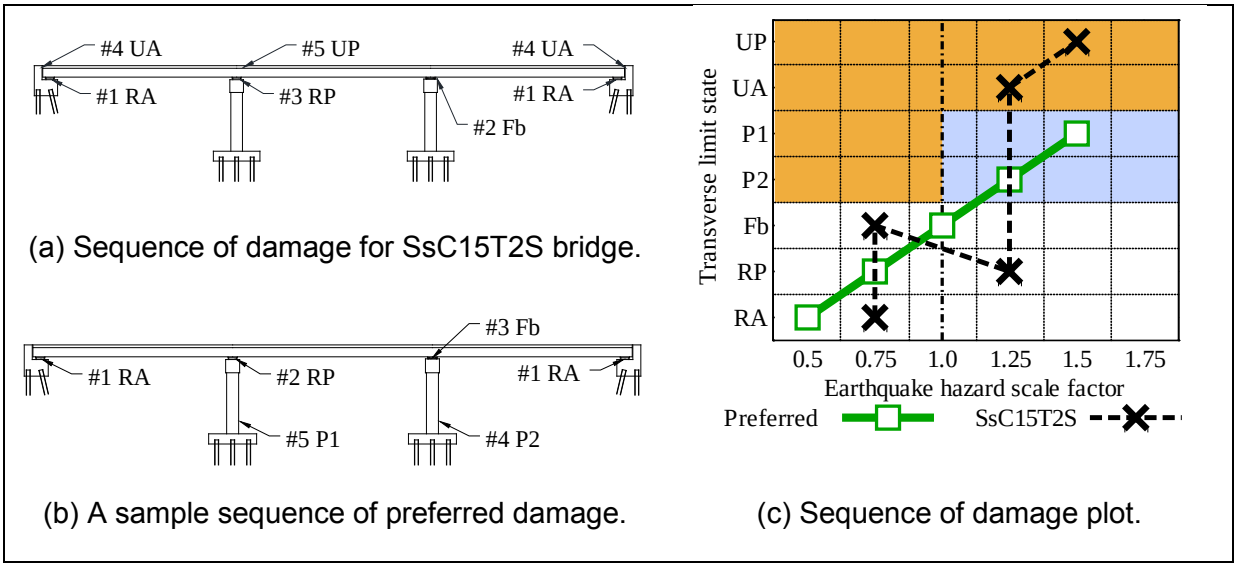

Figure 3.29. Sequence of damage representation for incremental transverse hazard.

CHAPTER 4 PARAMETRIC STUDY RESULTS

4.1 SYNTHESIS OF NUMERICAL RESULTS

The performance of the 48 parametric study bridges was assessed based on key response parameters such as superstructure displacements, relative bearing displacements, relative pier displacements, and base shears. To distill the thousands of time-history runs into summary tables and graphics, representative values of these response parameters were obtained for each bridge via a series of approximations:

1. At each time step in an individual time-history analysis, bearing displacement at a support was calculated by averaging the response of the six bearings. Similarly, displacement of the multi-column piers was calculated by averaging the response of the four piers. Backwall displacement was conservatively reported as the peak displacement over the eight backwall interaction nodes. Foundations and wall piers were modeled with single elements, so no averaging was required. Force response was always reported as the total for a support (e.g., the summation of forces for all six bearings).
2. For each time-history run, the peak force and displacement responses were extracted and then condensed into representative values for the Pa and CG ground motion suites by averaging over all ground motions in a suite. These tabulations are available in Appendix A. As discussed in Chapter 2, a full suite consisted of ten ground motions, but in some instances only eight or nine runs were successfully completed because of computational difficulties associated with achieving convergence during nonlinear time-history analysis of sliding systems with small tangent stiffness. According to the AASHTO Guide Specification for LRFD Seismic Bridge Design (AASHTO 2009), use of the mean response is acceptable when averaging over at least seven time histories.
3. Finally, results were grouped by bridge parameter to obtain characteristic system response values and to assess the influence of bridge parameter on system response. Such tabulations are included in this chapter for a scale factor (SF) of 1.0; while these tables cannot provide detailed information about trends or variability within the dataset, this approach was adequate to identify the one or two bridge parameters that most significantly influenced the system response.

4.1.1 Superstructure Displacements

Superstructure displacements were reported as the displacement of bearing top plate relative to ground and can be thought of as total system displacement. In the longitudinal direction, superstructure displacement was roughly the same at all supports. In the transverse direction, there was some variability along the spans resulting from rigid-body rotation of the superstructure about the vertical axis—a mild instance of the seismic response commonly seen in skewed bridge decks. Table 4.1 documents superstructure displacement at Abutment 1, which is considered sufficiently representative of global behavior to illustrate trends in system response.

Superstructure displacements, presented in Figure 4.1, were most influenced by pier height. Bridge systems with tall piers experienced larger displacements. This trend was noted particularly for the Pa ground motions applied in the longitudinal direction, possibly because the longitudinal fundamental period of most bridges was longer than the transverse

period, as discussed in Chapter 3. Thus, bridges were most affected by the long-period excitation of the Pa ground motions applied in the longitudinal direction.

Table 4.9. Average Superstructure Displacements (SF = 1.0)

Longitudinal Superstructure Displ. (in)

Pa Analyses			CG Analyses		
Ss	**Sl**	**Cs**	**Ss**	**Sl**	**Cs**
5.5	8.5	7.6	3.9	4.9	4.9
C	**W**	**Δ / C**	**C**	**W**	**Δ / C**
7.3	7.1	-4%	4.7	4.4	-6%
15'	**40'**	**Δ / 15**	**15'**	**40'**	**Δ / 15**
5.5	8.9	61%	3.8	5.3	39%
T1	**T2**	**Δ / T1**	**T1**	**T2**	**Δ / T1**
7.2	7.2	0%	4.8	4.4	-10%
F	**S**	**Δ / F**	**F**	**S**	**Δ / F**
6.8	7.6	11%	4.4	4.8	9%

Transverse Superstructure Displ. (in)

Pa Analyses			CG Analyses		
Ss	**Sl**	**Cs**	**Ss**	**Sl**	**Cs**
10.4	12.4	10.9	6.0	6.4	6.6
C	**W**	**Δ / C**	**C**	**W**	**Δ / C**
11.2	11.3	1%	6.2	6.4	3%
15'	**40'**	**Δ / 15**	**15'**	**40'**	**Δ / 15**
9.8	12.7	29%	6.0	6.6	10%
T1	**T2**	**Δ / T1**	**T1**	**T2**	**Δ / T1**
10.2	12.3	22%	6.2	6.5	5%
F	**S**	**Δ / F**	**F**	**S**	**Δ / F**
9.8	12.7	30%	6.5	6.2	-4%

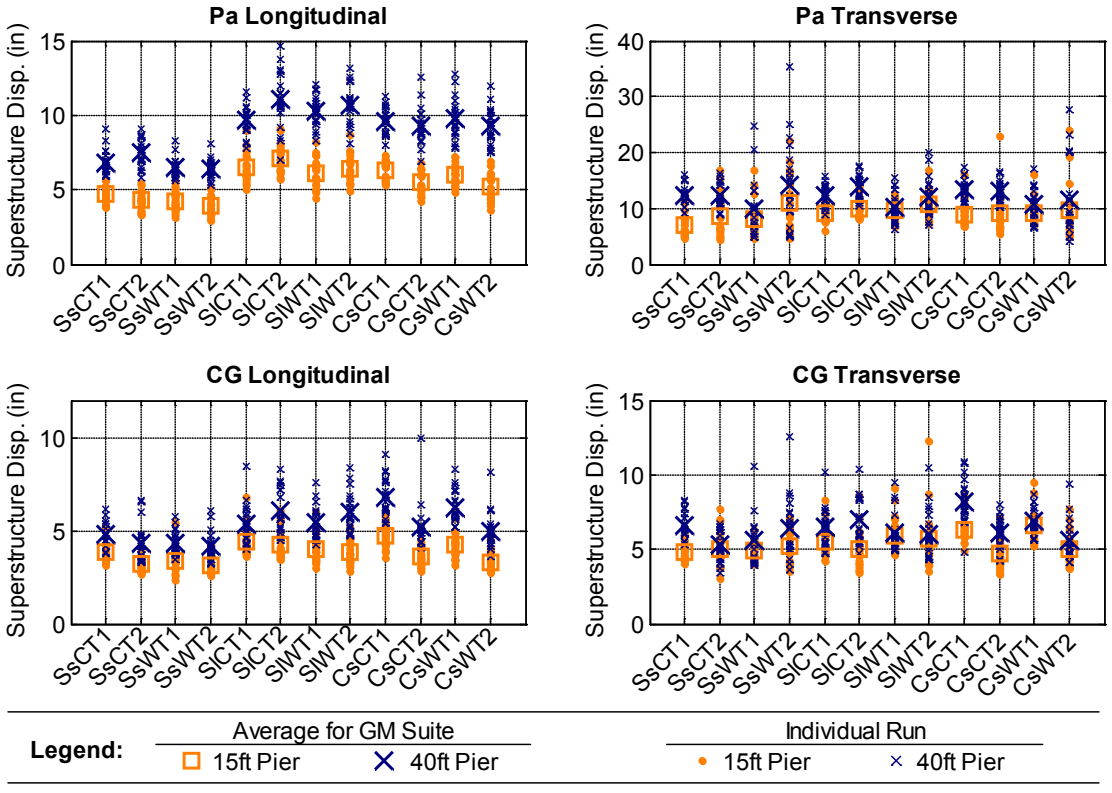

Figure 4.30. Superstructure displacements grouped by pier height (SF = 1.0).

4.1.2 Bearing Displacements

As discussed in Chapter 2, elastomeric bearings (either Type I or II) were modeled at the abutments and Pier 1, and low-profile fixed bearings were modeled at Pier 2. For elastomeric bearings, relative bearing displacement was calculated by subtracting elastic deformation from total deformation to obtain a sliding displacement at either the elastomer on concrete cap interface (Type I) or top plate on polytetrafluoroethylene (PTFE) pad interface (Type II). This calculation was not performed for the fixed bearings because there was relatively little elastic deformation. Instead, the total bearing displacement was directly reported.

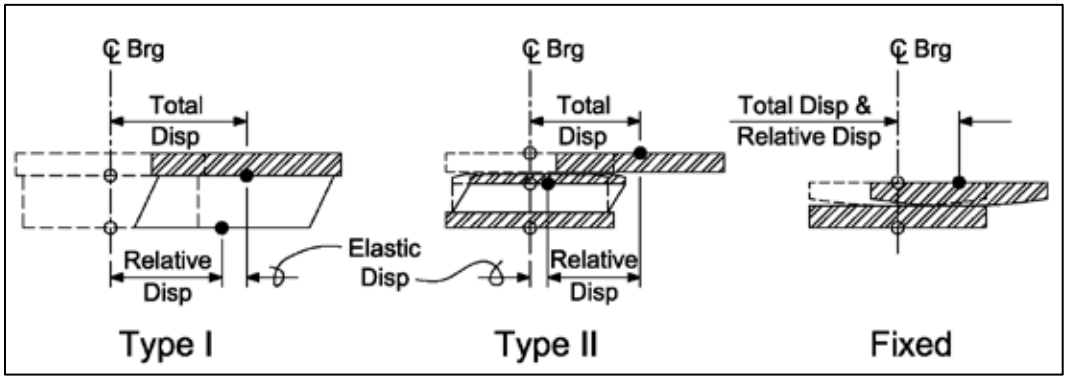

Figure 4.31. Measures of relative bearing displacement.

4.1.2.1 Abutment Bearings (Elastomeric Type I and Type II)

Table 4.2 shows Abutment 1 bearing displacements, and the Abutment 2 response was similar. In the longitudinal direction, abutment bearing displacement was primarily influenced by pier height (Figure 4.3), while in the transverse direction, bearing type was the most influential bridge characteristic (Figure 4.4). Abutment bearings in tall pier systems experienced larger displacements than those in short pier systems. Type II bearings experienced larger displacements than Type I.

Table 4.10. Average Abutment 1 Bearing Relative Displacements (SF = 1.0)

Longitudinal Bearing Displacement (in)

Pa Analyses			CG Analyses		
Ss	**Sl**	**Cs**	**Ss**	**Sl**	**Cs**
4.3	6.8	5.3	2.9	3.4	2.8
C	**W**	**Δ / C**	**C**	**W**	**Δ / C**
5.6	5.3	-4%	3.2	2.9	-10%
15'	**40'**	**Δ / 15**	**15'**	**40'**	**Δ / 15**
3.8	7.1	87%	2.3	3.8	63%
T1	**T2**	**Δ / T1**	**T1**	**T2**	**Δ / T1**
4.8	6.2	29%	2.6	3.5	32%
F	**S**	**Δ / F**	**F**	**S**	**Δ / F**
5.5	5.4	-3%	3.4	2.7	-18%

Transverse Bearing Displacement (in)

Pa Analyses			CG Analyses		
Ss	**Sl**	**Cs**	**Ss**	**Sl**	**Cs**
8.7	9.1	7.8	3.8	4.1	3.2
C	**W**	**Δ / C**	**C**	**W**	**Δ / C**
8.7	8.4	-4%	3.8	3.6	-3%
15'	**40'**	**Δ / 15**	**15'**	**40'**	**Δ / 15**
7.1	10.0	41%	3.2	4.2	29%
T1	**T2**	**Δ / T1**	**T1**	**T2**	**Δ / T1**
6.7	10.3	53%	2.8	4.6	63%
F	**S**	**Δ / F**	**F**	**S**	**Δ / F**
7.5	9.5	26%	3.7	3.7	-1%

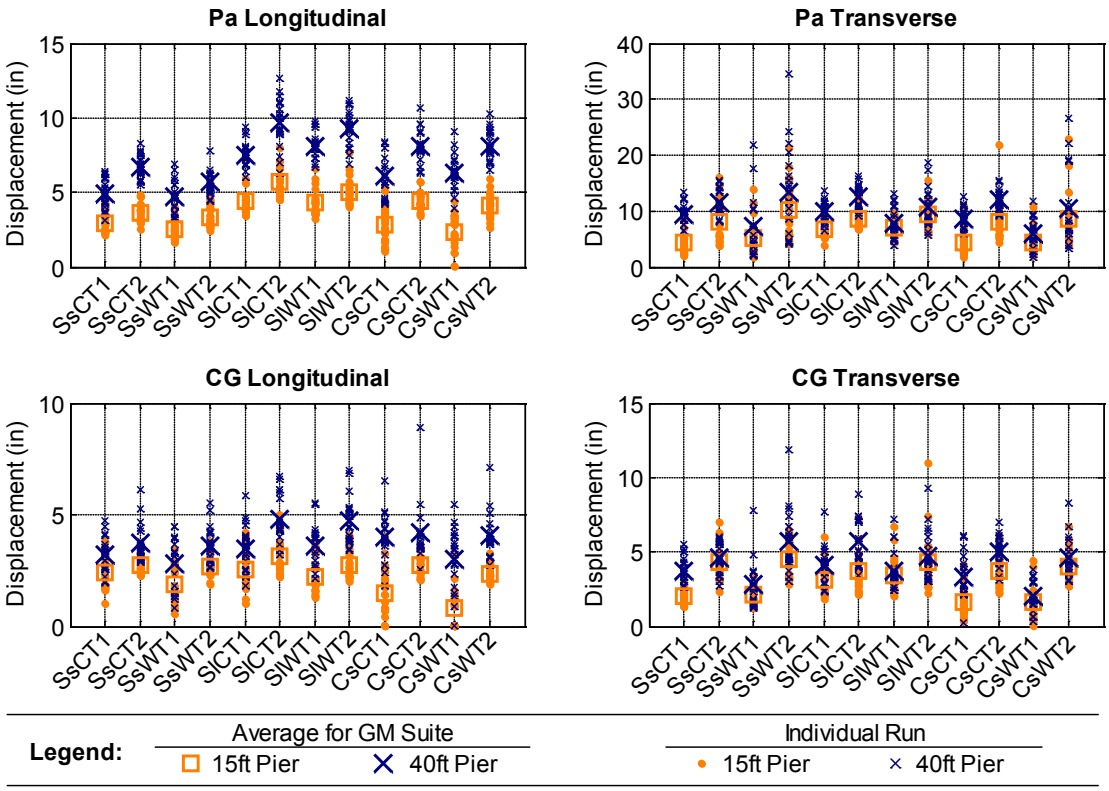

Figure 4.32. Abutment 1 bearing displacements grouped by pier height (SF= 1.0).

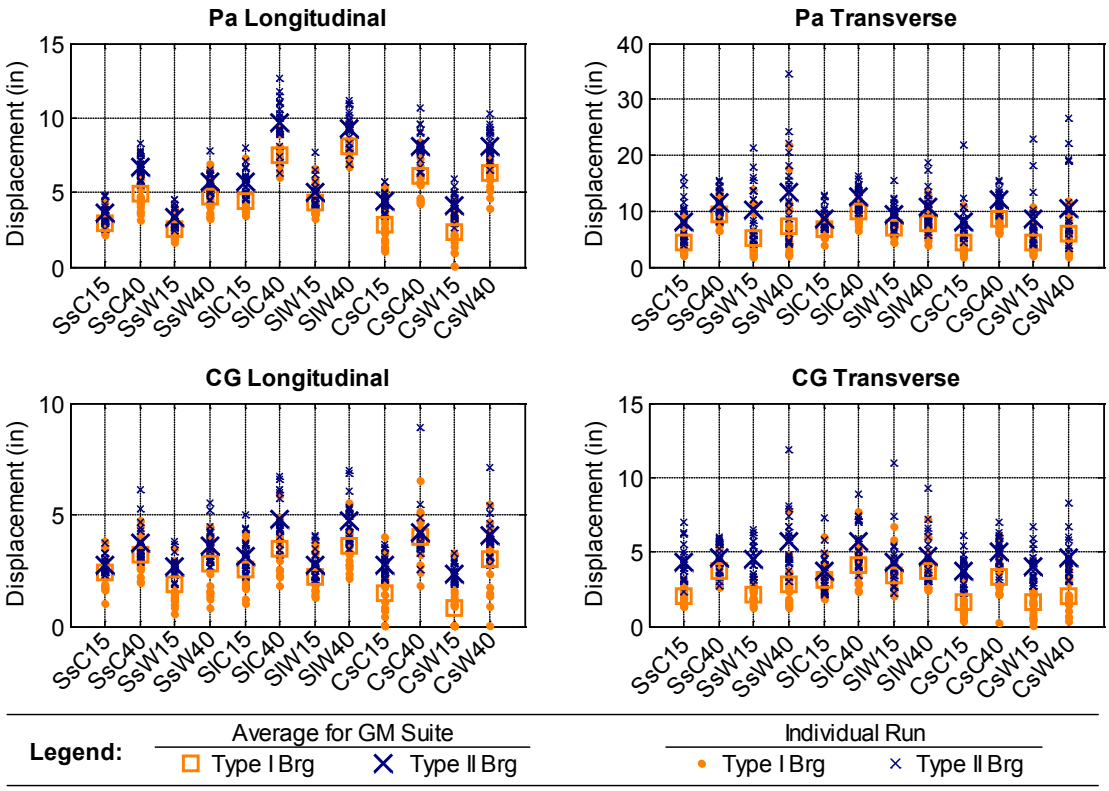

Figure 4.33. Abutment 1 bearing displacements grouped by bearing type (SF = 1.0).

4.1.2.2 Pier 1 Bearings (Elastomeric Type I and Type II

Table 4.3 shows results for Pier 1 bearing displacements; the data suggest that these displacements were most influenced by bearing type. Figure 4.5 shows that at SF = 1.0, Type II bearings at Pier 1 always fused, while Type I bearings often did not fuse because of their comparatively high coefficient of static friction (0.6 vs. 0.16). Thus, Type II bearings experienced significantly larger displacements on average than Type I bearings.

Table 4.11. Average Relative Pier 1 Bearing Displacements (SF = 1.0)

Longitudinal Bearing Displacement (in)

Pa Analyses			CG Analyses		
Ss	Sl	Cs	Ss	Sl	Cs
2.2	1.4	1.6	1.0	0.7	0.9
C	W	Δ / C	C	W	Δ / C
1.5	1.9	26%	0.8	0.9	12%
15'	40'	Δ / 15	15'	40'	Δ / 15
1.9	1.6	-15%	1.0	0.7	-25%
T1	T2	Δ / T1	T1	T2	Δ / T1
0.3	3.1	832%	0.1	1.6	1539%
F	S	Δ / F	F	S	Δ / F
1.5	1.9	31%	0.8	1.0	23%

Transverse Bearing Displacement (in)

Pa Analyses			CG Analyses		
Ss	Sl	Cs	Ss	Sl	Cs
4.1	2.1	3.2	1.0	0.4	0.8
C	W	Δ / C	C	W	Δ / C
1.5	4.7	214%	0.4	1.1	165%
15'	40'	Δ / 15	15'	40'	Δ / 15
3.2	3.1	-4%	0.7	0.8	3%
T1	T2	Δ / T1	T1	T2	Δ / T1
1.3	4.9	270%	0.2	1.4	802%
F	S	Δ / F	F	S	Δ / F
2.7	3.5	30%	0.8	0.7	-21%

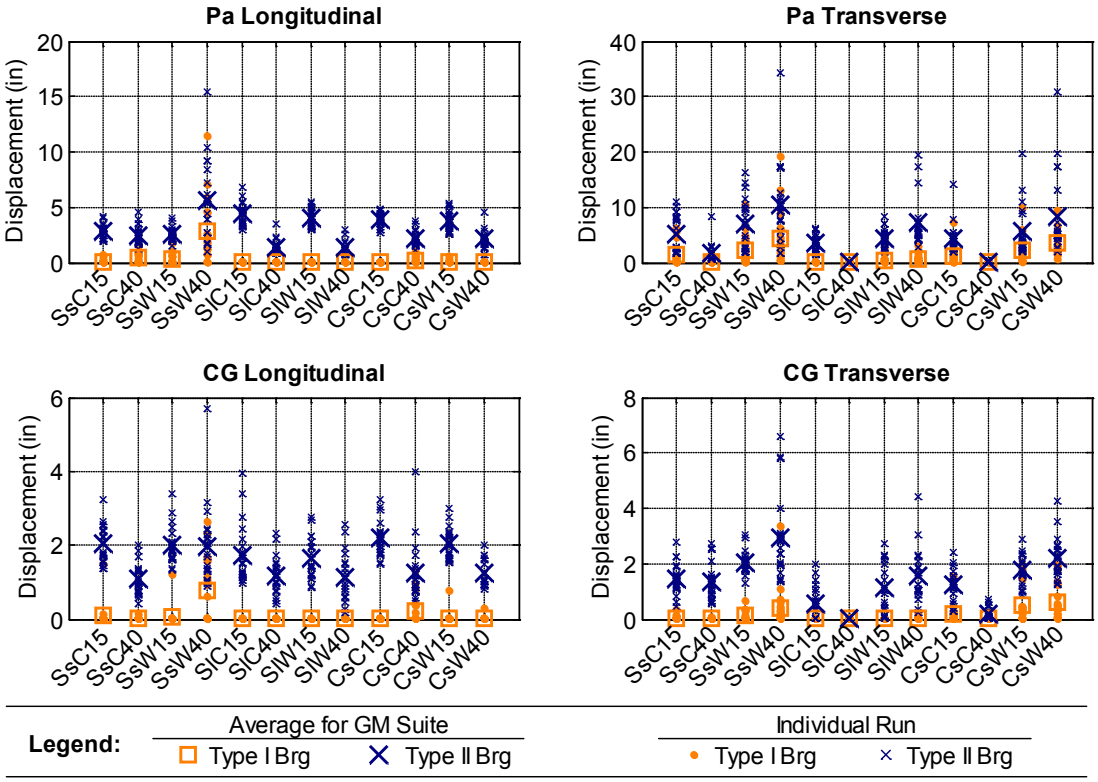

Figure 4.34. Pier 1 bearing displacements grouped by bearing type (SF = 1.0).

4.1.2.3 Pier 2 Bearing Displacement (Low-Profile Fixed)

Table 4.4 shows results for Pier 2 bearing displacements. Displacements were most influenced by substructure type (Figure 4.6). Fixed bearings installed on wall piers experienced larger deformations on average than those installed on column piers. In both the longitudinal and transverse directions, the wall piers had greater strength and stiffness than the column piers, which led to earlier fixed bearing fusing, and thus larger fixed bearing displacements. In the longitudinal direction, this meant the difference between the fixed

bearings remaining elastic (column piers) and just barely fusing (wall piers). In the transverse direction, the earlier fusing meant fixed bearings at wall piers were more likely to reach bearing unseating and also correlated with significantly increased variability in peak displacement.

Furthermore, in the longitudinal direction, Figure 4.6 suggests some sensitivity to superstructure type. In comparison with Ss superstructures, the Sl and Cs superstructures feature increased frictional resistance as a result of higher self-weights; they use larger anchor bolts, thus requiring larger forces and displacements to achieve fusing. Figure 4.6 reflects a case where the Ss bridge fixed bearings happened to be on the cusp of fusing. As discussed above, the wall pier variants then fused earlier than the column pier variants, resulting in a noticeable difference between fixed bearing displacements at column versus wall piers. However, for Sl and Cs bridges, the combined resistance of the frictional force and fixed bearing anchor bolts was high enough that elastic deformation rather than full fusing occurred. This highlights the importance of considering frictional force when selecting fuse capacities.

Table 4.12. Average Relative Pier 2 Fixed Bearing Displacements (SF = 1.0)

Longitudinal Bearing Displacement (in)

Pa Analyses

Ss	Sl	Cs
1.8	0.2	0.4

C	W	Δ / C
0.3	1.3	359%

15'	40'	Δ / 15
0.6	1.0	55%

T1	T2	Δ / T1
0.8	0.8	4%

F	S	Δ / F
0.8	0.8	-4%

CG Analyses

Ss	Sl	Cs
1.1	0.1	0.4

C	W	Δ / C
0.2	0.9	250%

15'	40'	Δ / 15
0.6	0.5	-15%

T1	T2	Δ / T1
0.6	0.5	-5%

F	S	Δ / F
0.5	0.6	6%

Transverse Bearing Displacement (in)

Pa Analyses

Ss	Sl	Cs
5.2	6.0	5.7

C	W	Δ / C
3.1	8.1	160%

15'	40'	Δ / 15
6.6	4.7	-28%

T1	T2	Δ / T1
4.8	6.5	36%

F	S	Δ / F
4.5	6.8	50%

CG Analyses

Ss	Sl	Cs
2.8	1.8	2.3

C	W	Δ / C
1.4	3.2	130%

15'	40'	Δ / 15
2.9	1.7	-40%

T1	T2	Δ / T1
1.9	2.7	42%

F	S	Δ / F
2.9	1.7	-40%

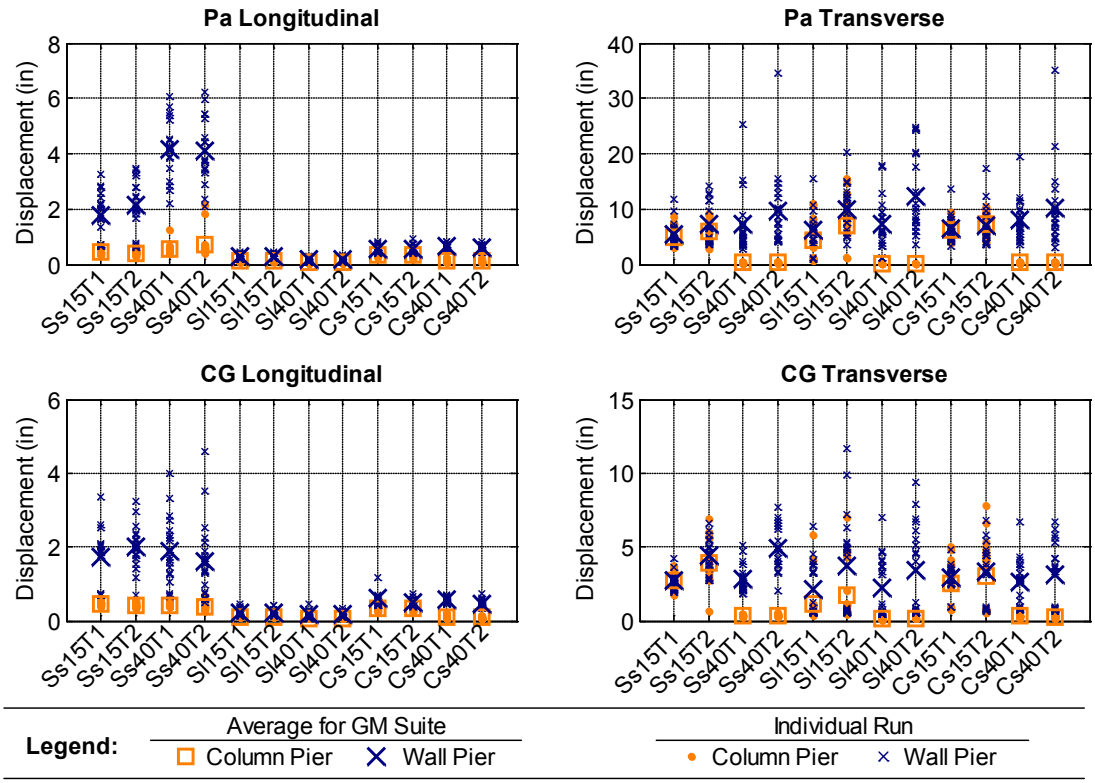

Figure 4.35. Pier 2 bearing displacements grouped by pier type (SF = 1.0).

4.1.3 Pier Displacements

Relative pier displacement (Figure 4.7) is reported as the top of pier displacement relative to bottom of pier displacement less any translation caused by rotation of the foundation element or the pier cap element.

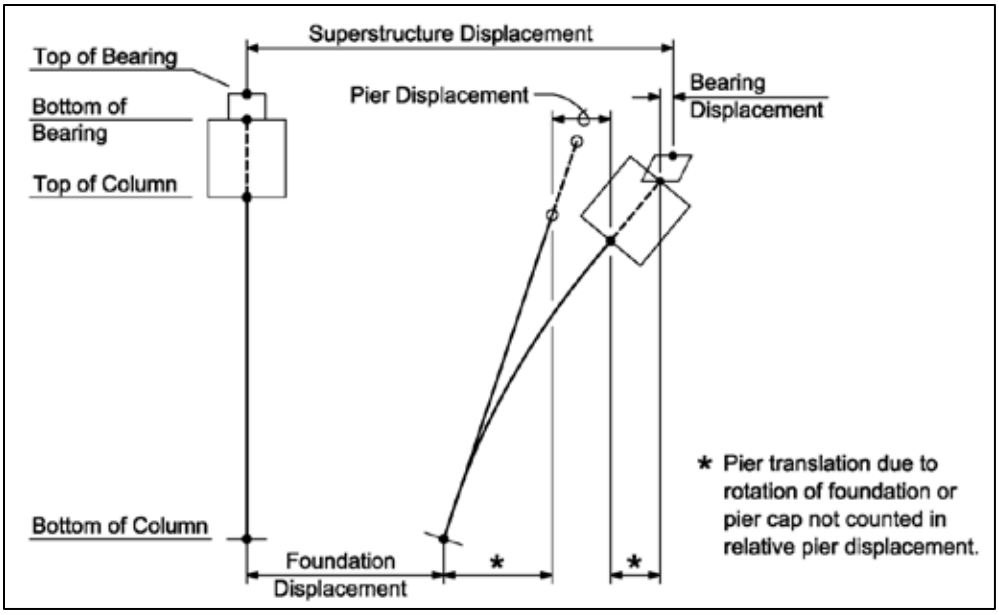

Figure 4.36. Relative pier displacement.

Table 4.5 shows relative pier displacements at Pier 1 (i.e., the elastomeric bearing pier). Displacements were most influenced by pier height, with tall piers displacing more than short piers (Figure 4.8). In the transverse direction, the substructure type was also significant in determining pier response because wall piers were essentially rigid and column piers experienced more deformation (Figure 4.9).

Table 4.13. Average Relative Pier 1 Displacements (SF = 1.0)

Longitudinal Pier Displacement (in)						Transverse Pier Displacement (in)					
Pa Analyses			CG Analyses			Pa Analyses			CG Analyses		
Ss	Sl	Cs	Ss	Sl	Cs	Ss	Sl	Cs	Ss	Sl	Cs
4.4	5.3	5.2	2.7	2.9	3.1	2.5	3.0	2.8	0.9	1.3	1.2
C	W	Δ / C	C	W	Δ / C	C	W	Δ / C	C	W	Δ / C
4.8	5.2	9%	3.0	2.8	-7%	5.5	0.0	-99%	2.2	0.0	-99%
15'	40'	Δ / 15	15'	40'	Δ / 15	15'	40'	Δ / 15	15'	40'	Δ / 15
1.0	9.0	772%	0.8	5.1	569%	0.4	5.2	1361%	0.2	2.1	971%
T1	T2	Δ / T1	T1	T2	Δ / T1	T1	T2	Δ / T1	T1	T2	Δ / T1
5.3	4.7	-12%	3.2	2.6	-19%	2.8	2.7	-2%	1.2	1.0	-15%
F	S	Δ / F	F	S	Δ / F	F	S	Δ / F	F	S	Δ / F
4.8	5.2	8%	2.8	3.0	7%	2.9	2.6	-9%	1.2	1.0	-20%

Table 4.6 shows relative pier displacements at Pier 2 (i.e., the fixed bearing pier). The displacement magnitudes differ somewhat from Pier 1, but the general response trends appear similar. Pier 2 displacements were most influenced by pier height, with tall piers displacing more than short piers (Figure 4.10). In the transverse direction, the substructure

type was also significant in determining pier response because wall piers were essentially rigid and column piers experienced more deformation (Figure 4.11).

Table 4.14. Average Relative Pier 2 Displacements (SF = 1.0)

Longitudinal Pier Displacement (in)

Pa Analyses			CG Analyses		
Ss	**Sl**	**Cs**	**Ss**	**Sl**	**Cs**
4.8	6.7	6.0	3.0	3.7	3.7
C	**W**	**Δ / C**	**C**	**W**	**Δ / C**
5.7	6.0	4%	3.5	3.5	0%
15'	**40'**	**Δ / 15**	**15'**	**40'**	**Δ / 15**
3.6	8.1	126%	2.3	4.6	98%
T1	**T2**	**Δ / T1**	**T1**	**T2**	**Δ / T1**
5.8	5.8	0%	3.7	3.3	-11%
F	**S**	**Δ / F**	**F**	**S**	**Δ / F**
5.9	5.8	-2%	3.6	3.4	-6%

Transverse Pier Displacement (in)

Pa Analyses			CG Analyses		
Ss	**Sl**	**Cs**	**Ss**	**Sl**	**Cs**
2.8	3.3	2.9	1.1	1.5	1.3
C	**W**	**Δ / C**	**C**	**W**	**Δ / C**
6.0	0.0	-99%	2.6	0.0	-99%
15'	**40'**	**Δ / 15**	**15'**	**40'**	**Δ / 15**
0.4	5.6	1261%	0.3	2.4	779%
T1	**T2**	**Δ / T1**	**T1**	**T2**	**Δ / T1**
2.9	3.1	5%	1.4	1.3	-5%
F	**S**	**Δ / F**	**F**	**S**	**Δ / F**
3.1	2.9	-7%	1.5	1.2	-22%

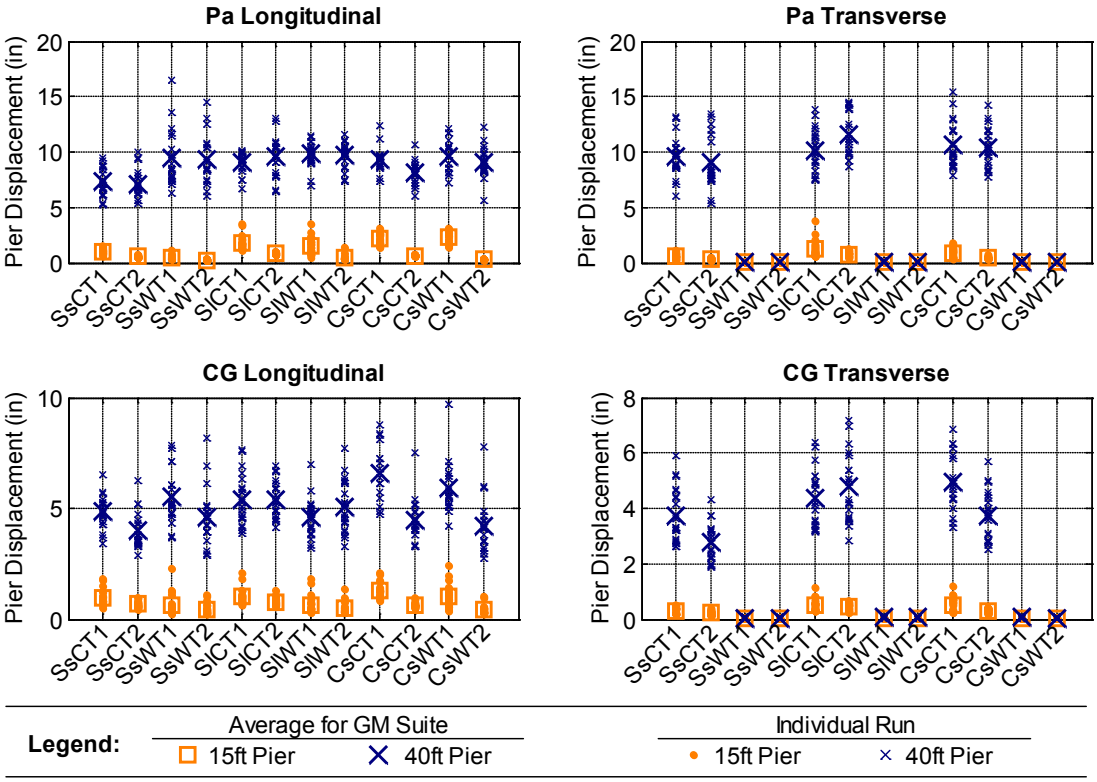

Figure 4.37. Pier 1 displacements grouped by pier height (SF = 1.0).

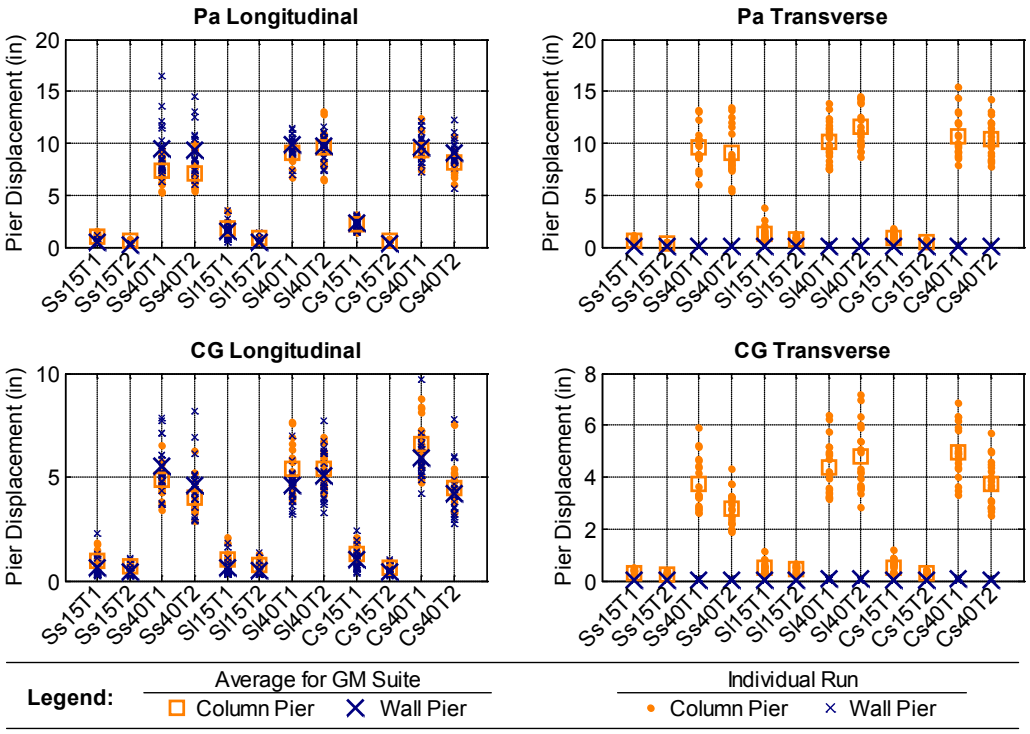

Figure 4.38. Pier 1 displacements grouped by pier type (SF = 1.0).

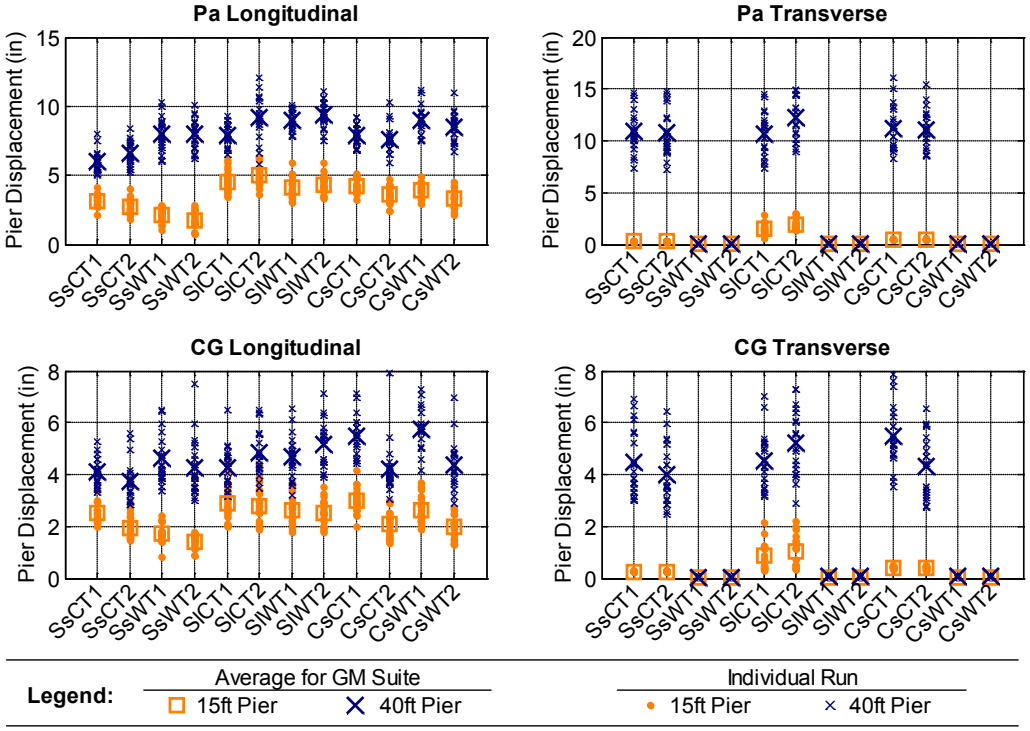

Figure 4.39. Pier 2 displacements grouped by pier height (SF = 1.0).

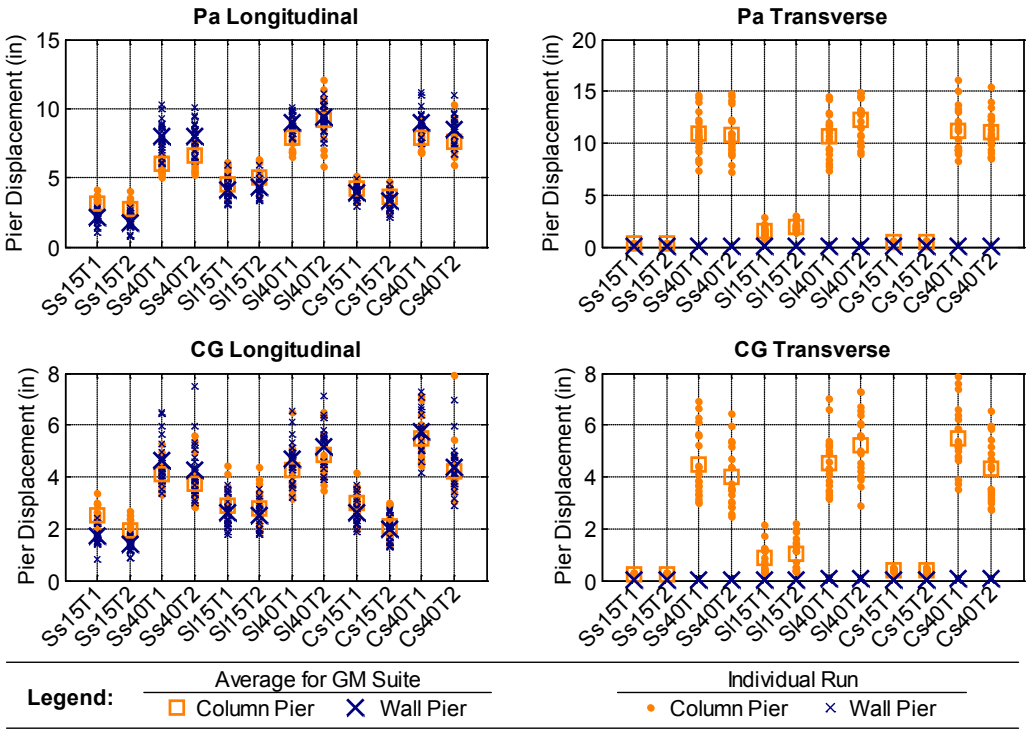

Figure 4.40. Pier 2 displacements grouped by pier type (SF = 1.0).

4.1.4 Base Shear

Base shears were recorded as reaction forces at each of the four foundation nodes. For reporting purposes, normalized base shear was obtained by dividing the support base shear by the dead load reaction at the support, as summarized in Table 4.7. At the piers, the dead load was inclusive of substructure self-weight. The unitless normalized base shear facilitates comparison between bridges with different self-weights and is helpful for conceptual comparison with bearing fuse design criteria.

Table 4.15. Unfactored Dead Load Reaction at Support (kips)

	Column Pier				Wall Pier			
	Short (15 ft)		Tall (40 ft)		Short (15 ft)		Tall (40 ft)	
	Abut	Pier	Abut	Pier	Abut	Pier	Abut	Pier
Steel short (Ss) superstructure	127	477	128	583	127	650	127	1044
Steel long (Sl) superstructure	184	909	184	1015	183	1082	183	1475
Concrete short (Cs) superstructure	198	671	199	776	198	844	198	1237

Table 4.8 shows normalized base shears at Abutment 1, and a similar response was observed at Abutment 2. In the longitudinal direction, normalized abutment base shears were most influenced by pier height, with tall pier systems showing higher normalized base shears (Figure 4.12). These longitudinal normalized base shears range roughly from 2 to 5 because of the interaction with the backwall and backfill, whereas the transverse normalized base shears are around 1. In the transverse direction, bearing type was the most significant

bridge parameter, and Type II bearings were associated with lower normalized base shears (Figure 4.13). Normalized base shears were higher for Ss superstructure bridges compared with Sl or Cs superstructure bridges, indicating there may also be a modest sensitivity to superstructure type.

Table 4.16. Average Abutment 1 Normalized Base Shears (SF = 1.0)

Longitudinal Base Shear (normalized)

Pa Analyses

Ss	Sl	Cs
5.24	2.77	2.91

C	W	Δ / C
3.68	3.60	-2%

15'	40'	Δ / 15
3.33	3.95	19%

T1	T2	Δ / T1
3.69	3.59	-3%

F	S	Δ / F
3.86	3.42	-11%

CG Analyses

Ss	Sl	Cs
4.50	2.37	2.42

C	W	Δ / C
3.11	3.08	-1%

15'	40'	Δ / 15
3.03	3.16	4%

T1	T2	Δ / T1
3.21	2.98	-7%

F	S	Δ / F
3.18	3.01	-6%

Transverse Base Shear (normalized)

Pa Analyses

Ss	Sl	Cs
0.89	0.96	0.81

C	W	Δ / C
0.89	0.89	0%

15'	40'	Δ / 15
0.88	0.89	1%

T1	T2	Δ / T1
0.95	0.83	-13%

F	S	Δ / F
0.88	0.89	1%

CG Analyses

Ss	Sl	Cs
0.88	0.96	0.80

C	W	Δ / C
0.88	0.88	0%

15'	40'	Δ / 15
0.88	0.88	0%

T1	T2	Δ / T1
0.94	0.83	-12%

F	S	Δ / F
0.88	0.88	0%

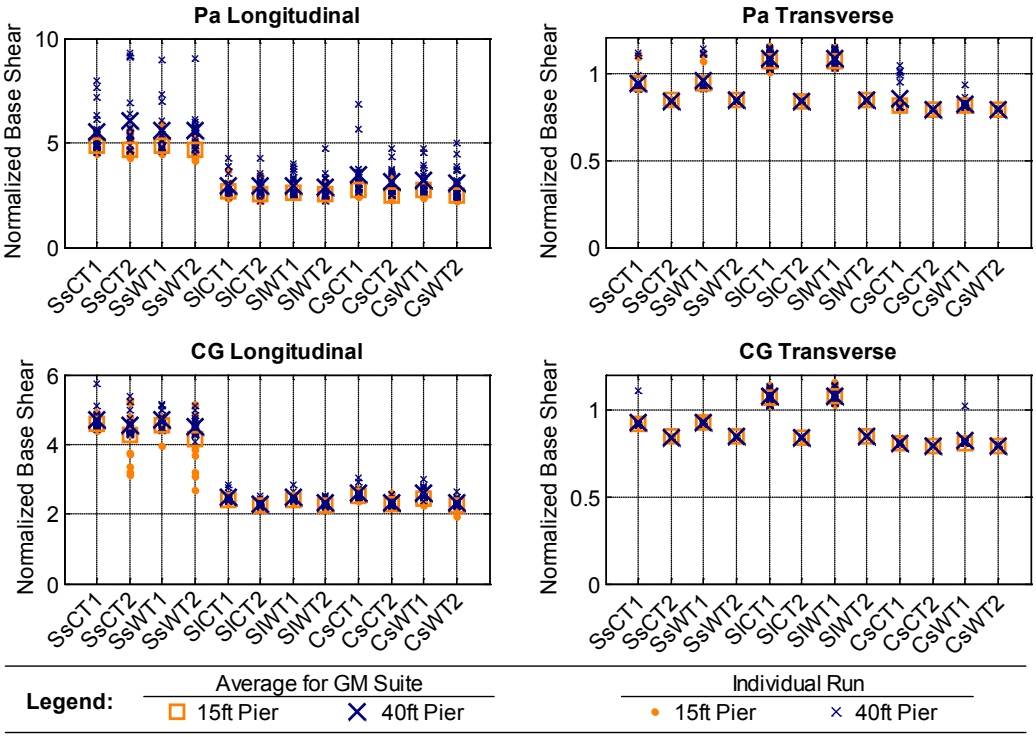

Figure 4.41. Abutment 1 base shears grouped by pier height (SF = 1.0).

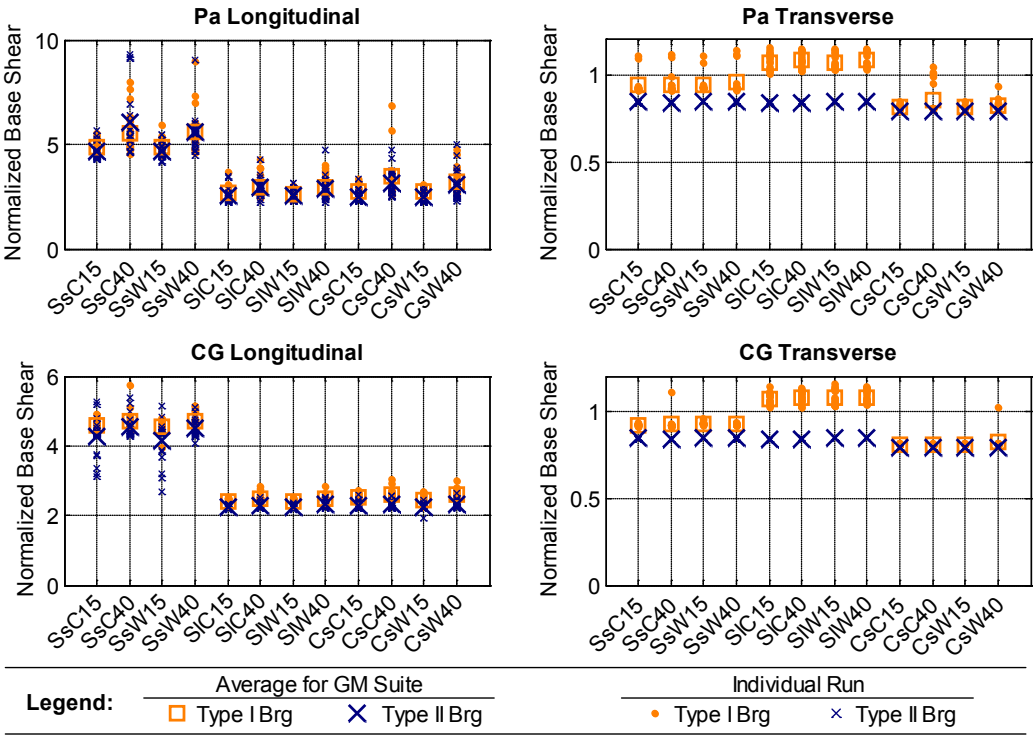

Figure 4.42. Abutment 1 base shears grouped by bearing type (SF = 1.0).

Table 4.9 shows normalized base shears at Pier 1, and a similar response was observed at Pier 2. Normalized pier base shears were most influenced by pier height, with tall pier systems showing lower normalized base shears (Figure 4.14). For tall pier bridges in the transverse direction, pier type was also significant, with wall pier systems showing higher normalized base shears than column pier systems (Figure 4.15).

Table 4.17. Average Pier 1 Normalized Base Shears (SF = 1.0)

Longitudinal Base Shear (normalized)

Pa Analyses

Ss	Sl	Cs
0.34	0.24	0.30

C	W	Δ / C
0.27	0.31	14%

15'	40'	Δ / 15
0.36	0.22	-38%

T1	T2	Δ / T1
0.31	0.27	-13%

F	S	Δ / F
0.26	0.32	21%

CG Analyses

Ss	Sl	Cs
0.39	0.25	0.32

C	W	Δ / C
0.28	0.36	29%

15'	40'	Δ / 15
0.38	0.26	-31%

T1	T2	Δ / T1
0.34	0.31	-7%

F	S	Δ / F
0.30	0.35	15%

Transverse Base Shear (normalized)

Pa Analyses

Ss	Sl	Cs
0.60	0.55	0.61

C	W	Δ / C
0.54	0.63	17%

15'	40'	Δ / 15
0.70	0.47	-33%

T1	T2	Δ / T1
0.63	0.54	-15%

F	S	Δ / F
0.60	0.57	-4%

CG Analyses

Ss	Sl	Cs
0.52	0.42	0.50

C	W	Δ / C
0.44	0.52	18%

15'	40'	Δ / 15
0.55	0.41	-26%

T1	T2	Δ / T1
0.51	0.45	-13%

F	S	Δ / F
0.56	0.40	-30%

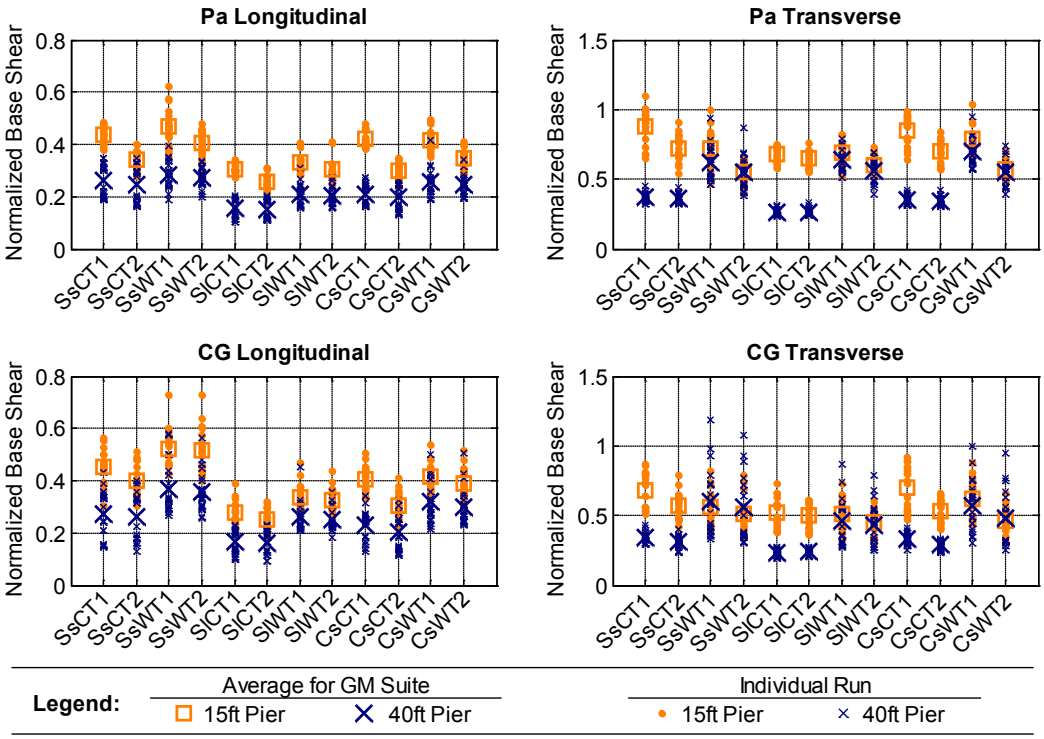

Figure 4.43. Pier 1 base shears grouped by pier height (SF = 1.0).

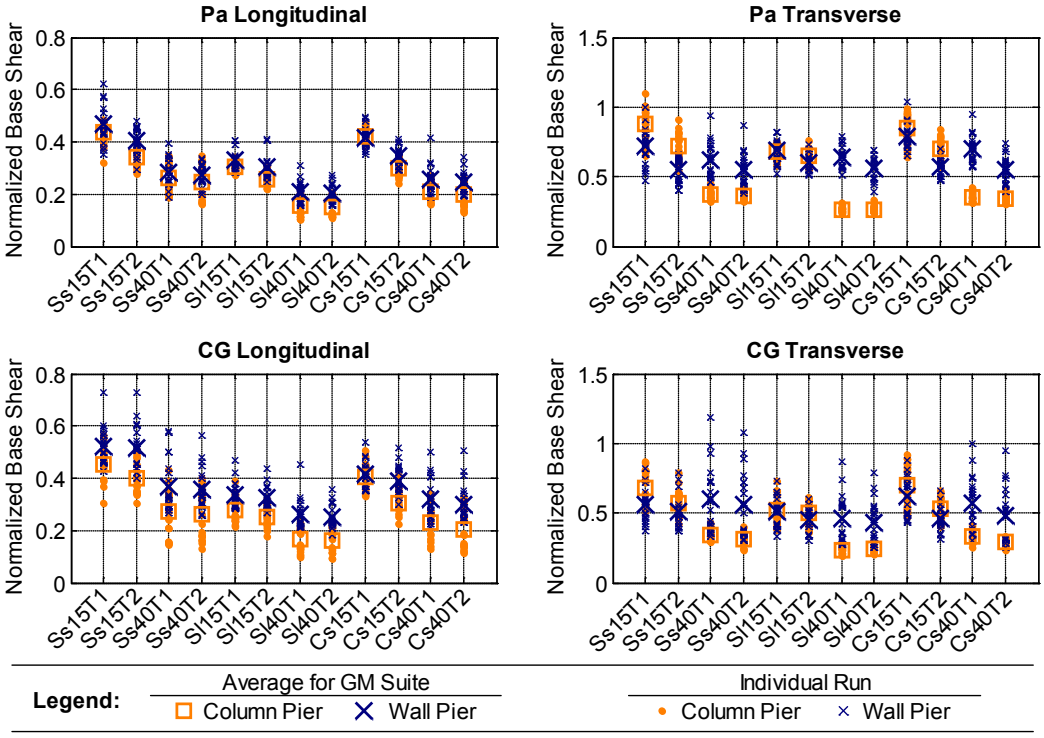

Figure 4.44. Pier 1 base shears grouped by pier type (SF = 1.0).

4.2 SEQUENCE OF DAMAGE

A list of limit states organized by scale factor of first occurrence constitutes the sequence of damage for a bridge. Such tabulations provide a valuable qualitative overview of performance, indicating at a glance what combination of bearing fusing, pier yielding, and bearing unseating occurred. The limit state abbreviations from Table 3.1 are used for shorthand notation, scale factors are separated by vertical lines, and the location of SF = 1.0 is indicated with a (1) to aid in quickly identifying system state at the design earthquake. Limit states that did not occur at any of the six scale factors are not listed. Taking the SsC15T2S bridge from Chapter 3 as an example case, the longitudinal sequence of damage for Pa ground motions is tabulated as | Bw EP | P2 | (1) | UA | | |. This denotes backwall yielding and sliding of Pier 1 bearings at SF = 0.5 followed by yielding of Pier 2 at SF = 0.75 and unseating of abutment bearings at SF = 1.25. Finally, this sequence of damage indicates that no further limit states were encountered at SF = 1.5 or SF = 1.75. Some of the more global sequence of damage phenomena are shown in Figure 4.16.

4.2.1 Longitudinal

Table 4.10 displays the longitudinal sequence of damage for Pa ground motions. The tabulation for CG ground motions is available in Appendix A. In the longitudinal direction, the bridges generally did not attain the ideal quasi-isolated sequence of damage because of substructure yielding prior to bearing fusing. This was particularly evident at the fixed bearing pier (Pier 2), where the pier generally yielded early in the response history and the fixed bearing generally did not fuse. Unseating of the abutment bearings was common for tall bridges with Type II bearings, whereas the backwall, which was engaged in every analysis run, prevented Type I bearings from experiencing displacements large enough to cause bearing unseating. Note that sliding of the abutment bearings always occurred (nearly always at SF = 0.5) and was thus omitted from the table for brevity.

4.2.2 Transverse

Table 4.11 displays the transverse sequence of damage for Pa ground motions (the tabulation for CG ground motions is available in Appendix A). In the transverse direction, many bridges achieved quasi-isolation, with all the bearings fusing and minimal damage to substructure components. Tall bridges with column piers continued to exhibit substructure yielding rather than fusing of the bearings, and transverse unseating was again a problem for tall bridges with Type II bearings.

Table 4.18. Longitudinal Sequence of Damage for Pa Ground Motions

(a) Short Steel (Ss) Superstructure Bridge Variants

			Short Pier (15 ft)	Tall Pier (40 ft)
Column Pier	Type I Bearings	Fixed base	| Bw P2 | | (1) | | P1 | |	| Bw | P1 | (1) P2 | EP | Fb | |
		Soft soil	| Bw P2 | | (1) | | EP P1 | |	| Bw | | (1) P1 P2 | | EP Fb | |
	Type II Bearings	Fixed base	| Bw EP P2 | | (1) | UA | | Fb |	| Bw | EP UA | (1) P1 P2 | Fb | | |
		Soft soil	| Bw EP | P2 | (1) | UA | | |	| Bw | EP UA | (1) P1 P2 | | Fb | |
Wall Pier	Type I Bearings	Fixed base	| Bw Fb P2 | (1) EP | P1 | | |	| Bw Fb P1 P2 | (1) EP | | | |
		Soft soil	| Bw P2 | Fb | (1) P1 | EP | | |	| Bw P1 P2 Fb | EP | (1) | | | |
	Type II Bearings	Fixed base	| Bw EP Fb P2 | | (1) | UA | | P1 |	| Bw EP P1 P2 | Fb UA | (1) | | UP | |
		Soft soil	| Bw EP P2 | Fb | (1) | UA | P1 | |	| Bw EP Fb P1 P2 | UA | (1) | UP | | |

(b) Long Steel (Sl) Superstructure Bridge Variants

			Short Pier (15 ft)	Tall Pier (40 ft)
Column Pier	Type I Bearings	Fixed base	| Bw P2 | | (1) P1 | | | |	| Bw | | (1) | P1 P2 | | |
		Soft soil	| Bw P2 | (1) P1 | | | |	| Bw | | (1) P1 P2 | | | |
	Type II Bearings	Fixed base	| Bw EP P2 | | (1) | UA | | |	| Bw | EP UA | (1) P1 P2 | | | |
		Soft soil	| Bw EP P2 | (1) UA | | | UP |	| Bw EP | UA | (1) P1 P2 | | | |
Wall Pier	Type I Bearings	Fixed base	| Bw P2 | P1 | (1) | | | |	| Bw P1 P2 | | (1) | | | |
		Soft soil	| Bw P2 | P1 | (1) | | | |	| Bw P1 P2 | | (1) | | | |
	Type II Bearings	Fixed base	| Bw EP P2 | (1) P1 | UA | | |	| Bw EP P1 P2 | UA | (1) | | | |
		Soft soil	| Bw EP P2 | (1) P1 | UA | | UP |	| Bw P1 P2 | EP UA | (1) | | | |

(c) Precast Concrete (Cs) Superstructure Bridge Variants

			Short Pier (15 ft)	Tall Pier (40 ft)
Column Pier	Type I Bearings	Fixed base	| Bw P2 | | (1) P1 | | | |	| Bw | P1 | (1) P2 | | | |
		Soft soil	| Bw P2 | | (1) P1 | | | |	| Bw | P1 | (1) P2 | | | |
	Type II Bearings	Fixed base	| Bw EP P2 | | (1) | UA | | |	| Bw | EP | (1) P1 P2 UA | | | |
		Soft soil	| Bw EP | P2 | (1) | UA | | UP |	| Bw | EP | (1) P1 P2 UA | | | |
Wall Pier	Type I Bearings	Fixed base	| Bw P2 | P1 | (1) | EP | | Fb |	| Bw P1 P2 | | (1) | | | Fb |
		Soft soil	| Bw P2 | P1 | (1) | | EP Fb | |	| Bw P1 P2 | | (1) | EP | Fb | |
	Type II Bearings	Fixed base	| Bw EP P2 | | (1) | | P1 UA | Fb |	| Bw EP P1 P2 | | (1) UA | | Fb | |
		Soft soil	| Bw EP P2 | | (1) | UA | P1 | Fb |	| Bw EP P1 P2 | | (1) UA | | | Fb |

Table 4.19. Transverse Sequence of Damage for Pa Ground Motions

(a) Short Steel (Ss) Superstructure Bridge Variants

			Short Pier (15 ft)	Tall Pier (40 ft)
Column Pier	Type I Bearings	Fixed base	| RA Fb | | (1) EP | | RP | UA UP |	| RA | P1 P2 | (1) | | | |
		Soft soil	| RA | Fb | (1) | EP | RP | UA UP |	| RA | P1 P2 | (1) | | | |
	Type II Bearings	Fixed base	| RA Fb | EP | (1) | RP UA | UP | |	| RA | P1 P2 | (1) EP UA | | RP | |
		Soft soil	| RA | Fb EP | (1) | RP UA | UP | |	| RA | P1 P2 UA | (1) EP | | RP | |
Wall Pier	Type I Bearings	Fixed base	| RA Fb | | (1) EP | | RP | UA |	| RA Fb | | (1) EP RP | | | |
		Soft soil	| RA Fb | | (1) EP | RP | UP | UA |	| RA Fb | | (1) EP RP | | UP | UA |
	Type II Bearings	Fixed base	| RA Fb | EP | (1) | RP UA | UP | |	| RA Fb | EP RP | (1) | UA | UP | |
		Soft soil	| RA | Fb EP | (1) UA | UP | | |	| RA Fb | EP RP | (1) UA UP | | | |

(b) Long Steel (Sl) Superstructure Bridge Variants

			Short Pier (15 ft)	Tall Pier (40 ft)
Column Pier	Type I Bearings	Fixed base	| RA | Fb P2 | (1) P1 | | | UA UP |	| RA P1 P2 | | (1) | | | |
		Soft soil	| RA | | (1) Fb P2 | P1 | UA | UP |	| RA | P1 P2 | (1) | | | |
	Type II Bearings	Fixed base	| RA | EP Fb P2 | (1) P1 UA | UP | |	| RA P1 P2 | | (1) UA | | |
		Soft soil	| RA | EP Fb P2 | (1) UA | P1 | UP | |	| RA P1 P2 | UA | (1) | | | |
Wall Pier	Type I Bearings	Fixed base	| RA | Fb | (1) | EP RP | | UA |	| RA | Fb | (1) | EP RP | | |
		Soft soil	| | RA Fb | (1) | EP | RP UA UP | |	| RA | | (1) Fb | EP RP | UA UP | |
	Type II Bearings	Fixed base	| RA | EP Fb | (1) | RP UA | UP | |	| RA | Fb EP RP | (1) | UA | | UP |
		Soft soil	| RA | Fb | (1) EP RP UA | UP | | |	| RA | Fb EP RP UA | (1) | | UP | |

(c) Precast Concrete (Cs) Superstructure Bridge Variants

			Short Pier (15 ft)	Tall Pier (40 ft)
Column Pier	Type I Bearings	Fixed base	| RA Fb | | (1) EP P1 | RP | | UA UP |	| RA P1 P2 | | (1) | | | |
		Soft soil	| RA | Fb | (1) | EP RP P1 | | UP |	| RA | P1 P2 | (1) | | | |
	Type II Bearings	Fixed base	| RA Fb | EP | (1) RP | UA | UP | |	| RA | P1 P2 UA | (1) | | | |
		Soft soil	| RA | Fb EP | (1) UA | RP | UP | |	| RA | P1 P2 UA | (1) | | | |
Wall Pier	Type I Bearings	Fixed base	| RA Fb | EP | (1) RP | | | UP |	| RA Fb | EP | (1) RP | | | |
		Soft soil	| RA | Fb | (1) EP RP | | UP | UA |	| RA | Fb | (1) EP RP | | UP | UA |
	Type II Bearings	Fixed base	| RA Fb | EP | (1) RP | UA | UP | |	| RA Fb | EP | (1) RP | UA | UP | |
		Soft soil	| | RA EP Fb | (1) UA | RP UP | | |	| RA EP | Fb | (1) UA | UP | | |

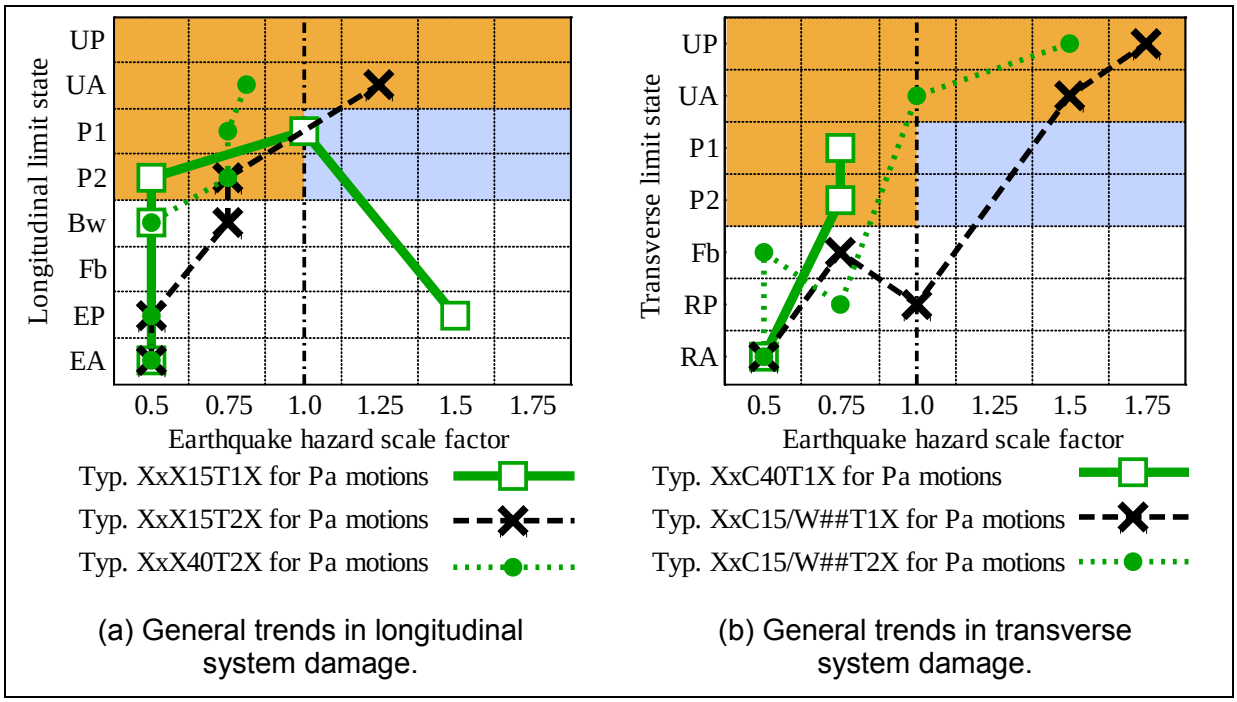

(a) General trends in longitudinal system damage.

(b) General trends in transverse system damage.

Figure 4.45. General trends of system damage for some typical bridge cases.

4.3 EFFECT OF PARAMETRIC VARIATIONS ON GLOBAL BRIDGE RESPONSE

Results from the entire parametric space were compared based on the observed sequence of damage, peak recorded displacements, and abutment and pier base shears. Comparison of these overall response parameters illustrates how variations in bearing type, substructure type, substructure height, superstructure configuration, foundation flexibility, and the applied ground motion can influence system response. Displacements are reported based on the maximum relative bearing displacement at a single support, and base shears are normalized with respect to the vertical dead load reaction at the foundation. Unless otherwise stated, the results presented below are for a scale factor (SF) of 1.0, which corresponds to the design earthquake.

4.3.1 Type I Versus Type II Bearings

In comparison with bridges with Type I bearings, when Type II bearings were used at the abutments and Pier 1, the result was a slight reduction (12%) in Pier 1 base shears, a slight reduction (13%) of transverse abutment base shears, and significantly higher displacements (29% for longitudinal, and 58% for transverse).

Type II bearings have a lower coefficient of friction, provide less resistance to sliding, and generally experience larger displacements than an equivalent Type I bridge. The larger Type II displacements, coupled with the more stringent unseating criteria used for Type II bearings, caused Type II systems to reach the bearing unseating limit state at much lower hazard levels than bridges with Type I bearings. When subjected to Pa longitudinal excitation, all bridges with tall substructures and Type II bearings (XxX40T2X) unseated at hazard levels at or lower than the design-level earthquake (SF = 1.0), and all Type II bearing systems unseated by SF = 1.75 for both the CG and Pa ground motions. In the transverse direction, bridges with tall substructures and Type II bearings were again vulnerable, with 15

out of the 24 Type II bridges unseating before SF = 1.0 for the Pa motions and all 24 Type II bridges unseating by SF = 1.75 for both Pa and CG motions.

Type I bearing systems, on the other hand, performed much better, with no unseating recorded for longitudinal excitation. For transverse excitation with Pa ground motions, no unseating was recorded at the design earthquake, seven out of 24 bridges unseated at SF = 1.5, and an additional eight bridge variants unseated at SF = 1.75. The bridges that unseated were primarily those with flexible foundation boundary conditions. No transverse unseating was recorded for Type I bearing systems for the CG ground motions, so these bridges are considered vulnerable only for very high seismic hazard conditions.

As discussed previously, the definition of “bearing unseating” in this research is distinct from “unseating” in IDOT and AASHTO design provisions. For example, for Type I bearings, unseating occurs when the leading edge of the bearing just reaches the edge of the abutment. AASHTO and IDOT provisions, by contrast, assume that loss of span is the critical behavior, which would occur only when the end of the girder reaches the edge of the abutment.

However, with the computational limitations of the OpenSees models, system behavior cannot accurately be predicted beyond the bearing unseating definitions used in this report. The conclusion drawn in regard to girder unseating is therefore practically limited to the qualitative observation that the risk of actual span loss at the design earthquake is very low for the bridges in the parametric study.

4.3.2 Pier Type and Height

For longitudinal analyses, most wall and multi-column pier bridges followed a sequence of damage where Pier 2 was damaged at low earthquake scale factors (SF = 0.5 or 0.75). Most tall structure variants (XxX40), and short pier structures with Type I bearings Sl and Cs variants (SlX15T1 and CsX15T1), experienced yielding in both the isolated and non-isolated piers (Piers 1 and 2, respectively) before the design-level earthquake. For the remaining short substructure bridge variants, Pier 1 was isolated and protected from damage up to the design-level earthquake, but above the design level, Pier 1 yielded in all variants except those having both 15 ft column piers and Type II bearings (XxC15T2).

As discussed in Section 3.1.2, drift ratios were used to assess the extent of substructure damage associated with the pier yielding limit state. Pier drift ratios between 2% and 4% were considered to represent moderate damage, and ratios in excess of 4% were considered to represent severe damage. At SF = 1.0, severe damage never occurred, but moderate damage occurred in roughly 15% of longitudinal Pa runs and 25% of transverse runs, distributed across the bridge variants, as indicated in Table 4.12 and Table 4.13. In the vast majority of CG runs, pier drifts remained below 2%. For wall piers in the transverse direction, onset of damage would be expected well before the 2% limit selected for column piers and out-of-plane wall piers. However, recorded in-plane wall pier displacement demands were nearly zero, no damage was anticipated at SF = 1.0, and unique drift limits were therefore considered unnecessary.

Table 4.20. Number of Longitudinal Pa Runs with Moderate Pier Damage (2% to 4% Drift)

			Ss Superstructure				Sl Superstructure				Cs Superstructure			
			Short (15 ft)		Tall (40 ft)		Short (15 ft)		Tall (40 ft)		Short (15 ft)		Tall (40 ft)	
			Pier 1	Pier 2	Pier 1	Pier 2	Pier 1	Pier 2	Pier 1	Pier 2	Pier 1	Pier 2	Pier 1	Pier 2
Column Pier	Type I Brg	Fixed base	NA	2	NA	NA	NA	10	3	NA	NA	10	2	NA
		Soft soil	NA	1	NA	NA	NA	8	3	NA	NA	9	3	NA
	Type II Brg	Fixed base	NA	1	NA	NA	NA	10	2	2	NA	7	NA	NA
		Soft soil	NA	NA	1	NA	NA	10	8	5	NA	4	1	1
Wall Pier	Type I Brg	Fixed base	NA	NA	2	2	NA	9	5	3	NA	9	3	NA
		Soft soil	NA	NA	5	NA	NA	6	8	3	NA	6	7	4
	Type II Brg	Fixed base	NA	NA	2	1	NA	10	5	4	NA	4	1	NA
		Soft soil	NA	NA	5	NA	NA	7	7	4	NA	2	5	2

Table 4.21. Number of Transverse Pa Runs with Moderate Damage (2-4% Drift)

			Ss Superstructure				Sl Superstructure				Cs Superstructure			
			Short (15 ft)		Tall (40 ft)		Short (15 ft)		Tall (40 ft)		Short (15 ft)		Tall (40 ft)	
			Pier 1	Pier 2	Pier 1	Pier 2	Pier 1	Pier 2	Pier 1	Pier 2	Pier 1	Pier 2	Pier 1	Pier 2
Column Pier	Type I Brg	Fixed base	NA	NA	5	8	1	NA	7	8	NA	NA	7	7
		Soft soil	NA	NA	5	8	NA	NA	5	5	NA	NA	5	5
	Type II Brg	Fixed base	NA	NA	3	8	NA	NA	9	9	NA	NA	7	8
		Soft soil	NA	NA	3	5	NA	NA	8	9	NA	NA	6	7
Wall Pier	Type I Brg	Fixed base	NA	NA	NA	NA	NA	NA	NA	NA	NA	NA	NA	NA
		Soft soil	NA	NA	NA	NA	NA	NA	NA	NA	NA	NA	NA	NA
	Type II Brg	Fixed base	NA	NA	NA	NA	NA	NA	NA	NA	NA	NA	NA	NA
		Soft soil	NA	NA	NA	NA	NA	NA	NA	NA	NA	NA	NA	NA

For transverse excitation, short multi-column pier substructures and all wall substructures were typically strong enough that the fixed bearings and Pier 1 retainers failed, thereby allowing for effective quasi-isolation. One exception was the long steel bridges (Sl), where some pier yielding was noted to occur before the design-level earthquake for the short column pier variants. When subject to transverse excitation, most tall multi-column pier substructures yielded before reaching the design-level earthquake, and the Pier 1 retainers and low-profile fixed bearings remained essentially elastic even at high levels of seismic excitation.

Bridges with tall pier substructures on average experienced maximum deformations that were 74% and 24% larger than their short pier equivalents for longitudinal and transverse excitation, respectively. These higher displacements often resulted in unseating failures, as was noted in Section 4.3.1. The tall pier substructures experienced lower normalized base shears than short pier bridges by 39% for longitudinal and 30% for transverse excitation. The difference in base shears can be attributed to the fact that the base shears were capped by the lateral yield capacity of the substructures, which were lower for the taller piers. Backwall forces, however, increased by 12% for the taller bridge

variations. In comparison with column pier bridges, the normalized base shears at wall piers were 20% higher in the longitudinal and 18% higher in the transverse directions, which can again be attributed to the yield capacity of the different systems. The abutment force and displacement response did not vary significantly between column and wall pier systems, and the longitudinal pier response was similar for the two systems. In the transverse direction however, wall piers are much stiffer than column piers and experienced 177% higher pier bearing displacements and roughly 20% higher normalized pier base shears.

4.3.3 Superstructure Configuration

The long steel (Sl) superstructures often experienced pier yielding earlier than the other superstructures. This can be attributed to the higher axial load at the substructures, as well as the higher bearing fuse capacities, because these components are designed to resist a percentage of the dead load. System displacements increased with superstructure length, and the short steel (Ss) superstructure generally had slightly higher normalized base shears. This is primarily because the substructure mass was higher when compared with the superstructure. There were slight differences in displacement between the three cases because the bridges differ in structural period. However, the systems performed about equivalently in terms of unseating, so the seat width equations effectively incorporate superstructure length.

4.3.4 Foundation Flexibility

Bridge cases with flexible foundation conditions experienced generally small differences in bearing displacement and normalized base shear when compared with the fixed foundation variations. Because the flexible foundations could accommodate some displacement, their presence at times altered the sequence of damage such that piers and fixed bearings experienced lower forces and were thereby damaged at higher scale factors of excitation or were not damaged at all. Owing to the higher displacement demands, flexible variations were somewhat more prone to unseating, typically reaching the UA or UP limit state at a scale factor of about 0.25 lower than what was observed for fixed foundation cases (i.e., unseating at SF = 1.5 vs. SF = 1.75).

4.3.5 Ground Motion Type

Results for all 48 bridge variants subjected to Pa ground motions were compared with results from the CG ground motions at the design-level earthquake hazard. Under longitudinal excitation, Pa ground motions resulted in 81% higher bearing displacements, 4% lower intermediate substructure base shears, and 20% higher abutment backwall forces than the CG counterparts. For transverse excitation, the Pa motions resulted in 116% higher bearing displacements and 18% higher base shears at the intermediate substructures, and the abutment base shears remained equivalent because they were limited by the retainer and bearing sliding force capacity for both types of excitation. The increase in base shear and displacements was more significant in structures with longer periods (i.e., Sl vs. Ss superstructure, tall vs. short substructures, and flexible vs. fixed base), which were again more susceptible to longer-period excitation. By general observation of damage patterns in the entire parametric space, it was noted that the Pa and CG motions produced approximately the same sequence of damage, but the Pa motions normally resulted in limit states being reached at lower scale factors of excitation than with the CG motions. For example, in the transverse direction, 31% more bridges experienced unseating when subject to the Pa than to the CG motions.

4.3.6 Non-Orthogonal Ground Motion

Non-orthogonal seismic excitation was found to be equal or less critical compared with a uni-directional ground motion application for the quasi-isolated systems studied in this project. The SsC15T2S, SlW15T1F, and CsC40T1S bridge variations were studied with both uni-directional and non-orthogonal excitation, and it was determined that mean bridge response was less for non-orthogonal ground motion applications. As discussed in Chapter 3, non-orthogonal excitation can often alter the sequence of damage (e.g., it can cause bearing failure or pier yielding before it would occur in one of the orthogonal directions), but peak displacements and base shears would still be due to pure orthogonal excitation. The explanation for this behavior is that the bridges evaluated with non-orthogonal excitation take advantage of multiple lateral systems, including the side retainers and strong axis of the pier substructures, for the transverse force component and the abutment backwall for the longitudinal force component.

4.3.7 Sensitivity to Variations in Bearing and Backwall Fuse Capacities

Supplementary analyses of the prototype bridge (SsC15T1F) were conducted to assess the influence of restraining elements, such as the fixed bearings, retainers, and backwalls, on local and global bridge seismic response. A summary of key observations is provided below, with reference to Filipov et al. (2012) for full details of this additional supplementary sensitivity study.

In the longitudinal direction, the study looked at the effect of reducing the number of “active” fixed bearings (i.e., the number of fixed bearings with anchor bolts). With the original six active fixed bearings, the bridge was not considered quasi-isolated because the fixed bearing pier yielded while the fixed bearings themselves remained essentially elastic at the design earthquake. Reducing the number of active fixed bearings to two allowed the fixed bearings to fuse while the pier remained elastic, precisely as desired for quasi-isolation. Although reducing the number of active fixed bearings strongly influenced local response at the fixed bearing pier, it did not have much effect on global bridge response. In the average response to the ten Paducah ground motions, maximum base shears and longitudinal superstructure displacements were essentially uninfluenced by the number of active (and fusing) fixed bearings.

The study also looked at the influence of backwall and backfill capacities on longitudinal bridge response. A comparison between a model with neither backwall nor backfill and a model incorporating the hyperbolic backfill element from the parametric study confirmed that backfill response is significant in controlling longitudinal superstructure displacement. Augmenting the backfill with increasingly strong backwalls, however, did not provide further reduction in system displacements, but it did lead to increased base shears for the abutment piles.

Similar to the longitudinal fixed bearing sensitivity study, in the transverse direction the study looked at the effect of simultaneously reducing the number of active fixed bearings and retainers. A reduction in the number of restraining elements produced a concomitant reduction in total bridge base shear, but it did not have a predictable effect on system displacements. Reducing the number of restraints sometimes caused the fixed bearings and retainers to fuse earlier in the time history, with the superstructure then experiencing an increased number of cycles in which the only transverse restraint was bearing friction. The magnitude of the impact this has on residual system displacements was largely a function of the dynamic characteristics of the input ground motion, and thus not readily predicted.

4.3.8 Other Observations on Bridge Performance

It is important to remember that results presented in this report are based on a superstructure that remains essentially elastic for all analyses. However, current IDOT standard diaphragm details have not been specifically designed for seismic effects and are therefore likely vulnerable to suffering significant permanent deformation of the diaphragm channel or failure of the connections. This would be expected to result in significant damage to the girders and could lead to superstructure collapse. It is therefore imperative that diaphragms near abutments and intermediate supports be designed and detailed to remain elastic at the design hazard.

When looking at the results of this study, it is important to note that the ground motions were initially normalized to design spectra for Cairo, Illinois, which is nearly the highest hazard for Illinois and the NMSZ in general. This level of hazard was chosen as the baseline for this study to establish an upper bound on response for Illinois bridges. Bridges with quasi-isolation systems farther away from the NMSZ and with lower hazard levels are expected to experience significantly less damage than those shown in this study. The parametric variations used in this study provide a representative sample of modern bridges in Illinois that employ elastomeric bearings and simply supported abutment conditions. The chosen pier heights, span lengths, foundation stiffnesses, and ground motions provide a reasonable selection of common bridge cases in the NMSZ, and it is reasonable to apply the results and recommendations presented herein to similar structures.

The results from this research are generally consistent with other studies on bridges in the NMSZ. When studying fragilities of wall pier bridges in Illinois, Bignell, LaFave, and Hawkins (2005) found that overall, bridge systems in the region are expected to experience only moderate damage for MCE-level hazards, which is similar to the conclusions herein. Similarly, Bignell, LaFave, and Hawkins (2005) noted that pier properties were important in the general bridge response, but in contrast to the study presented in this paper, they found that bearings (steel roller, low-profile fixed, and elastomeric in some cases) had little influence on the bridge fragility. A study of multi-span simply supported bridges by Nielson and DesRoches (2007) showed that for MCE-level hazards, significant vulnerabilities exist at the piers, abutments, and in the unseating of girders. The study found that longitudinal and transverse displacement demands were of the same order, whereas the IDA results shown herein indicate that for continuous bridges, transverse deformations tend to be much greater than longitudinal deformations, especially at higher degrees of excitation. The difference in deformation demand can be attributed to the bearings used in the previous research, where steel dowels at the intermediate substructures did not fuse and permit sliding as is intended for quasi-isolated systems.

CHAPTER 5 FUSE DESIGN RECOMMENDATIONS

5.1 OBSERVATIONS OF FUSE BEHAVIOR

Elastomeric bearings possessed significantly higher observed capacities relative to predicted capacities. For Type I bearings, in particular, the standardized retainer designs in use by IDOT at the time of the testing program resulted in experimental fuse capacities approximately three to four times the predicted value. This is a significant overstrength factor, which could defeat the fundamental purpose of the fuse components (i.e., to provide an upper limit on the magnitude of load that will be transmitted from the superstructure to the substructure during a seismic event). The large overstrength factors derive from the combined effects of four primary sources:

- The horizontal reaction developed at the toe (accounts for 34% to 48% of total experimental fuse capacities).
- The shear load carried in the elastomer (14% to 21% of total experimental fuse capacities).
- The material overstrength of anchors (16% to 22% higher than nominal material ultimate strength for experiments).
- The vertical bearing load transferred to a retainer, reducing tension demand on an anchor (tension demand typically estimated to be about 26% to 43% of anchor tension capacity, rather than the 56% implicitly assumed by the 0.75 factor used in the current IDOT design equation).

Additionally, the mechanical response of the retainers was significantly different for short (7c/11b) versus tall (9c/13c) bearings, with respect to their interaction with both the concrete and the bearing. The response observed for the short bearings is recommended as a preferred mechanical response. For tall bearings, the response was influenced by crushing of concrete at the toe, which manifests as a hysteretic response with a higher apparent energy dissipation capacity than for short bearings. However, the additional energy dissipation is available for a single cycle only, when the concrete at the toe is experiencing crushing, and the subsequent cycles are pinched. Furthermore, when the retainer crushes concrete at the toe, it then rotates significantly and the transmission of horizontal load occurs through the elastomer and reinforcing shims to the retainer heel, rather than through the thick bearing top plate to the initially vertical face of the retainer. Subjecting the reinforced elastomer to a concentrated load from the retainer heel may not be advisable, particularly considering that the behavior has been observed only for controlled experimental conditions during quasi-static tests rather than in the more random dynamic scenarios typical of earthquakes.

5.2 FORMULATION OF RETAINER MECHANICAL RESPONSE

The experimental data and fuse capacities presented in Volume 1 of this report represent combined resistance of elastomeric bearings and retainers. To isolate the load effects and behavior of retainers, data for the horizontal load and moment acting at the top of the bearing (and how these quantities varied with shear strain, in the absence of retainer interaction) were used to infer the loads acting between the bearing and a retainer (Figure 5.1).

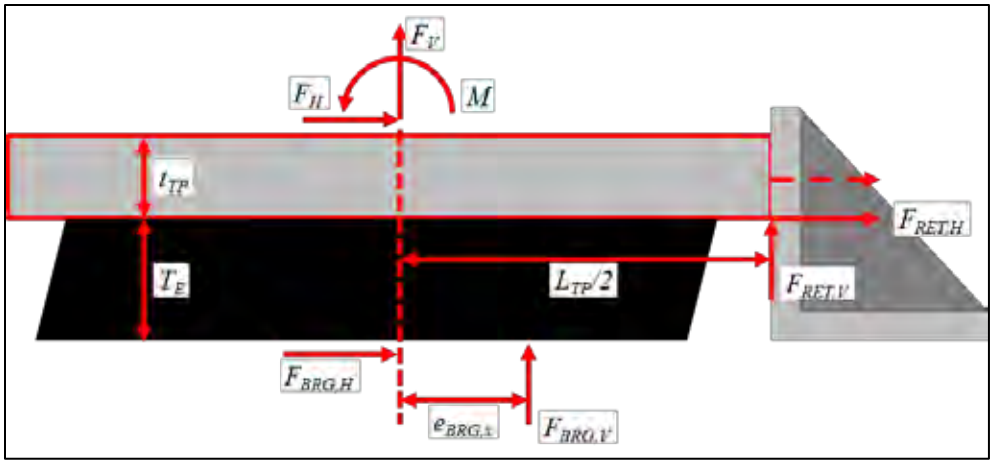

Figure 5.46. Schematic of bearing reaction forces and moments.

When the bearing initially contacts the retainer, there may be a short sliding segment where the horizontal reaction centroid is closer to the center of the top plate, as shown with a dashed arrow in Figure 5.1. However, once the retainer slides sufficiently to engage the steel anchor in the concrete, the retainer will pivot at a location between the toe and the anchor, rotating the vertical face of the retainer to accommodate the bearing top plate displacement. The contact surface will be reduced to a knife-edge condition at the bottom edge of the top plate.

With the magnitudes of the reaction components acting between the bearing and retainer, the local loading effects at the retainer were evaluated according to the configuration shown in Figure 5.2. (Further discussion of the data processing performed to determine loads and displacements at retainers is available Appendix D.)

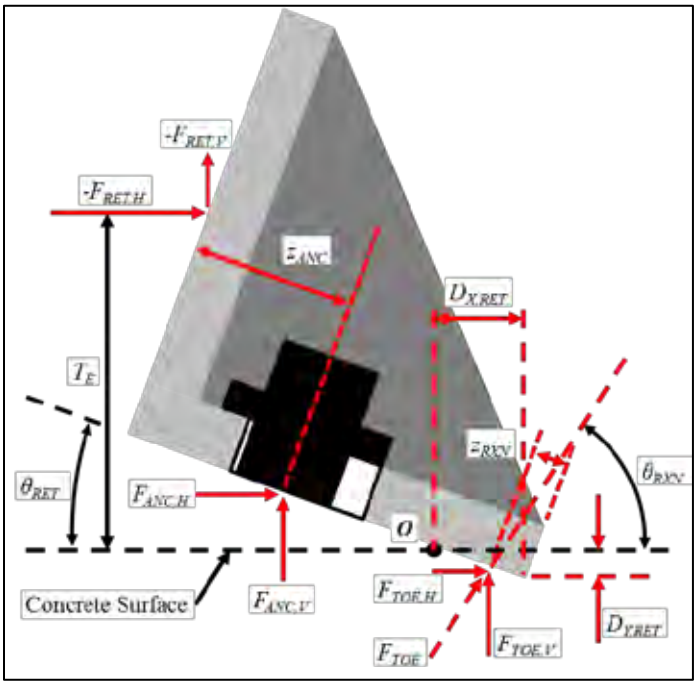

Figure 5.47. Local bearing reaction components.

The $F_{RET,H}$ and $F_{RET,V}$ loads are determined from bearing response data obtained during experiments, but the retainer is statically indeterminate, with four unknown quantities. To circumvent this difficulty, the concrete reaction orientation term, θ_{RXN}, was parameterized, and the resulting $F_{ANC,H}$ and $F_{ANC,V}$ terms were transformed to normal and shear components, $F_{ANC,n}$ and $F_{ANC,v}$, respectively, and combined and evaluated according to ACI 318, Appendix D (2008), in accordance with AASHTO (2008).

5.3 SUMMARY OF FUSE RESPONSE QUANTITIES

Response quantities obtained through investigation of local retainer force components are presented in Table 5.1 through Table 5.3 for the short bearing experiments and for the alternate retainer designs tested with a 13c bearing. The data shown in Table 5.1 correspond to the peak load capacity observed in the ramp for each retainer when the retainer anchor ruptured. For the alternate retainers, the West retainer is included to represent a condition at incipient crushing rather than anchor rupture. Approximately 50% to 65% of the applied horizontal load was developed as a vertical reaction acting on the vertical face of the retainer for the 7c and 11b bearings, but the ratio was slightly lower for the 13c. The surface condition of the retainers may have influenced the ratio. For the alternate retainers tested with the 13c, they were fabricated from sections of angles, and the surface layer was mill scale, whereas the retainers tested with the 7c and 11b bearings were built up from plates and painted. The vertical load was a redistribution of gravity load from the elastomer, so the direction of the applied load acted to resist the overturning effect of the horizontal load.

Table 5.22. Applied Loading Summary

Bearing	Direction	F_H	F_V	F_V / F_H
		kips	kips	
7c	West	31.2	16.3	0.52
	East	29.5	14.4	0.49
11b	West	67.5	43.8	0.65
	East	67.1	39.6	0.59
13c (ALT)	*West*	*72.1*	*32.9*	*0.46*
	East	72.2	25.3	0.35

The concrete reactions corresponding to the anchors reaching a value of unity for combined load effects are presented in Table 5.2. The inclination of the reaction resultant relative to horizontal was approximately 55° to 65°, with an average of about 60°. The average concrete stress at the toe, $f_{c,avg}$, was not a limiting factor for either the 7c or 11b bearing. Only localized minor crushing was evident after these tests, which was insignificant in comparison with the response of 9c or 13c bearings, or the West 13c alternate retainer. The concrete dry-cured strength was about 5 ksi. The estimated compression stress for 11b bearings is significantly in excess of the cylinder compression test strengths, but the loading condition (bearing on a wide area, rather than compressing an unconfined concrete cylinder) is expected to permit higher strength than cylinder tests would indicate. Also, it should be noted that the 11b retainers were installed with rebar passing beneath the toe, but the 13c alternate retainer toes were several inches away from rebar. Therefore, the difference in performance between the two cases is probably not attributable solely to the relatively small discrepancy in concrete stress.

Table 5.23. Concrete Reaction Summary

Bearing	Direction	θ_{RXN}	F_{TOE}	$F_{TOE, H}$	$F_{TOE, V}$	$f_{c,avg}$
		deg	kips	kips	kips	ksi
7c	West	53.8	27.7	16.4	22.3	3.2
	East	58.6	29.7	15.5	25.3	3.6
11b	West	63.2	63.3	28.5	56.5	6.3
	East	64.5	68.3	29.4	61.6	6.8
13c (ALT)	*West*	*60.0*	*84.0*	*42.0*	*72.7*	*7.3*
	East	58.5	57.2	29.9	48.8	2.4

Anchor reactions were determined from equilibrium with the loads from the bearing and at the toe. Retainer rotations were about 3° for the 7c bearing and about 8° to 9° for the 11b bearing. The rotation for the East 13c alternate retainer was about 6° at anchor failure, and the rotation for the West retainer was approximately 8° at the development of significant concrete crushing (which led to much larger rotations, eventually reaching about 90°). At shallow angles, there are only minor differences between horizontal and vertical reactions compared with normal and shear components. The combined load capacities for anchors were primarily driven by shear demands, but tension demand was also significant, at about 25% to 50% of nominal pure tension capacity.

Table 5.24. Anchor Reaction Summary

Bearing	Direction	$F_{ANC, H}$	$F_{ANC, V}$	$F_{ANC, n}$	$F_{ANC, v}$	$F_{ANC, n} / T_n$	$F_{ANC, v} / V_n$
		kips	kips	kips	kips		
7c	West	14.8	6.0	6.8	14.5	0.26	0.93
	East	14.0	11.0	12.7	12.5	0.49	0.80
11b	West	39.0	12.7	18.0	36.8	0.27	0.93
	East	37.7	22.1	27.8	33.7	0.42	0.85
13c (ALT)	*West*	*30.1*	*39.8*	*43.8*	*24.1*	*0.58*	*0.54*
	East	42.3	23.5	27.8	39.6	0.37	0.88

5.4 RECOMMENDED REVISIONS TO DESIGN PROCEDURE

The recommended revisions to retainer design are outlined below. The proposed sequence of steps is intended to account for the loading effects inferred for the bearing-retainer interaction and the retainer toe reaction, as determined from the experimental data. The proposed procedure also aims to reduce the likelihood of concrete crushing at the toe and thereby provide a more reliable mechanical force-displacement response for the retainers during fusing. Additional data and supplemental equations may be found in Appendix D of this report.

Step 1: Calculate an initial required anchor diameter, assuming that the nominal tension capacity of the anchor is equal to about V_{fuse} / 1.2.

Step 2: Estimate shear load demand on the retainer by reducing V_{fuse} to account for the contribution of the elastomer ($GA\ \gamma$, where G is about 120 psi, A is the footprint area of the elastomer in units of in^2, and γ is about 0.5).

Step 3: Estimate the vertical load acting on the vertical face of the retainer with a ratio of about 0.5 times the horizontal load.

Step 4: Assume that an average of 5 ksi acts on a 1-in. strip at the retainer toe (corresponding to a 40-kip vertical reaction on the toe for a standard 8-in. retainer length). Sum the moments about the anchor centroid to determine how wide the retainer will need to be to satisfy equilibrium.

Step 5: Assume that the concrete reaction acts at an inclination from horizontal of about 60° (corresponding to about 23 kips acting horizontally with a 40-kip vertical reaction). Balance the equilibrium of horizontal and vertical forces to find anchor reaction components.

Step 6: Perform an interaction check for combined loading on the anchor per the commentary of ACI 318 Appendix D (2008).

Step 7: Scale the anchor size as needed to provide the required capacity.

Step 8: If the anchor position relative to the heel increases, return to Step 4 and verify that the moment arm to the toe is still sufficient to limit the concrete stress to 5 ksi.

CHAPTER 6 CONCLUSIONS AND RECOMMENDATIONS

This research investigated the seismic performance of typical bearings and bridge configurations currently used in Illinois. Experimental and analytical research programs provided data to characterize the behavior of both bearing assemblies and global bridge systems. Overall, this can support future calibration and further refinement of the IDOT ERS as the philosophy evolves toward a performance-based design method that is well-suited to the bridge configurations and seismic hazards encountered in Illinois.

6.1 CONCLUSIONS FROM THE ANALYTICAL STUDY

The parametric study evaluated anticipated behavior of existing IDOT bridges in a significant earthquake and assessed how closely this performance matched the objectives of quasi-isolated seismic response. The analyzed bridges featured different superstructures, substructures, foundation stiffnesses, and types of elastomeric bearings. The structures were selected as a representative sample of bridges in southern Illinois, and performance observations can be generalized to similar systems in the region. Bridge response was studied using nonlinear numerical models in which transient seismic analyses were carried out for incremental hazard levels.

The dynamic parametric analyses point to the following primary conclusions:

- From the current parametric study, only a few bridge variants were noted to unseat for design-level earthquakes, indicating that most structures in Illinois would not experience severe damage during their typical design life. Because a high hazard level was used as a baseline to scale the ground motions, unseating and span loss are not likely for regions with moderate seismic hazard.
- Bridges with Type II IDOT bearings were shown to be more prone to unseating because the area of the bearing surface was often insufficient given the magnitude of the displacement demand. Unseating of the bearings is an unstable and unpredictable behavior leading to large displacements, potential damage to deck and diaphragm elements, and possible local or global collapse. Tall structures with Type II bearings experienced longitudinal unseating before design-level earthquakes, and nearly all bridges with Type II bearings experienced both transverse and longitudinal unseating for MCE-level hazards. However, unseating in this context was defined based on the bearing behavior and does not necessarily represent span loss.
- Bridges with Type I bearings showed reliable behavior in preventing system collapse. No unseating was noted for longitudinal excitation of these bridges, and transverse unseating of the bearings was observed only at MCE-level hazards for ground motions scaled based on a design spectrum for Soil Class D ground motions.
- The sequence of damage of most bridge structures indicated yielding of the piers with fixed bearings for small earthquakes and potential unseating of some bridges for large seismic events, which are both discouraged for quasi-isolation. Calibration of fuse component capacities and revision of seat width equations can improve the sequence of damage for many bridge systems.
- Displacements in the longitudinal direction are generally much lower than in the transverse direction because of the influence of the backwall elements. For design-level earthquakes, transverse bearing displacements were roughly 36%

higher than the longitudinal, and the transverse displacements increased more severely as the intensity of the earthquake increased. This difference arises because after the retainers and fixed bearings have failed, there is no active restraint of the system in the transverse direction, whereas the backwall and backfill continue to provide resistance in the longitudinal direction.

- Bridge displacement response was noted to be significantly larger for systems with tall pier substructures and Type II bearings.
- Ground motions simulating soil site conditions and scaled based on a design spectrum for Soil Class D typically resulted in larger force and displacement demands than rock ground motions, which were scaled based on a design spectrum for Soil Class B, of similar intensity. The soil ground motions also resulted in more limit states being reached at lower hazard levels.

6.2 PRELIMINARY RECOMMENDATIONS FOR CALIBRATION OF THE ERS

On the basis of the research findings presented in this report, the following items are recommended for improving the quasi-isolated design methodology:

- Consider limiting use of Type II bearings to regions of low or moderate seismicity, where bearing unseating is less likely. If use of Type II bearings in higher seismic zones is desired, consider increasing the size of the bearing surface to increase travel capacity and reduce the potential for bearing unseating.
- Type I bearings are appropriate for use with all seismic hazard levels and most soil types in Illinois (excluding soil conditions susceptible to special geotechnical concerns such as liquefaction).
- Design and detail diaphragms to remain essentially elastic under seismic effects in order to protect the girders from damage and prevent superstructure collapse. Current IDOT standard diaphragm details likely need to be revised in order to satisfy this criterion.
- Modify seat width requirements to be based on bearing unseating rather than girder unseating, and consider independent calibration of longitudinal and transverse seat width requirements.
- Identify acceptable substructure damage at the design earthquake in terms of ductility demand. This is essential to fully define the ERS and to effectively calibrate the fuse component capacities in future research. Such ductility demand limits can vary based on the Seismic Performance Zone.
- Fixed bearings and retainers were generally found to have higher fuse capacities than predicted by current IDOT equations. Consider reducing the strength of bearing and retainer fuse components by one or more of the following methods:
  - Place more stringent constraints on anchor bolt material classification, and use smaller-diameter bolts for both retainers and fixed bearings.
  - Use fewer fixed bearings, or use fewer anchor bolts with the existing number of fixed bearings.
  - Replace all fixed bearings with Type I or II elastomeric bearings.
  - Replace the current fixed bearings with a new bearing type that will more reliably allow fusing to occur.
  - Revise the current design and selection method for retainers to more accurately estimate fuse capacity and ensure a preferred fusing mechanism.

- Provide procedures and encourage designers to consider the backwall contribution for seismic design. This can allow for significant cost savings in substructure material, which would otherwise be required to limit longitudinal response.

6.3 RECOMMENDATIONS FOR FURTHER RESEARCH

Additional research needs have been identified as follows.

6.3.1 Further Research on ERS Calibration

- Conduct a sensitivity study on the superstructure-to-substructure connecting elements (i.e., retainers, fixed bearings, and backwalls) that will determine which components are most critical, and seek improved system behavior. The optimization process will weigh the benefits of controlling the force-based fuse capacity of sliding components against the competing interest of predicting superstructure displacement. The sensitivity of displacement response to input ground motion should be considered from the standpoint of developing simplified design methods. The effect of using different backwall capacities and lower-capacity fixed bearing components and retainers should be investigated.
- The OpenSees backwall elements did not account for the influence of wingwalls or an approach slab, and the backfill response was based on limited data for compacted Nevada sands. Refined models could more accurately capture the backwall-backfill response by accounting for these additional structural components and adjusting backfill response to reflect the uncompacted fill typically used in Illinois.
- The OpenSees bearing and retainer models were based on experimental tests of individual bearings and retainers. When tested together, retainers and bearings have more complex behavior, and the numerical element models could be updated to incorporate interaction behaviors between the two components.

6.3.2 Further Research on Limits of ERS Feasibility

- This current research considered only regular three-span bridges without skew. Skew effects in particular should be studied in more detail because they can influence bridge behavior significantly.
- Study other types of bridge irregularity to determine the feasibility of applying a quasi-isolated design approach.
- The current research considered only H-pile foundations, so analysis of bridges with other foundation systems common in Illinois would be beneficial. Foundation types such as drilled shafts or spread footings may alter system response, potentially impacting the feasibility and benefits of quasi-isolated design.
- The cost of a bridge designed with a quasi-isolation system is expected to be significantly less than that of a classical isolation system because complex design and high-cost components are not necessary. A benefit-cost analysis that compares quasi-isolation systems with classical isolation systems and with fixed bearing systems (i.e., conventional ductile substructure seismic design) should be performed to more clearly quantify the feasibility and benefits of quasi-isolation.

- The quasi-isolation design methodology can potentially be adapted to locations outside the New Madrid Seismic Zone. Investigation with synthetic and natural time-history records that are representative of other locations in the United States should be performed to see whether the quasi-isolated ERS might be suitable for other locations.

REFERENCES

American Association of State Highway and Transportation Officials (AASHTO). 2008. *LRFD Bridge Design Specifications*, Washington, DC: AASHTO.

American Association of State Highway and Transportation Officials (AASHTO). 2009. *Guide Specifications for LRFD Seismic Bridge Design*, Washington, DC: AASHTO.

American Concrete Institute (ACI). 2008. *Building Code Requirements for Structural Concrete (ACI 318-08) and Commentary*. Farmington Hills, MI: ACI.

ASTM International (ASTM). 2007. *Standard Specification for Anchor Bolts, Steel, 36, 55, and 105-ksi Yield Strength, Designation: F 1554-07a*, West Conshohocken, PA: ASTM.

Barth, K.E., and H. Wu. 2006. "Efficient Nonlinear Finite Element Modeling of Slab on Steel Stringer Bridges." *Finite Elements in Analysis and Design* 42(14–15):1304–1313.

Becker, T.C., and S.A. Mahin. 2011. "Experimental and Analytical Study of the Bi-Directional Behavior of the Triple Friction Pendulum Isolator." *Earthquake Engineering & Structural Dynamics* 41(3):355–373.

Bignell, J.L., J.M. LaFave, and N.M. Hawkins. 2005. "Seismic Vulnerability Assessment of Wall Pier Supported Highway Bridges Using Nonlinear Pushover Analyses." *Engineering Structures* 27(14):2044–2063.

Bisadi, V., and M. Head. 2010. "Orthogonal Effects in Nonlinear Analysis of Bridges Subjected to Multicomponent Earthquake Excitation," pp. 204-215. In *Proceedings of ASCE 2010 Structures* Congress, Orlando, FL, May 12–15, 2010.

Buckle, I., M. Constantinou, M. Dicleli, and H. Ghasemi. 2006. *Seismic Isolation of Highway Bridges.* Special Report MCEER06-SP07. Buffalo, NY: Multidisciplinary Center for Earthquake Engineering Research.

Building Seismic Safety Council (BSSC), 2000. *Prestandard and Commentary for the Seismic Rehabilitation of Buildings, FEMA-356*. Washington, DC: Federal Emergency Management Agency.

Chang, C., and D. White. 2008. "An Assessment of Modeling Strategies for Composite Curved Steel I-Girder Bridges." *Engineering Structures* 30(11):2991–3002.

Constantinou, M., A. Mokha, and A. Reinhorn. 1990. "Teflon Bearings in Base Isolation II: Modeling." *Journal of Structural Engineering* 116(2):455–474.

Ensoft Inc. 2010. Ensoft, Inc. Austin, Texas: http://www.ensoftinc.com/, July 4, 2010.

Fernandez, J.A., and G.J. Rix. 2008. "Seismic Hazard Analysis and Probabilistic Ground Motions in the Upper Mississippi Embayment." *Geotechnical Earthquake Engineering and Soil Dynamics Geotechnical Special Publication n181*. American Society of Civil Engineers.

Filipov, E.T. 2012. *Nonlinear Seismic Analysis of Quasi-Isolation Systems for Earthquake Protection of Bridges*. MS Thesis, University of Illinois at Urbana-Champaign, Urbana, IL.

Filipov, E.T., J.R. Revell, J.S. Steelman, L.A. Fahnestock, J.M. LaFave, D.A. Foutch, and J.F. Hajjar. 2012. "Sensitivity of Quasi-Isolated Bridge Seismic Response to Variations in Bearing and Backwall Elements." Paper No. 2978, *Proceedings of the*

15th World Conference on Earthquake Engineering, Lisbon, Portugal, September 24–28, 2012.

Gomez, I., A. Kavinde, C. Smith, and G. Deierlein. 2009 (Mar.). *Shear Transfer in Exposed Column Base Plates*. Report to the American Institute of Steel Construction. National Science Foundation Grant Number NSF-CMMI 0421492.

Ibarra, I.F., R.A. Medina, and H. Krawinkler. 2005. "Hysteretic Models That Incorporate Strength and Stiffness Deterioration." *Earthquake Engineering & Structural Dynamics* 34(12):1489–1511.

Illinois Department of Transportation (IDOT), *Bridge Manual*. 2009. Springfield, IL: IDOT.

Klinger, R.E., J.A. Mendonca, and J.B. Malik. 1982. "Effect of Reinforcing Details on the Shear Resistance of Anchor Bolts Under Reversed Cyclic Loading." *Journal of the American Concrete Institute* (79)1:3–12.

McKenna, F., S. Mazzoni, and G.L. Fenves. 2011. Open System for Earthquake Engineering Simulation (OpenSees) Software Version 2.2.0. University of California, Berkeley, CA. Available from http://opensees.berkeley.edu/.

Mackie, K.R., K.J. Cronin, and B.G. Nielson. 2011. "Response Sensitivity of Highway Bridges to Randomly Oriented Multi-Component Earthquake Excitation." *Journal of Earthquake Engineering* 15(6):850–876.

Mander, J.B., D.K. Kim, S.S. Chen, and G.J. Premus. 1996 (Nov.). *Response of Steel Bridge Bearings to Reversed Cyclic Loading*. Technical Report NCEER-96-0014. Buffalo NY: State University of New York at Buffalo.

Mosqueda, G., A.W. Whittaker, and G.L. Fenves. 2004. "Characterization and Modeling of Friction Pendulum Bearings Subjected to Multiple Components of Excitation." *Journal of Structural Engineering* 130(3):433–442.

Nielson, B.G., and R. DesRoches. 2007. "Seismic Performance Assessment of Simply Supported and Continuous Multispan Concrete Girder Highway Bridges." *Journal of Bridge Engineering* 12(5):611–620.

Roeder, C.W., and J.F. Stanton. 1991. "State of the Art Elastomeric Bridge Bearing Design." *ACI Structural Journal* 88(1):31–41.

Scott, M.H., and G.L. Fenves. 2006. "Plastic Hinge Integration Methods for Force-Based Beam-Column Elements." *Journal of Structural Engineering* 132(2):244–252.

Shamsabadi, A., K.M. Rollins, and M. Kapuskar. 2007. "Nonlinear Soil-Abutment-Bridge Structure Interaction for Seismic Performance-Based Design." *Journal of Geotechnical and Geoenvironmental Engineering* 133(6):707–720.

Somerville, P., N. Smith, S. Punyamurthula, and J. Sun. 1997 (Oct.). *Development of Ground Motion Time Histories for Phase 2 of the FEMA/SAC Steel Project*. SAC/BD-97/04, Sacramento, CA: SAC Joint Venture.

Vamvatsikos, D., and C.A. Cornell. 2002. "Incremental Dynamic Analysis." *Earthquake Engineering & Structural Dynamics* 31(3):491–514.

Wilson, P., and A. Elgamal. 2010. "Bridge-Abutment-Backfill Dynamic Interaction Modeling Based on Full Scale Tests." In *Proceedings of the 9th U.S. National and 10th Canadian Conference on Earthquake Engineering*. EERI Publication. Toronto, ON, July 25–29, 2010.

Zandieh, A., and S. Pezeshk. 2011. “A Study of Horizontal-to-Vertical Component Spectral Ratio in the New Madrid Seismic Zone.” *Bulletin of the Seismological Society of America* 101(1):287–296.

APPENDIX A NUMERICAL RESULTS

The organization of all tables in this appendix is outlined below for convenience. The first 56 tables present numerical results at SF = 1.0 for the 48 bridge variants in the parametric study. Results were tabulated for each of the Pa and CG ground motion suites in the longitudinal and transverse directions. As discussed in Chapter 4, each value in these tables was obtained by extracting the peak response from a set of individual time history runs, and then averaging the peak response over all ground motions in a suite. The remaining tables (Tables A.57 through A.62) were included to provide results of interest that were not specific to SF = 1.0. Supplemental information regarding interpretation of data in specific tables is given below.

Table No.	Content
1 - 4	Superstructure Displacement
5 - 20	Bearing Displacement
21 - 28	Pier Displacement
29 - 32	Foundation Displacement
33 - 48	Base Shear
49 - 56	Normalized Base Shear
57 - 60	Bearing Unseating Scale Factor
61 - 62	Fundamental Period of Vibration
63 - 66	Sequence of Damage

Tables 1-4 Superstructure Displacement

Superstructure displacements were reported at Abutment 1, and measured as indicated in Figure A.2.

Tables 5-20 Bearing Displacement

Relative displacements were reported for bearing elements as defined in Figure A.2. This meant that elastic deformation was subtracted from total deformation to obtain a sliding displacement at either the elastomer on concrete cap interface (Type I) or top plate on PTFE pad interface (Type II). This calculation was not performed for the fixed bearings because there was relatively little elastic deformation. Instead, the total bearing displacement was directly reported.

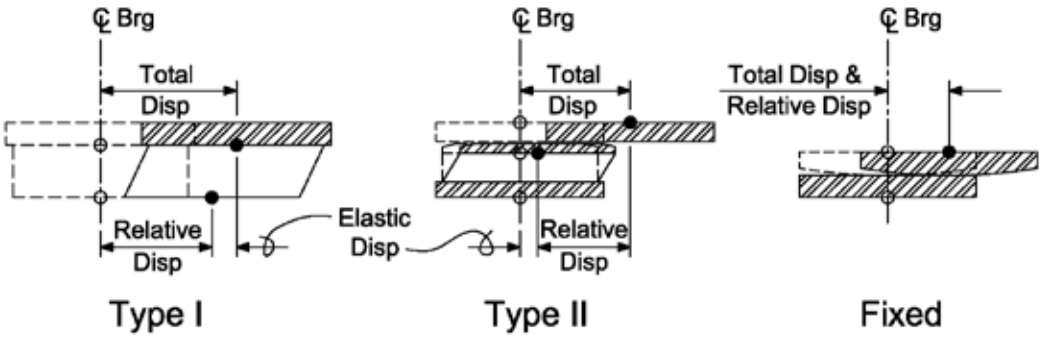

Figure A.48. Definitions of relative bearing displacement.

Tables 21-28 Pier Displacement

Relative pier displacement (Figure A.2) was reported as the top of pier displacement relative to bottom of pier displacement less any translation caused by rotation of the foundation element or the pier cap element.

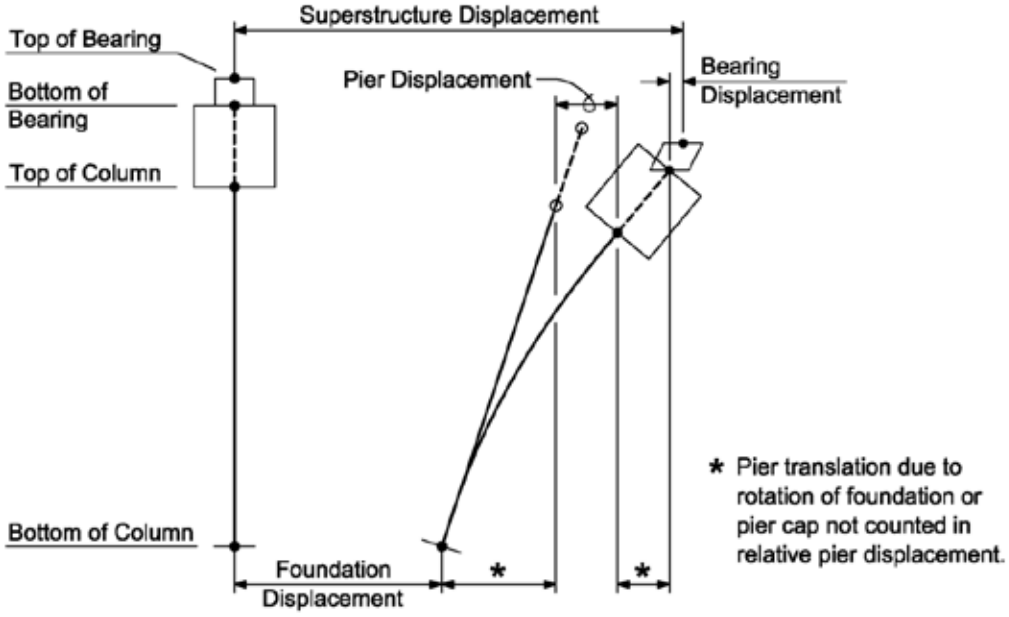

Figure A.49. Displacement definitions.

Tables 29-32 Foundation Displacement

Foundation displacements were reported at each substructure, and measured as indicated in Figure A.2. For fixed foundation bridge variants, the displacement is zero.

Table A.25. Peak Longitudinal Superstructure Displacement (in) - Pa Ground Motions at SF = 1.0

			Steel short (Ss) superstructure				Steel long (Sl) superstructure				Concrete short (Cs) superstructure			
			Short (15 ft)		Tall (40 ft)		Short (15 ft)		Tall (40 ft)		Short (15 ft)		Tall (40 ft)	
			Avg	StdDev	Avg	StdDev	Avg	StdDev	Avg	StdDev	Avg	StdDev	Avg	StdDev
Column pier substructure	Type I Bearings	Fixed base	4.58	0.50	6.59	0.70	6.14	0.85	9.26	0.98	5.96	0.59	9.28	0.81
		Soft soil	4.87	0.53	7.06	0.91	6.83	1.08	10.06	0.93	6.61	0.53	9.89	0.94
	Type II Bearings	Fixed base	4.19	0.66	7.13	0.77	6.71	0.77	10.12	1.54	5.27	0.63	8.66	1.00
		Soft soil	4.35	0.59	7.78	1.00	7.41	1.05	12.03	1.77	5.67	0.81	9.92	1.25
Wall pier substructure	Type I Bearings	Fixed base	3.90	0.63	6.58	0.77	5.73	0.97	9.63	0.82	5.62	0.48	8.89	0.80
		Soft soil	4.66	0.50	6.41	0.61	6.47	0.94	10.86	0.81	6.44	0.64	10.63	1.30
	Type II Bearings	Fixed base	3.63	0.50	6.50	0.73	5.90	0.79	9.95	1.07	4.85	0.84	8.55	0.78
		Soft soil	4.20	0.69	6.35	0.57	6.91	0.84	11.42	1.14	5.55	0.96	10.02	1.13

Table A.26. Peak Longitudinal Superstructure Displacement (in) – CG Ground Motions at SF = 1.0

			Steel short (Ss) superstructure				Steel long (Sl) superstructure				Concrete short (Cs) superstructure			
			Short (15 ft)		Tall (40 ft)		Short (15 ft)		Tall (40 ft)		Short (15 ft)		Tall (40 ft)	
			Avg	StdDev	Avg	StdDev	Avg	StdDev	Avg	StdDev	Avg	StdDev	Avg	StdDev
Column pier substructure	Type I Bearings	Fixed base	3.66	0.43	4.72	0.68	4.23	0.58	5.09	0.68	4.50	0.60	6.37	0.85
		Soft soil	4.05	0.44	4.95	0.62	4.63	0.99	5.67	1.31	5.00	0.58	7.23	1.06
	Type II Bearings	Fixed base	3.09	0.44	4.26	0.99	4.14	0.74	5.78	1.13	3.50	0.45	5.01	0.73
		Soft soil	3.29	0.38	4.48	1.05	4.40	0.86	6.39	1.18	3.72	0.64	5.46	1.64
Wall pier substructure	Type I Bearings	Fixed base	3.05	0.41	4.49	0.61	3.74	0.59	5.17	0.67	3.91	0.63	5.95	0.65
		Soft soil	3.75	0.66	4.27	0.68	4.23	0.76	5.71	0.99	4.56	0.73	6.58	0.97
	Type II Bearings	Fixed base	3.04	0.52	4.25	0.70	3.58	0.57	5.61	0.87	3.17	0.39	4.79	0.65
		Soft soil	3.22	0.47	4.08	0.89	4.15	0.70	6.39	1.12	3.48	0.53	5.19	1.21

Table A.27. Peak Transverse Superstructure Displacement (in) – Pa Ground Motions at SF = 1.0

			Steel short (Ss) superstructure				Steel long (Sl) superstructure				Concrete short (Cs) superstructure			
			Short (15 ft)		Tall (40 ft)		Short (15 ft)		Tall (40 ft)		Short (15 ft)		Tall (40 ft)	
			Avg	StdDev	Avg	StdDev	Avg	StdDev	Avg	StdDev	Avg	StdDev	Avg	StdDev
Column pier substructure	Type I Bearings	Fixed base	7.01	2.61	12.52	3.68	8.47	1.62	12.64	2.44	8.97	2.72	13.51	2.13
		Soft soil	7.14	2.36	12.51	2.11	9.59	1.37	12.36	1.69	8.98	1.38	13.26	1.90
	Type II Bearings	Fixed base	8.70	4.22	12.17	2.12	11.40	4.54	13.76	2.48	9.03	5.19	13.01	1.86
		Soft soil	8.73	3.42	12.28	2.28	14.00	5.77	14.53	2.52	11.26	3.10	13.09	1.80
Wall pier substructure	Type I Bearings	Fixed base	7.59	2.94	7.45	3.00	8.47	1.32	8.27	1.29	8.52	1.68	9.15	2.47
		Soft soil	8.32	3.66	12.65	5.73	10.62	1.22	13.41	5.51	9.94	2.33	12.37	2.21
	Type II Bearings	Fixed base	9.30	3.84	9.00	4.05	9.65	3.40	9.27	1.16	8.92	4.64	7.80	4.47
		Soft soil	12.54	5.81	19.25	7.40	18.42	5.40	22.89	9.05	10.17	5.07	17.21	9.21

Table A.28. Peak Transverse Superstructure Displacement (in) – CG Ground Motions at SF = 1.0

			Steel short (Ss) superstructure				Steel long (Sl) superstructure				Concrete short (Cs) superstructure			
			Short (15 ft)		Tall (40 ft)		Short (15 ft)		Tall (40 ft)		Short (15 ft)		Tall (40 ft)	
			Avg	StdDev	Avg	StdDev	Avg	StdDev	Avg	StdDev	Avg	StdDev	Avg	StdDev
Column pier substructure	Type I Bearings	Fixed base	4.60	0.38	6.47	0.00	5.50	0.00	6.27	0.00	6.34	0.86	8.42	1.90
		Soft soil	5.00	0.00	6.68	0.00	5.57	0.00	6.80	0.00	6.37	1.11	8.04	0.95
	Type II Bearings	Fixed base	7.20	0.00	5.55	0.00	6.04	0.00	7.11	0.00	8.14	2.48	5.98	1.20
		Soft soil	5.85	0.00	5.44	0.00	5.06	0.00	6.92	0.00	4.37	0.92	6.16	0.82
Wall pier substructure	Type I Bearings	Fixed base	4.60	0.00	4.55	0.00	6.01	1.19	6.06	1.27	6.81	0.84	6.77	0.87
		Soft soil	5.23	0.00	6.64	0.00	5.79	1.26	6.22	1.35	6.49	1.26	7.04	0.92
	Type II Bearings	Fixed base	6.07	0.00	6.55	0.00	8.44	3.00	8.16	3.38	6.84	2.47	6.80	2.43
		Soft soil	7.43	0.00	8.82	0.00	6.49	5.11	6.01	3.09	4.92	1.55	5.56	1.54

Table A.29. Peak Longitudinal Abutment 1 Bearing Displacement (in) – Pa Ground Motions at SF = 1.0

			Steel short (Ss) superstructure				Steel long (Sl) superstructure				Concrete short (Cs) superstructure			
			Short (15 ft)		Tall (40 ft)		Short (15 ft)		Tall (40 ft)		Short (15 ft)		Tall (40 ft)	
			Avg	StdDev	Avg	StdDev	Avg	StdDev	Avg	StdDev	Avg	StdDev	Avg	StdDev
Column pier substructure	Type I Bearings	Fixed base	3.22	0.78	5.46	0.90	4.42	0.63	7.49	0.96	3.68	1.22	6.79	1.40
		Soft soil	2.69	0.37	4.34	0.88	4.44	1.18	7.60	0.96	1.95	0.69	5.39	0.96
	Type II Bearings	Fixed base	3.75	0.64	6.74	0.77	5.65	0.81	9.06	1.43	4.46	0.64	7.76	0.94
		Soft soil	3.51	0.67	6.68	0.90	5.76	1.06	10.32	1.65	4.37	0.66	8.39	1.22
Wall pier substructure	Type I Bearings	Fixed base	2.87	0.63	5.57	0.83	4.26	0.90	7.81	0.79	3.06	0.93	6.38	0.96
		Soft soil	2.27	0.46	3.93	0.70	4.33	0.94	8.46	0.92	1.63	1.11	6.27	1.50
	Type II Bearings	Fixed base	3.30	0.61	6.12	0.82	4.75	0.78	8.82	1.06	4.04	0.75	7.71	0.74
		Soft soil	3.31	0.73	5.28	0.53	5.35	0.98	9.72	1.20	4.17	0.94	8.57	1.14

Table A.30. Peak Longitudinal Abutment 1 Bearing Displacement (in) – CG Ground Motions at SF = 1.0

			Steel short (Ss) superstructure				Steel long (Sl) superstructure				Concrete short (Cs) superstructure			
			Short (15 ft)		Tall (40 ft)		Short (15 ft)		Tall (40 ft)		Short (15 ft)		Tall (40 ft)	
			Avg	StdDev	Avg	StdDev	Avg	StdDev	Avg	StdDev	Avg	StdDev	Avg	StdDev
Column pier substructure	Type I Bearings	Fixed base	2.97	0.36	3.71	0.61	2.88	0.62	3.80	0.65	2.29	0.90	4.72	0.86
		Soft soil	1.93	0.72	2.67	0.53	2.22	1.03	3.21	1.28	0.67	0.74	3.28	0.85
	Type II Bearings	Fixed base	2.89	0.45	3.84	0.93	3.18	0.65	4.71	1.02	2.89	0.49	4.18	0.63
		Soft soil	2.63	0.33	3.68	0.76	3.09	0.94	4.94	1.16	2.56	0.46	4.17	1.73
Wall pier substructure	Type I Bearings	Fixed base	2.22	0.73	3.76	0.49	2.38	0.70	3.93	0.66	1.38	1.13	4.03	0.68
		Soft soil	1.52	0.84	1.81	0.74	2.06	0.84	3.31	1.03	0.31	0.71	2.05	1.18
	Type II Bearings	Fixed base	2.83	0.42	3.92	0.57	2.75	0.58	4.66	0.93	2.45	0.46	4.12	0.62
		Soft soil	2.52	0.56	3.35	0.92	2.79	0.75	4.81	1.18	2.30	0.31	4.00	1.28

Table A.31. Peak Transverse Abutment 1 Bearing Displacement (in) – Pa Ground Motions at SF = 1.0

			Steel short (Ss) superstructure				Steel long (Sl) superstructure				Concrete short (Cs) superstructure			
			Short (15 ft)		Tall (40 ft)		Short (15 ft)		Tall (40 ft)		Short (15 ft)		Tall (40 ft)	
			Avg	StdDev	Avg	StdDev	Avg	StdDev	Avg	StdDev	Avg	StdDev	Avg	StdDev
Column pier substructure	Type I Bearings	Fixed base	4.42	2.64	9.20	1.60	6.30	1.58	10.13	2.10	4.51	2.61	8.73	2.10
		Soft soil	4.32	2.36	9.68	2.10	7.07	1.32	9.80	1.63	4.05	1.42	8.26	1.83
	Type II Bearings	Fixed base	8.04	4.21	11.52	2.11	8.45	1.86	12.47	2.49	8.03	5.19	12.00	1.86
		Soft soil	8.04	3.42	11.59	2.25	8.97	2.09	12.71	1.78	8.32	2.15	12.02	1.77
Wall pier substructure	Type I Bearings	Fixed base	4.84	2.94	4.75	2.99	6.10	1.32	5.97	1.29	3.65	1.67	4.51	2.44
		Soft soil	5.47	3.64	9.81	5.71	8.06	1.20	9.83	2.20	4.86	2.32	7.42	2.19
	Type II Bearings	Fixed base	8.64	3.85	8.33	4.05	7.80	1.44	7.97	1.16	7.91	4.64	6.79	4.47
		Soft soil	11.86	5.81	18.56	7.40	10.83	2.22	13.33	2.67	9.11	5.07	14.34	6.79

Table A.32. Peak Transverse Abutment 1 Bearing Displacement (in) – CG Ground Motions at SF = 1.0

			Steel short (Ss) superstructure				Steel long (Sl) superstructure				Concrete short (Cs) superstructure			
			Short (15 ft)		Tall (40 ft)		Short (15 ft)		Tall (40 ft)		Short (15 ft)		Tall (40 ft)	
			Avg	StdDev	Avg	StdDev	Avg	StdDev	Avg	StdDev	Avg	StdDev	Avg	StdDev
Column pier substructure	Type I Bearings	Fixed base	1.96	0.42	3.74	0.97	3.30	1.15	3.88	1.18	1.87	0.93	3.62	1.86
		Soft soil	2.17	0.60	3.80	0.96	3.06	1.00	4.29	1.40	1.38	1.07	3.07	0.88
	Type II Bearings	Fixed base	4.64	1.20	4.75	1.06	4.29	1.51	5.82	1.49	4.34	0.86	4.97	1.20
		Soft soil	4.00	1.18	4.54	1.13	3.21	0.86	5.57	1.63	3.06	0.78	5.08	0.81
Wall pier substructure	Type I Bearings	Fixed base	1.87	0.49	1.84	0.55	3.66	1.19	3.71	1.29	1.93	0.89	1.99	0.89
		Soft soil	2.42	0.51	3.82	1.53	3.24	1.28	3.78	1.37	1.33	1.31	2.02	1.10
	Type II Bearings	Fixed base	4.28	1.17	4.61	1.10	4.59	1.24	4.76	1.45	4.38	1.35	4.67	1.10
		Soft soil	4.78	1.18	6.87	2.24	4.14	2.53	4.67	1.98	3.66	0.88	4.51	1.54

Table A.33. Peak Longitudinal Abutment 2 Bearing Displacement (in) – Pa Ground Motions at SF = 1.0

			Steel short (Ss) superstructure				Steel long (Sl) superstructure				Concrete short (Cs) superstructure			
			Short (15 ft)		Tall (40 ft)		Short (15 ft)		Tall (40 ft)		Short (15 ft)		Tall (40 ft)	
			Avg	StdDev	Avg	StdDev	Avg	StdDev	Avg	StdDev	Avg	StdDev	Avg	StdDev
Column pier substructure	Type I Bearings	Fixed base	3.67	0.51	4.97	0.94	4.30	0.76	7.34	0.94	3.56	0.80	6.74	1.25
		Soft soil	2.52	0.75	4.50	0.74	4.69	1.13	7.68	0.97	2.55	0.86	5.28	0.95
	Type II Bearings	Fixed base	3.81	0.69	6.65	0.72	5.73	0.85	8.95	1.56	4.52	0.62	7.87	1.03
		Soft soil	3.56	0.61	6.95	1.05	6.15	1.02	10.46	1.79	4.51	0.94	8.61	1.28
Wall pier substructure	Type I Bearings	Fixed base	3.04	0.66	5.12	1.14	4.23	0.82	7.62	0.89	3.35	0.76	5.82	1.19
		Soft soil	2.53	0.76	4.07	0.73	4.47	1.08	8.24	0.76	2.70	0.66	6.09	1.33
	Type II Bearings	Fixed base	3.26	0.50	6.13	0.65	4.93	0.81	8.82	1.03	4.05	0.80	7.72	0.85
		Soft soil	3.55	0.68	5.57	0.61	5.58	0.86	9.82	1.12	4.45	1.00	8.65	1.22

Table A.34. Peak Longitudinal Abutment 2 Bearing Displacement (in) – CG Ground Motions at SF = 1.0

			Steel short (Ss) superstructure				Steel long (Sl) superstructure				Concrete short (Cs) superstructure			
			Short (15 ft)		Tall (40 ft)		Short (15 ft)		Tall (40 ft)		Short (15 ft)		Tall (40 ft)	
			Avg	StdDev	Avg	StdDev	Avg	StdDev	Avg	StdDev	Avg	StdDev	Avg	StdDev
Column pier substructure	Type I Bearings	Fixed base	2.85	0.35	3.86	0.72	2.62	0.59	3.50	0.71	2.27	0.73	4.25	1.01
		Soft soil	1.70	0.54	2.72	0.66	2.49	1.16	3.37	1.06	0.86	0.63	2.59	1.11
	Type II Bearings	Fixed base	2.68	0.35	3.96	1.06	3.15	0.77	4.77	1.16	2.76	0.54	4.30	0.87
		Soft soil	2.63	0.35	3.76	1.07	3.04	0.74	4.88	1.18	2.72	0.70	4.22	1.42
Wall pier substructure	Type I Bearings	Fixed base	2.31	0.69	3.80	0.75	2.41	0.48	3.54	0.75	1.85	0.53	3.73	0.99
		Soft soil	1.72	0.84	1.90	0.69	2.19	1.08	3.33	1.03	0.59	0.92	2.10	1.38
	Type II Bearings	Fixed base	2.70	0.58	3.97	0.76	2.60	0.57	4.54	0.91	2.47	0.45	4.02	0.70
		Soft soil	2.57	0.38	3.32	0.75	2.90	0.64	4.93	0.96	2.58	0.58	3.92	1.10

Table A.35. Peak Transverse Abutment 2 Bearing Displacement (in) – Pa Ground Motions at SF = 1.0

			Steel short (Ss) superstructure				Steel long (Sl) superstructure				Concrete short (Cs) superstructure			
			Short (15 ft)		Tall (40 ft)		Short (15 ft)		Tall (40 ft)		Short (15 ft)		Tall (40 ft)	
			Avg	StdDev	Avg	StdDev	Avg	StdDev	Avg	StdDev	Avg	StdDev	Avg	StdDev
Column pier substructure	Type I Bearings	Fixed base	2.67	1.96	9.87	3.72	5.11	2.62	10.35	2.40	2.50	2.08	8.50	2.55
		Soft soil	2.86	2.32	9.47	2.15	6.29	3.95	9.52	1.80	3.21	2.44	7.75	1.80
	Type II Bearings	Fixed base	5.88	2.45	11.14	2.12	10.15	4.51	11.96	2.51	7.97	2.52	11.78	2.14
		Soft soil	6.65	2.12	11.39	2.44	12.65	5.77	13.18	2.51	10.21	3.09	11.91	1.87
Wall pier substructure	Type I Bearings	Fixed base	2.15	2.12	2.25	2.17	5.02	2.66	4.35	2.65	2.05	1.90	1.62	1.95
		Soft soil	4.57	2.68	7.47	5.22	7.67	4.25	10.90	5.49	3.77	3.47	5.72	2.84
	Type II Bearings	Fixed base	6.16	1.30	6.23	1.53	8.35	3.40	7.59	2.27	5.97	2.39	6.46	2.27
		Soft soil	9.19	3.65	13.54	8.38	17.06	5.40	21.55	9.06	9.05	3.52	16.17	9.20

Table A.36. Peak Transverse Abutment 2 Bearing Displacement (in) – CG Ground Motions at SF = 1.0

			Steel short (Ss) superstructure				Steel long (Sl) superstructure				Concrete short (Cs) superstructure			
			Short (15 ft)		Tall (40 ft)		Short (15 ft)		Tall (40 ft)		Short (15 ft)		Tall (40 ft)	
			Avg	StdDev	Avg	StdDev	Avg	StdDev	Avg	StdDev	Avg	StdDev	Avg	StdDev
Column pier substructure	Type I Bearings	Fixed base	0.43	0.37	2.98	1.28	2.39	1.42	3.47	1.07	0.21	0.44	2.98	1.20
		Soft soil	1.42	0.38	2.88	1.34	1.80	0.77	3.21	1.01	1.07	0.57	1.84	0.99
	Type II Bearings	Fixed base	6.54	2.56	4.89	1.29	4.76	2.66	5.73	1.22	7.13	2.48	4.74	1.55
		Soft soil	5.16	2.41	4.75	1.26	3.74	1.57	5.55	1.27	3.31	0.94	4.74	1.34
Wall pier substructure	Type I Bearings	Fixed base	0.10	0.20	0.08	0.11	2.79	1.59	3.12	1.85	0.00	0.00	0.08	0.26
		Soft soil	0.84	0.63	1.78	1.17	1.71	0.82	2.19	1.32	0.27	0.54	0.53	0.81
	Type II Bearings	Fixed base	5.41	2.44	5.90	2.51	7.14	3.00	6.87	3.39	5.83	2.47	5.79	2.43
		Soft soil	6.74	2.40	8.13	2.25	5.15	5.10	4.69	3.09	3.87	1.55	4.39	2.10

Table A.37. Peak Longitudinal Pier 1 Bearing Displacement (in) – Pa Ground Motions at SF = 1.0

			Steel short (Ss) superstructure				Steel long (Sl) superstructure				Concrete short (Cs) superstructure			
			Short (15 ft)		Tall (40 ft)		Short (15 ft)		Tall (40 ft)		Short (15 ft)		Tall (40 ft)	
			Avg	StdDev	Avg	StdDev	Avg	StdDev	Avg	StdDev	Avg	StdDev	Avg	StdDev
Column pier substructure	Type I Bearings	Fixed base	0.03	0.11	0.29	0.69	0.00	0.00	0.00	0.00	0.00	0.00	0.11	0.23
		Soft soil	0.15	0.29	0.57	0.49	0.00	0.00	0.00	0.00	0.00	0.00	0.41	0.42
	Type II Bearings	Fixed base	2.86	0.66	2.31	0.70	4.17	0.82	1.16	0.24	3.75	0.69	2.34	0.58
		Soft soil	2.89	0.59	2.62	1.06	4.65	1.14	1.66	0.82	4.11	0.58	2.08	0.75
Wall pier substructure	Type I Bearings	Fixed base	0.39	0.59	1.24	1.89	0.00	0.00	0.00	0.00	0.09	0.20	0.00	0.00
		Soft soil	0.28	0.43	4.37	3.17	0.00	0.00	0.00	0.00	0.00	0.00	0.00	0.00
	Type II Bearings	Fixed base	2.48	0.52	3.62	2.50	3.80	0.76	1.21	0.33	3.67	0.85	1.89	0.53
		Soft soil	2.76	0.71	7.77	3.32	4.33	0.75	1.49	0.75	4.00	0.90	2.38	0.91

Table A.38. Peak Longitudinal Pier 1 Bearing Displacement (in) – CG Ground Motions at SF = 1.0

			Steel short (Ss) superstructure				Steel long (Sl) superstructure				Concrete short (Cs) superstructure			
			Short (15 ft)		Tall (40 ft)		Short (15 ft)		Tall (40 ft)		Short (15 ft)		Tall (40 ft)	
			Avg	StdDev	Avg	StdDev	Avg	StdDev	Avg	StdDev	Avg	StdDev	Avg	StdDev
Column pier substructure	Type I Bearings	Fixed base	0.00	0.00	0.00	0.00	0.00	0.00	0.00	0.00	0.00	0.00	0.05	0.13
		Soft soil	0.16	0.47	0.02	0.05	0.00	0.00	0.00	0.00	0.00	0.00	0.41	0.48
	Type II Bearings	Fixed base	1.89	0.42	1.18	0.52	1.78	0.88	1.06	0.56	2.17	0.50	1.26	0.59
		Soft soil	2.18	0.57	0.97	0.33	1.70	0.81	1.29	0.49	2.21	0.49	1.22	1.01
Wall pier substructure	Type I Bearings	Fixed base	0.00	0.00	0.00	0.00	0.00	0.00	0.00	0.00	0.00	0.00	0.00	0.00
		Soft soil	0.12	0.38	1.52	0.62	0.00	0.00	0.00	0.00	0.08	0.24	0.03	0.09
	Type II Bearings	Fixed base	1.91	0.43	1.34	0.45	1.58	0.49	1.03	0.65	1.94	0.30	1.37	0.38
		Soft soil	2.08	0.61	2.57	1.24	1.71	0.67	1.27	0.65	2.17	0.49	1.11	0.26

Table A.39. Peak Transverse Pier 1 Bearing Displacement (in) – Pa Ground Motions at SF = 1.0

			Steel short (Ss) superstructure				Steel long (Sl) superstructure				Concrete short (Cs) superstructure			
			Short (15 ft)		Tall (40 ft)		Short (15 ft)		Tall (40 ft)		Short (15 ft)		Tall (40 ft)	
			Avg	StdDev	Avg	StdDev	Avg	StdDev	Avg	StdDev	Avg	StdDev	Avg	StdDev
Column pier substructure	Type I Bearings	Fixed base	1.96	2.15	0.00	0.00	0.00	0.00	0.00	0.00	2.12	1.90	0.00	0.00
		Soft soil	0.83	1.99	0.00	0.00	0.00	0.00	0.00	0.00	0.51	0.82	0.00	0.00
	Type II Bearings	Fixed base	5.61	3.22	2.27	2.24	4.15	1.35	0.00	0.00	5.29	3.54	0.24	0.16
		Soft soil	4.94	3.59	1.37	0.84	3.25	1.70	0.00	0.00	3.47	1.25	0.15	0.16
Wall pier substructure	Type I Bearings	Fixed base	2.48	2.04	2.44	2.11	0.69	0.92	0.83	1.00	2.84	1.38	3.25	1.63
		Soft soil	1.91	3.39	6.25	5.84	0.11	0.25	0.45	0.36	1.42	3.05	3.73	3.20
	Type II Bearings	Fixed base	5.45	3.10	5.31	2.95	4.89	1.32	5.10	1.35	5.25	3.39	4.91	3.17
		Soft soil	8.83	5.37	15.68	7.47	4.07	2.04	9.41	5.51	6.25	5.56	11.86	8.95

Table A.40. Peak Transverse Pier 1 Bearing Displacement (in) – CG Ground Motions at SF = 1.0

			Steel short (Ss) superstructure				Steel long (Sl) superstructure				Concrete short (Cs) superstructure			
			Short (15 ft)		Tall (40 ft)		Short (15 ft)		Tall (40 ft)		Short (15 ft)		Tall (40 ft)	
			Avg	StdDev	Avg	StdDev	Avg	StdDev	Avg	StdDev	Avg	StdDev	Avg	StdDev
Column pier substructure	Type I Bearings	Fixed base	0.06	0.12	0.00	0.00	0.00	0.00	0.00	0.00	0.32	0.46	0.00	0.00
		Soft soil	0.00	0.00	0.01	0.03	0.00	0.00	0.00	0.00	0.00	0.00	0.00	0.00
	Type II Bearings	Fixed base	1.57	0.56	1.43	0.69	1.02	0.57	0.00	0.00	1.61	0.45	0.31	0.26
		Soft soil	1.36	0.56	1.27	0.64	0.12	0.25	0.00	0.00	0.83	0.44	0.11	0.10
Wall pier substructure	Type I Bearings	Fixed base	0.14	0.22	0.20	0.27	0.00	0.00	0.02	0.06	0.88	0.71	0.94	0.65
		Soft soil	0.07	0.15	0.61	1.02	0.00	0.00	0.00	0.00	0.08	0.18	0.31	0.53
	Type II Bearings	Fixed base	1.94	0.44	2.07	0.61	1.76	0.62	1.82	0.67	2.07	0.46	2.24	0.52
		Soft soil	2.16	0.40	3.79	1.71	0.48	0.67	1.35	1.22	1.50	0.49	2.12	0.97

Table A.41. Peak Longitudinal Pier 2 Bearing Displacement (in) – Pa Ground Motions at SF = 1.0

			Steel short (Ss) superstructure				Steel long (Sl) superstructure				Concrete short (Cs) superstructure			
			Short (15 ft)		Tall (40 ft)		Short (15 ft)		Tall (40 ft)		Short (15 ft)		Tall (40 ft)	
			Avg	StdDev	Avg	StdDev	Avg	StdDev	Avg	StdDev	Avg	StdDev	Avg	StdDev
Column pier substructure	Type I Bearings	Fixed base	0.49	0.10	0.61	0.23	0.11	0.00	0.08	0.01	0.37	0.03	0.14	0.07
		Soft soil	0.38	0.03	0.51	0.08	0.11	0.00	0.05	0.01	0.32	0.04	0.08	0.01
	Type II Bearings	Fixed base	0.47	0.04	0.91	0.62	0.12	0.00	0.08	0.01	0.36	0.02	0.14	0.04
		Soft soil	0.37	0.04	0.54	0.08	0.11	0.00	0.06	0.01	0.29	0.06	0.07	0.01
Wall pier substructure	Type I Bearings	Fixed base	2.26	0.74	3.47	0.85	0.31	0.07	0.22	0.06	0.67	0.08	0.62	0.08
		Soft soil	1.33	0.75	4.85	0.80	0.25	0.04	0.14	0.05	0.49	0.06	0.67	0.11
	Type II Bearings	Fixed base	2.42	0.86	3.64	1.06	0.33	0.07	0.23	0.07	0.65	0.14	0.58	0.07
		Soft soil	1.86	0.94	4.62	1.07	0.27	0.03	0.15	0.03	0.48	0.06	0.58	0.12

Table A.42. Peak Longitudinal Pier 2 Bearing Displacement (in) – CG Ground Motions at SF = 1.0

			Steel short (Ss) superstructure				Steel long (Sl) superstructure				Concrete short (Cs) superstructure			
			Short (15 ft)		Tall (40 ft)		Short (15 ft)		Tall (40 ft)		Short (15 ft)		Tall (40 ft)	
			Avg	StdDev	Avg	StdDev	Avg	StdDev	Avg	StdDev	Avg	StdDev	Avg	StdDev
Column pier substructure	Type I Bearings	Fixed base	0.49	0.04	0.42	0.08	0.11	0.00	0.07	0.01	0.39	0.02	0.12	0.04
		Soft soil	0.43	0.04	0.44	0.06	0.10	0.00	0.05	0.01	0.31	0.04	0.08	0.01
	Type II Bearings	Fixed base	0.47	0.05	0.39	0.12	0.12	0.00	0.08	0.01	0.37	0.02	0.11	0.02
		Soft soil	0.39	0.03	0.40	0.06	0.11	0.01	0.05	0.01	0.29	0.04	0.07	0.01
Wall pier substructure	Type I Bearings	Fixed base	2.01	0.31	1.31	0.55	0.27	0.11	0.22	0.09	0.68	0.17	0.53	0.04
		Soft soil	1.45	0.89	2.49	0.75	0.20	0.06	0.12	0.06	0.52	0.09	0.63	0.07
	Type II Bearings	Fixed base	2.24	0.40	0.91	0.38	0.26	0.10	0.24	0.06	0.56	0.09	0.42	0.04
		Soft soil	1.74	0.63	2.32	1.00	0.21	0.05	0.13	0.03	0.47	0.07	0.50	0.12

Table A.43. Peak Transverse Pier 2 Bearing Displacement (in) – Pa Ground Motions at SF = 1.0

			Steel short (Ss) superstructure				Steel long (Sl) superstructure				Concrete short (Cs) superstructure			
			Short (15 ft)		Tall (40 ft)		Short (15 ft)		Tall (40 ft)		Short (15 ft)		Tall (40 ft)	
			Avg	StdDev	Avg	StdDev	Avg	StdDev	Avg	StdDev	Avg	StdDev	Avg	StdDev
Column pier substructure	Type I Bearings	Fixed base	4.96	1.63	0.27	0.03	5.36	2.48	0.17	0.02	5.72	1.36	0.29	0.03
		Soft soil	4.84	1.93	0.28	0.04	3.43	4.17	0.16	0.02	6.65	1.61	0.26	0.03
	Type II Bearings	Fixed base	5.97	2.04	0.31	0.04	7.43	3.41	0.16	0.02	6.83	1.95	0.27	0.02
		Soft soil	6.09	2.07	0.30	0.03	6.76	5.55	0.16	0.02	7.99	2.04	0.27	0.03
Wall pier substructure	Type I Bearings	Fixed base	4.82	1.47	4.78	1.67	5.89	1.93	5.50	1.93	5.78	1.34	5.60	1.38
		Soft soil	6.19	2.58	9.96	6.53	6.53	4.26	9.32	5.81	7.44	2.75	10.34	3.79
	Type II Bearings	Fixed base	5.65	1.96	5.69	1.67	7.39	2.72	7.13	2.02	5.99	1.99	5.98	1.79
		Soft soil	9.13	3.79	13.72	7.97	12.24	3.84	17.63	6.16	8.14	4.26	14.20	8.31

Table A.44. Peak Transverse Pier 2 Bearing Displacement (in) – CG Ground Motions at SF = 1.0

			Steel short (Ss) superstructure				Steel long (Sl) superstructure				Concrete short (Cs) superstructure			
			Short (15 ft)		Tall (40 ft)		Short (15 ft)		Tall (40 ft)		Short (15 ft)		Tall (40 ft)	
			Avg	StdDev	Avg	StdDev	Avg	StdDev	Avg	StdDev	Avg	StdDev	Avg	StdDev
Column pier substructure	Type I Bearings	Fixed base	2.53	0.46	0.30	0.03	1.84	1.69	0.14	0.02	3.17	0.61	0.31	0.02
		Soft soil	2.93	0.49	0.38	0.05	0.52	0.14	0.11	0.02	1.92	1.81	0.30	0.05
	Type II Bearings	Fixed base	4.45	1.13	0.37	0.07	2.84	2.16	0.17	0.03	5.05	1.25	0.28	0.06
		Soft soil	3.46	1.47	0.39	0.06	0.62	0.22	0.14	0.03	1.05	1.27	0.26	0.06
Wall pier substructure	Type I Bearings	Fixed base	2.44	0.39	2.42	0.43	3.76	1.29	3.93	1.47	3.08	0.47	3.10	0.51
		Soft soil	2.95	0.57	3.30	1.10	0.60	0.10	0.57	0.14	2.75	1.16	2.25	2.06
	Type II Bearings	Fixed base	4.15	1.09	4.34	1.21	5.75	1.69	5.51	2.25	4.59	1.08	4.47	1.12
		Soft soil	4.61	1.22	5.56	1.50	1.76	3.49	1.25	1.98	2.04	1.73	1.82	2.14

Table A.45. Peak Longitudinal Pier 1 Displacement (in) – Pa Ground Motions at SF = 1.0

			Steel short (Ss) superstructure				Steel long (Sl) superstructure				Concrete short (Cs) superstructure			
			Short (15 ft)		Tall (40 ft)		Short (15 ft)		Tall (40 ft)		Short (15 ft)		Tall (40 ft)	
			Avg	StdDev	Avg	StdDev	Avg	StdDev	Avg	StdDev	Avg	StdDev	Avg	StdDev
Column pier substructure	Type I Bearings	Fixed base	0.96	0.20	7.23	1.54	1.79	0.71	8.99	1.10	2.14	0.58	9.34	1.04
		Soft soil	1.08	0.25	7.37	0.99	1.73	0.67	9.15	0.90	2.15	0.50	9.32	1.27
	Type II Bearings	Fixed base	0.50	0.07	6.92	0.78	0.81	0.05	8.79	1.29	0.64	0.07	7.70	0.95
		Soft soil	0.60	0.08	7.36	1.69	0.88	0.12	10.29	1.93	0.66	0.07	8.53	1.03
Wall pier substructure	Type I Bearings	Fixed base	0.42	0.13	8.70	2.11	1.62	0.89	9.63	1.23	2.28	0.59	9.15	1.20
		Soft soil	0.54	0.26	10.18	2.86	1.53	0.70	10.02	1.09	2.32	0.57	10.13	1.50
	Type II Bearings	Fixed base	0.25	0.04	8.77	2.07	0.38	0.07	9.56	1.37	0.31	0.03	8.48	1.20
		Soft soil	0.27	0.02	9.85	2.43	0.49	0.34	9.83	1.09	0.32	0.05	9.67	1.36

Table A.46. Peak Longitudinal Pier 1 Displacement (in) – CG Ground Motions at SF = 1.0

			Steel short (Ss) superstructure				Steel long (Sl) superstructure				Concrete short (Cs) superstructure			
			Short (15 ft)		Tall (40 ft)		Short (15 ft)		Tall (40 ft)		Short (15 ft)		Tall (40 ft)	
			Avg	StdDev	Avg	StdDev	Avg	StdDev	Avg	StdDev	Avg	StdDev	Avg	StdDev
Column pier substructure	Type I Bearings	Fixed base	1.00	0.44	4.63	0.92	1.06	0.41	5.01	0.79	1.25	0.37	6.16	1.23
		Soft soil	0.99	0.34	5.07	0.49	0.97	0.35	5.83	1.35	1.32	0.35	7.04	1.13
	Type II Bearings	Fixed base	0.69	0.19	3.85	0.94	0.80	0.20	5.34	0.90	0.66	0.16	4.39	0.74
		Soft soil	0.64	0.11	4.18	0.68	0.77	0.14	5.46	0.84	0.64	0.06	4.54	1.13
Wall pier substructure	Type I Bearings	Fixed base	0.72	0.36	4.87	0.97	0.77	0.42	4.51	0.72	1.11	0.41	5.77	0.79
		Soft soil	0.53	0.63	6.17	1.02	0.53	0.40	4.72	1.05	0.94	0.65	6.04	1.49
	Type II Bearings	Fixed base	0.59	0.29	4.27	1.20	0.60	0.32	4.76	1.00	0.54	0.26	4.11	1.13
		Soft soil	0.33	0.13	4.92	1.37	0.37	0.14	5.40	1.31	0.32	0.08	4.31	1.36

Table A.47. Peak Transverse Pier 1 Displacement (in) – Pa Ground Motions at SF = 1.0

			Steel short (Ss) superstructure				Steel long (Sl) superstructure				Concrete short (Cs) superstructure			
			Short (15 ft)		Tall (40 ft)		Short (15 ft)		Tall (40 ft)		Short (15 ft)		Tall (40 ft)	
			Avg	StdDev	Avg	StdDev	Avg	StdDev	Avg	StdDev	Avg	StdDev	Avg	StdDev
Column pier substructure	Type I Bearings	Fixed base	0.68	0.14	9.64	1.63	1.68	0.92	10.71	2.11	1.21	0.31	11.13	2.26
		Soft soil	0.44	0.25	9.56	2.12	0.74	0.24	9.66	1.70	0.58	0.23	10.21	1.84
	Type II Bearings	Fixed base	0.36	0.06	9.16	2.47	0.88	0.15	12.14	2.17	0.51	0.07	10.77	1.91
		Soft soil	0.29	0.07	8.93	2.41	0.68	0.24	11.11	1.71	0.40	0.07	10.12	1.79
Wall pier substructure	Type I Bearings	Fixed base	0.00	0.00	0.08	0.02	0.01	0.00	0.12	0.02	0.00	0.00	0.11	0.01
		Soft soil	0.00	0.00	0.07	0.02	0.00	0.00	0.11	0.02	0.00	0.00	0.10	0.02
	Type II Bearings	Fixed base	0.00	0.00	0.05	0.01	0.00	0.00	0.10	0.01	0.00	0.00	0.07	0.01
		Soft soil	0.00	0.00	0.04	0.01	0.00	0.00	0.09	0.02	0.00	0.00	0.07	0.01

Table A.48. Peak Transverse Pier 1 Displacement (in) – CG Ground Motions at SF = 1.0

			Steel short (Ss) superstructure				Steel long (Sl) superstructure				Concrete short (Cs) superstructure			
			Short (15 ft)		Tall (40 ft)		Short (15 ft)		Tall (40 ft)		Short (15 ft)		Tall (40 ft)	
			Avg	StdDev	Avg	StdDev	Avg	StdDev	Avg	StdDev	Avg	StdDev	Avg	StdDev
Column pier substructure	Type I Bearings	Fixed base	0.41	0.05	4.07	1.05	0.68	0.20	4.79	1.18	0.75	0.18	5.34	1.11
		Soft soil	0.19	0.03	3.42	0.87	0.33	0.06	3.93	0.71	0.30	0.07	4.58	0.75
	Type II Bearings	Fixed base	0.28	0.05	2.99	0.73	0.56	0.06	5.27	1.22	0.37	0.03	4.02	1.00
		Soft soil	0.17	0.03	2.62	0.59	0.32	0.06	4.28	1.10	0.23	0.04	3.47	0.77
Wall pier substructure	Type I Bearings	Fixed base	0.00	0.00	0.06	0.01	0.00	0.00	0.09	0.01	0.00	0.00	0.09	0.01
		Soft soil	0.00	0.00	0.04	0.01	0.00	0.00	0.05	0.01	0.00	0.00	0.06	0.01
	Type II Bearings	Fixed base	0.00	0.00	0.05	0.02	0.00	0.00	0.07	0.01	0.00	0.00	0.05	0.01
		Soft soil	0.00	0.00	0.03	0.00	0.00	0.00	0.05	0.01	0.00	0.00	0.04	0.00

Table A.49. Peak Longitudinal Pier 2 Displacement (in) – Pa Ground Motions at SF = 1.0

			Steel short (Ss) superstructure				Steel long (Sl) superstructure				Concrete short (Cs) superstructure			
			Short (15 ft)		Tall (40 ft)		Short (15 ft)		Tall (40 ft)		Short (15 ft)		Tall (40 ft)	
			Avg	StdDev	Avg	StdDev	Avg	StdDev	Avg	StdDev	Avg	StdDev	Avg	StdDev
Column pier substructure	Type I Bearings	Fixed base	3.33	0.41	5.96	0.65	4.69	0.69	7.83	0.89	4.38	0.49	7.94	0.77
		Soft soil	2.98	0.44	5.97	0.88	4.42	0.86	7.96	0.86	4.08	0.40	7.87	0.85
	Type II Bearings	Fixed base	2.98	0.53	6.62	0.91	5.16	0.65	8.63	1.37	3.81	0.51	7.35	0.92
		Soft soil	2.57	0.43	6.62	0.99	4.93	0.85	9.79	1.60	3.35	0.62	7.91	1.12
Wall pier substructure	Type I Bearings	Fixed base	2.01	0.64	8.50	1.13	4.45	0.77	8.97	0.76	4.22	0.39	8.59	0.74
		Soft soil	2.31	0.29	7.45	1.14	3.78	0.55	9.06	0.68	3.65	0.42	9.34	1.26
	Type II Bearings	Fixed base	1.57	0.70	8.51	0.88	4.58	0.64	9.24	1.02	3.54	0.63	8.28	0.75
		Soft soil	1.96	0.42	7.54	1.13	4.05	0.51	9.59	0.96	3.08	0.59	8.71	1.24

Table A.50. Peak Longitudinal Pier 2 Displacement (in) – CG Ground Motions at SF = 1.0

			Steel short (Ss) superstructure				Steel long (Sl) superstructure				Concrete short (Cs) superstructure			
			Short (15 ft)		Tall (40 ft)		Short (15 ft)		Tall (40 ft)		Short (15 ft)		Tall (40 ft)	
			Avg	StdDev	Avg	StdDev	Avg	StdDev	Avg	StdDev	Avg	StdDev	Avg	StdDev
Column pier substructure	Type I Bearings	Fixed base	2.56	0.35	4.11	0.56	3.11	0.47	4.21	0.56	3.17	0.50	5.37	0.79
		Soft soil	2.45	0.38	4.09	0.54	2.64	0.80	4.31	1.02	2.84	0.45	5.61	0.84
	Type II Bearings	Fixed base	2.08	0.35	3.70	0.82	3.06	0.61	4.81	0.96	2.36	0.37	4.19	0.60
		Soft soil	1.78	0.30	3.74	0.84	2.49	0.71	4.91	0.91	1.83	0.51	4.19	1.34
Wall pier substructure	Type I Bearings	Fixed base	1.65	0.41	4.75	0.88	2.93	0.43	4.86	0.63	2.83	0.49	5.77	0.63
		Soft soil	1.78	0.30	4.47	0.99	2.31	0.51	4.49	1.02	2.42	0.48	5.70	0.95
	Type II Bearings	Fixed base	1.47	0.29	4.28	0.84	2.78	0.44	5.28	0.83	2.28	0.30	4.61	0.67
		Soft soil	1.34	0.25	4.26	1.39	2.30	0.44	5.05	0.94	1.69	0.39	4.17	1.13

Table A.51. Peak Transverse Pier 2 Displacement (in) – Pa Ground Motions at SF = 1.0

			Steel short (Ss) superstructure				Steel long (Sl) superstructure				Concrete short (Cs) superstructure			
			Short (15 ft)		Tall (40 ft)		Short (15 ft)		Tall (40 ft)		Short (15 ft)		Tall (40 ft)	
			Avg	StdDev	Avg	StdDev	Avg	StdDev	Avg	StdDev	Avg	StdDev	Avg	StdDev
Column pier substructure	Type I Bearings	Fixed base	0.26	0.04	11.16	1.94	1.65	0.28	11.47	2.09	0.45	0.04	11.77	2.36
		Soft soil	0.29	0.05	10.66	2.13	1.29	0.64	9.94	1.79	0.49	0.04	10.60	1.86
	Type II Bearings	Fixed base	0.28	0.03	11.06	2.09	1.91	0.44	12.39	2.22	0.45	0.04	11.54	1.95
		Soft soil	0.30	0.04	10.43	2.35	2.02	0.54	12.03	2.00	0.47	0.04	10.70	1.86
Wall pier substructure	Type I Bearings	Fixed base	0.00	0.00	0.04	0.02	0.00	0.00	0.11	0.02	0.00	0.00	0.07	0.02
		Soft soil	0.00	0.00	0.06	0.02	0.00	0.00	0.12	0.01	0.00	0.00	0.09	0.02
	Type II Bearings	Fixed base	0.00	0.00	0.04	0.02	0.00	0.00	0.11	0.02	0.00	0.00	0.07	0.02
		Soft soil	0.00	0.00	0.05	0.02	0.00	0.00	0.12	0.01	0.00	0.00	0.07	0.01

Table A.52. Peak Transverse Pier 2 Displacement (in) – CG Ground Motions at SF = 1.0

			Steel short (Ss) superstructure				Steel long (Sl) superstructure				Concrete short (Cs) superstructure			
			Short (15 ft)		Tall (40 ft)		Short (15 ft)		Tall (40 ft)		Short (15 ft)		Tall (40 ft)	
			Avg	StdDev	Avg	StdDev	Avg	StdDev	Avg	StdDev	Avg	StdDev	Avg	StdDev
Column pier substructure	Type I Bearings	Fixed base	0.25	0.03	4.85	1.32	1.31	0.36	5.01	1.15	0.45	0.02	6.11	1.18
		Soft soil	0.24	0.02	4.11	1.23	0.43	0.13	4.01	0.76	0.40	0.04	4.91	0.97
	Type II Bearings	Fixed base	0.26	0.03	4.28	1.25	1.52	0.39	5.78	1.14	0.44	0.03	4.74	1.31
		Soft soil	0.24	0.03	3.67	1.08	0.54	0.30	4.66	1.19	0.35	0.06	3.90	0.95
Wall pier substructure	Type I Bearings	Fixed base	0.00	0.00	0.05	0.02	0.00	0.00	0.10	0.01	0.00	0.00	0.06	0.01
		Soft soil	0.00	0.00	0.04	0.01	0.00	0.00	0.06	0.01	0.00	0.00	0.06	0.01
	Type II Bearings	Fixed base	0.00	0.00	0.05	0.01	0.00	0.00	0.09	0.01	0.00	0.00	0.06	0.01
		Soft soil	0.00	0.00	0.03	0.01	0.00	0.00	0.06	0.01	0.00	0.00	0.05	0.01

Table A.53. Peak Longitudinal Foundation Displacement (in) – Pa Ground Motions at SF = 1.0

			Steel short (Ss) superstructure				Steel long (Sl) superstructure				Concrete short (Cs) superstructure			
			Short (15 ft)		Tall (40 ft)		Short (15 ft)		Tall (40 ft)		Short (15 ft)		Tall (40 ft)	
			Avg	StdDev	Avg	StdDev	Avg	StdDev	Avg	StdDev	Avg	StdDev	Avg	StdDev
Column pier substructure	Type I Bearings	Abut 1	1.06	0.04	1.15	0.13	0.81	0.06	0.90	0.12	0.93	0.07	1.08	0.15
		Pier 1	0.51	0.08	0.38	0.05	0.83	0.09	0.39	0.06	0.91	0.10	0.41	0.06
		Pier 2	0.67	0.07	0.36	0.05	0.98	0.08	0.41	0.06	1.00	0.06	0.41	0.07
		Abut 2	1.08	0.05	1.16	0.11	0.81	0.08	0.90	0.20	0.92	0.08	1.02	0.18
	Type II Bearings	Abut 1	1.01	0.03	1.20	0.13	0.79	0.09	0.91	0.14	0.84	0.07	1.02	0.17
		Pier 1	0.32	0.04	0.36	0.06	0.67	0.13	0.39	0.05	0.48	0.10	0.37	0.05
		Pier 2	0.68	0.08	0.36	0.05	0.99	0.07	0.41	0.05	0.94	0.09	0.42	0.09
		Abut 2	1.01	0.06	1.16	0.11	0.78	0.11	0.95	0.20	0.82	0.06	0.96	0.20
Wall pier substructure	Type I Bearings	Abut 1	1.05	0.04	1.13	0.09	0.80	0.05	0.93	0.17	0.92	0.06	1.05	0.17
		Pier 1	1.06	0.22	1.10	0.22	1.32	0.19	1.11	0.29	1.28	0.16	1.20	0.32
		Pier 2	1.49	0.16	1.05	0.20	1.74	0.26	1.15	0.24	1.73	0.19	1.16	0.24
		Abut 2	1.07	0.04	1.11	0.07	0.80	0.06	0.93	0.16	0.92	0.06	1.06	0.17
	Type II Bearings	Abut 1	1.02	0.06	1.16	0.12	0.77	0.09	0.90	0.15	0.83	0.07	1.02	0.18
		Pier 1	0.87	0.09	0.99	0.15	1.17	0.26	1.06	0.23	0.98	0.12	1.08	0.24
		Pier 2	1.34	0.19	1.04	0.20	1.73	0.27	1.12	0.19	1.57	0.25	1.09	0.26
		Abut 2	1.01	0.07	1.10	0.10	0.76	0.08	0.96	0.21	0.80	0.07	0.98	0.17

Note: Tabulated data is for flexible foundation bridge variants only. All fixed foundation bridges have zero foundation displacement.

Table A.54. Peak Longitudinal Foundation Displacement (in) – CG Ground Motions at SF = 1.0

			Steel short (Ss) superstructure				Steel long (Sl) superstructure				Concrete short (Cs) superstructure			
			Short (15 ft)		Tall (40 ft)		Short (15 ft)		Tall (40 ft)		Short (15 ft)		Tall (40 ft)	
			Avg	StdDev	Avg	StdDev	Avg	StdDev	Avg	StdDev	Avg	StdDev	Avg	StdDev
Column pier substructure	Type I Bearings	Abut 1	1.02	0.03	1.04	0.03	0.75	0.02	0.76	0.02	0.85	0.03	0.87	0.03
		Pier 1	0.60	0.11	0.47	0.11	0.73	0.26	0.49	0.07	0.88	0.16	0.53	0.14
		Pier 2	0.60	0.05	0.46	0.08	0.88	0.05	0.49	0.10	0.92	0.06	0.49	0.09
		Abut 2	1.02	0.02	1.04	0.03	0.74	0.02	0.75	0.01	0.84	0.02	0.87	0.06
	Type II Bearings	Abut 1	0.86	0.13	1.02	0.06	0.69	0.02	0.71	0.03	0.77	0.03	0.78	0.02
		Pier 1	0.43	0.15	0.46	0.09	0.62	0.16	0.50	0.09	0.51	0.14	0.47	0.11
		Pier 2	0.60	0.03	0.48	0.11	0.86	0.04	0.48	0.08	0.82	0.03	0.46	0.08
		Abut 2	0.89	0.11	1.00	0.03	0.69	0.02	0.71	0.02	0.76	0.01	0.79	0.05
Wall pier substructure	Type I Bearings	Abut 1	1.00	0.05	1.02	0.03	0.75	0.02	0.77	0.02	0.82	0.04	0.86	0.02
		Pier 1	1.20	0.27	1.41	0.51	1.32	0.31	1.47	0.52	1.28	0.20	1.48	0.51
		Pier 2	1.29	0.11	1.40	0.49	1.40	0.13	1.52	0.55	1.45	0.15	1.53	0.46
		Abut 2	1.00	0.08	1.02	0.03	0.74	0.01	0.76	0.01	0.81	0.02	0.87	0.04
	Type II Bearings	Abut 1	0.83	0.16	0.99	0.05	0.69	0.02	0.70	0.01	0.75	0.05	0.77	0.02
		Pier 1	1.12	0.35	1.32	0.48	1.20	0.29	1.35	0.35	1.07	0.26	1.40	0.54
		Pier 2	1.10	0.13	1.29	0.49	1.32	0.14	1.47	0.47	1.22	0.14	1.53	0.62
		Abut 2	0.78	0.21	0.99	0.03	0.68	0.02	0.71	0.02	0.75	0.02	0.78	0.04

Note: Tabulated data is for flexible foundation bridge variants only. All fixed foundation bridges have zero foundation displacement.

Table A.55. Peak Transverse Foundation Displacement (in) – Pa Ground Motions at SF = 1.0

			Steel short (Ss) superstructure				Steel long (Sl) superstructure				Concrete short (Cs) superstructure			
			Short (15 ft)		Tall (40 ft)		Short (15 ft)		Tall (40 ft)		Short (15 ft)		Tall (40 ft)	
			Avg	StdDev	Avg	StdDev	Avg	StdDev	Avg	StdDev	Avg	StdDev	Avg	StdDev
Column pier substructure	Type I Bearings	Abut 1	0.33	0.03	0.33	0.03	0.62	0.03	0.63	0.02	0.48	0.01	0.50	0.06
		Pier 1	2.25	0.52	1.03	0.12	3.76	0.39	1.44	0.17	3.25	0.52	1.51	0.17
		Pier 2	1.86	0.35	1.11	0.13	4.22	0.37	1.42	0.11	3.20	0.20	1.51	0.14
		Abut 2	0.33	0.03	0.33	0.03	0.63	0.02	0.62	0.03	0.48	0.01	0.49	0.05
	Type II Bearings	Abut 1	0.28	0.00	0.28	0.00	0.45	0.00	0.45	0.00	0.46	0.00	0.46	0.00
		Pier 1	1.79	0.41	0.96	0.14	3.61	0.51	1.45	0.20	2.69	0.44	1.45	0.15
		Pier 2	1.91	0.31	1.02	0.14	4.52	0.17	1.37	0.17	3.14	0.29	1.43	0.14
		Abut 2	0.28	0.00	0.28	0.00	0.45	0.00	0.45	0.00	0.46	0.00	0.46	0.00
Wall pier substructure	Type I Bearings	Abut 1	0.33	0.02	0.34	0.04	0.62	0.03	0.64	0.02	0.48	0.01	0.49	0.03
		Pier 1	2.69	0.83	4.08	1.23	4.80	0.75	6.34	0.86	4.42	0.71	5.77	1.15
		Pier 2	2.44	0.52	4.45	1.25	5.55	0.92	7.35	0.85	3.89	0.68	6.23	1.13
		Abut 2	0.33	0.03	0.34	0.04	0.62	0.03	0.63	0.03	0.48	0.01	0.50	0.06
	Type II Bearings	Abut 1	0.28	0.00	0.28	0.00	0.45	0.00	0.45	0.00	0.46	0.00	0.46	0.00
		Pier 1	1.82	0.46	3.53	1.19	4.53	0.45	5.29	1.00	2.99	0.34	4.53	0.99
		Pier 2	2.21	0.54	3.91	1.33	5.83	0.69	8.05	0.73	3.89	0.55	5.67	0.79
		Abut 2	0.28	0.00	0.28	0.00	0.45	0.00	0.45	0.00	0.46	0.00	0.46	0.00

Note: Tabulated data is for flexible foundation bridge variants only. All fixed foundation bridges have zero foundation displacement.

Table A.56. Peak Transverse Flexible Foundation Displacement (in) – CG Ground Motions at SF = 1.0

			Steel short (Ss) superstructure				Steel long (Sl) superstructure				Concrete short (Cs) superstructure			
			Short (15 ft)		Tall (40 ft)		Short (15 ft)		Tall (40 ft)		Short (15 ft)		Tall (40 ft)	
			Avg	StdDev	Avg	StdDev	Avg	StdDev	Avg	StdDev	Avg	StdDev	Avg	StdDev
Column pier substructure	Type I Bearings	Abut 1	0.32	0.00	0.32	0.00	0.62	0.02	0.62	0.01	0.47	0.00	0.47	0.00
		Pier 1	1.32	0.17	0.89	0.17	2.32	0.38	1.11	0.18	2.12	0.39	1.34	0.23
		Pier 2	1.59	0.16	0.92	0.16	2.75	0.53	1.10	0.22	2.66	0.23	1.30	0.23
		Abut 2	0.32	0.00	0.32	0.00	0.61	0.03	0.63	0.02	0.48	0.00	0.47	0.00
	Type II Bearings	Abut 1	0.28	0.00	0.28	0.00	0.45	0.00	0.45	0.00	0.46	0.00	0.46	0.00
		Pier 1	1.09	0.18	0.75	0.15	2.24	0.36	1.15	0.15	1.60	0.25	1.00	0.19
		Pier 2	1.56	0.18	0.87	0.13	2.99	0.63	1.19	0.19	2.40	0.32	1.02	0.23
		Abut 2	0.28	0.00	0.28	0.00	0.45	0.00	0.45	0.00	0.46	0.00	0.46	0.00
Wall pier substructure	Type I Bearings	Abut 1	0.32	0.00	0.32	0.00	0.62	0.03	0.62	0.02	0.48	0.00	0.47	0.00
		Pier 1	1.64	0.33	2.54	0.44	2.73	0.43	2.96	0.50	2.50	0.37	3.22	0.66
		Pier 2	1.75	0.27	2.89	0.38	3.22	0.66	3.78	1.01	3.00	0.36	3.81	0.63
		Abut 2	0.32	0.00	0.32	0.00	0.60	0.02	0.63	0.02	0.47	0.00	0.48	0.00
	Type II Bearings	Abut 1	0.28	0.00	0.28	0.00	0.45	0.00	0.45	0.00	0.46	0.00	0.46	0.00
		Pier 1	1.46	0.25	2.21	0.44	2.45	0.46	2.74	0.48	1.90	0.35	2.34	0.56
		Pier 2	1.70	0.20	2.67	0.37	3.38	0.75	3.85	0.97	2.62	0.37	3.31	0.56
		Abut 2	0.28	0.00	0.28	0.00	0.45	0.00	0.45	0.00	0.46	0.00	0.46	0.00

Note: Tabulated data is for flexible foundation bridge variants only. All fixed foundation bridges have zero foundation displacement.

Table A.57. Peak Longitudinal Abutment 1 Base Shear (kip) – Pa Ground Motions at SF = 1.0

			Steel short (Ss) superstructure				Steel long (Sl) superstructure				Concrete short (Cs) superstructure			
			Short (15 ft)		Tall (40 ft)		Short (15 ft)		Tall (40 ft)		Short (15 ft)		Tall (40 ft)	
			Avg	StdDev	Avg	StdDev	Avg	StdDev	Avg	StdDev	Avg	StdDev	Avg	StdDev
Column pier substructure	Type I Bearings	Fixed base	636	39	777	146	518	69	577	115	563	68	767	308
		Soft soil	597	22	645	65	470	29	515	63	531	36	609	76
	Type II Bearings	Fixed base	622	57	893	224	478	84	553	100	505	72	671	152
		Soft soil	574	15	666	66	457	47	520	69	484	34	577	87
Wall pier substructure	Type I Bearings	Fixed base	647	52	787	167	496	38	561	102	555	41	677	158
		Soft soil	594	20	631	46	466	26	530	87	522	33	594	89
	Type II Bearings	Fixed base	618	56	770	147	475	66	547	134	497	54	638	183
		Soft soil	576	30	649	61	449	44	516	79	480	36	574	94

Table A.58. Peak Longitudinal Abutment 1 Base Shear (kip) – CG Ground Motions at SF = 1.0

			Steel short (Ss) superstructure				Steel long (Sl) superstructure				Concrete short (Cs) superstructure			
			Short (15 ft)		Tall (40 ft)		Short (15 ft)		Tall (40 ft)		Short (15 ft)		Tall (40 ft)	
			Avg	StdDev	Avg	StdDev	Avg	StdDev	Avg	StdDev	Avg	StdDev	Avg	StdDev
Column pier substructure	Type I Bearings	Fixed base	598	16	617	48	452	8	470	24	506	21	540	38
		Soft soil	576	14	585	17	437	9	445	9	488	15	502	16
	Type II Bearings	Fixed base	588	44	587	50	418	10	422	13	461	23	472	24
		Soft soil	497	66	575	30	409	9	419	17	447	13	452	11
Wall pier substructure	Type I Bearings	Fixed base	590	12	622	26	450	8	464	22	487	22	536	26
		Soft soil	567	27	579	17	437	10	449	8	473	23	497	13
	Type II Bearings	Fixed base	573	33	592	30	412	7	436	20	452	13	467	25
		Soft soil	482	81	559	24	410	10	416	8	440	23	450	12

Table A.59. Peak Transverse Abutment 1 Base Shear (kip) – Pa Ground Motions at SF = 1.0

			Steel short (Ss) superstructure				Steel long (Sl) superstructure				Concrete short (Cs) superstructure			
			Short (15 ft)		Tall (40 ft)		Short (15 ft)		Tall (40 ft)		Short (15 ft)		Tall (40 ft)	
			Avg	StdDev	Avg	StdDev	Avg	StdDev	Avg	StdDev	Avg	StdDev	Avg	StdDev
Column pier substructure	Type I Bearings	Fixed base	120	7	121	8	193	8	196	9	161	2	172	19
		Soft soil	120	8	121	8	200	8	204	5	161	2	168	17
	Type II Bearings	Fixed base	107	0	108	0	154	1	155	0	157	0	157	0
		Soft soil	107	0	108	0	155	0	155	0	157	0	157	0
Wall pier substructure	Type I Bearings	Fixed base	119	6	120	7	192	6	193	6	161	1	162	3
		Soft soil	120	7	124	11	200	7	206	5	162	2	164	8
	Type II Bearings	Fixed base	107	0	107	0	155	0	155	0	157	0	157	0
		Soft soil	108	0	108	0	155	0	155	0	157	0	157	0

Table A.60. Peak Transverse Abutment 1 Base Shear (kip) – CG Ground Motions at SF = 1.0

			Steel short (Ss) superstructure				Steel long (Sl) superstructure				Concrete short (Cs) superstructure			
			Short (15 ft)		Tall (40 ft)		Short (15 ft)		Tall (40 ft)		Short (15 ft)		Tall (40 ft)	
			Avg	StdDev	Avg	StdDev	Avg	StdDev	Avg	StdDev	Avg	StdDev	Avg	StdDev
Column pier substructure	Type I Bearings	Fixed base	117	1	120	8	193	5	197	7	160	1	160	1
		Soft soil	117	1	117	0	200	6	201	4	160	1	160	1
	Type II Bearings	Fixed base	107	0	108	0	154	0	155	0	157	0	157	0
		Soft soil	107	0	108	0	154	0	155	0	157	0	157	0
Wall pier substructure	Type I Bearings	Fixed base	118	2	117	0	194	6	195	5	160	0	165	13
		Soft soil	118	1	118	1	201	9	202	6	160	1	161	1
	Type II Bearings	Fixed base	107	0	107	0	155	0	155	0	157	0	157	0
		Soft soil	107	0	108	0	155	0	155	0	157	0	157	0

Table A.61. Peak Longitudinal Abutment 2 Base Shear (kip) – Pa Ground Motions at SF = 1.0

			Steel short (Ss) superstructure				Steel long (Sl) superstructure				Concrete short (Cs) superstructure			
			Short (15 ft)		Tall (40 ft)		Short (15 ft)		Tall (40 ft)		Short (15 ft)		Tall (40 ft)	
			Avg	StdDev	Avg	StdDev	Avg	StdDev	Avg	StdDev	Avg	StdDev	Avg	StdDev
Column pier substructure	Type I Bearings	Fixed base	659	46	768	130	485	39	561	138	539	28	729	171
		Soft soil	606	27	649	58	471	43	515	101	525	41	576	91
	Type II Bearings	Fixed base	605	54	695	66	472	74	596	148	491	43	650	212
		Soft soil	571	30	650	54	454	57	543	103	473	33	545	100
Wall pier substructure	Type I Bearings	Fixed base	613	28	749	134	493	49	586	107	562	77	697	148
		Soft soil	604	23	625	36	466	32	532	81	525	30	598	87
	Type II Bearings	Fixed base	583	39	805	212	461	76	592	181	499	90	625	146
		Soft soil	573	33	616	53	446	44	544	107	466	35	555	86

Table A.62. Peak Longitudinal Abutment 2 Base Shear (kip) – CG Ground Motions at SF = 1.0

			Steel short (Ss) superstructure				Steel long (Sl) superstructure				Concrete short (Cs) superstructure			
			Short (15 ft)		Tall (40 ft)		Short (15 ft)		Tall (40 ft)		Short (15 ft)		Tall (40 ft)	
			Avg	StdDev	Avg	StdDev	Avg	StdDev	Avg	StdDev	Avg	StdDev	Avg	StdDev
Column pier substructure	Type I Bearings	Fixed base	606	33	642	63	447	9	460	14	505	32	546	48
		Soft soil	577	12	584	17	435	10	441	7	481	8	502	28
	Type II Bearings	Fixed base	565	19	588	41	411	7	449	79	449	8	475	37
		Soft soil	511	58	567	18	409	10	417	11	444	7	457	23
Wall pier substructure	Type I Bearings	Fixed base	586	16	616	27	448	12	458	8	491	19	565	121
		Soft soil	566	44	575	15	436	7	444	7	468	11	499	23
	Type II Bearings	Fixed base	566	30	612	69	408	7	432	29	446	10	462	13
		Soft soil	454	105	561	16	405	8	417	13	439	8	453	20

Table A.63. Peak Transverse Abutment 2 Base Shear (kip) – Pa Ground Motions at SF = 1.0

			Steel short (Ss) superstructure				Steel long (Sl) superstructure				Concrete short (Cs) superstructure			
			Short (15 ft)		Tall (40 ft)		Short (15 ft)		Tall (40 ft)		Short (15 ft)		Tall (40 ft)	
			Avg	StdDev	Avg	StdDev	Avg	StdDev	Avg	StdDev	Avg	StdDev	Avg	StdDev
Column pier substructure	Type I Bearings	Fixed base	121	9	120	8	195	6	197	8	165	15	164	12
		Soft soil	121	9	121	9	204	7	201	7	161	3	166	14
	Type II Bearings	Fixed base	107	0	107	0	155	0	155	1	156	1	157	0
		Soft soil	107	0	107	0	155	0	155	1	157	0	157	0
Wall pier substructure	Type I Bearings	Fixed base	121	9	121	9	198	11	196	10	164	12	166	16
		Soft soil	121	9	125	10	202	8	204	8	161	2	167	15
	Type II Bearings	Fixed base	107	0	107	0	154	1	155	1	157	0	157	1
		Soft soil	107	0	108	0	155	0	155	0	157	0	157	0

Table A.64. Peak Transverse Abutment 2 Base Shear (kip) – CG Ground Motions at SF = 1.0

			Steel short (Ss) superstructure				Steel long (Sl) superstructure				Concrete short (Cs) superstructure			
			Short (15 ft)		Tall (40 ft)		Short (15 ft)		Tall (40 ft)		Short (15 ft)		Tall (40 ft)	
			Avg	StdDev	Avg	StdDev	Avg	StdDev	Avg	StdDev	Avg	StdDev	Avg	StdDev
Column pier substructure	Type I Bearings	Fixed base	118	0	117	0	195	6	196	6	160	0	160	1
		Soft soil	117	0	117	0	198	7	204	5	160	0	160	0
	Type II Bearings	Fixed base	107	0	107	0	155	1	155	1	156	0	157	0
		Soft soil	107	0	107	0	155	0	154	0	157	0	157	0
Wall pier substructure	Type I Bearings	Fixed base	117	0	118	1	192	5	193	7	163	8	160	0
		Soft soil	117	0	118	0	195	6	204	5	160	0	160	1
	Type II Bearings	Fixed base	107	0	107	0	154	0	155	0	157	0	157	0
		Soft soil	107	0	107	0	155	0	155	0	157	0	157	0

Table A.65. Peak Longitudinal Pier 1 Base Shear (kip) – Pa Ground Motions at SF = 1.0

			Steel short (Ss) superstructure				Steel long (Sl) superstructure				Concrete short (Cs) superstructure			
			Short (15 ft)		Tall (40 ft)		Short (15 ft)		Tall (40 ft)		Short (15 ft)		Tall (40 ft)	
			Avg	StdDev	Avg	StdDev	Avg	StdDev	Avg	StdDev	Avg	StdDev	Avg	StdDev
Column pier substructure	Type I Bearings	Fixed base	200	19	119	9	270	8	124	16	270	8	134	7
		Soft soil	216	17	187	10	281	20	190	12	291	22	194	12
	Type II Bearings	Fixed base	153	15	106	9	222	16	121	8	193	19	118	11
		Soft soil	174	13	183	13	249	26	191	9	208	21	187	12
Wall pier substructure	Type I Bearings	Fixed base	279	33	256	34	334	22	282	40	331	25	278	35
		Soft soil	327	45	334	45	379	40	336	61	372	31	353	67
	Type II Bearings	Fixed base	239	24	259	35	308	24	270	32	277	24	280	33
		Soft soil	287	18	310	32	349	52	326	48	309	24	329	50

Table A.66. Peak Longitudinal Pier 1 Base Shear (kip) – CG Ground Motions at SF = 1.0

			Steel short (Ss) superstructure				Steel long (Sl) superstructure				Concrete short (Cs) superstructure			
			Short (15 ft)		Tall (40 ft)		Short (15 ft)		Tall (40 ft)		Short (15 ft)		Tall (40 ft)	
			Avg	StdDev	Avg	StdDev	Avg	StdDev	Avg	StdDev	Avg	StdDev	Avg	StdDev
Column pier substructure	Type I Bearings	Fixed base	199	31	114	28	245	33	127	17	255	25	143	37
		Soft soil	233	21	205	21	259	52	208	15	289	32	218	30
	Type II Bearings	Fixed base	184	26	106	22	220	39	123	23	196	32	112	19
		Soft soil	195	30	203	19	236	32	211	18	214	27	202	24
Wall pier substructure	Type I Bearings	Fixed base	329	32	377	108	346	38	363	51	328	36	379	93
		Soft soil	350	56	394	104	377	63	406	107	369	40	409	103
	Type II Bearings	Fixed base	341	39	378	70	351	33	364	65	335	41	353	74
		Soft soil	333	72	373	99	351	59	382	70	324	54	391	109

Table A.67. Peak Transverse Pier 1 Base Shear (kip) – Pa Ground Motions at SF = 1.0

			Steel short (Ss) superstructure				Steel long (Sl) superstructure				Concrete short (Cs) superstructure			
			Short (15 ft)		Tall (40 ft)		Short (15 ft)		Tall (40 ft)		Short (15 ft)		Tall (40 ft)	
			Avg	StdDev	Avg	StdDev	Avg	StdDev	Avg	StdDev	Avg	StdDev	Avg	StdDev
Column pier substructure	Type I Bearings	Fixed base	453	22	203	10	645	26	258	13	623	19	256	12
		Soft soil	387	70	229	15	587	52	284	22	520	68	293	22
	Type II Bearings	Fixed base	359	30	203	12	614	26	258	14	497	29	254	14
		Soft soil	330	54	221	19	567	67	285	26	447	58	285	20
Wall pier substructure	Type I Bearings	Fixed base	488	55	671	95	778	84	972	122	655	49	878	89
		Soft soil	446	109	628	161	724	99	925	113	672	94	850	152
	Type II Bearings	Fixed base	379	48	599	93	623	44	867	101	484	56	687	107
		Soft soil	333	61	554	157	688	59	787	132	486	45	687	130

Table A.68. Peak Transverse Pier 1 Base Shear (kip) – CG Ground Motions at SF = 1.0

			Steel short (Ss) superstructure				Steel long (Sl) superstructure				Concrete short (Cs) superstructure			
			Short (15 ft)		Tall (40 ft)		Short (15 ft)		Tall (40 ft)		Short (15 ft)		Tall (40 ft)	
			Avg	StdDev	Avg	StdDev	Avg	StdDev	Avg	StdDev	Avg	StdDev	Avg	StdDev
Column pier substructure	Type I Bearings	Fixed base	380	23	190	17	557	50	243	27	564	35	248	30
		Soft soil	267	22	212	22	398	52	240	23	370	52	269	31
	Type II Bearings	Fixed base	311	28	174	28	523	26	243	21	411	22	224	26
		Soft soil	237	23	192	20	388	47	245	19	304	32	226	26
Wall pier substructure	Type I Bearings	Fixed base	420	54	824	197	648	71	890	172	628	55	901	155
		Soft soil	306	43	424	58	449	56	480	66	421	49	515	88
	Type II Bearings	Fixed base	379	72	787	172	554	47	836	157	437	60	790	184
		Soft soil	282	33	380	58	413	61	451	63	342	46	397	73

Table A.69. Peak Longitudinal Pier 2 Base Shear (kip) – Pa Ground Motions at SF = 1.0

			Steel short (Ss) superstructure				Steel long (Sl) superstructure				Concrete short (Cs) superstructure			
			Short (15 ft)		Tall (40 ft)		Short (15 ft)		Tall (40 ft)		Short (15 ft)		Tall (40 ft)	
			Avg	StdDev	Avg	StdDev	Avg	StdDev	Avg	StdDev	Avg	StdDev	Avg	StdDev
Column pier substructure	Type I Bearings	Fixed base	222	9	118	7	281	8	119	13	281	8	123	9
		Soft soil	244	12	184	12	308	15	194	11	312	12	193	15
	Type II Bearings	Fixed base	223	9	115	14	282	8	116	11	281	9	120	11
		Soft soil	249	15	184	12	311	16	196	10	301	16	196	19
Wall pier substructure	Type I Bearings	Fixed base	327	30	252	37	410	30	274	45	399	31	278	41
		Soft soil	413	35	323	42	463	53	343	49	463	38	345	50
	Type II Bearings	Fixed base	314	38	257	42	412	27	277	48	384	46	274	35
		Soft soil	382	41	321	42	466	54	336	39	431	51	332	53

Table A.70. Peak Longitudinal Pier 2 Base Shear (kip) – CG Ground Motions at SF = 1.0

			Steel short (Ss) superstructure				Steel long (Sl) superstructure				Concrete short (Cs) superstructure			
			Short (15 ft)		Tall (40 ft)		Short (15 ft)		Tall (40 ft)		Short (15 ft)		Tall (40 ft)	
			Avg	StdDev	Avg	StdDev	Avg	StdDev	Avg	StdDev	Avg	StdDev	Avg	StdDev
Column pier substructure	Type I Bearings	Fixed base	211	5	113	24	271	5	117	17	271	3	125	27
		Soft soil	232	9	200	16	285	10	208	20	293	12	210	18
	Type II Bearings	Fixed base	214	6	109	18	269	6	122	21	269	6	115	23
		Soft soil	231	7	207	23	279	8	208	16	275	7	203	17
Wall pier substructure	Type I Bearings	Fixed base	293	19	379	101	356	23	361	70	361	33	385	101
		Soft soil	371	24	391	102	395	28	417	112	403	31	419	93
	Type II Bearings	Fixed base	292	17	369	84	346	24	375	83	326	25	372	86
		Soft soil	332	26	367	100	377	28	405	96	354	32	417	128

Table A.71. Peak Transverse Pier 2 Base Shear (kip) – Pa Ground Motions at SF = 1.0

			Steel short (Ss) superstructure				Steel long (Sl) superstructure				Concrete short (Cs) superstructure			
			Short (15 ft)		Tall (40 ft)		Short (15 ft)		Tall (40 ft)		Short (15 ft)		Tall (40 ft)	
			Avg	StdDev	Avg	StdDev	Avg	StdDev	Avg	StdDev	Avg	StdDev	Avg	StdDev
Column pier substructure	Type I Bearings	Fixed base	300	33	205	13	658	12	258	13	466	30	256	10
		Soft soil	336	47	240	16	646	50	280	14	511	27	291	19
	Type II Bearings	Fixed base	318	27	204	13	660	15	258	13	469	28	256	12
		Soft soil	342	42	229	19	686	22	274	23	504	38	281	18
Wall pier substructure	Type I Bearings	Fixed base	333	66	552	131	722	55	908	135	525	63	685	163
		Soft soil	411	70	676	165	821	121	1057	112	603	89	911	149
	Type II Bearings	Fixed base	343	60	559	126	718	62	893	143	525	62	696	151
		Soft soil	382	72	606	174	857	91	1150	96	603	73	837	104

Table A.72. Peak Transverse Pier 2 Base Shear (kip) – CG Ground Motions at SF = 1.0

			Steel short (Ss) superstructure				Steel long (Sl) superstructure				Concrete short (Cs) superstructure			
			Short (15 ft)		Tall (40 ft)		Short (15 ft)		Tall (40 ft)		Short (15 ft)		Tall (40 ft)	
			Avg	StdDev	Avg	StdDev	Avg	StdDev	Avg	StdDev	Avg	StdDev	Avg	StdDev
Column pier substructure	Type I Bearings	Fixed base	289	20	196	16	637	17	250	24	460	16	257	26
		Soft soil	298	22	214	20	451	70	239	29	439	30	264	31
	Type II Bearings	Fixed base	299	21	195	27	646	17	254	20	463	18	241	28
		Soft soil	295	23	209	17	482	83	251	26	404	43	228	31
Wall pier substructure	Type I Bearings	Fixed base	384	74	789	207	691	48	882	97	497	36	800	157
		Soft soil	319	38	470	50	513	87	587	134	484	48	592	84
	Type II Bearings	Fixed base	377	63	777	165	699	39	870	86	514	25	799	159
		Soft soil	312	26	441	49	534	100	597	129	435	49	525	75

Table A.73. Peak Normalized Longitudinal Abutment Base Shear (no units) – Pa Ground Motions at SF = 1.0

			Steel short (Ss) superstructure				Steel long (Sl) superstructure				Concrete short (Cs) superstructure			
			Short (15 ft)		Tall (40 ft)		Short (15 ft)		Tall (40 ft)		Short (15 ft)		Tall (40 ft)	
			A1	A2	A1	A2	A1	A2	A1	A2	A1	A2	A1	A2
Column pier substructure	Type I Bearings	Fixed base	4.99	5.17	6.09	6.01	2.82	2.64	3.14	3.05	2.84	2.72	3.86	3.67
		Soft soil	4.68	4.75	5.04	5.08	2.56	2.57	2.80	2.80	2.68	2.64	3.06	2.90
	Type II Bearings	Fixed base	4.88	4.75	7.00	5.44	2.61	2.57	3.01	3.25	2.55	2.48	3.37	3.27
		Soft soil	4.50	4.47	5.21	5.08	2.49	2.47	2.83	2.95	2.44	2.38	2.90	2.74
Wall pier substructure	Type I Bearings	Fixed base	5.09	4.82	6.18	5.88	2.71	2.69	3.06	3.20	2.81	2.84	3.43	3.53
		Soft soil	4.67	4.74	4.95	4.90	2.54	2.54	2.89	2.90	2.64	2.65	3.00	3.02
	Type II Bearings	Fixed base	4.85	4.58	6.05	6.32	2.59	2.51	2.98	3.23	2.51	2.52	3.22	3.16
		Soft soil	4.52	4.50	5.09	4.83	2.45	2.43	2.81	2.97	2.42	2.35	2.90	2.80

Table A.74. Peak Normalized Longitudinal Abutment Base Shear (no units) – CG Ground Motions at SF = 1.0

			Steel short (Ss) superstructure				Steel long (Sl) superstructure				Concrete short (Cs) superstructure			
			Short (15 ft)		Tall (40 ft)		Short (15 ft)		Tall (40 ft)		Short (15 ft)		Tall (40 ft)	
			A1	A2	A1	A2	A1	A2	A1	A2	A1	A2	A1	A2
Column pier substructure	Type I Bearings	Fixed base	4.69	4.76	4.83	5.03	2.46	2.43	2.56	2.50	2.55	2.55	2.72	2.75
		Soft soil	4.51	4.53	4.58	4.57	2.38	2.37	2.42	2.40	2.46	2.42	2.53	2.53
	Type II Bearings	Fixed base	4.61	4.43	4.60	4.61	2.28	2.24	2.30	2.44	2.32	2.27	2.38	2.39
		Soft soil	3.90	4.01	4.50	4.44	2.23	2.23	2.28	2.27	2.25	2.24	2.27	2.30
Wall pier substructure	Type I Bearings	Fixed base	4.63	4.61	4.88	4.84	2.45	2.44	2.53	2.50	2.47	2.49	2.71	2.86
		Soft soil	4.45	4.45	4.54	4.51	2.38	2.38	2.45	2.42	2.39	2.37	2.51	2.52
	Type II Bearings	Fixed base	4.51	4.45	4.65	4.81	2.25	2.23	2.38	2.36	2.28	2.26	2.36	2.33
		Soft soil	3.78	3.57	4.39	4.40	2.23	2.21	2.27	2.27	2.22	2.22	2.27	2.29

Table A.75. Peak Normalized Transverse Abutment Base Shear (no units) – Pa Ground Motions at SF = 1.0

			Steel short (Ss) superstructure				Steel long (Sl) superstructure				Concrete short (Cs) superstructure			
			Short (15 ft)		Tall (40 ft)		Short (15 ft)		Tall (40 ft)		Short (15 ft)		Tall (40 ft)	
			A1	A2	A1	A2	A1	A2	A1	A2	A1	A2	A1	A2
Column pier substructure	Type I Bearings	Fixed base	0.94	0.95	0.95	0.94	1.05	1.06	1.07	1.07	0.81	0.83	0.87	0.83
		Soft soil	0.94	0.95	0.94	0.95	1.09	1.11	1.11	1.10	0.81	0.81	0.85	0.83
	Type II Bearings	Fixed base	0.84	0.84	0.84	0.84	0.84	0.84	0.84	0.84	0.79	0.79	0.79	0.79
		Soft soil	0.84	0.84	0.84	0.84	0.84	0.84	0.84	0.84	0.79	0.79	0.79	0.79
Wall pier substructure	Type I Bearings	Fixed base	0.94	0.95	0.94	0.95	1.05	1.08	1.05	1.07	0.81	0.83	0.82	0.84
		Soft soil	0.94	0.95	0.97	0.98	1.09	1.10	1.12	1.11	0.82	0.81	0.83	0.84
	Type II Bearings	Fixed base	0.84	0.84	0.84	0.84	0.84	0.84	0.85	0.84	0.79	0.79	0.79	0.79
		Soft soil	0.84	0.84	0.84	0.84	0.84	0.84	0.84	0.84	0.79	0.79	0.79	0.79

Table A.76. Peak Normalized Transverse Abutment Base Shear (no units) – CG Ground Motions at SF = 1.0

			Steel short (Ss) superstructure				Steel long (Sl) superstructure				Concrete short (Cs) superstructure			
			Short (15 ft)		Tall (40 ft)		Short (15 ft)		Tall (40 ft)		Short (15 ft)		Tall (40 ft)	
			A1	A2	A1	A2	A1	A2	A1	A2	A1	A2	A1	A2
Column pier substructure	Type I Bearings	Fixed base	0.92	0.92	0.94	0.92	1.05	1.06	1.07	1.07	0.81	0.81	0.81	0.81
		Soft soil	0.92	0.92	0.92	0.92	1.09	1.08	1.09	1.11	0.81	0.81	0.81	0.81
	Type II Bearings	Fixed base	0.84	0.84	0.84	0.84	0.84	0.84	0.84	0.84	0.79	0.79	0.79	0.79
		Soft soil	0.84	0.84	0.84	0.84	0.84	0.84	0.84	0.84	0.79	0.79	0.79	0.79
Wall pier substructure	Type I Bearings	Fixed base	0.93	0.92	0.92	0.92	1.06	1.05	1.06	1.05	0.81	0.82	0.83	0.81
		Soft soil	0.92	0.92	0.92	0.92	1.09	1.06	1.10	1.11	0.81	0.81	0.81	0.81
	Type II Bearings	Fixed base	0.84	0.84	0.84	0.84	0.84	0.84	0.84	0.84	0.79	0.79	0.79	0.79
		Soft soil	0.84	0.84	0.84	0.84	0.84	0.84	0.84	0.84	0.79	0.79	0.79	0.79

Table A.77. Peak Normalized Longitudinal Pier Base Shear (no units) – Pa Ground Motions at SF = 1.0

			Steel short (Ss) superstructure				Steel long (Sl) superstructure				Concrete short (Cs) superstructure			
			Short (15 ft)		Tall (40 ft)		Short (15 ft)		Tall (40 ft)		Short (15 ft)		Tall (40 ft)	
			P1	P2	P1	P2	P1	P2	P1	P2	P1	P2	P1	P2
Column pier substructure	Type I Bearings	Fixed base	0.42	0.47	0.20	0.20	0.30	0.31	0.12	0.12	0.40	0.42	0.17	0.16
		Soft soil	0.45	0.51	0.32	0.32	0.31	0.34	0.19	0.19	0.43	0.46	0.25	0.25
	Type II Bearings	Fixed base	0.32	0.47	0.18	0.20	0.24	0.31	0.12	0.11	0.29	0.42	0.15	0.15
		Soft soil	0.37	0.52	0.31	0.32	0.27	0.34	0.19	0.19	0.31	0.45	0.24	0.25
Wall pier substructure	Type I Bearings	Fixed base	0.43	0.50	0.25	0.24	0.31	0.38	0.19	0.19	0.39	0.47	0.22	0.22
		Soft soil	0.50	0.64	0.32	0.31	0.35	0.43	0.23	0.23	0.44	0.55	0.29	0.28
	Type II Bearings	Fixed base	0.37	0.48	0.25	0.25	0.29	0.38	0.18	0.19	0.33	0.46	0.23	0.22
		Soft soil	0.44	0.59	0.30	0.31	0.32	0.43	0.22	0.23	0.37	0.51	0.27	0.27

Table A.78. Peak Normalized Longitudinal Pier Base Shear (no units) – CG Ground Motions at SF = 1.0

			Steel short (Ss) superstructure				Steel long (Sl) superstructure				Concrete short (Cs) superstructure			
			Short (15 ft)		Tall (40 ft)		Short (15 ft)		Tall (40 ft)		Short (15 ft)		Tall (40 ft)	
			P1	P2	P1	P2	P1	P2	P1	P2	P1	P2	P1	P2
Column pier substructure	Type I Bearings	Fixed base	0.42	0.44	0.20	0.19	0.27	0.30	0.13	0.11	0.38	0.40	0.18	0.16
		Soft soil	0.49	0.49	0.35	0.34	0.28	0.31	0.21	0.21	0.43	0.44	0.28	0.27
	Type II Bearings	Fixed base	0.39	0.45	0.18	0.19	0.24	0.30	0.12	0.12	0.29	0.40	0.14	0.15
		Soft soil	0.41	0.48	0.35	0.36	0.26	0.31	0.21	0.21	0.32	0.41	0.26	0.26
Wall pier substructure	Type I Bearings	Fixed base	0.51	0.45	0.36	0.36	0.32	0.33	0.25	0.24	0.39	0.43	0.31	0.31
		Soft soil	0.54	0.57	0.38	0.37	0.35	0.37	0.28	0.28	0.44	0.48	0.33	0.34
	Type II Bearings	Fixed base	0.52	0.45	0.36	0.35	0.32	0.32	0.25	0.25	0.40	0.39	0.29	0.30
		Soft soil	0.51	0.51	0.36	0.35	0.32	0.35	0.26	0.27	0.38	0.42	0.32	0.34

Table A.79. Peak Normalized Transverse Pier Base Shear (no units) – Pa Ground Motions at SF = 1.0

			Steel short (Ss) superstructure				Steel long (Sl) superstructure				Concrete short (Cs) superstructure			
			Short (15 ft)		Tall (40 ft)		Short (15 ft)		Tall (40 ft)		Short (15 ft)		Tall (40 ft)	
			P1	P2	P1	P2	P1	P2	P1	P2	P1	P2	P1	P2
Column pier substructure	Type I Bearings	Fixed base	0.95	0.63	0.35	0.35	0.71	0.72	0.25	0.25	0.93	0.70	0.33	0.33
		Soft soil	0.81	0.71	0.39	0.41	0.65	0.71	0.28	0.28	0.78	0.76	0.38	0.37
	Type II Bearings	Fixed base	0.75	0.67	0.35	0.35	0.68	0.73	0.25	0.25	0.74	0.70	0.33	0.33
		Soft soil	0.69	0.72	0.38	0.39	0.62	0.76	0.28	0.27	0.67	0.75	0.37	0.36
Wall pier substructure	Type I Bearings	Fixed base	0.75	0.51	0.64	0.53	0.72	0.67	0.66	0.62	0.78	0.62	0.71	0.55
		Soft soil	0.69	0.63	0.60	0.65	0.67	0.76	0.63	0.72	0.80	0.72	0.69	0.74
	Type II Bearings	Fixed base	0.58	0.53	0.57	0.54	0.58	0.66	0.59	0.60	0.57	0.62	0.56	0.56
		Soft soil	0.51	0.59	0.53	0.58	0.64	0.79	0.53	0.78	0.58	0.71	0.56	0.68

Table A.80. Peak Normalized Transverse Pier Base Shear (no units) – CG Ground Motions at SF = 1.0

			Steel short (Ss) superstructure				Steel long (Sl) superstructure				Concrete short (Cs) superstructure			
			Short (15 ft)		Tall (40 ft)		Short (15 ft)		Tall (40 ft)		Short (15 ft)		Tall (40 ft)	
			P1	P2	P1	P2	P1	P2	P1	P2	P1	P2	P1	P2
Column pier substructure	Type I Bearings	Fixed base	0.80	0.61	0.33	0.34	0.61	0.70	0.24	0.25	0.84	0.69	0.32	0.33
		Soft soil	0.56	0.63	0.36	0.37	0.44	0.50	0.24	0.24	0.55	0.65	0.35	0.34
	Type II Bearings	Fixed base	0.65	0.63	0.30	0.33	0.58	0.71	0.24	0.25	0.61	0.69	0.29	0.31
		Soft soil	0.50	0.62	0.33	0.36	0.43	0.53	0.24	0.25	0.45	0.60	0.29	0.29
Wall pier substructure	Type I Bearings	Fixed base	0.65	0.59	0.79	0.76	0.60	0.64	0.60	0.60	0.74	0.59	0.73	0.65
		Soft soil	0.47	0.49	0.41	0.45	0.42	0.47	0.33	0.40	0.50	0.57	0.42	0.48
	Type II Bearings	Fixed base	0.58	0.58	0.75	0.74	0.51	0.65	0.57	0.59	0.52	0.61	0.64	0.65
		Soft soil	0.43	0.48	0.36	0.42	0.38	0.49	0.31	0.40	0.41	0.52	0.32	0.42

Table A.81. Scale Factor at which Longitudinal Bearing Unseating Occurs – Pa Ground Motions

			Steel short (Ss) superstructure		Steel long (Sl) superstructure		Concrete (Cs) superstructure	
			Short (15 ft)	Tall (40 ft)	Short (15 ft)	Tall (40 ft)	Short (15 ft)	Tall (40 ft)
Column pier substructure	Type I Bearings	Fixed base	NA	NA	NA	NA	NA	NA
		Soft soil	NA	NA	NA	NA	NA	NA
	Type II Bearings	Fixed base	1.25	0.75	1.25	0.75	1.25	1.00
		Soft soil	1.25	0.75	1.00	0.75	1.25	1.00
Wall pier substructure	Type I Bearings	Fixed base	NA	NA	NA	NA	NA	NA
		Soft soil	NA	NA	NA	NA	NA	NA
	Type II Bearings	Fixed base	1.25	0.75	1.25	0.75	1.50	1.00
		Soft soil	1.25	0.75	1.25	0.75	1.25	1.00

Table A.82. Scale Factor at which Longitudinal Bearing Unseating Occurs – CG Ground Motions

			Steel short (Ss) superstructure		Steel long (Sl) superstructure		Concrete (Cs) superstructure	
			Short (15 ft)	Tall (40 ft)	Short (15 ft)	Tall (40 ft)	Short (15 ft)	Tall (40 ft)
Column pier substructure	Type I Bearings	Fixed base	NA	NA	NA	NA	NA	NA
		Soft soil	NA	NA	NA	NA	NA	NA
	Type II Bearings	Fixed base	1.50	1.25	NA	1.25	NA	1.50
		Soft soil	1.50	1.25	1.75	1.25	NA	1.50
Wall pier substructure	Type I Bearings	Fixed base	NA	NA	NA	NA	NA	NA
		Soft soil	NA	NA	NA	NA	NA	NA
	Type II Bearings	Fixed base	1.50	1.25	NA	1.25	NA	1.50
		Soft soil	1.75	1.25	1.75	1.25	NA	1.50

Table A.83. Scale Factor at which Transverse Bearing Unseating Occurs – Pa Ground Motions

			Steel short (Ss) superstructure		Steel long (Sl) superstructure		Concrete (Cs) superstructure	
			Short (15 ft)	Tall (40 ft)	Short (15 ft)	Tall (40 ft)	Short (15 ft)	Tall (40 ft)
Column pier substructure	Type I Bearings	Fixed base	1.75	NA	1.75	NA	1.75	NA
		Soft soil	1.75	NA	1.50	NA	1.75	NA
	Type II Bearings	Fixed base	1.25	1.00	1.00	1.00	1.25	0.75
		Soft soil	1.25	1.00	1.00	0.75	1.00	0.75
Wall pier substructure	Type I Bearings	Fixed base	1.75	NA	1.75	NA	1.75	NA
		Soft soil	1.50	1.50	1.50	1.50	1.50	1.50
	Type II Bearings	Fixed base	1.25	1.25	1.25	1.25	1.25	1.25
		Soft soil	1.00	1.00	1.00	0.75	1.00	1.00

Table A.84. Scale Factor at which Transverse Bearing Unseating Occurs – CG Ground Motions

			Steel short (Ss) superstructure		Steel long (Sl) superstructure		Concrete (Cs) superstructure	
			Short (15 ft)	Tall (40 ft)	Short (15 ft)	Tall (40 ft)	Short (15 ft)	Tall (40 ft)
Column pier substructure	Type I Bearings	Fixed base	NA	NA	NA	NA	NA	NA
		Soft soil	NA	NA	NA	NA	NA	NA
	Type II Bearings	Fixed base	1.25	1.75	1.25	1.75	1.25	1.75
		Soft soil	1.25	1.75	1.75	1.50	1.50	1.75
Wall pier substructure	Type I Bearings	Fixed base	NA	NA	NA	NA	NA	NA
		Soft soil	NA	NA	NA	NA	NA	NA
	Type II Bearings	Fixed base	1.50	1.50	1.25	1.25	1.25	1.25
		Soft soil	1.25	1.25	1.50	1.50	1.50	1.50

Table A.85. Longitudinal Fundamental Period of Vibration (sec)

			Steel short (Ss) superstructure				Steel long (Sl) superstructure				Concrete short (Cs) superstructure			
			Short (15 ft)		Tall (40 ft)		Short (15 ft)		Tall (40 ft)		Short (15 ft)		Tall (40 ft)	
			Elast.	Fused	Elast.	Fused	Elast.	Fused	Elast.	Fused	Elast.	Fused	Elast.	Fused
Column pier substructure	Type I Bearings	Fixed base	0.65	0.73	1.32	1.32	0.84	0.95	1.52	1.52	0.78	0.89	1.65	1.66
		Soft soil	0.73	0.80	1.35	1.35	0.94	1.02	1.54	1.55	0.88	0.97	1.69	1.70
	Type II Bearings	Fixed base	0.63	0.70	1.19	1.20	0.88	1.01	1.80	1.81	0.75	0.84	1.43	1.43
		Soft soil	0.71	0.76	1.22	1.22	1.00	1.10	1.84	1.84	0.84	0.91	1.45	1.46
Wall pier substructure	Type I Bearings	Fixed base	0.37	0.58	0.93	0.95	0.57	0.78	1.12	1.15	0.44	0.71	1.09	1.13
		Soft soil	0.58	0.69	1.07	1.08	0.74	0.89	1.26	1.28	0.69	0.83	1.27	1.29
	Type II Bearings	Fixed base	0.37	0.57	0.89	0.90	0.57	0.81	1.21	1.26	0.43	0.68	1.03	1.05
		Soft soil	0.57	0.66	1.01	1.02	0.77	0.94	1.39	1.42	0.67	0.79	1.17	1.18

Table A.86. Transverse Fundamental Period of Vibration (sec)

			Steel short (Ss) superstructure				Steel long (Sl) superstructure				Concrete short (Cs) superstructure			
			Short (15 ft)		Tall (40 ft)		Short (15 ft)		Tall (40 ft)		Short (15 ft)		Tall (40 ft)	
			Elast.	Fused	Elast.	Fused	Elast.	Fused	Elast.	Fused	Elast.	Fused	Elast.	Fused
Column pier substructure	Type I Bearings	Fixed base	0.24	0.80	0.33	0.96	0.37	0.93	0.53	1.19	0.29	0.97	0.40	1.17
		Soft soil	0.33	0.82	0.41	1.01	0.48	0.98	0.62	1.25	0.40	1.00	0.49	1.23
	Type II Bearings	Fixed base	0.24	0.73	0.33	0.91	0.37	1.06	0.53	1.32	0.29	0.84	0.40	1.07
		Soft soil	0.33	0.75	0.41	0.95	0.48	1.11	0.62	1.38	0.40	0.88	0.49	1.13
Wall pier substructure	Type I Bearings	Fixed base	0.19	0.78	0.19	0.78	0.28	0.91	0.29	0.91	0.22	0.95	0.23	0.95
		Soft soil	0.33	0.81	0.41	0.82	0.46	0.96	0.53	0.98	0.39	0.98	0.46	0.99
	Type II Bearings	Fixed base	0.19	0.71	0.19	0.71	0.28	1.04	0.29	1.04	0.22	0.83	0.23	0.83
		Soft soil	0.33	0.74	0.41	0.75	0.46	1.08	0.53	1.10	0.39	0.86	0.46	0.88

Table A.87. Longitudinal Sequence of Damage – Pa Ground Motions

(a) Short Steel (Ss) Superstructure

			Short Pier (15 ft)	Tall Pier (40 ft)
Column Pier	Type I Bearings	Fixed base	| Bw P2 | | (1) | | P1 | |	| Bw | P1 | (1) P2 | EP | Fb | |
		Soft soil	| Bw P2 | | (1) | | EP P1 | |	| Bw | | (1) P1 P2 | | EP Fb | |
	Type II Bearings	Fixed base	| Bw EP P2 | | (1) | UA | | Fb |	| Bw | EP UA | (1) P1 P2 | Fb | | |
		Soft soil	| Bw EP | P2 | (1) | UA | | |	| Bw | EP UA | (1) P1 P2 | | Fb | |
Wall Pier	Type I Bearings	Fixed base	| Bw Fb P2 | (1) EP | P1 | | |	| Bw Fb P1 P2 | (1) EP | | | |
		Soft soil	| Bw P2 | Fb | (1) P1 | EP | | |	| Bw P1 P2 Fb | EP | (1) | | | |
	Type II Bearings	Fixed base	| Bw EP Fb P2 | | (1) | UA | | P1 |	| Bw EP P1 P2 | Fb UA | (1) | | UP | |
		Soft soil	| Bw EP P2 | Fb | (1) | UA | P1 | |	| Bw EP Fb P1 P2 | UA | (1) | UP | | |

(b) Long Steel (Sl) Superstructure

			Short Pier (15 ft)	Tall Pier (40 ft)
Column Pier	Type I Bearings	Fixed base	| Bw P2 | | (1) P1 | | | |	| Bw | | (1) | P1 P2 | | |
		Soft soil	| Bw P2 | (1) P1 | | | |	| Bw | | (1) P1 P2 | | | |
	Type II Bearings	Fixed base	| Bw EP P2 | | (1) | UA | | |	| Bw | EP UA | (1) P1 P2 | | | |
		Soft soil	| Bw EP P2 | (1) UA | | | UP |	| Bw EP | UA | (1) P1 P2 | | | |
Wall Pier	Type I Bearings	Fixed base	| Bw P2 | P1 | (1) | | | |	| Bw P1 P2 | | (1) | | | |
		Soft soil	| Bw P2 | P1 | (1) | | | |	| Bw P1 P2 | | (1) | | | |
	Type II Bearings	Fixed base	| Bw EP P2 | (1) P1 | UA | | |	| Bw EP P1 P2 | UA | (1) | | | |
		Soft soil	| Bw EP P2 | (1) P1 | UA | | UP |	| Bw P1 P2 | EP UA | (1) | | | |

(c) Precast Concrete (Cs) Superstructure

			Short Pier (15 ft)	Tall Pier (40 ft)
Column Pier	Type I Bearings	Fixed base	| Bw P2 | | (1) P1 | | | |	| Bw | P1 | (1) P2 | | | |
		Soft soil	| Bw P2 | | (1) P1 | | | |	| Bw | P1 | (1) P2 | | | |
	Type II Bearings	Fixed base	| Bw EP P2 | | (1) | UA | | |	| Bw | EP | (1) P1 P2 UA | | | |
		Soft soil	| Bw EP | P2 | (1) | UA | | UP |	| Bw | EP | (1) P1 P2 UA | | | |
Wall Pier	Type I Bearings	Fixed base	| Bw P2 | P1 | (1) | EP | | Fb |	| Bw P1 P2 | | (1) | | | Fb |
		Soft soil	| Bw P2 | P1 | (1) | | EP Fb | |	| Bw P1 P2 | | (1) | EP | Fb | |
	Type II Bearings	Fixed base	| Bw EP P2 | | (1) | | P1 UA | Fb |	| Bw EP P1 P2 | | (1) UA | | Fb | |
		Soft soil	| Bw EP P2 | | (1) | UA | P1 | Fb |	| Bw EP P1 P2 | | (1) UA | | | Fb |

Table A.88. Longitudinal Sequence of Damage – CG Ground Motions

(a) Short Steel (Ss) Superstructure

			Short Pier (15 ft)	Tall Pier (40 ft)
Column Pier	Type I Bearings	Fixed base	| Bw P2 | | (1) | | EP P1 | |	| Bw | | (1) | | P1 P2 | Fb |
		Soft soil	| Bw | P2 | (1) | | EP | P1	| Bw | | (1) | P1 | P2 | |
	Type II Bearings	Fixed base	| EP | Bw P2 | (1) | | UA | Fb |	| Bw | EP | (1) | UA | P1 P2 | Fb |
		Soft soil	| EP | Bw | (1) | P2 | UA | |	| Bw | EP | (1) | UA | P1 P2 | |
Wall Pier	Type I Bearings	Fixed base	| Fb P2 | Bw | (1) P1 | | EP | |	| Bw P1 P2 | Fb | (1) | | | |
		Soft soil	| Bw P2 | Fb | (1) P1 | EP | | |	| Bw P1 P2 | Fb | (1) EP | | | |
	Type II Bearings	Fixed base	| EP P2 | Bw Fb | (1) P1 | | UA | |	| Bw EP P2 | P1 | (1) Fb | UA | | |
		Soft soil	| EP P2 | Bw Fb | (1) | P1 | | UA |	| Bw EP | Fb P1 P2 | (1) | UA | | |

(b) Long Steel (Sl) Superstructure

			Short Pier (15 ft)	Tall Pier (40 ft)
Column Pier	Type I Bearings	Fixed base	| Bw P2 | | (1) | | P1 | |	| Bw | | (1) | | | P1 |
		Soft soil	| Bw | P2 | (1) | | P1 | |	| Bw | | (1) | | | P1 P2 |
	Type II Bearings	Fixed base	| Bw EP P2 | | (1) | | | |	| Bw | | (1) EP | UA | P1 | P2 |
		Soft soil	| Bw | EP P2 | (1) | | | UA |	| Bw | EP | (1) | UA | P1 P2 | |
Wall Pier	Type I Bearings	Fixed base	| Bw P2 | | (1) P1 | | | |	| Bw | P1 P2 | (1) | | | |
		Soft soil	| Bw P2 | | (1) P1 | | | |	| Bw | P1 P2 | (1) | | | |
	Type II Bearings	Fixed base	| Bw EP P2 | (1) P1 | | | |	| Bw EP | P1 P2 | (1) | UA | | |
		Soft soil	| Bw EP P2 | (1) | P1 | | UA |	| Bw | EP P1 P2 | (1) | UA | | |

(c) Precast Concrete (Cs) Superstructure

			Short Pier (15 ft)	Tall Pier (40 ft)
Column Pier	Type I Bearings	Fixed base	| Bw P2 | EA | (1) | P1 | | |	| Bw | | (1) | P1 | P2 | |
		Soft soil	| Bw | P2 | (1) | P1 | | |	| Bw | | (1) | P1 | P2 | |
	Type II Bearings	Fixed base	| Bw EP P2 | | (1) | | | |	| Bw | EP | (1) | | P1 UA | P2 |
		Soft soil	| Bw EP | | (1) P2 | | | |	| Bw | EP | (1) | | P1 P2 UA | |
Wall Pier	Type I Bearings	Fixed base	| Bw P2 | | (1) P1 | | EP Fb | |	| Bw P1 P2 | | (1) | | | Fb |
		Soft soil	| Bw P2 | | (1) P1 | | EP Fb | |	| Bw P1 P2 | | (1) | | | |
	Type II Bearings	Fixed base	| Bw EP P2 | | (1) | P1 | | Fb |	| Bw EP | P2 | (1) P1 | | UA |
		Soft soil	| Bw EP P2 | | (1) | | P1 Fb | |	| Bw EP | | (1) P1 P2 | | UA | |

Table A.89. Transverse Sequence of Damage – Pa Ground Motions

(a) Short Steel (Ss) Superstructure

			Short Pier (15 ft)	Tall Pier (40 ft)
Column Pier	Type I Bearings	Fixed base	| RA Fb | | (1) EP | | RP | UA UP |	| RA | P1 P2 | (1) | | | |
		Soft soil	| RA | Fb | (1) | EP | RP | UA UP |	| RA | P1 P2 | (1) | | | |
	Type II Bearings	Fixed base	| RA Fb | EP | (1) | RP UA | UP | |	| RA | P1 P2 | (1) EP UA | | RP | |
		Soft soil	| RA | Fb EP | (1) | RP UA | UP | |	| RA | P1 P2 UA | (1) EP | | RP | |
Wall Pier	Type I Bearings	Fixed base	| RA Fb | | (1) EP | | RP | UA |	| RA Fb | | (1) EP RP | | | |
		Soft soil	| RA Fb | | (1) EP | RP | UP | UA |	| RA Fb | | (1) EP RP | | UP | UA |
	Type II Bearings	Fixed base	| RA Fb | EP | (1) | RP UA | UP | |	| RA Fb | EP RP | (1) | UA | UP | |
		Soft soil	| RA | Fb EP | (1) UA | UP | | |	| RA Fb | EP RP | (1) UA UP | | | |

(b) Long Steel (Sl) Superstructure

			Short Pier (15 ft)	Tall Pier (40 ft)
Column Pier	Type I Bearings	Fixed base	| RA | Fb P2 | (1) P1 | | | UA UP |	| RA P1 P2 | | (1) | | | |
		Soft soil	| RA | | (1) Fb P2 | P1 | UA | UP |	| RA | P1 P2 | (1) | | | |
	Type II Bearings	Fixed base	| RA | EP Fb P2 | (1) P1 UA | UP | |	| RA P1 P2 | | (1) UA | | |
		Soft soil	| RA | EP Fb P2 | (1) UA | P1 | UP | |	| RA P1 P2 | UA | (1) | | | |
Wall Pier	Type I Bearings	Fixed base	| RA | Fb | (1) | EP RP | | UA |	| RA | Fb | (1) | EP RP | | |
		Soft soil	| | RA Fb | (1) | EP | RP UA UP | |	| RA | | (1) Fb | EP RP | UA UP | |
	Type II Bearings	Fixed base	| RA | EP Fb | (1) | RP UA | UP | |	| RA | Fb EP RP | (1) | UA | | UP |
		Soft soil	| RA | Fb | (1) EP RP UA | UP | | |	| RA | Fb EP RP UA | (1) | | UP | |

(c) Precast Concrete (Cs) Superstructure

			Short Pier (15 ft)	Tall Pier (40 ft)
Column Pier	Type I Bearings	Fixed base	| RA Fb | | (1) EP P1 | RP | | UA UP |	| RA P1 P2 | | (1) | | | |
		Soft soil	| RA | Fb | (1) | EP RP P1 | | UP |	| RA | P1 P2 | (1) | | | |
	Type II Bearings	Fixed base	| RA Fb | EP | (1) RP | UA | UP | |	| RA | P1 P2 UA | (1) | | | |
		Soft soil	| RA | Fb EP | (1) UA | RP | UP | |	| RA | P1 P2 UA | (1) | | | |
Wall Pier	Type I Bearings	Fixed base	| RA Fb | EP | (1) RP | | | UP |	| RA Fb | EP | (1) RP | | | |
		Soft soil	| RA | Fb | (1) EP RP | | UP | UA |	| RA | Fb | (1) EP RP | | UP | UA |
	Type II Bearings	Fixed base	| RA Fb | EP | (1) RP | UA | UP | |	| RA Fb | EP | (1) RP | UA | UP | |
		Soft soil	| | RA EP Fb | (1) UA | RP UP | | |	| RA EP | Fb | (1) UA | UP | | |

Table A.90. Transverse Sequence of Damage – CG Ground Motions

(a) Short Steel (Ss) Superstructure

			Short Pier (15 ft)	Tall Pier (40 ft)
Column Pier	Type I Bearings	Fixed base	| RA Fb | | (1) | | EP | RP |	| RA | | (1) | P2 | P1 | |
		Soft soil	| RA | Fb | (1) | | EP | RP |	| RA | | (1) | P2 | P1 | |
	Type II Bearings	Fixed base	| RA Fb | | (1) EP | UA | RP | UP |	| RA | | (1) EP | P2 | P1 RP | UA |
		Soft soil	| RA | Fb | (1) EP | UA | RP | UP |	| RA | | (1) EP | P2 | P1 RP | UA |
Wall Pier	Type I Bearings	Fixed base	| RA Fb | | (1) | | EP | RP |	| RA Fb | | (1) | EP RP | | |
		Soft soil	| RA Fb | | (1) | | EP RP |	| RA | Rb | (1) | EP RP | | |
	Type II Bearings	Fixed base	| RA Fb | | (1) EP | RP | UA | UP |	| RA Fb | | (1) EP RP | | UA | UP |
		Soft soil	| RA | Fb | (1) | UA | UP | |	| RA | Fb EP | (1) RP | UA | UP | |

(b) Long Steel (Sl) Superstructure

			Short Pier (15 ft)	Tall Pier (40 ft)
Column Pier	Type I Bearings	Fixed base	| RA | Fb P2 | (1) | P1 | | |	| RA | | (1) P1 P2 | | |
		Soft soil	| RA | | (1) | | Fb P2 | |	| RA | | (1) | P1 P2 | | |
	Type II Bearings	Fixed base	| RA | Fb P2 | (1) EP | P1 UA | | UP |	| RA | | (1) P1 P2 | | | UA |
		Soft soil	| RA | | (1) | EP Fb P2 | | UA |	| RA | | (1) | P1 P2 | UA | |
Wall Pier	Type I Bearings	Fixed base	| RA | Fb | (1) | | EP RP | |	| RA | Fb | (1) | | EP RP | |
		Soft soil	| | RA | (1) | Fb | | |	| RA | | (1) | Fb | | EP RP |
	Type II Bearings	Fixed base	| RA | EP Fb | (1) | RP UA | | UP |	| RA | Fb | (1) EP RP | UA | | |
		Soft soil	| RA | | (1) Fb | EP RP | UA | |	| RA | | (1) Fb EP RP | | UA | |

(c) Precast Concrete (Cs) Superstructure

			Short Pier (15 ft)	Tall Pier (40 ft)
Column Pier	Type I Bearings	Fixed base	| RA Fb | | (1) | EP P1 | RP | |	| RA | P2 | (1) P1 | | | |
		Soft soil	| RA | | (1) Fb | | | EP RP |	| RA | | (1) P2 | P1 | | |
	Type II Bearings	Fixed base	| RA Fb | | (1) EP | RP UA | | |	| RA | | (1) | | P2 | P1 UA |
		Soft soil	| RA | | (1) Fb EP | | RP UA | |	| RA | | (1) | P2 | P1 | UA |
Wall Pier	Type I Bearings	Fixed base	| RA Fb | | (1) EP | | RP | |	| RA Fb | | (1) EP | RP | | |
		Soft soil	| Ra Fb | | (1) | | RP | |	| RA | Fb | (1) | EP | RP | |
	Type II Bearings	Fixed base	| RA Fb | EP | (1) RP | UA | | UP |	| RA Fb | EP | (1) | RP UA | | |
		Soft soil	| | RA | (1) EP Fb | | RP UA | UP |	| RA | EP | (1) Fb | | UA | UP |

APPENDIX B GROUND MOTIONS

Results of time history analyses are, in general, markedly dependent on ground motion characteristics. Thus, every effort was made to select ground motions and scaling methods appropriate for southern Illinois. Table B.1 summarizes key ground motion characteristics, including the scale factor applied to the original record to produce the input ground motion at SF = 1.0. This value was applied to all ordinates of the raw time history, and to reach scale factors other than 1.0, a secondary factor equal to the SF of interest was applied. Figures B.1 through B.20 show the soil (Pa) and rock (CG) ground motions as scaled to SF = 1.0. Among the 20 ground motions, there were noticeable differences in duration, total number of cycles, and number of extreme cycles. These ground motion characteristics can be an important factor in determining seismic response of a nonlinear system.

Table B.91. Ground Motion Characteristics

Record ID	Record Length (s)	Scale Factor at SF = 1.0	Unscaled PGA	Scaled to SF = 1.0			V_{max}/A_{max}	Significant Duration (s)
				PGA (g)	PGV (in/s)	PGD (in)		
Pa01	43	1.86	0.45	0.83	41.7	41.0	0.13	19.7
Pa02	88	1.74	0.33	0.58	30.4	20.1	0.14	33.2
Pa03	58	1.81	0.39	0.70	27.7	14.4	0.10	29.7
Pa04	85	1.94	0.35	0.67	24.2	21.8	0.09	29.5
Pa05	88	1.92	0.32	0.62	29.5	96.8	0.12	28.6
Pa06	58	1.87	0.37	0.70	30.4	47.8	0.11	29.8
Pa07	45	1.52	0.39	0.59	29.8	15.6	0.13	19.8
Pa08	49	1.55	0.37	0.58	29.8	10.2	0.13	23.8
Pa09	42	1.34	0.51	0.68	25.8	14.5	0.10	22.9
Pa10	42	1.91	0.35	0.67	34.3	19.7	0.13	21.8
CG01	42	4.33	0.49	2.13	32.5	15.0	0.04	23.6
CG02	42	3.39	0.31	1.06	25.2	53.3	0.06	23.5
CG03	50	3.99	0.42	1.67	27.8	48.9	0.04	22.9
CG04	50	3.59	0.45	1.60	25.1	25.7	0.04	25.9
CG05	65	2.80	0.37	1.04	25.6	11.5	0.06	42.4
CG06	76	3.18	0.38	1.21	21.5	26.8	0.05	47.9
CG07	76	2.77	0.41	1.13	18.9	104.7	0.04	49.1
CG08	123	3.84	0.29	1.13	18.1	136.7	0.04	55.3
CG09	65	3.04	0.30	0.90	20.4	19.5	0.06	43.5
CG10	93	3.44	0.34	1.15	23.9	14.7	0.05	58.5

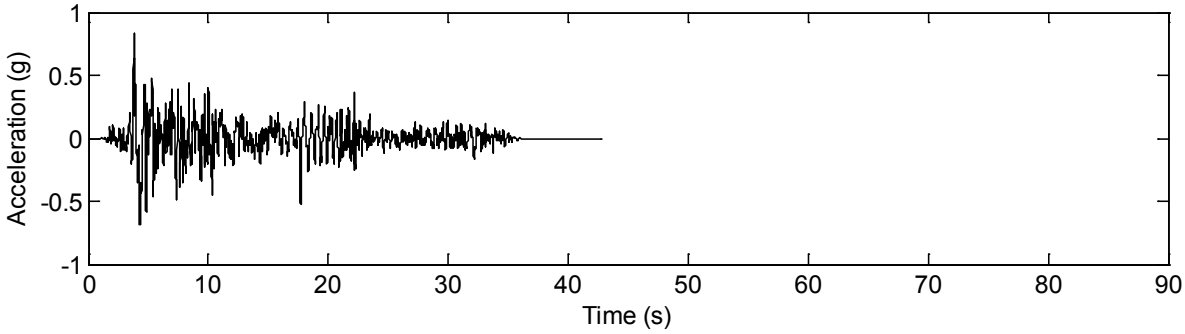

Figure B.50. Paducah 01 ground motion at SF = 1.0.

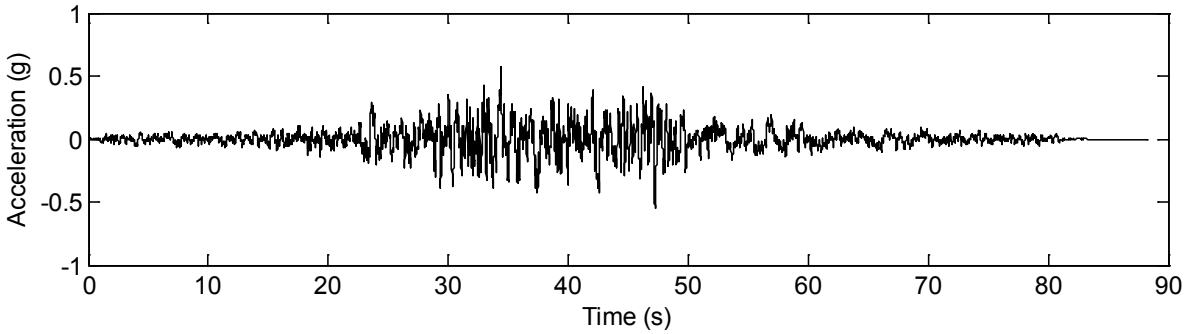

Figure B.51. Paducah 02 ground motion at SF = 1.0.

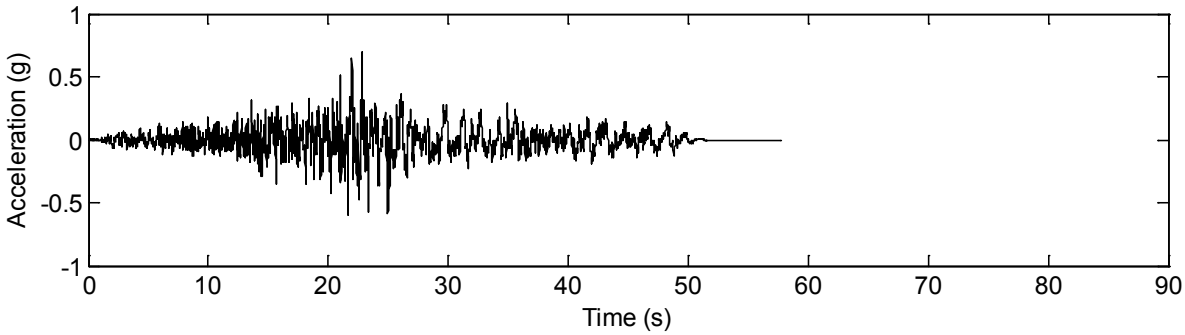

Figure B.52. Paducah 03 ground motion at SF = 1.0.

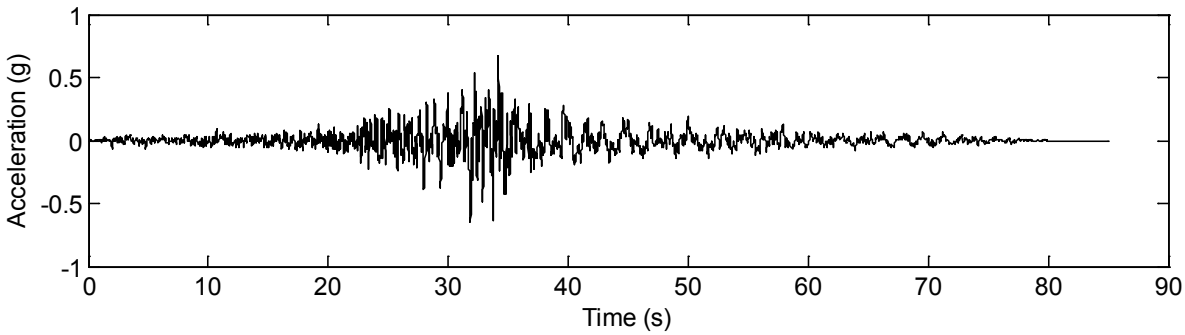

Figure B.53. Paducah 04 ground motion at SF = 1.0.

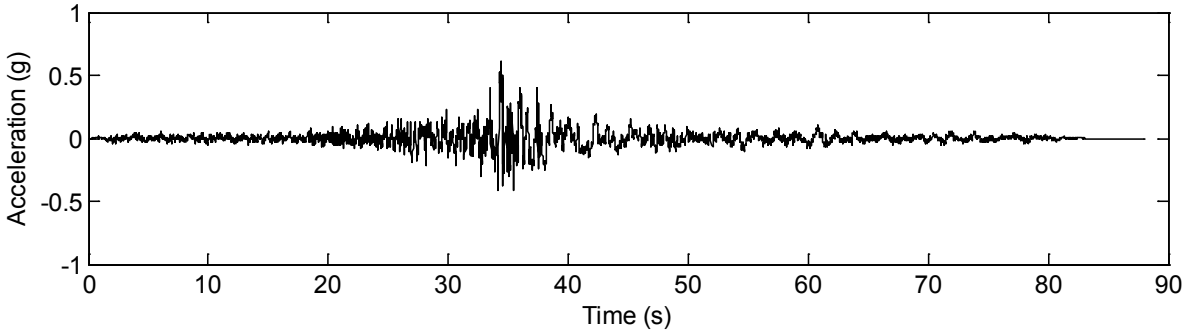

Figure B.54. Paducah 05 ground motion at SF = 1.0.

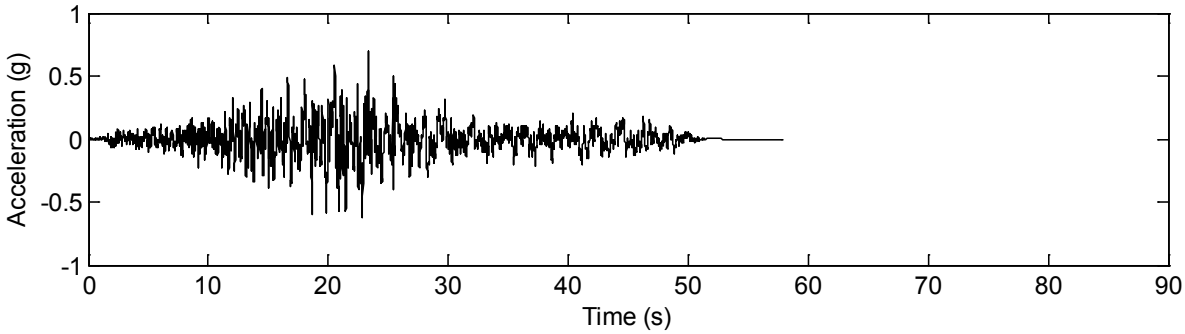

Figure B.55. Paducah 06 ground motion at SF = 1.0.

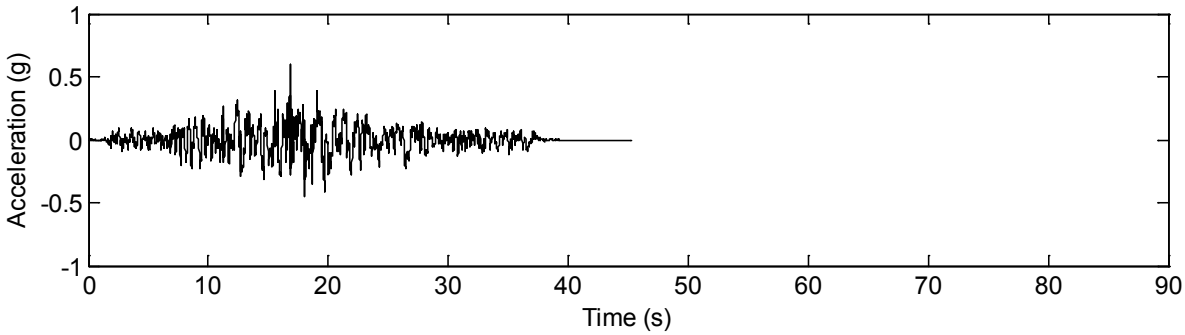

Figure B.56. Paducah 07 ground motion at SF = 1.0.

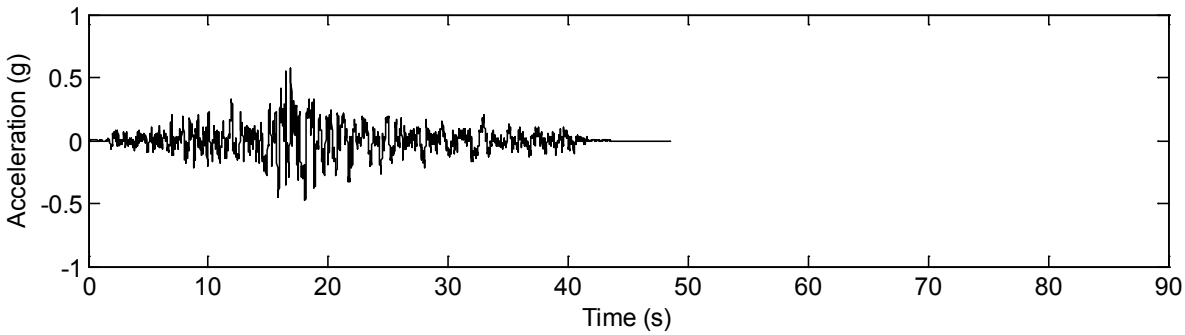

Figure B.57. Paducah 08 ground motion at SF = 1.0.

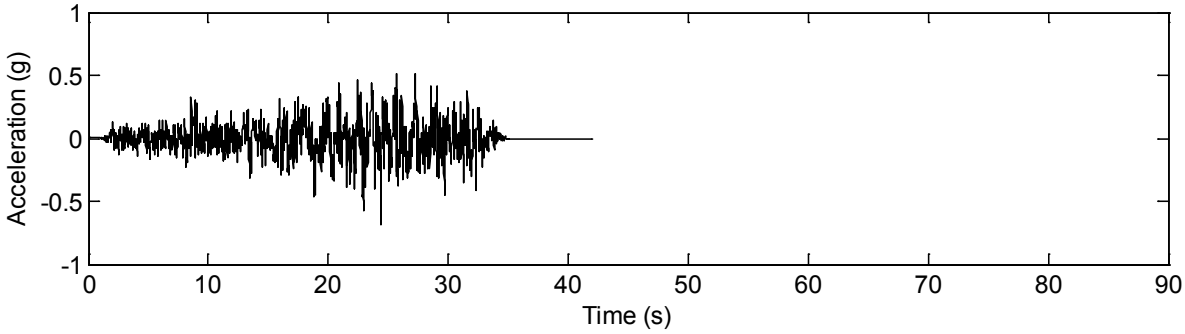

Figure B.58. Paducah 09 ground motion at SF = 1.0.

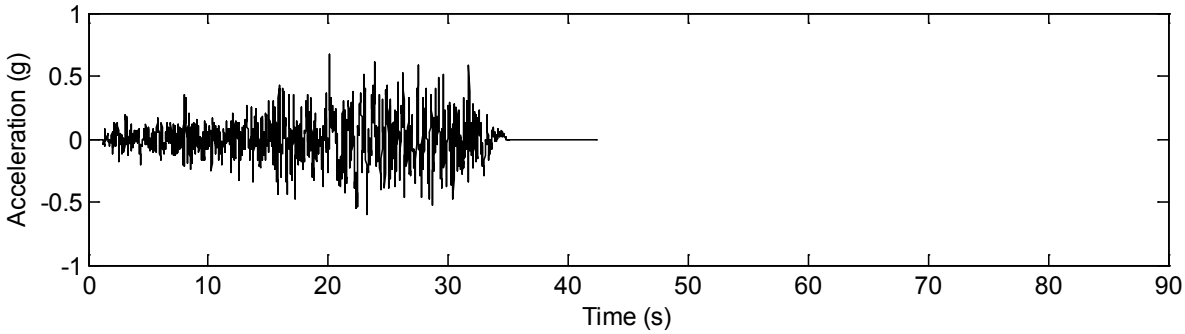

Figure B.59. Paducah 10 ground motion at SF = 1.0.

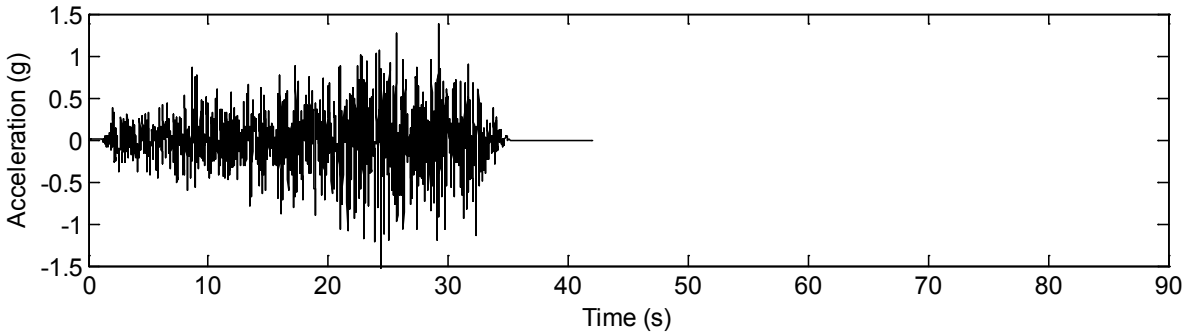

Figure B.60. Cape Girardeau 01 ground motion at SF = 1.0.

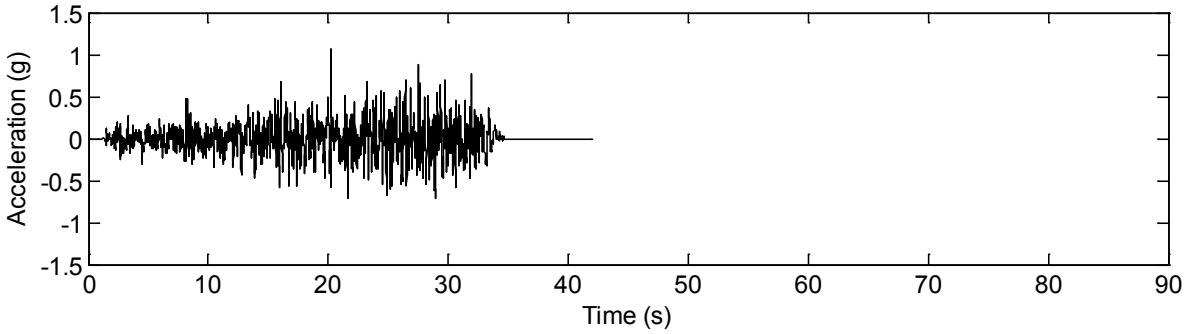

Figure B.61. Cape Girardeau 02 ground motion at SF = 1.0.

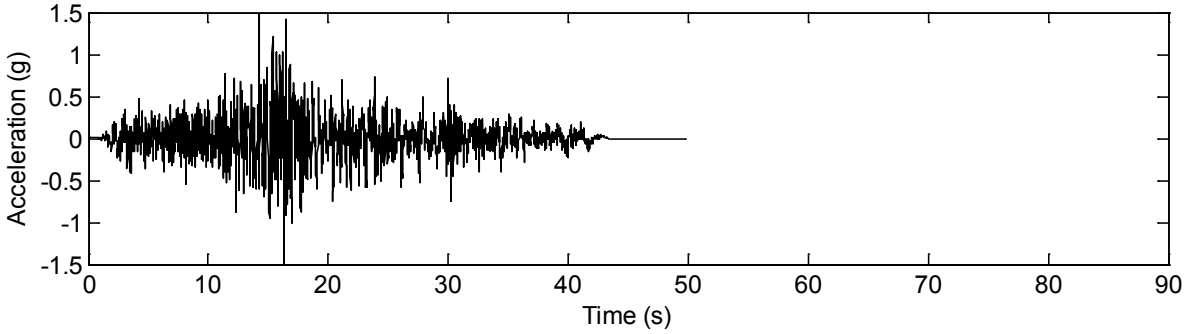

Figure B.62. Cape Girardeau 03 ground motion at SF = 1.0.

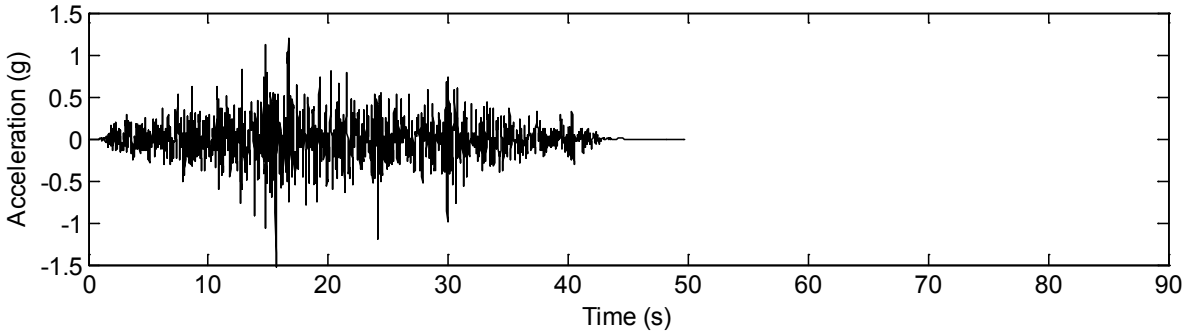

Figure B.63. Cape Girardeau 04 ground motion at SF = 1.0.

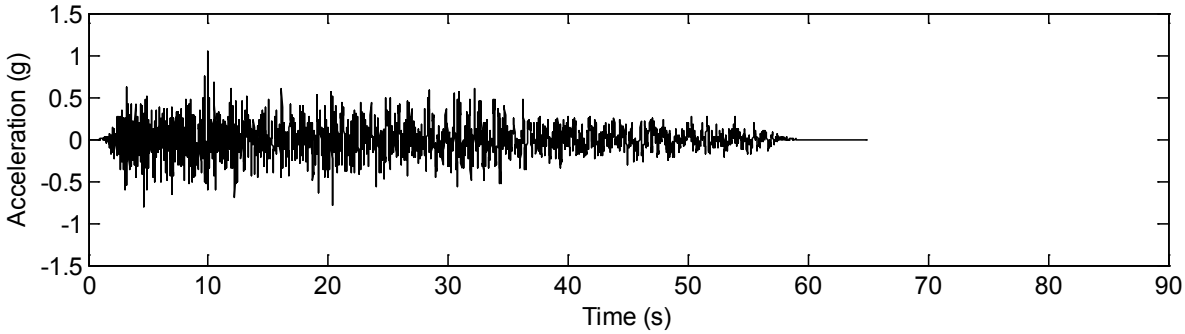

Figure B.64. Cape Girardeau 05 ground motion at SF = 1.0.

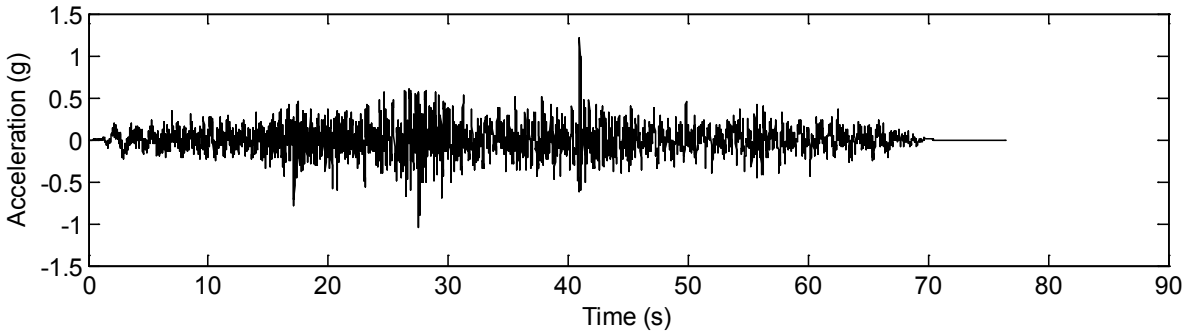

Figure B.65. Cape Girardeau 06 ground motion at SF = 1.0.

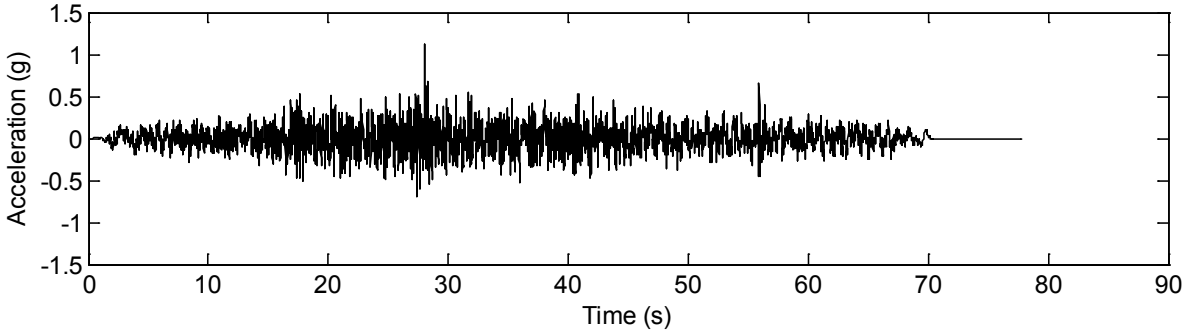

Figure B.66. Cape Girardeau 07 ground motion at SF = 1.0.

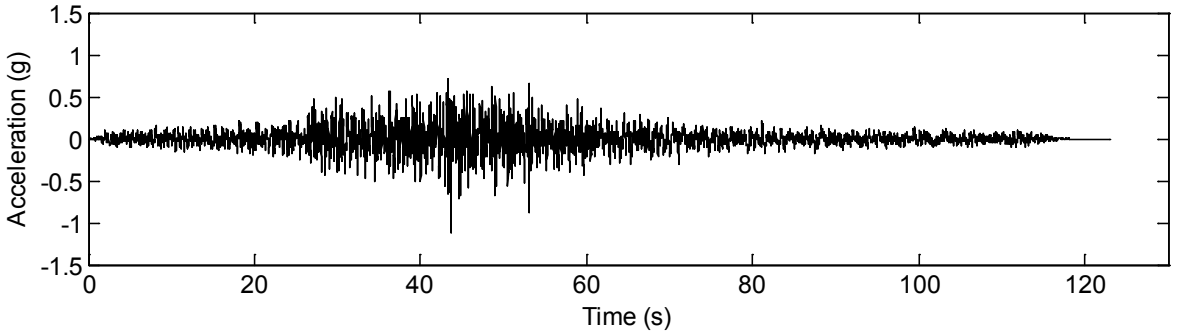

Figure B.67. Cape Girardeau 08 ground motion at SF = 1.0.

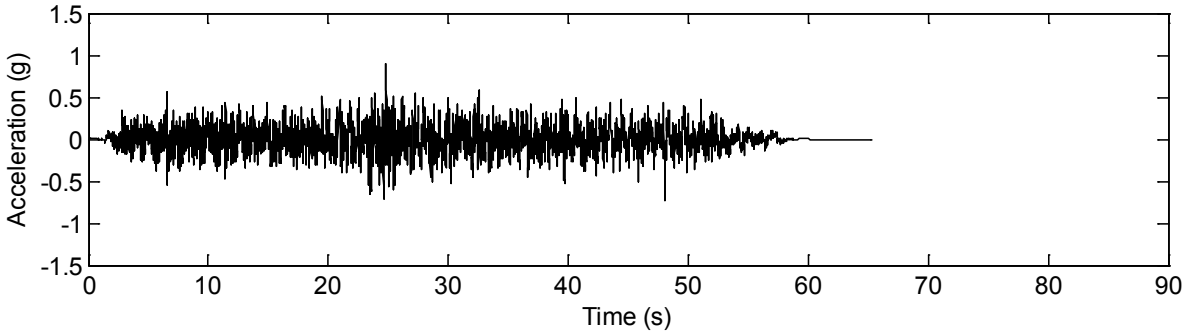

Figure B.68. Cape Girardeau 09 ground motion at SF = 1.0.

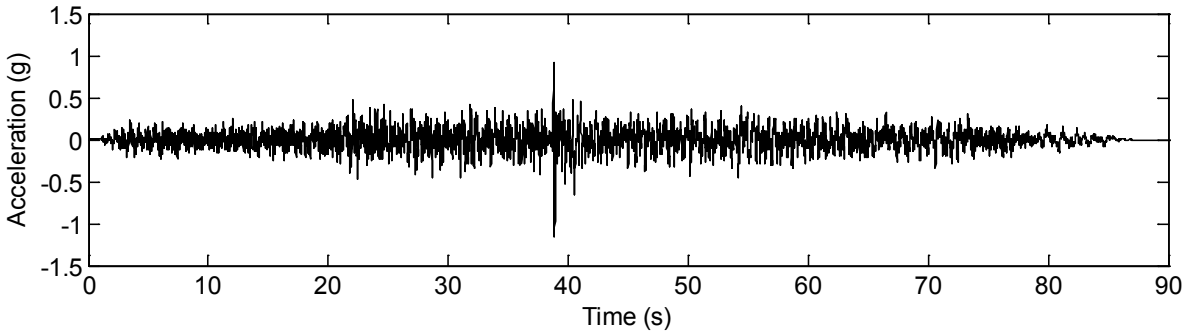

Figure B.69. Cape Girardeau 10 ground motion at SF = 1.0.

APPENDIX C RAW DATA FROM PARAMETRIC STUDY

Results for the 48 bridges are included in this appendix, organized as indicated in Table C.1. Two figures are provided for each bridge - the first figure presents longitudinal and transverse force results, while the subsequent figure provides longitudinal and transverse displacement data. Responses from rock (CG) and soil (Pa) ground motions are shown on the same plot.

This appendix uses the compact graphical form of Incremental Dynamic Analysis (IDA) curves to present more complete parametric study results than can be made available in numerical form. The curves are similar to those discussed in Chapter 3, and present the maximum force and displacement results obtained from nonlinear dynamic analyses conducted at a range of scale factors. At each scale factor, a suite of ten scaled ground motions was applied to a bridge, and the peak response varied among these ground motions. In the IDAs, rather than attempt to show individual data points, a circular marker indicates the average of the peak response for the entire suite, and side bars indicate a range of plus or minus one standard deviation. A thick line is drawn through the mean response at each scale factor to generate the IDA curve.

Figures are displayed in metric units. For conversion to English units:

1 kip = 4.448 kN
1 inch = 2.54 cm

Table C.92. Organization of Figures

Bridge Group		Figure Numbers
Ss	C 15	C.1 - C.8
	C 40	C.9 - C.16
	W 15	C.17 - C.24
	W 40	C.25 - C.32
Sl	C 15	C.33 - C.40
	C 40	C.41 - C.48
	W 15	C.49 - C.56
	W 40	C.57 - C.64
Cs	C 15	C.65 - C.72
	C 40	C.73 - C.80
	W 15	C.81 - C.88
	W 40	C.89 - C.96

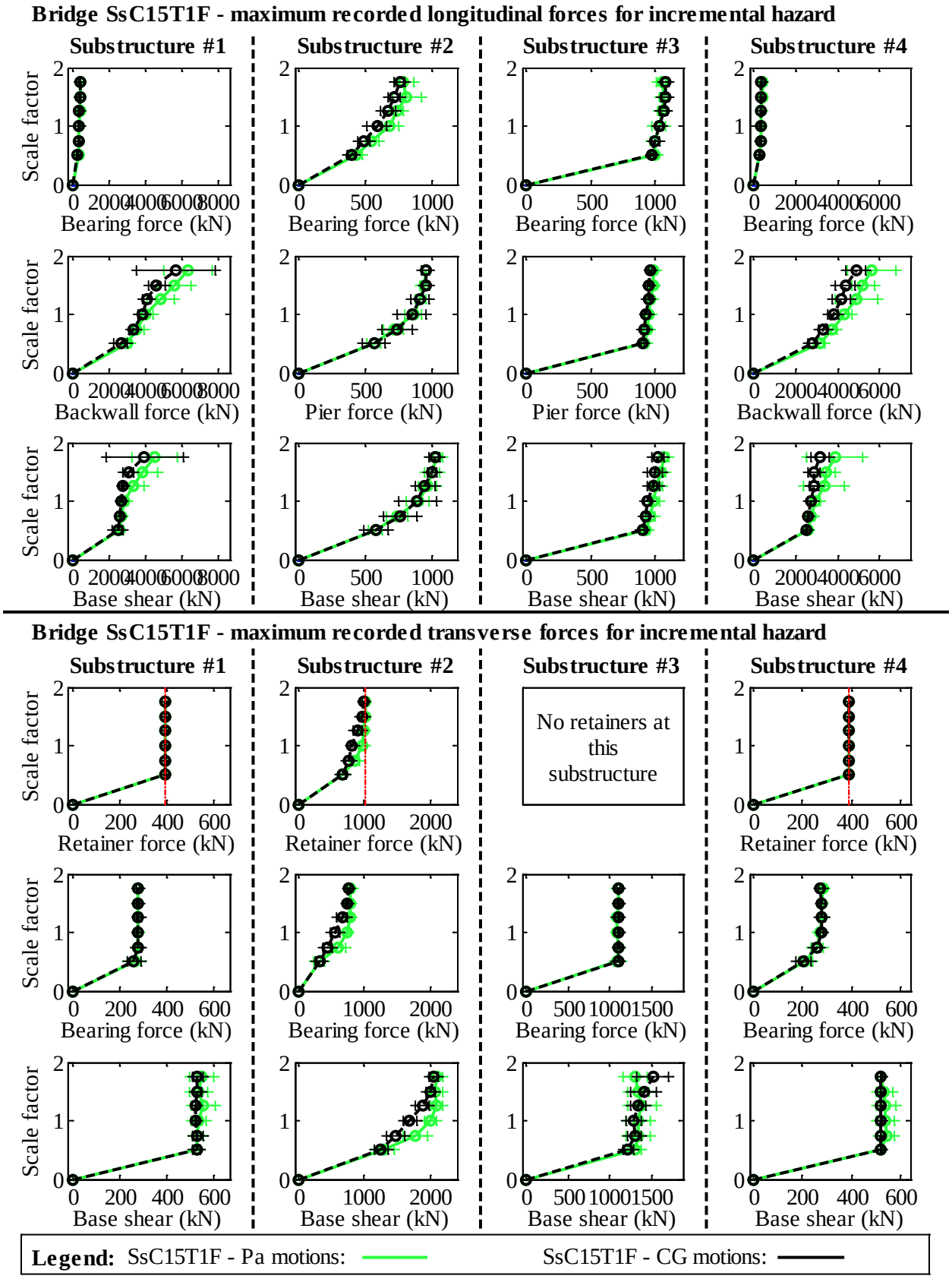

Figure C.70. Bridge SsC15T1F – force results.

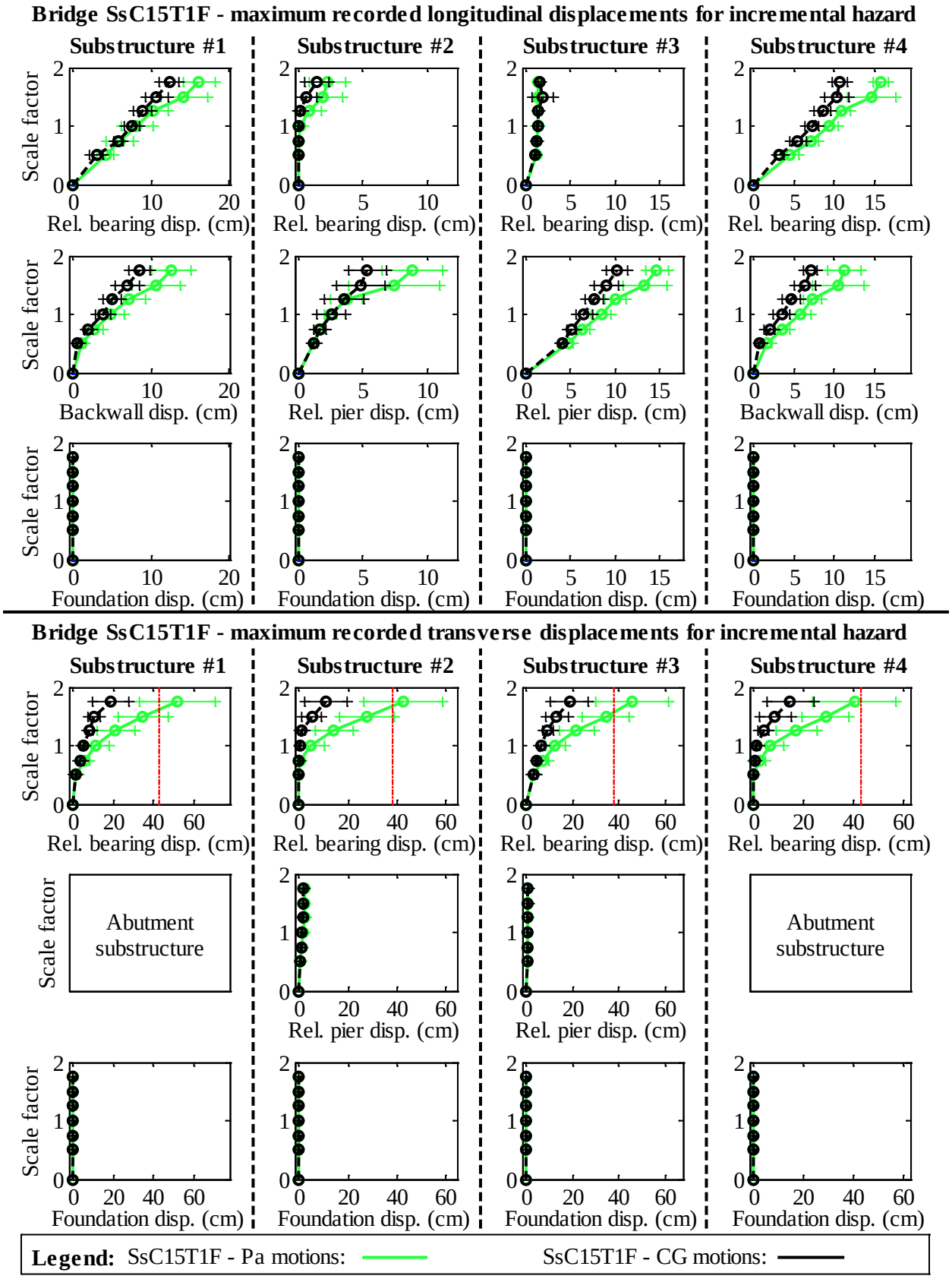

Figure C.71. Bridge SsC15T1F – displacement results.

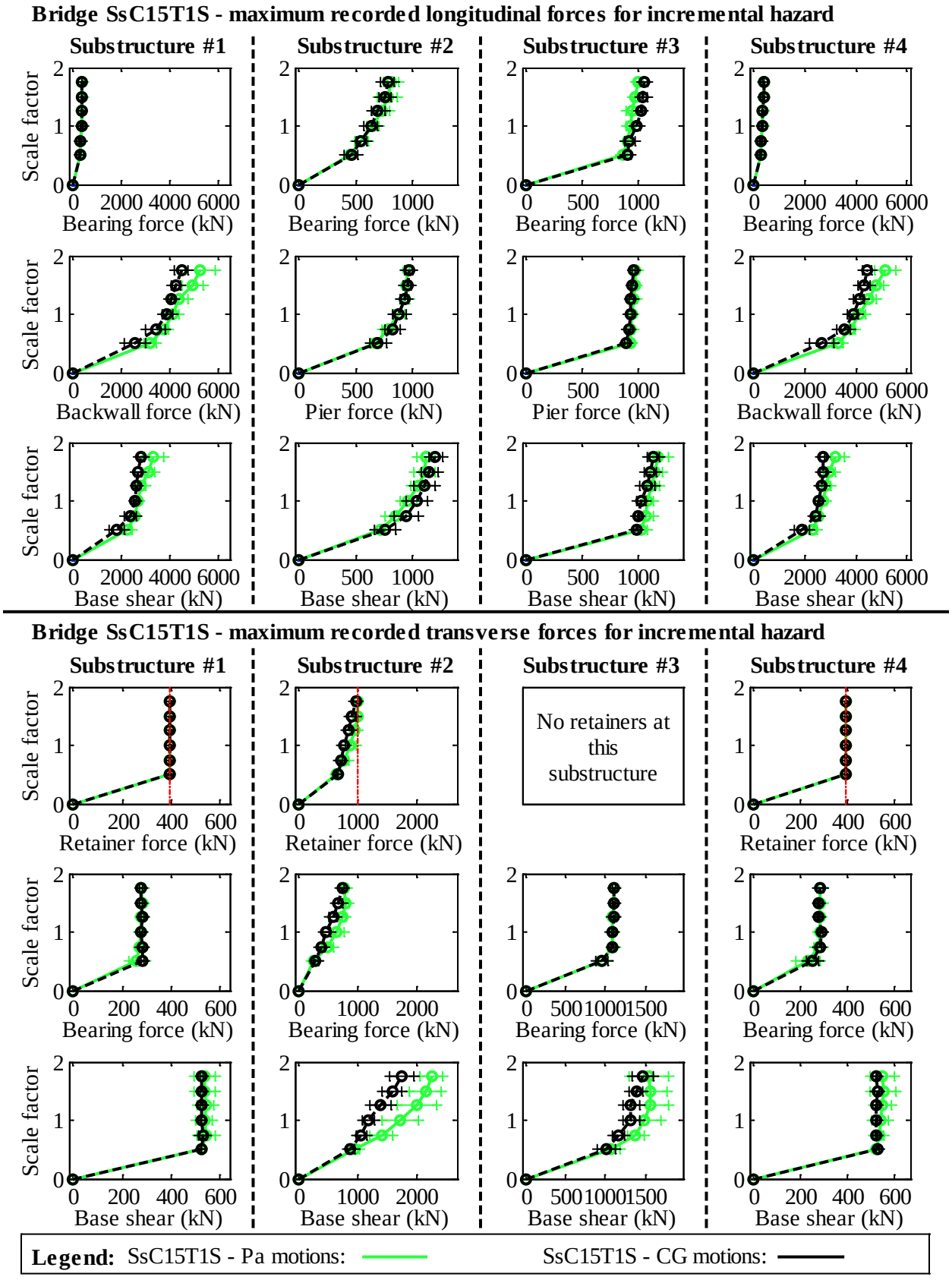

Figure C.72. Bridge SsC15T1S – force results.

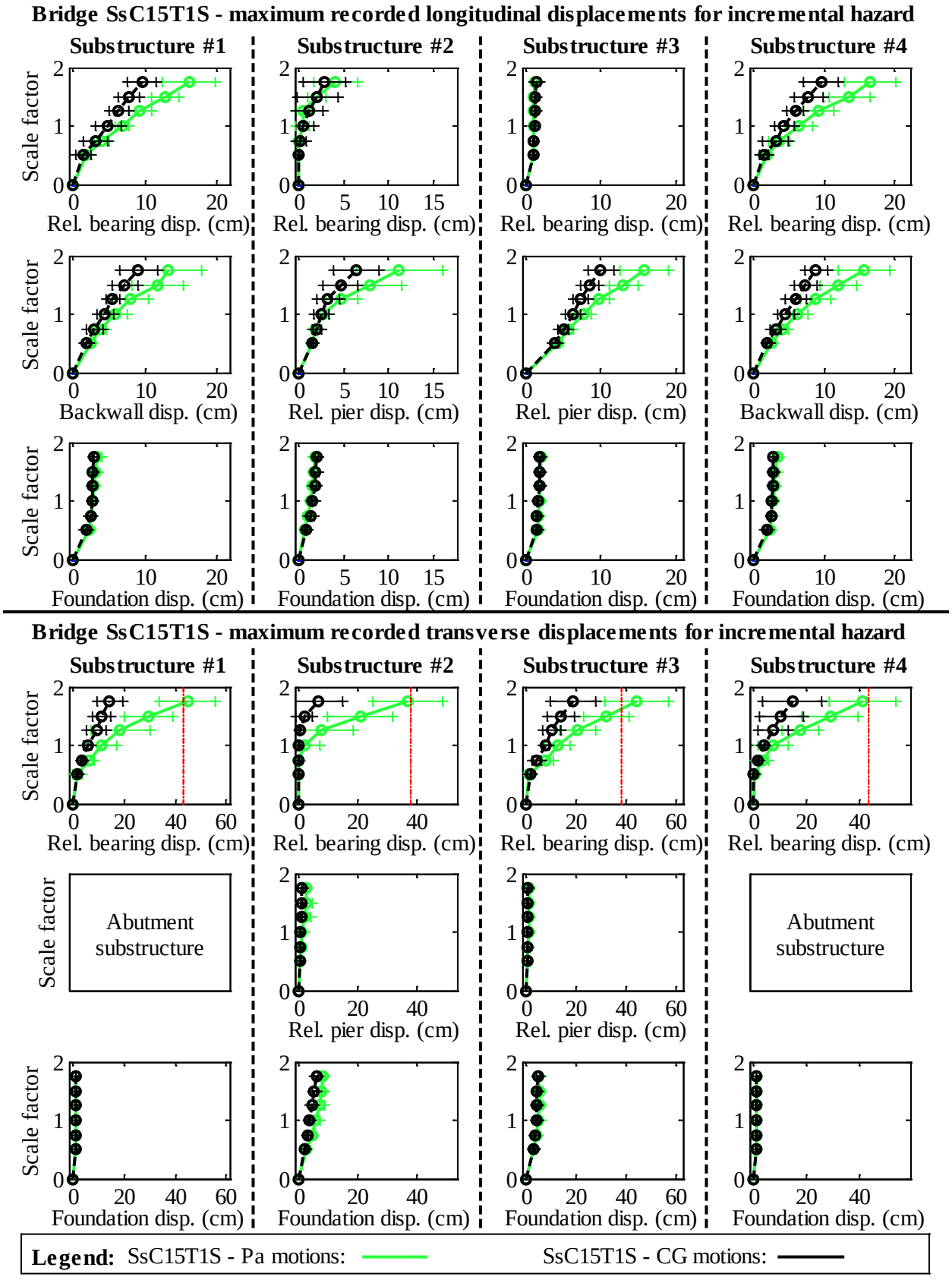

Figure C.73. Bridge SsC15T1S – displacement results.

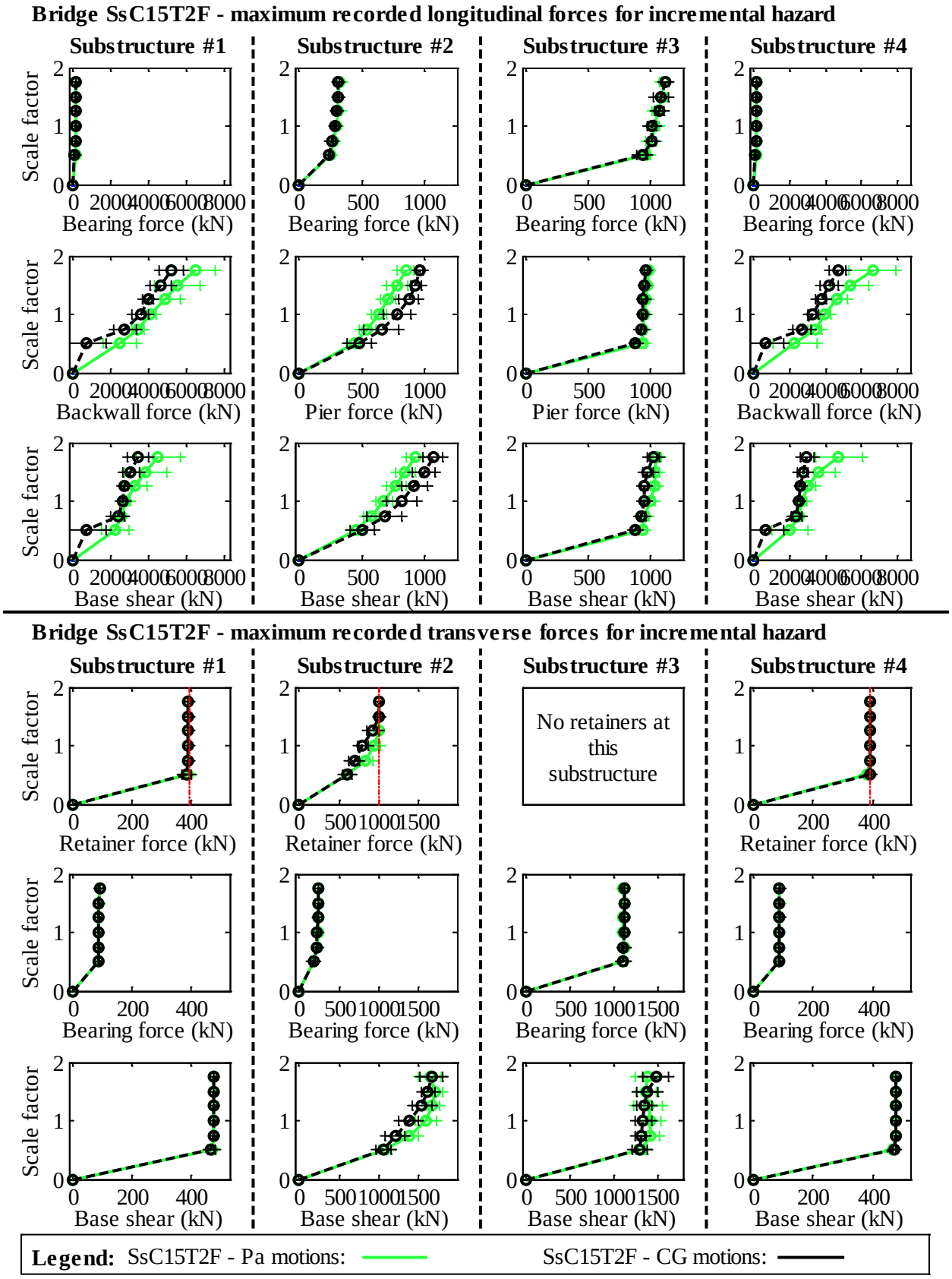

Figure C.74. Bridge SsC15T2F – force results.

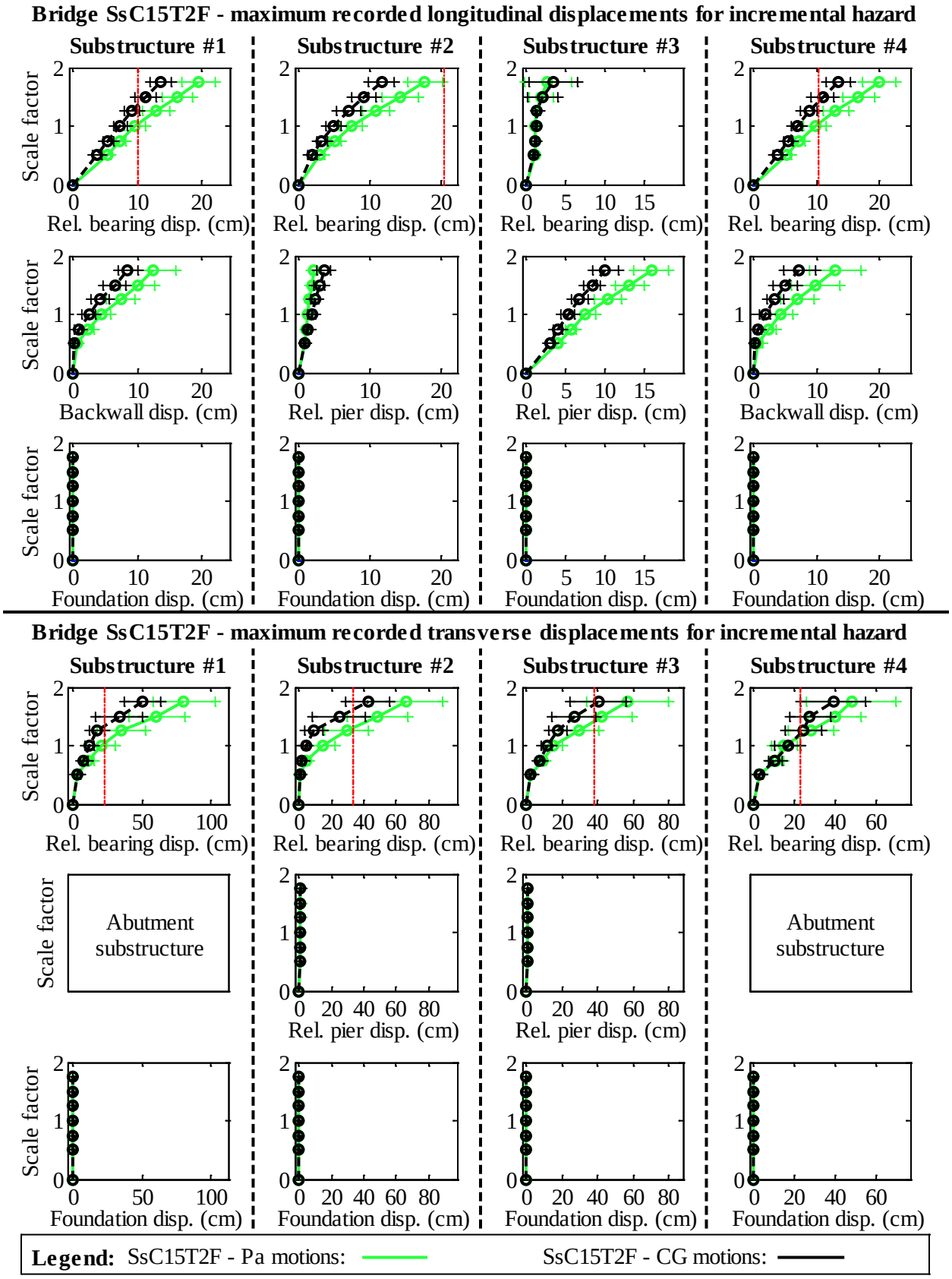

Figure C.75. Bridge SsC15T2F – displacement results.

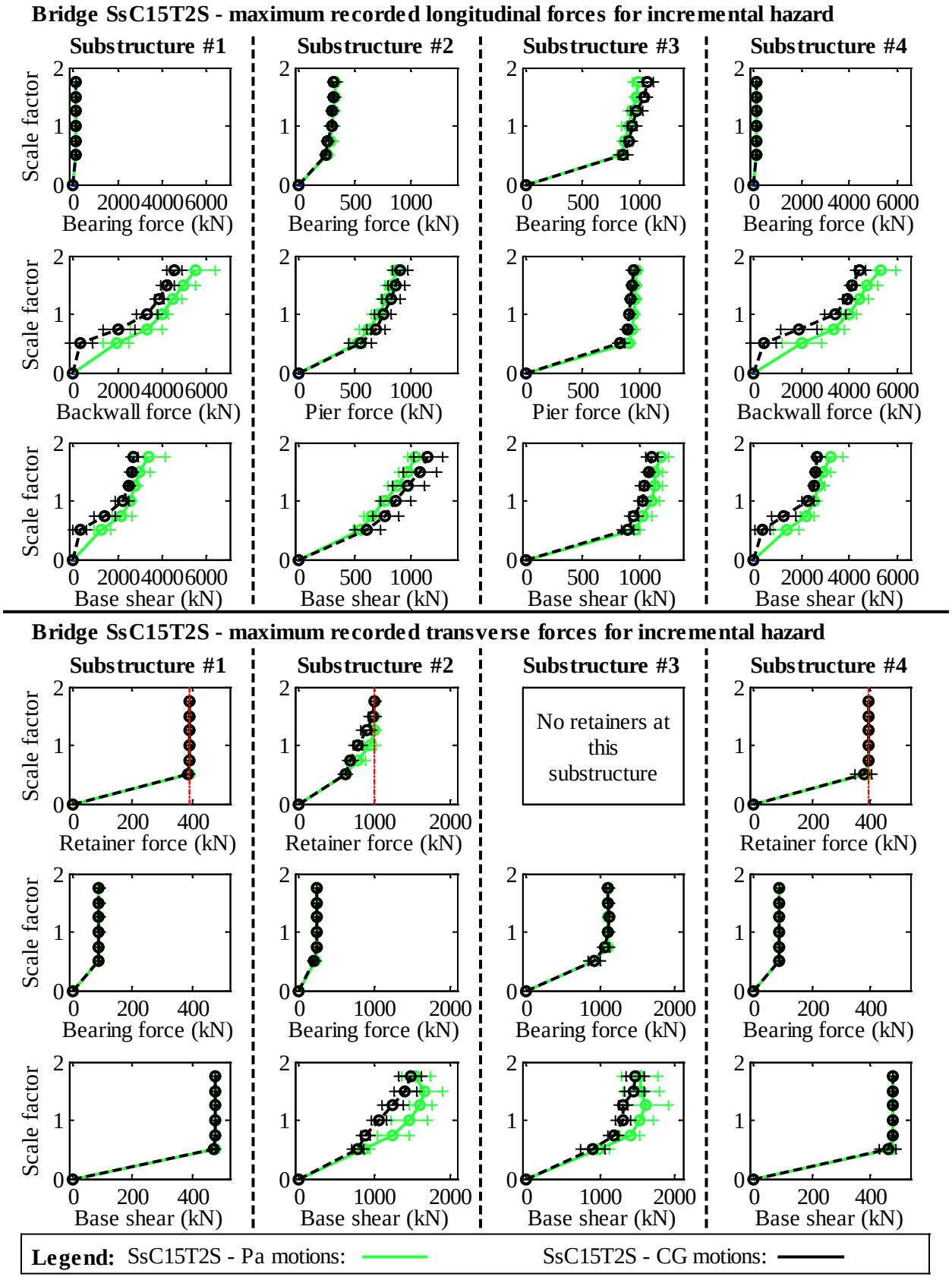

Figure C.76. Bridge SsC15T2S – force results.

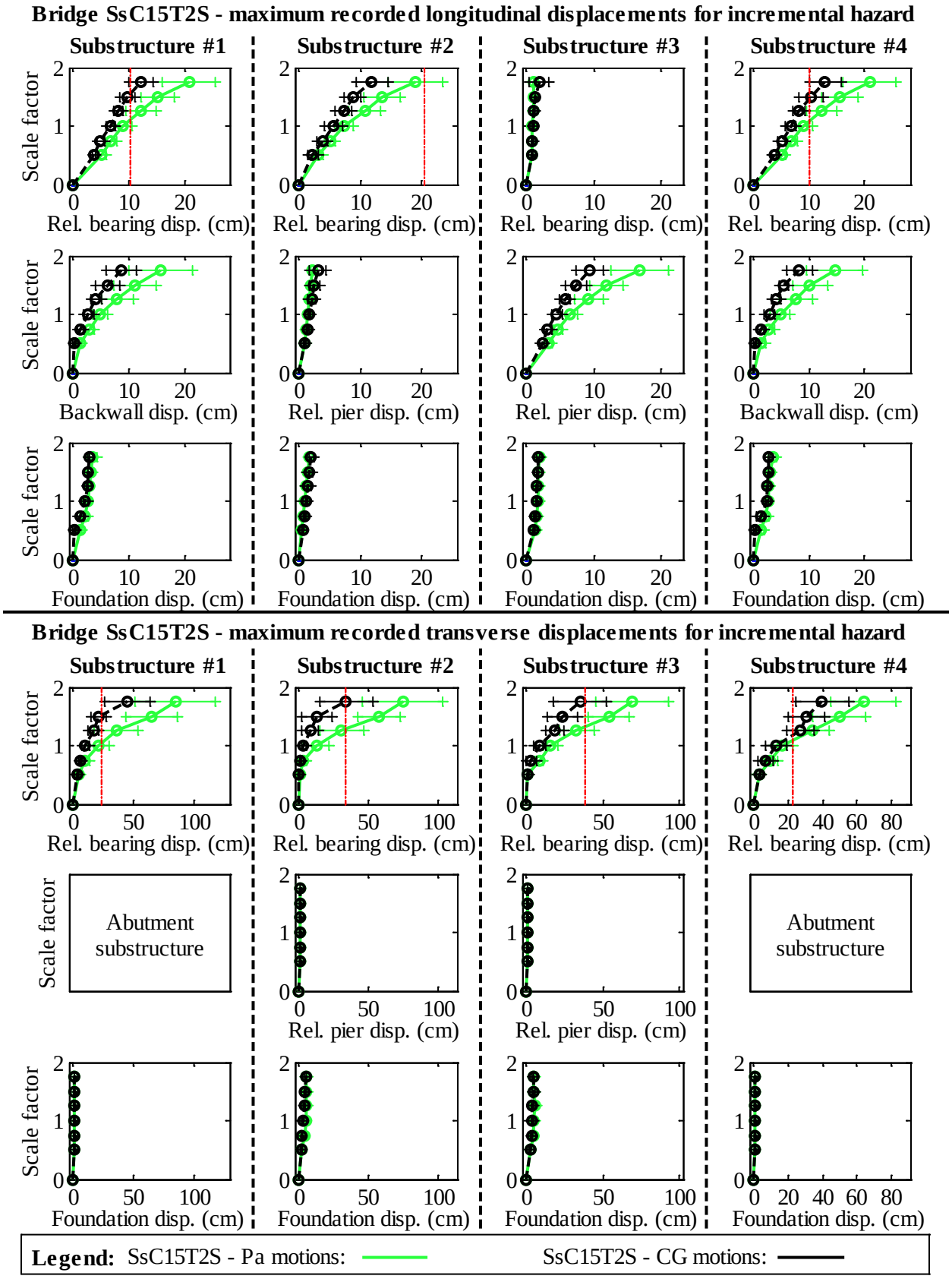

Figure C.77. Bridge SsC15T2S – displacement results.

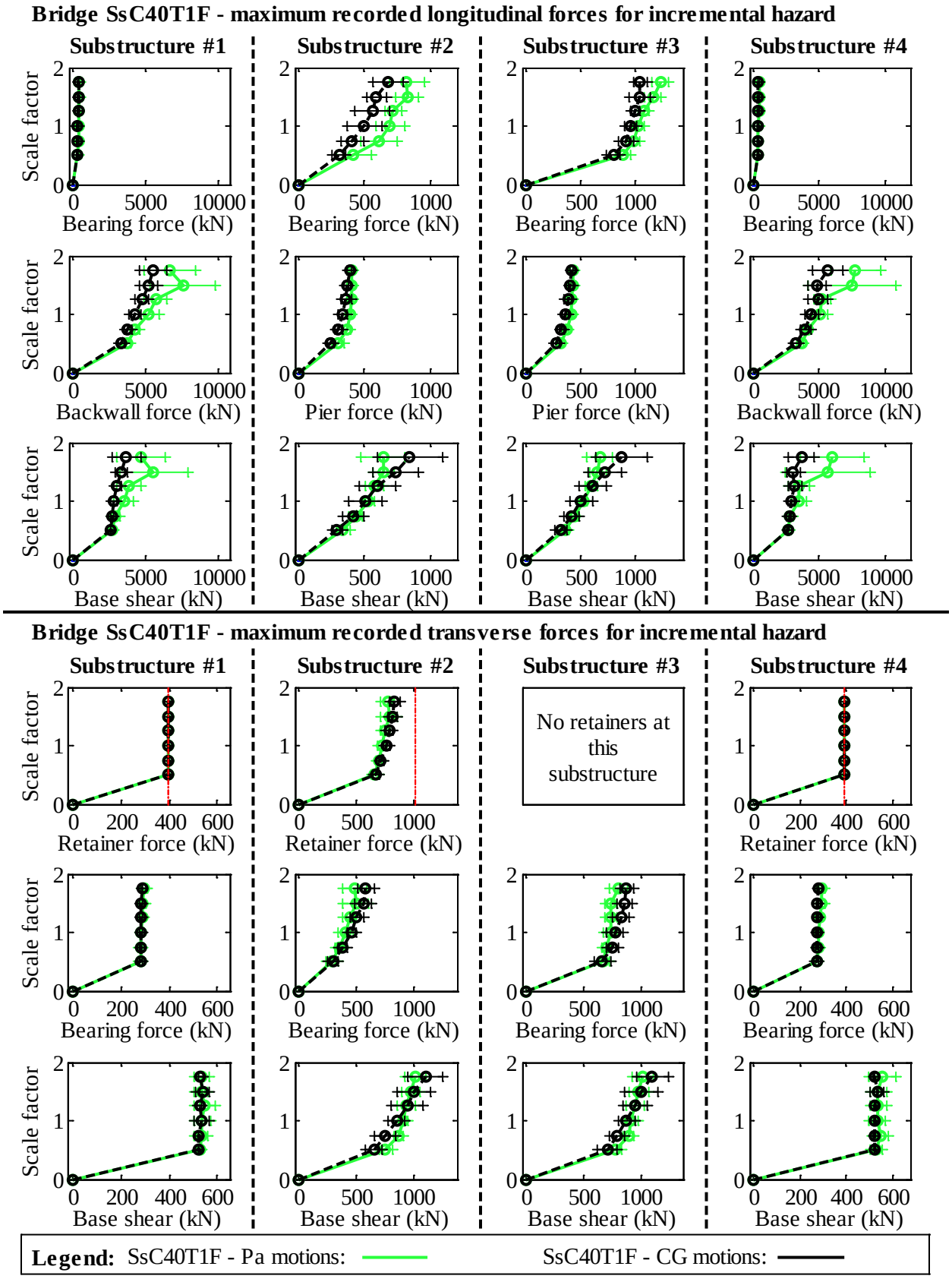

Figure C.78. Bridge SsC40T1F – force results.

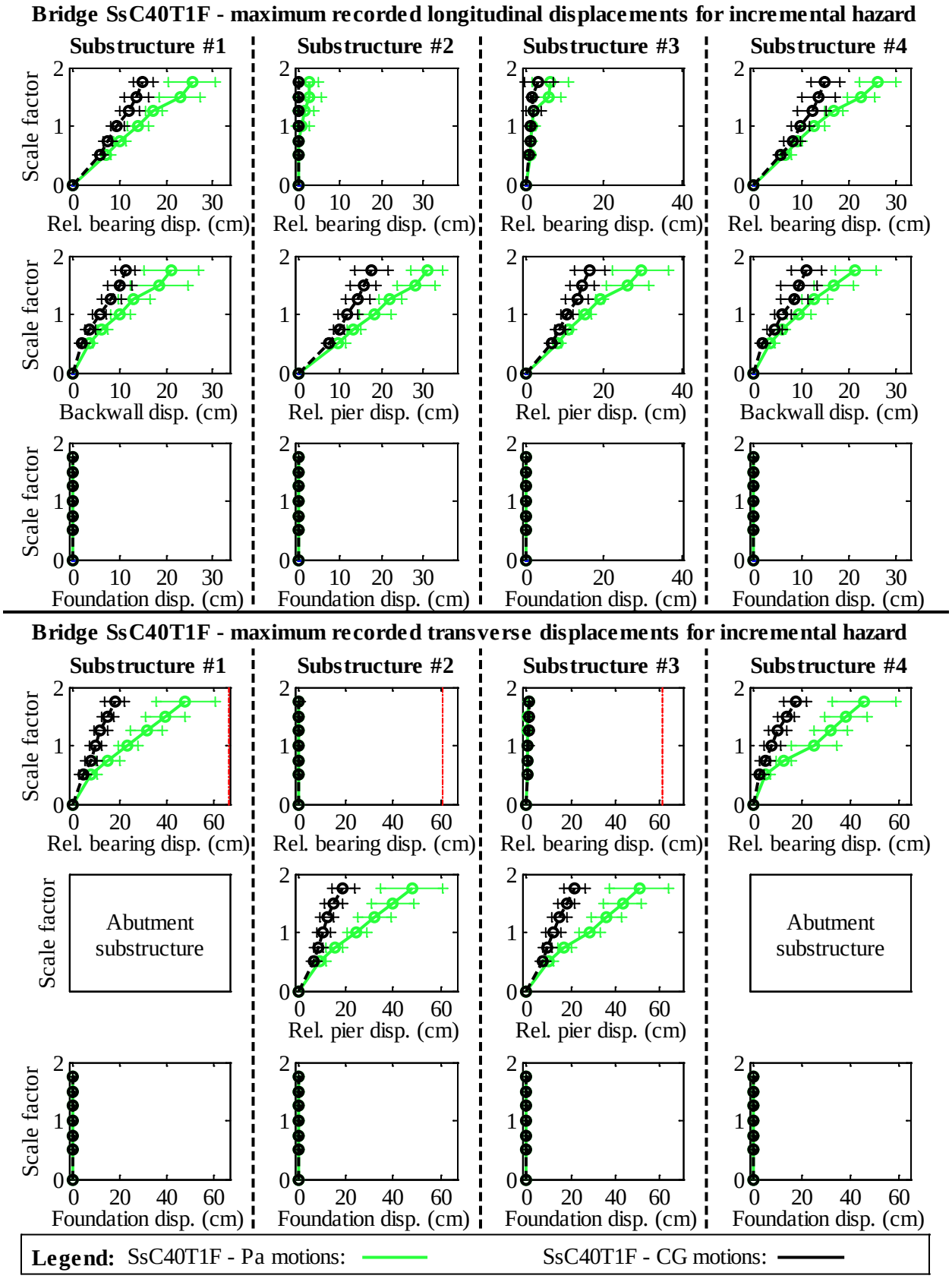

Figure C.79. Bridge SsC40T1F – displacement results.

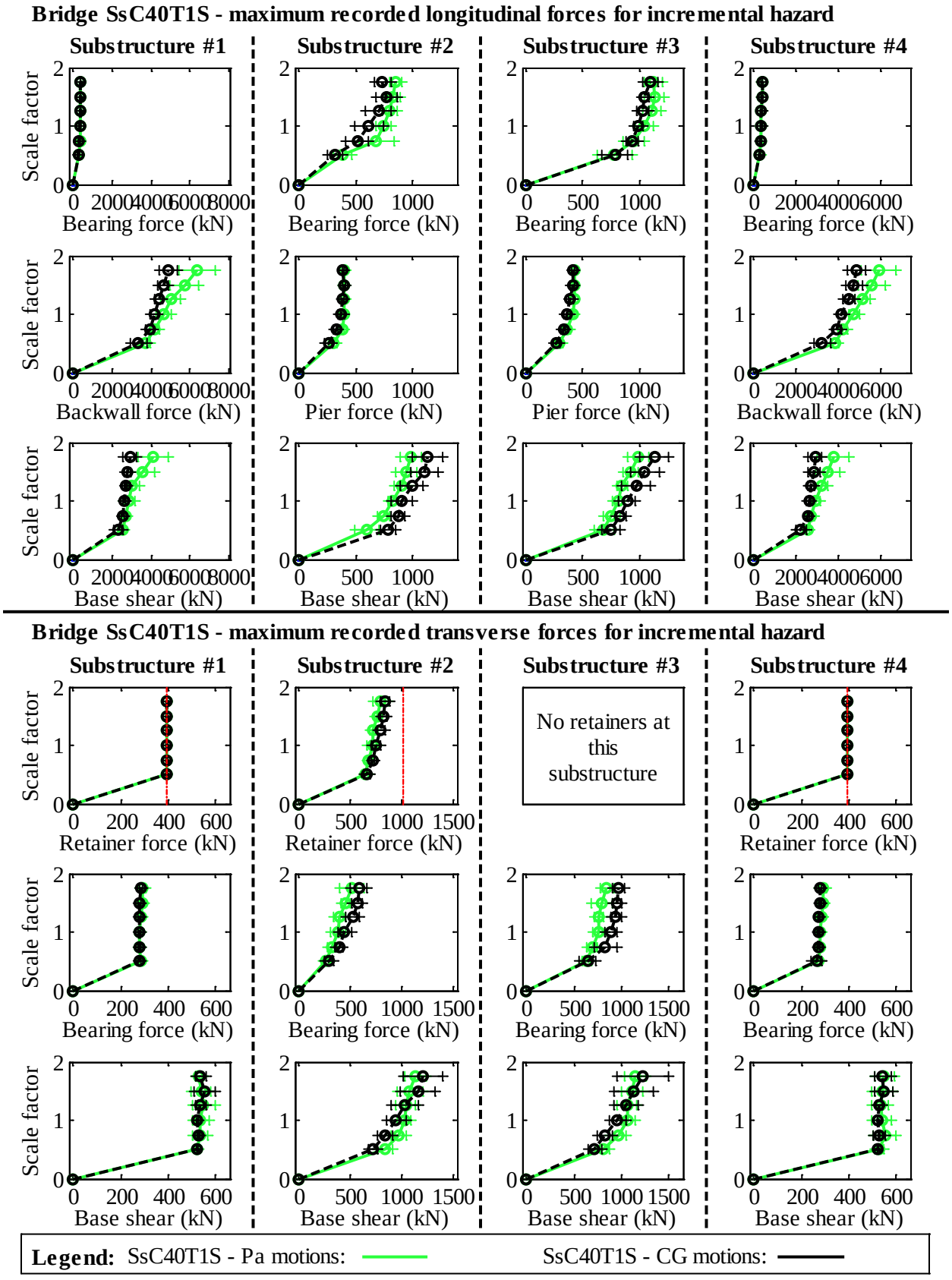

Figure C.80. Bridge SsC40T1S – force results.

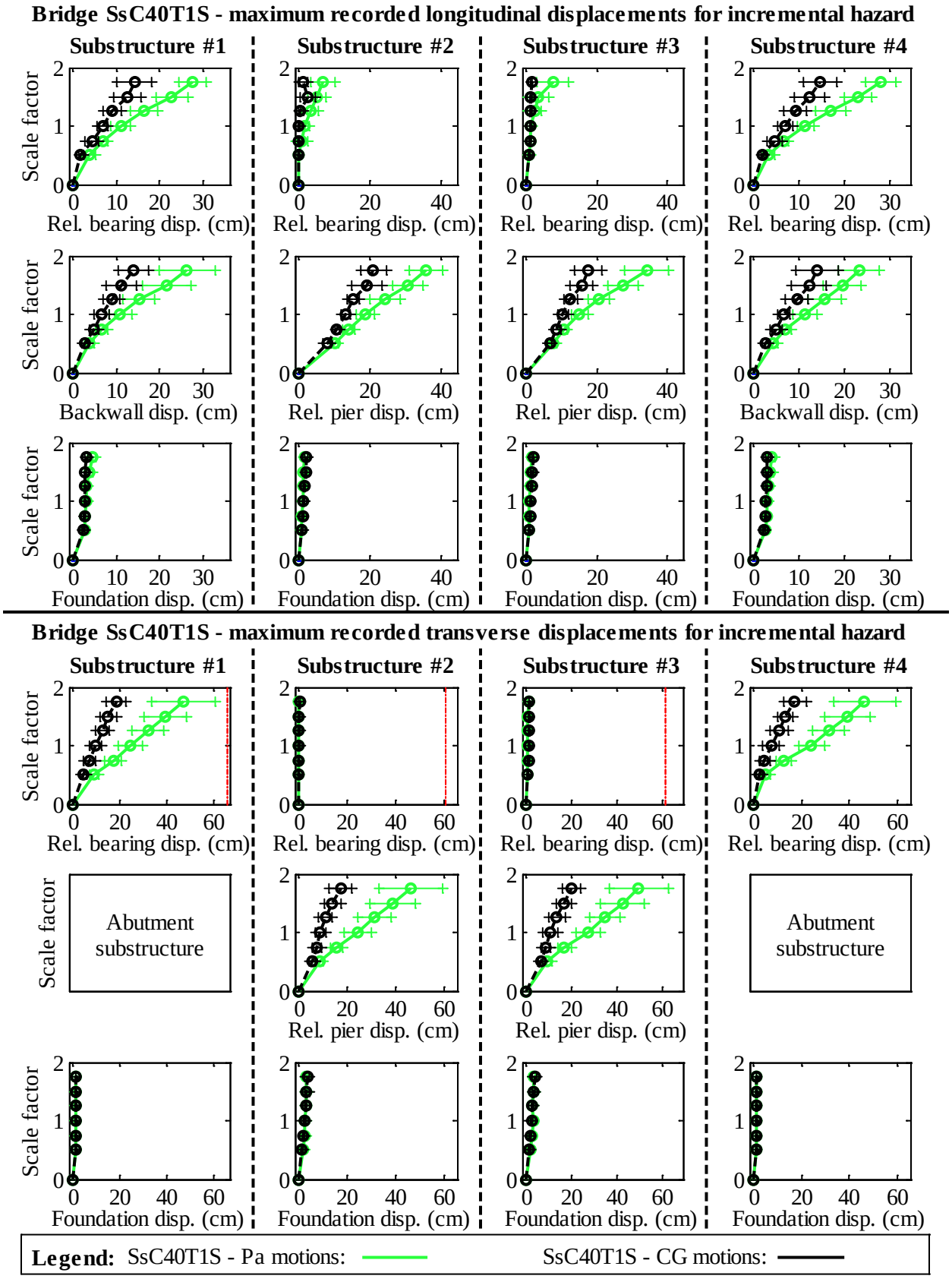

Figure C.81. Bridge SsC40T1S – displacement results.

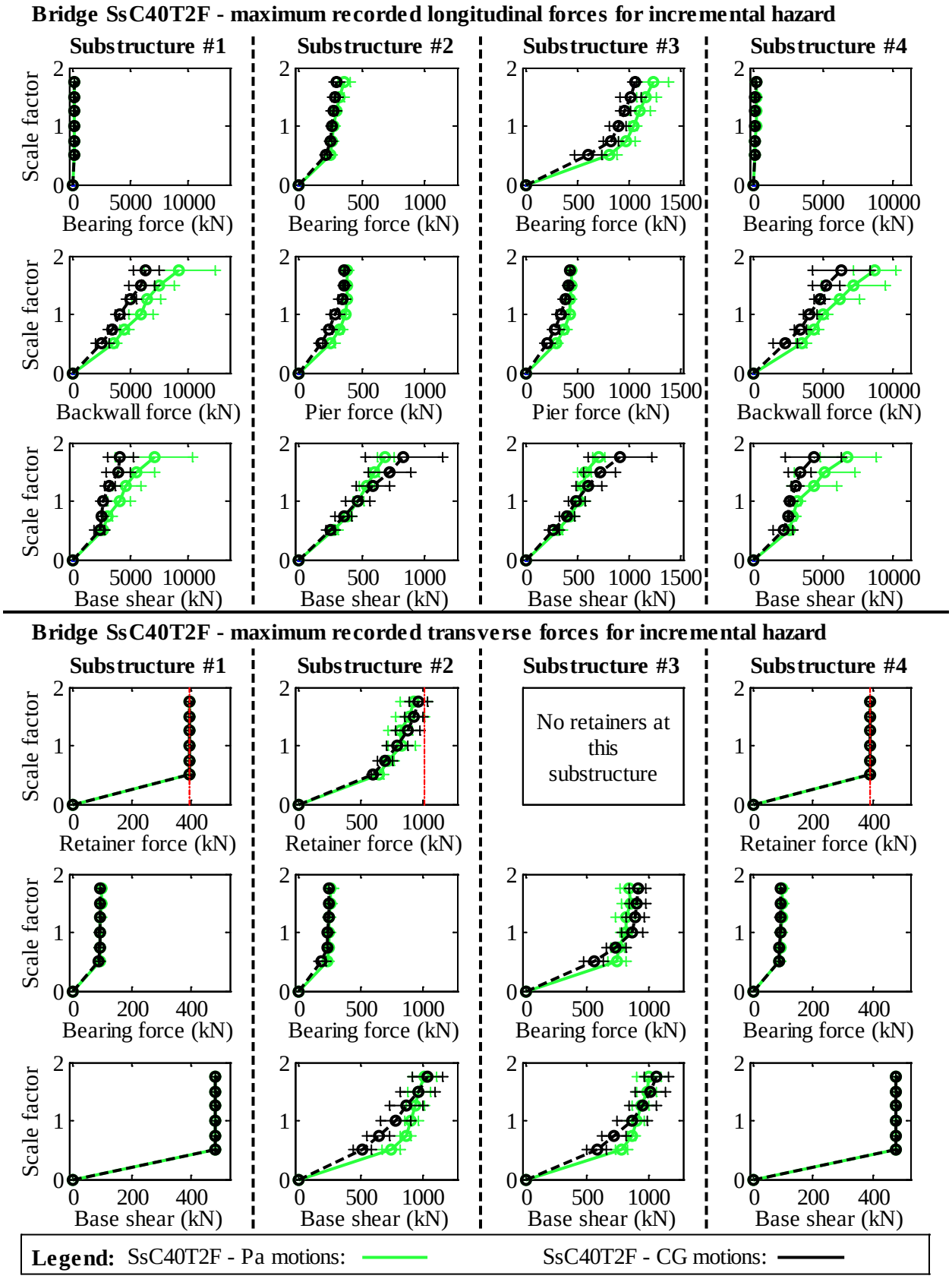

Figure C.82. Bridge SsC40T2F – force results.

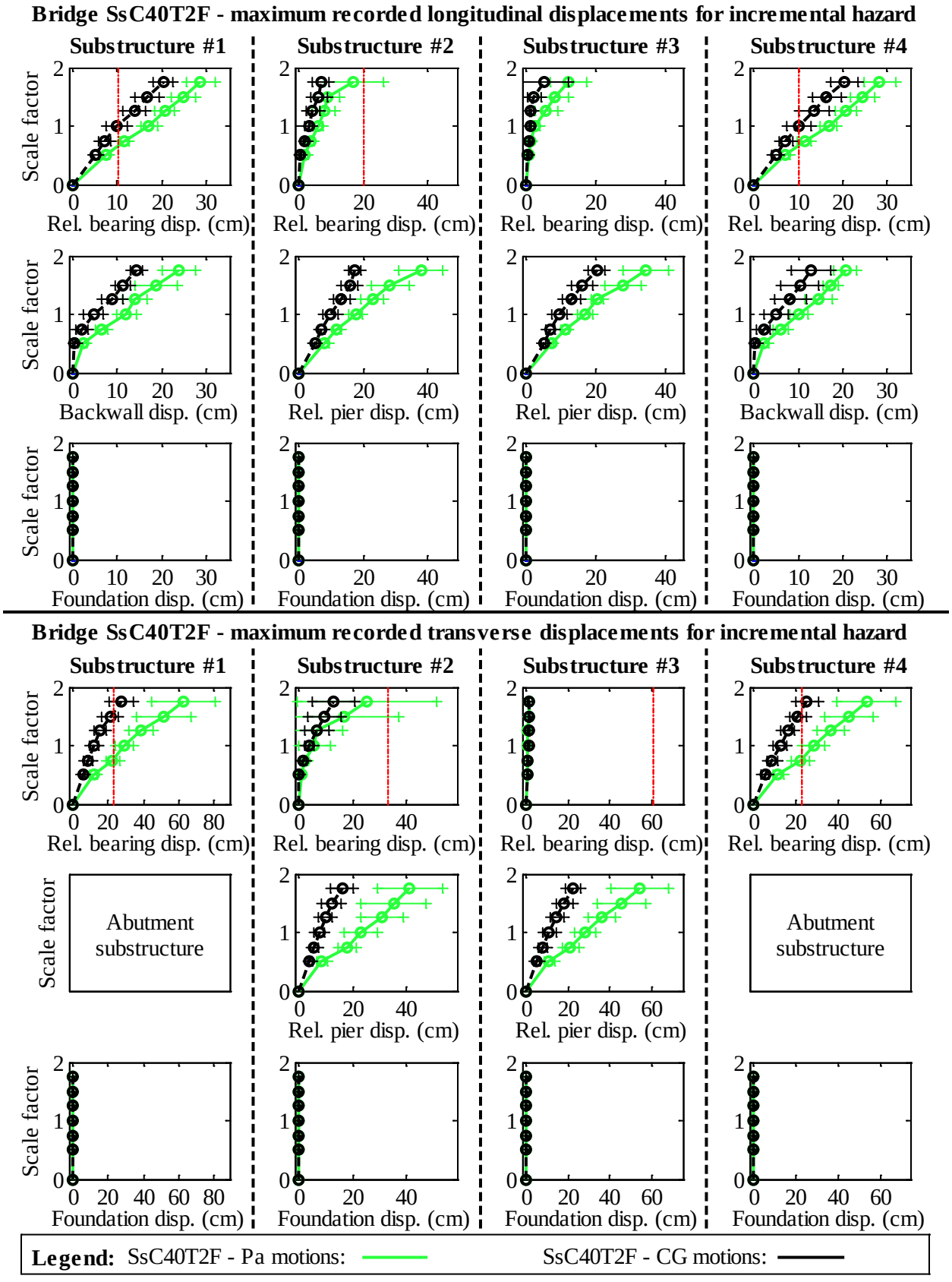

Figure C.83. Bridge SsC40T2F – displacement results.

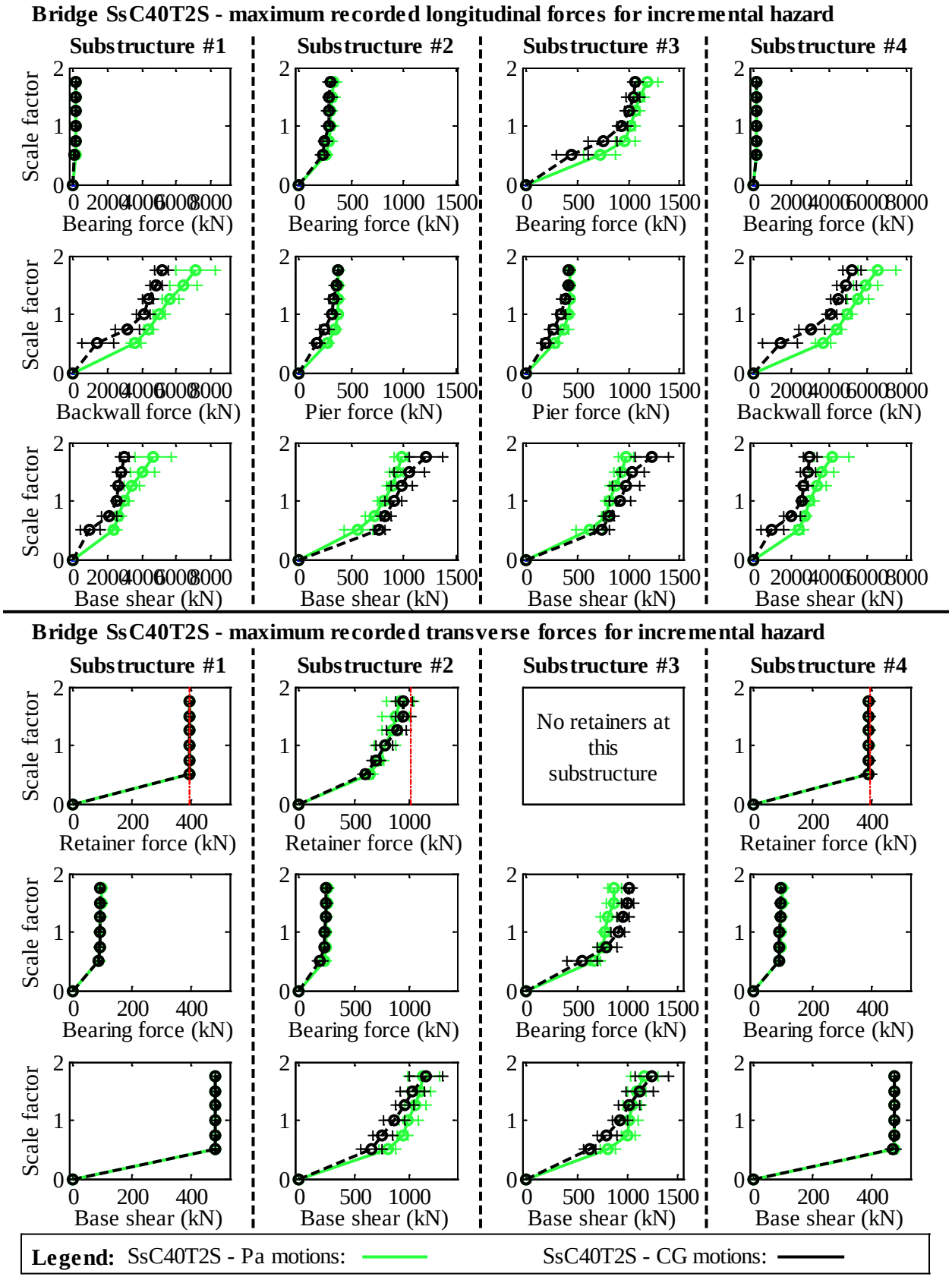

Figure C.84. Bridge SsC40T2S – force results.

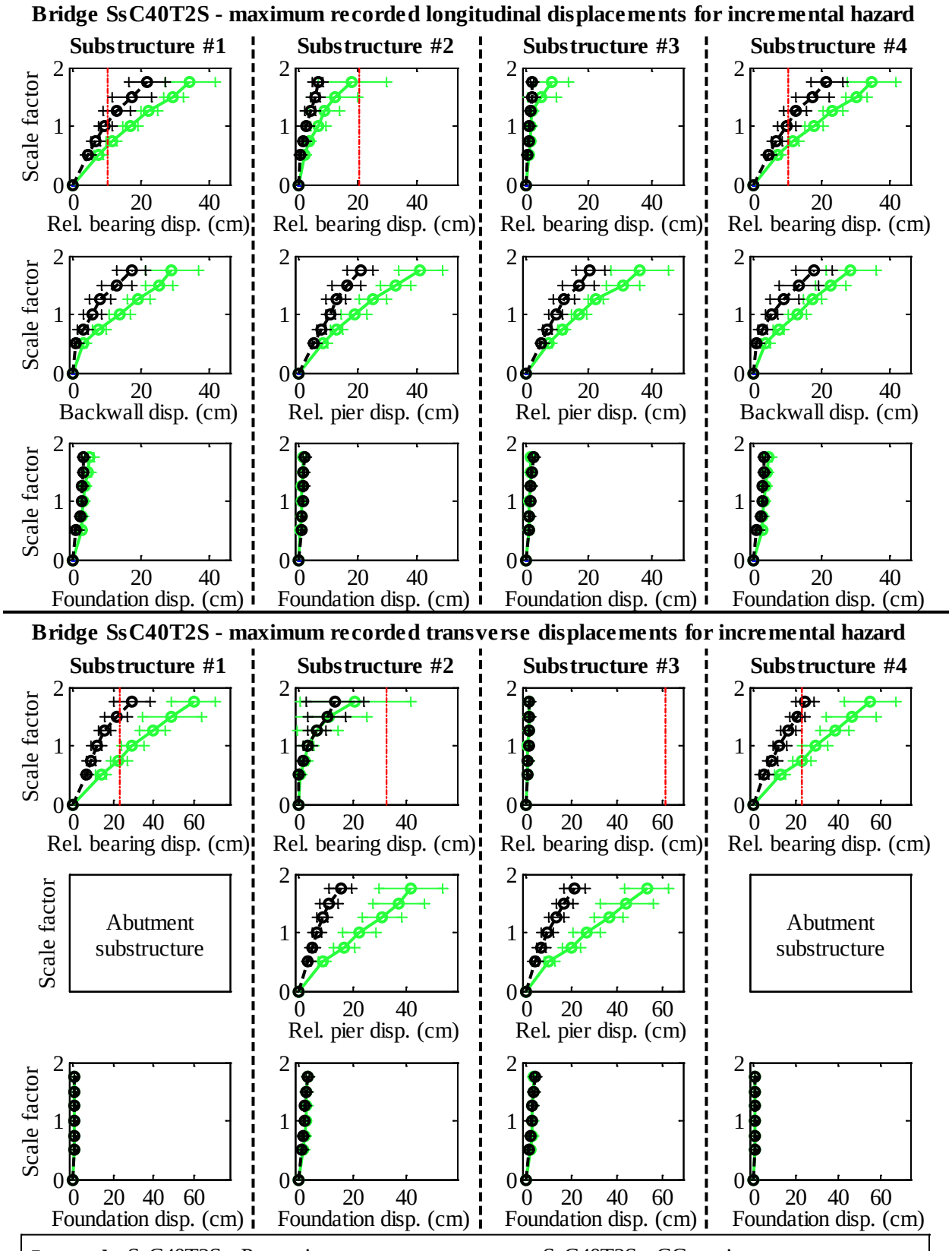

Figure C.85. Bridge SsC40T2S – displacement results.

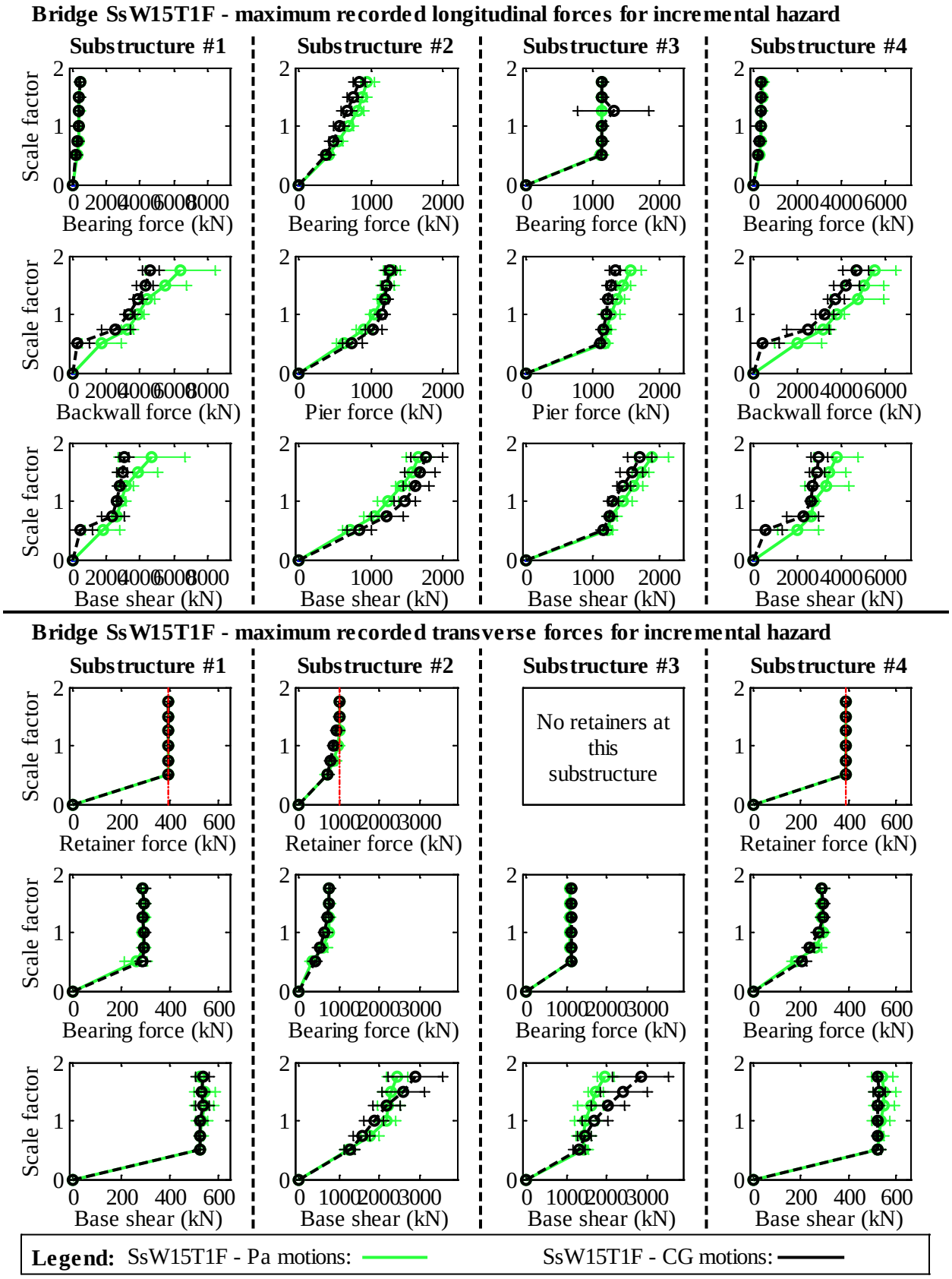

Figure C.86. Bridge SsW15T1F – force results.

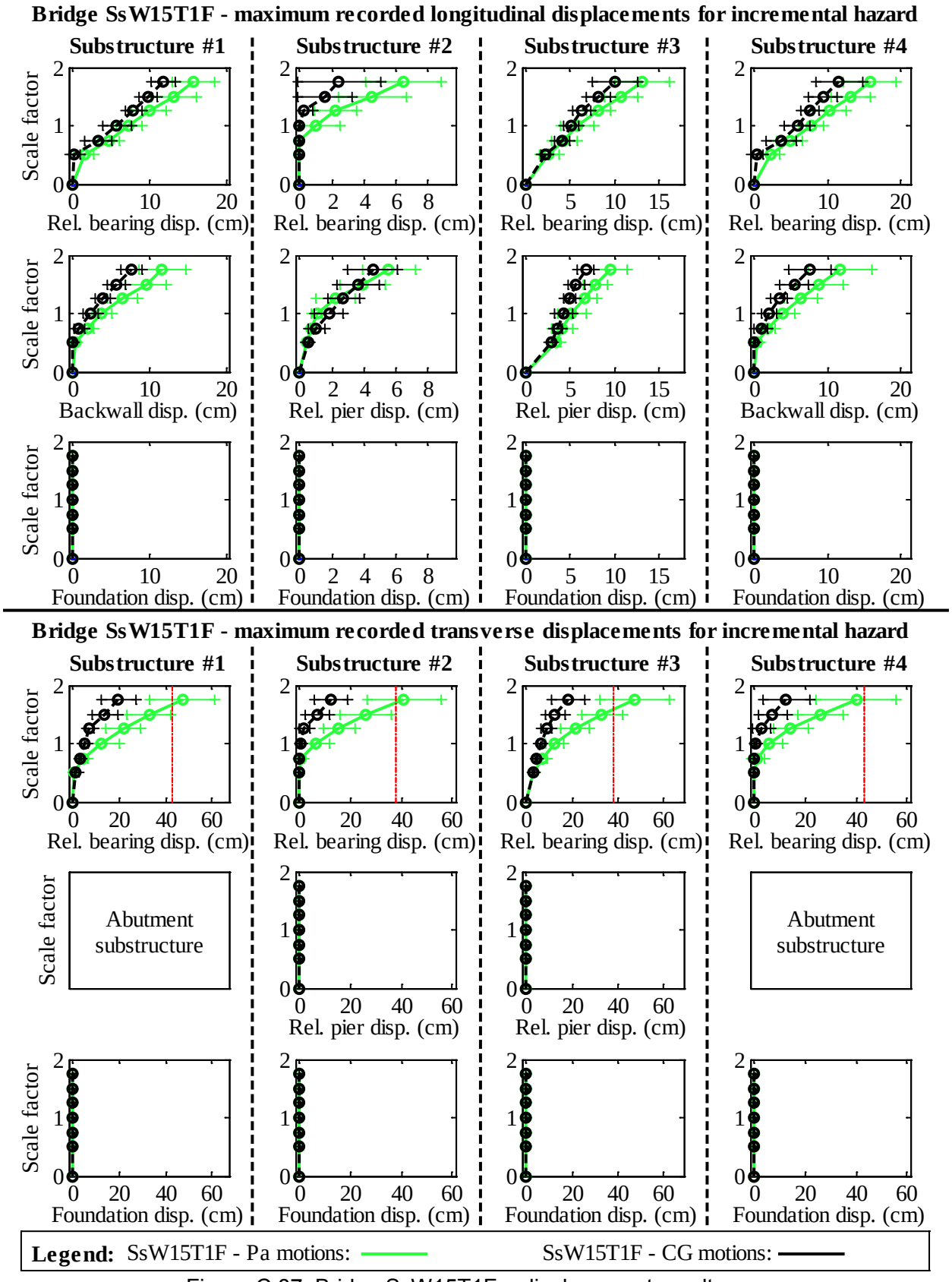

Figure C.87. Bridge SsW15T1F – displacement results.

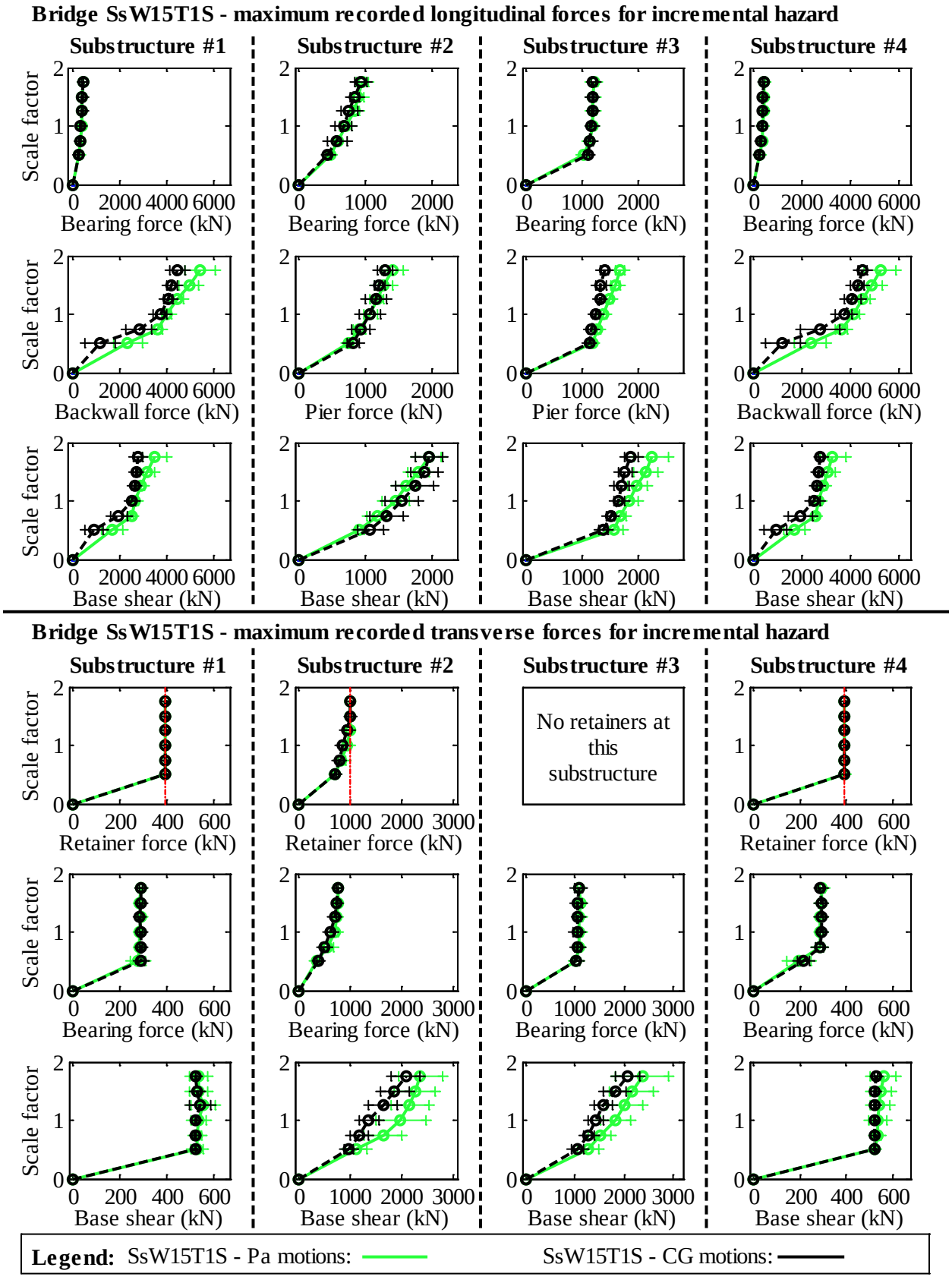

Figure C.88. Bridge SsW15T1S – force results.

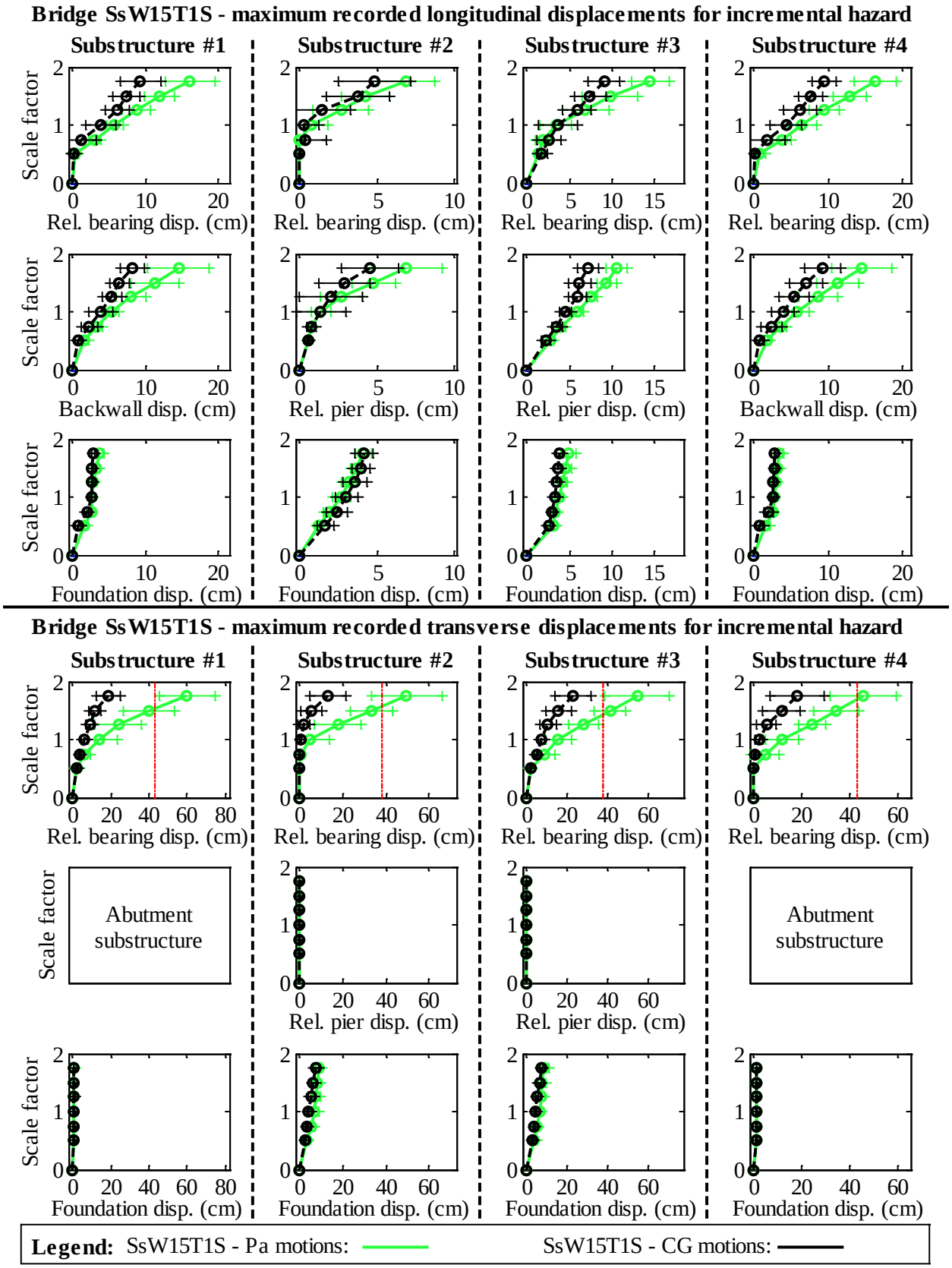

Figure C.89. Bridge SsW15T1S – displacement results.

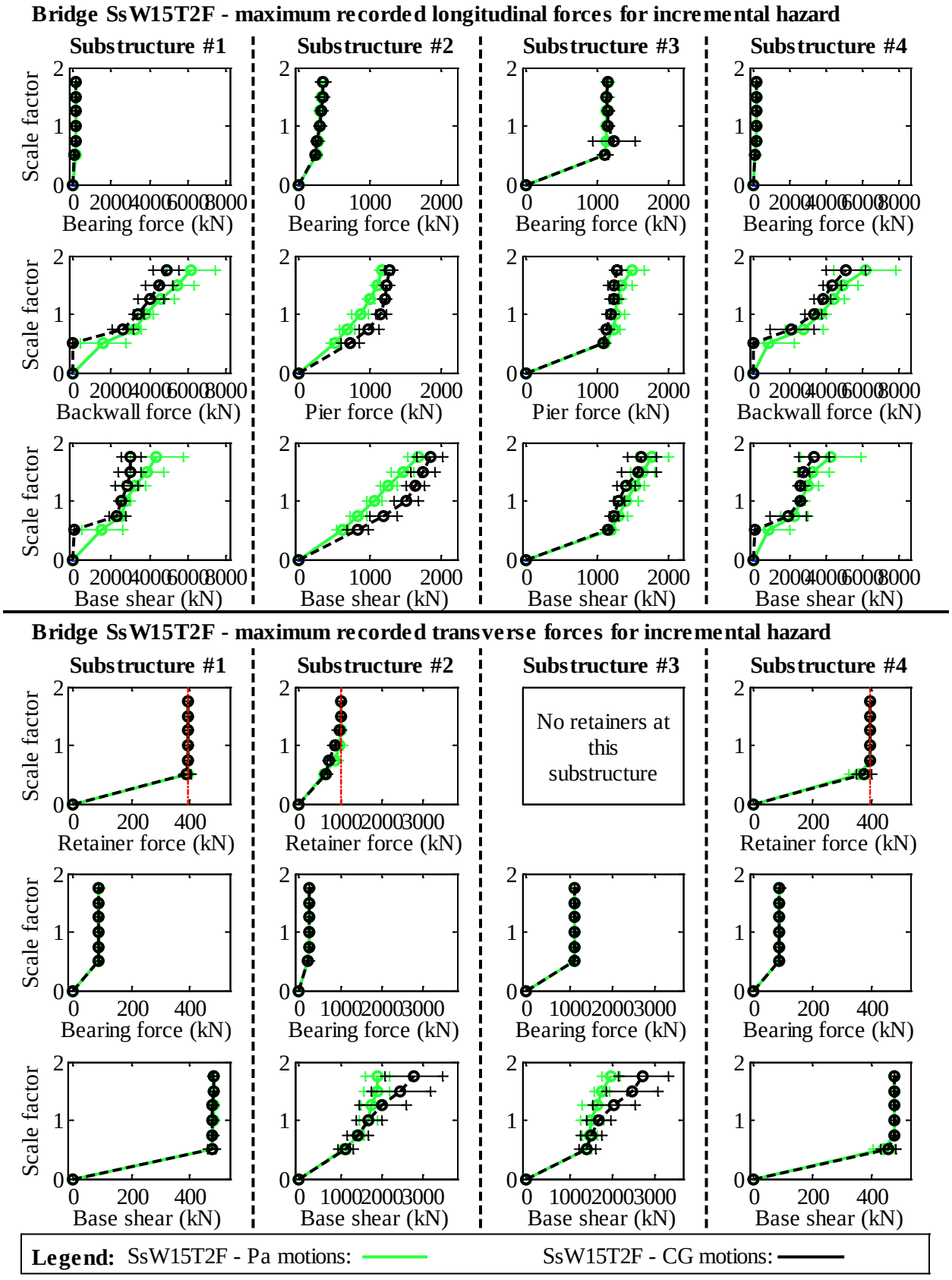

Figure C.90. Bridge SsW15T2F – force results.

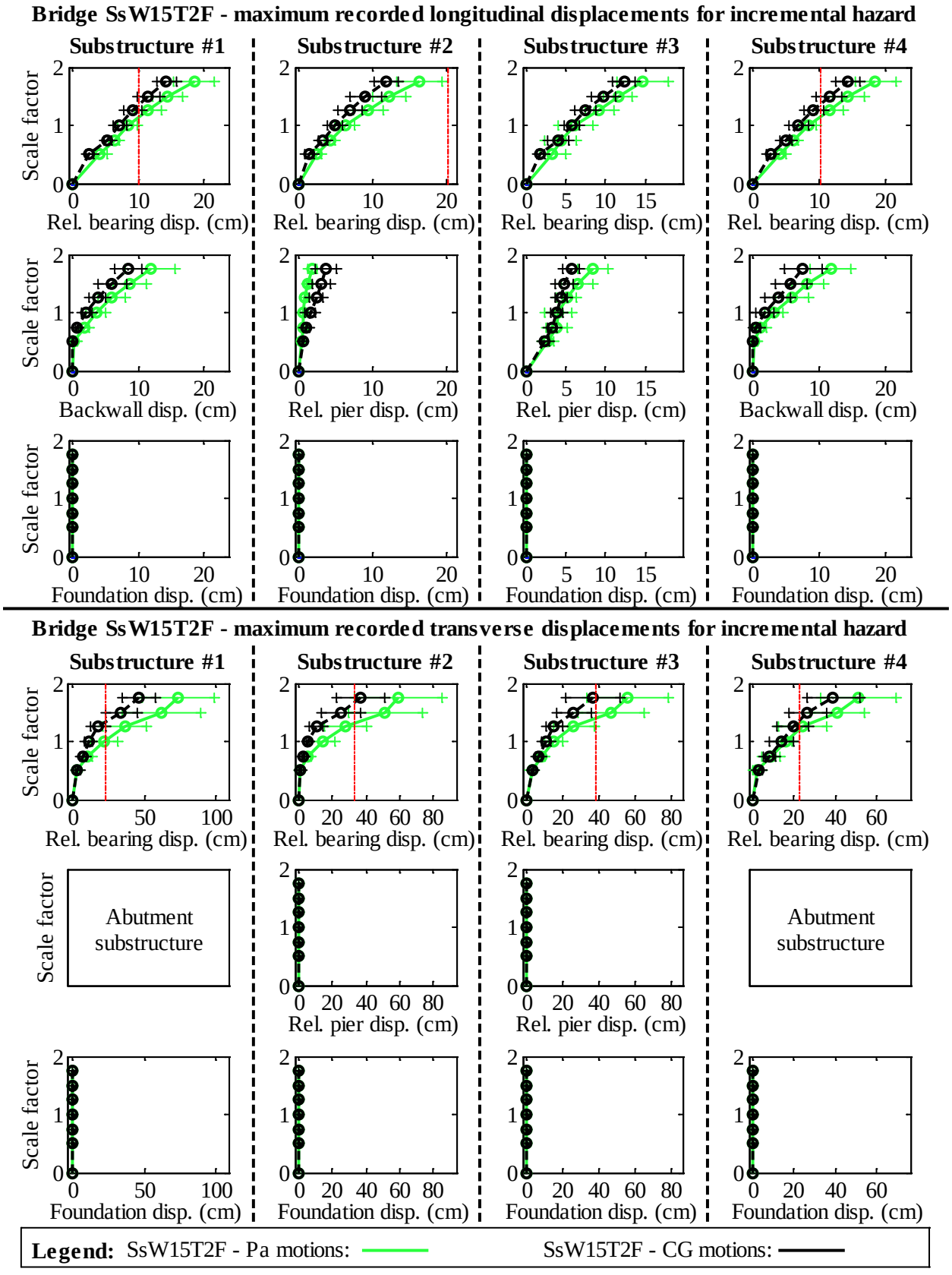

Figure C.91. Bridge SsW15T2F – displacement results.

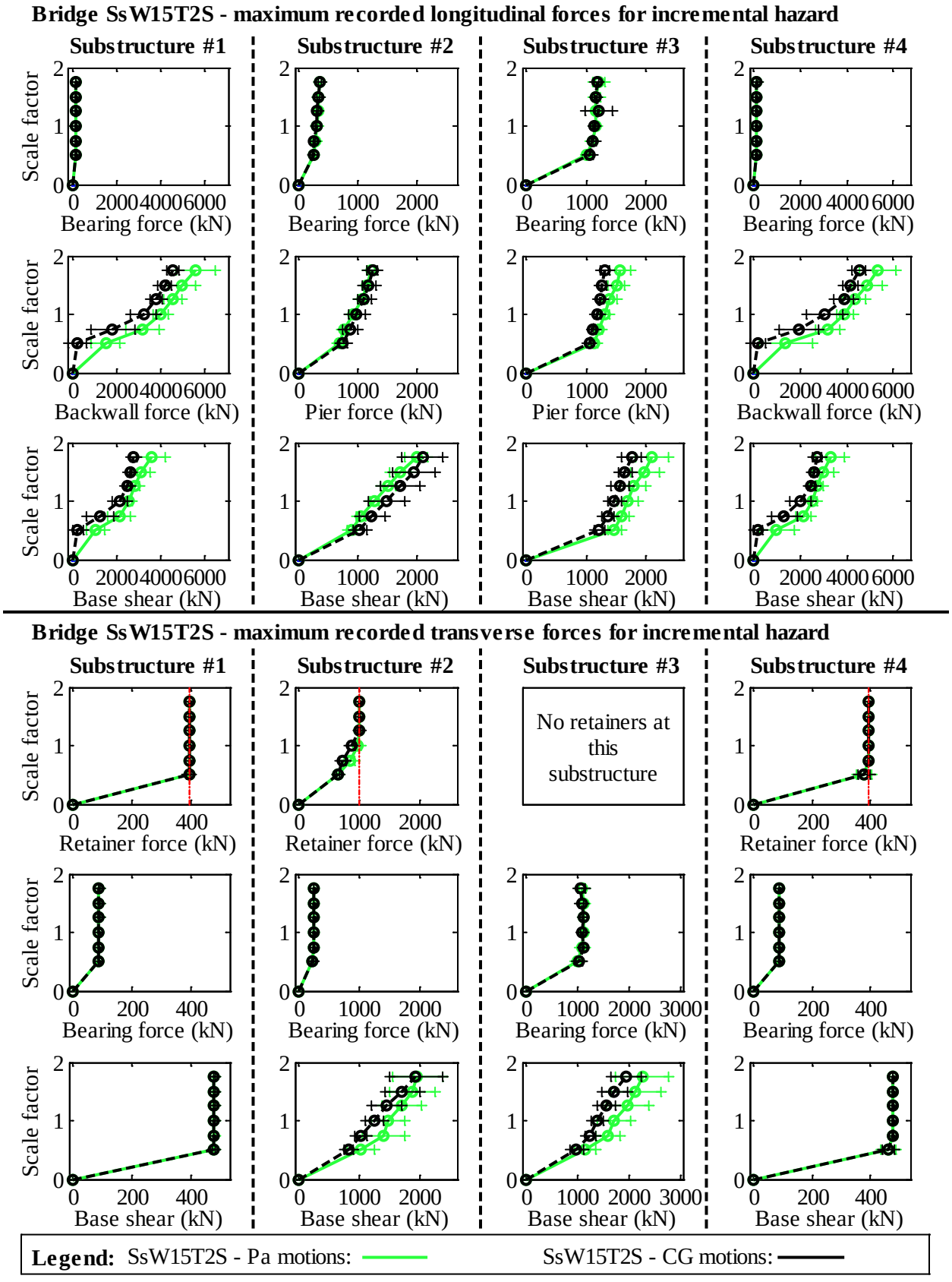

Figure C.92. Bridge SsW15T2S – force results.

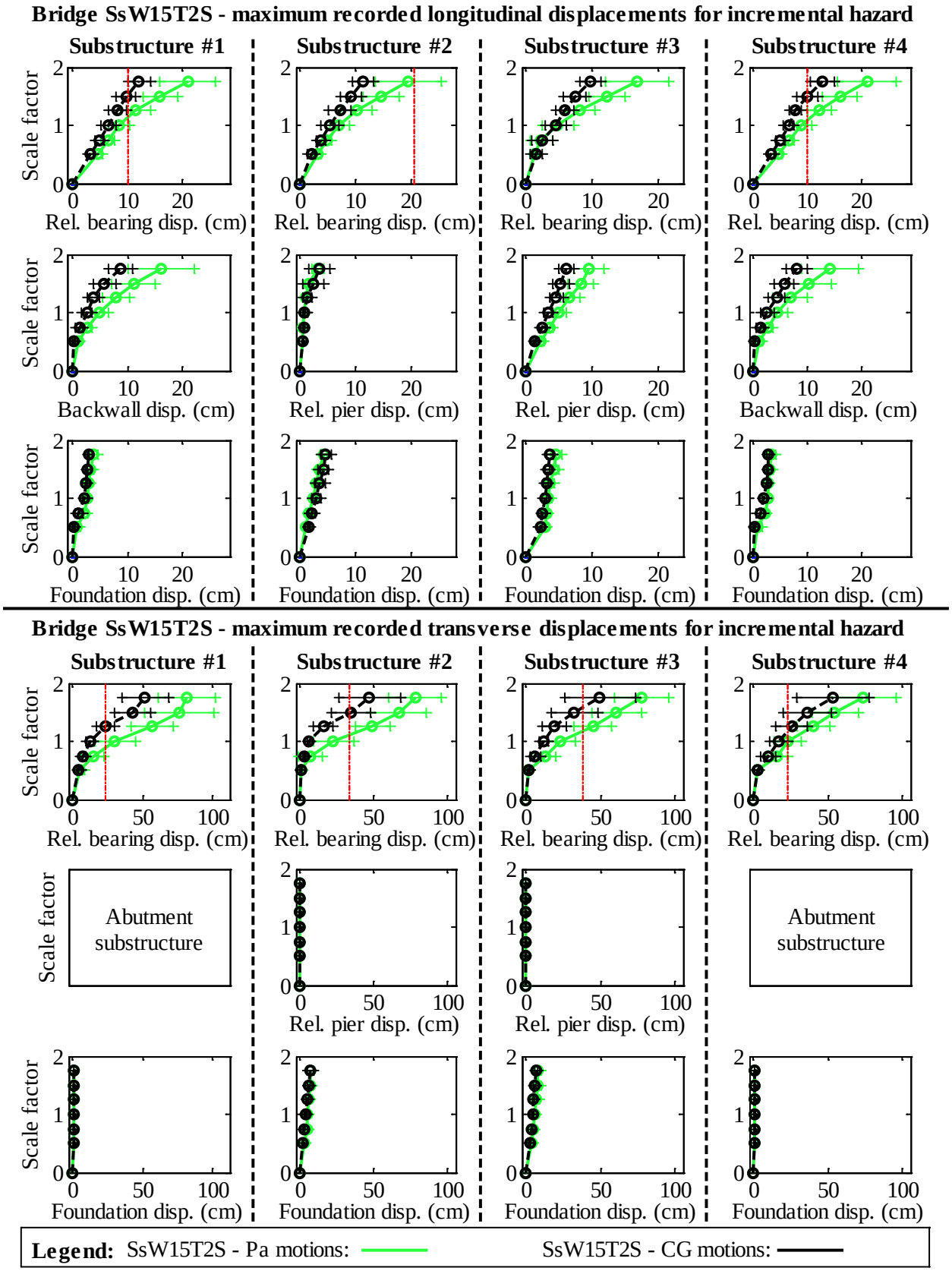

Figure C.93. Bridge SsW15T2S – displacement results.

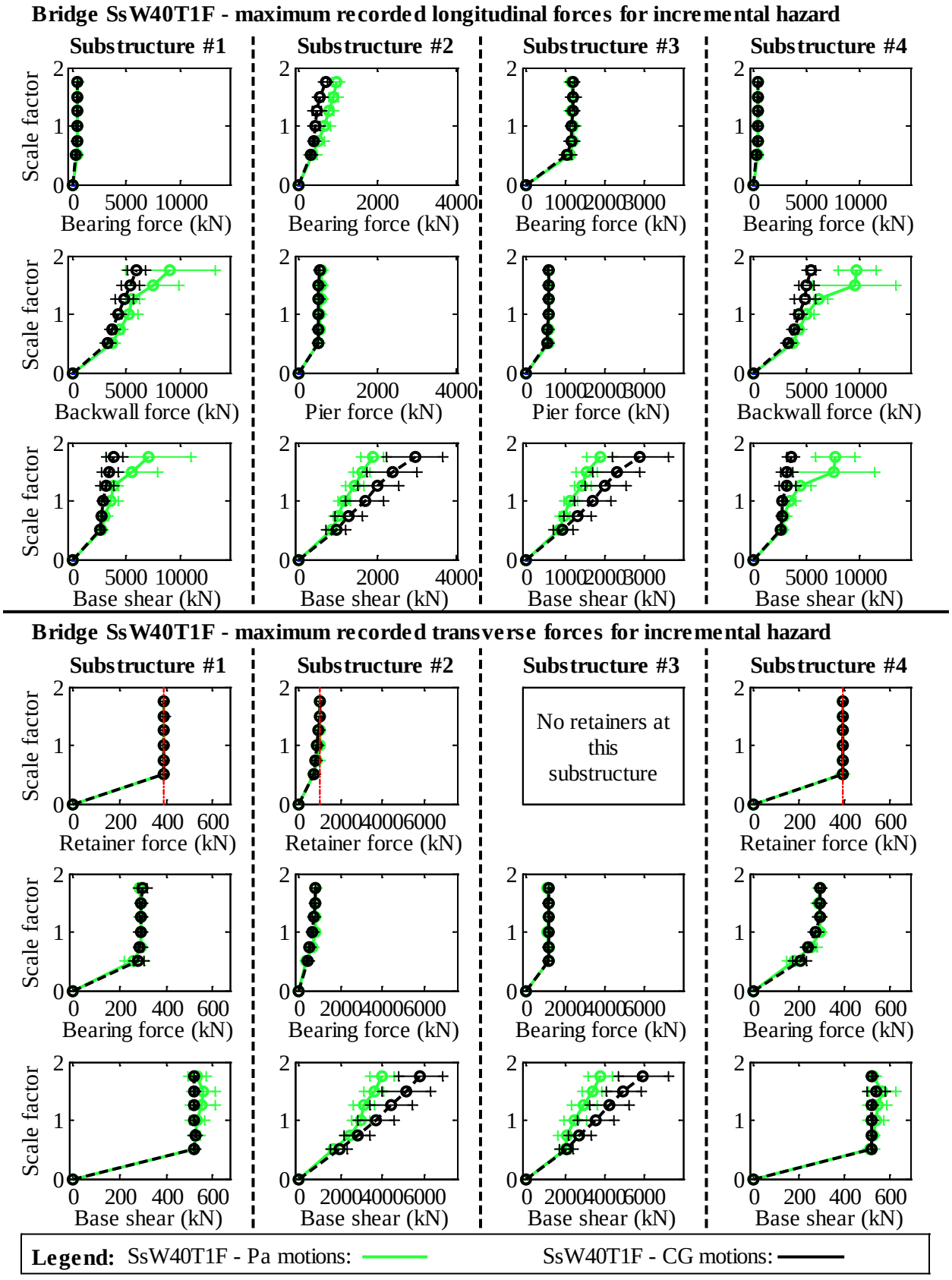

Figure C.94. Bridge SsW40T1F – force results.

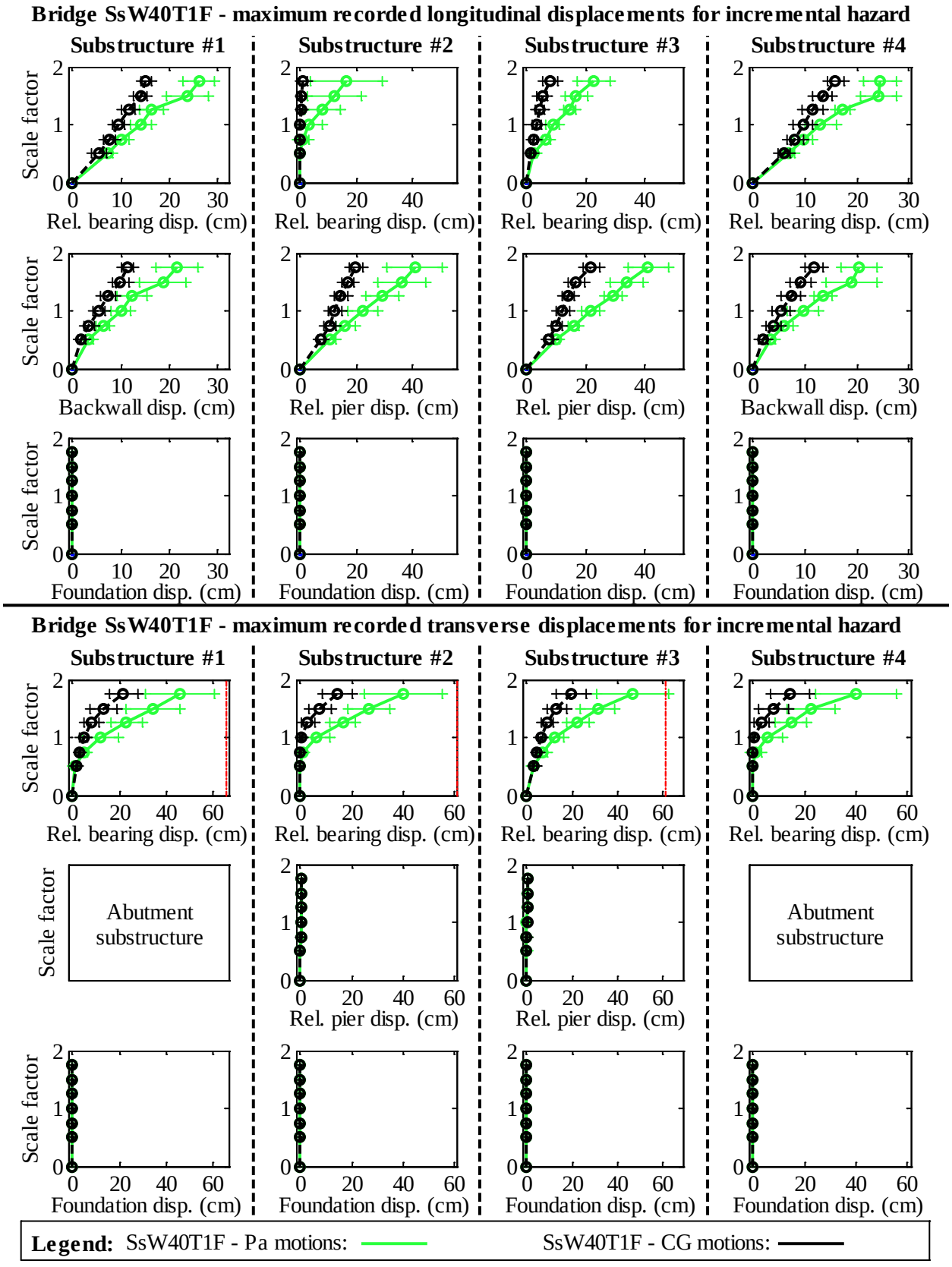

Figure C.95. Bridge SsW40T1F – displacement results.

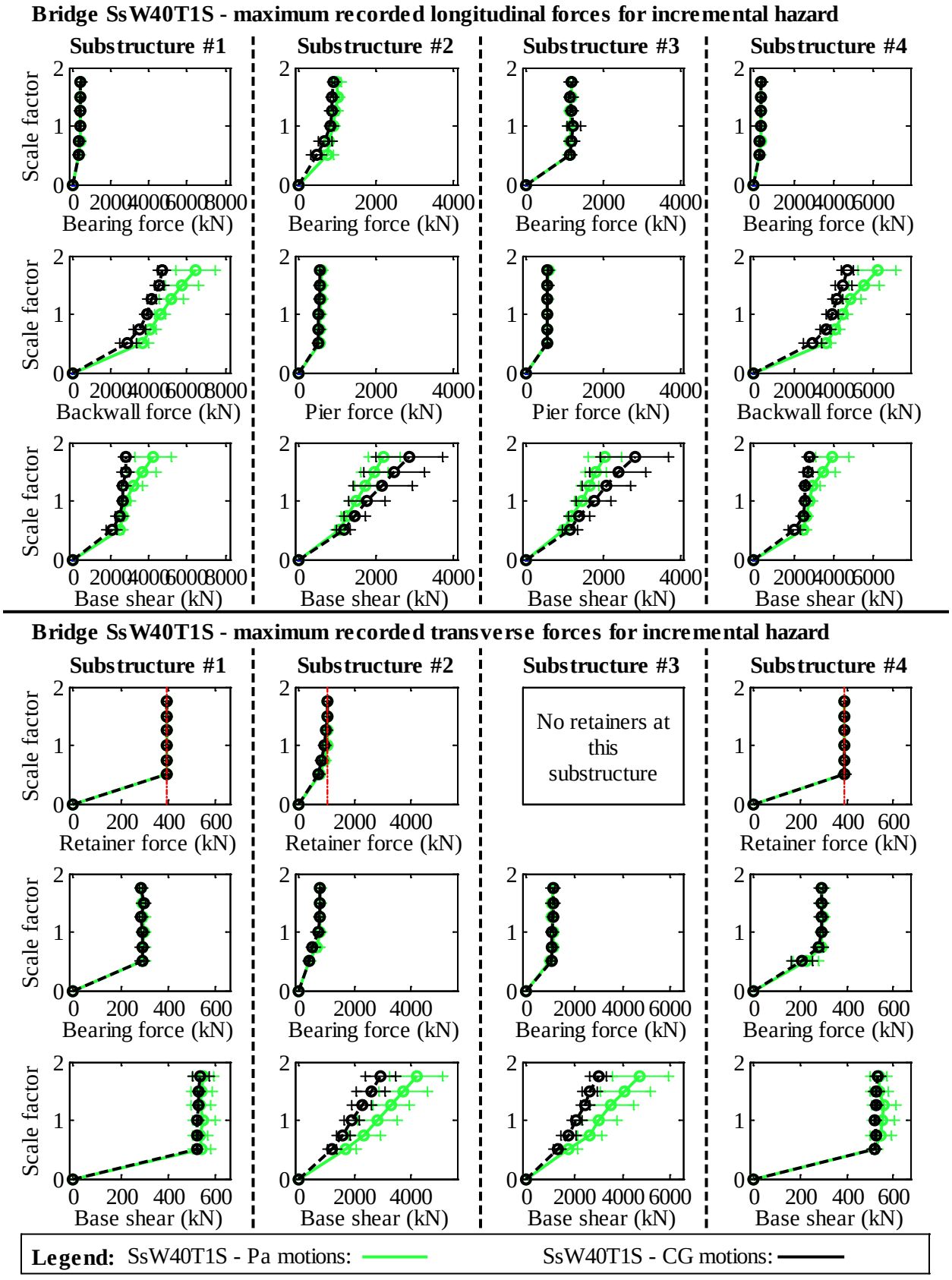

Figure C.96. Bridge SsW40T1F – force results.

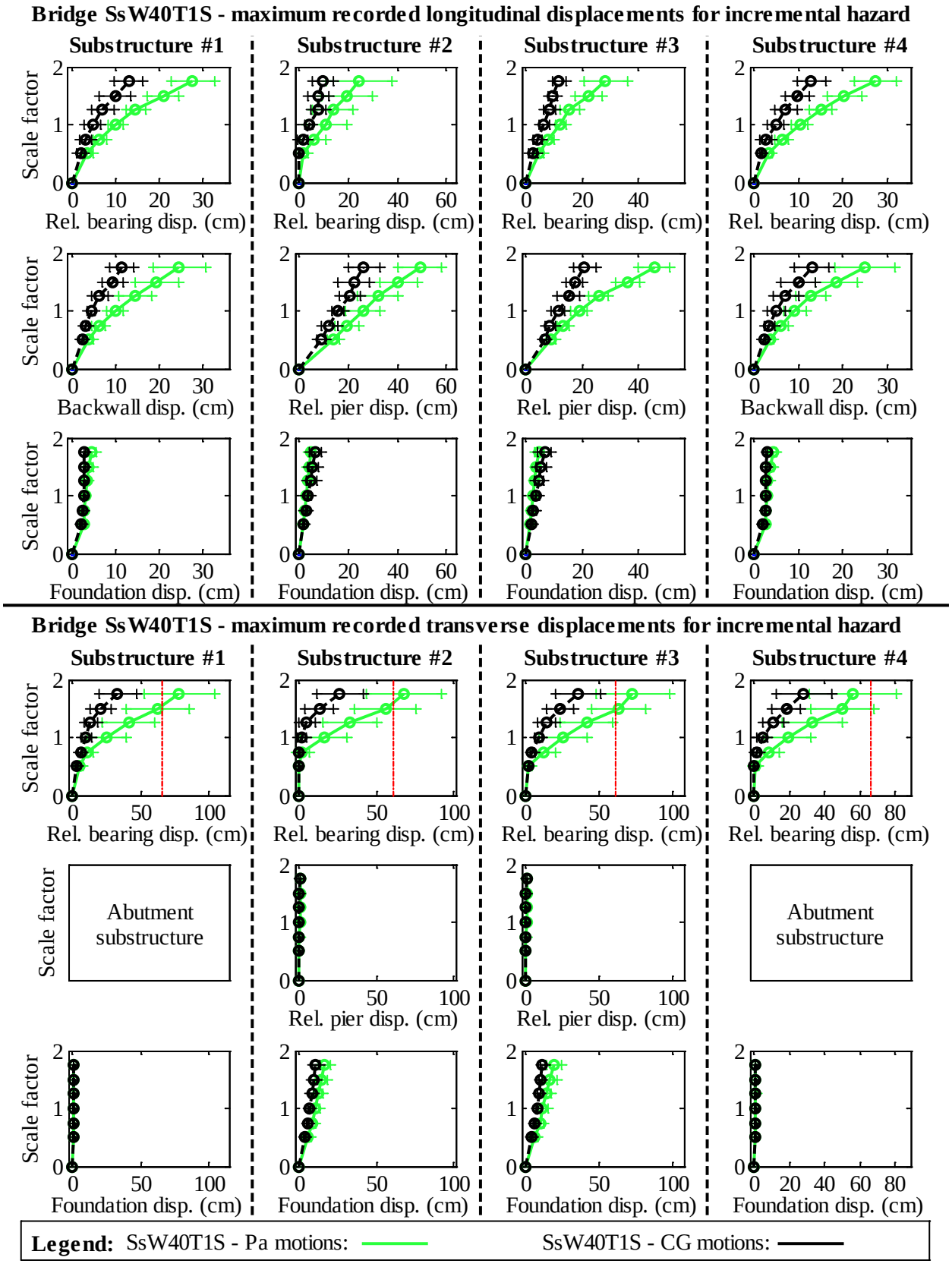

Figure C.97. Bridge SsW40T1S – displacement results.

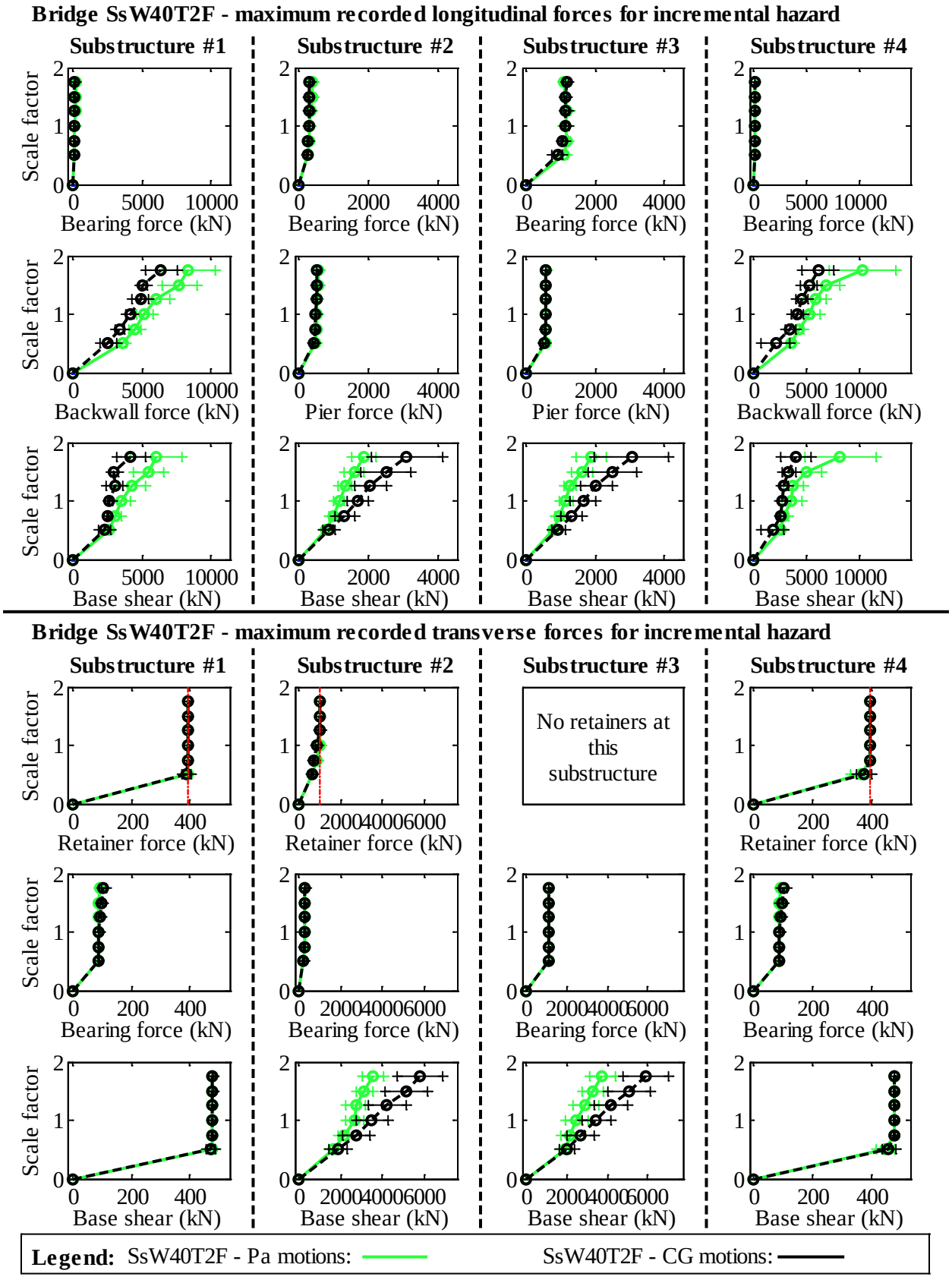

Figure C.98. Bridge SsW40T2F – force results.

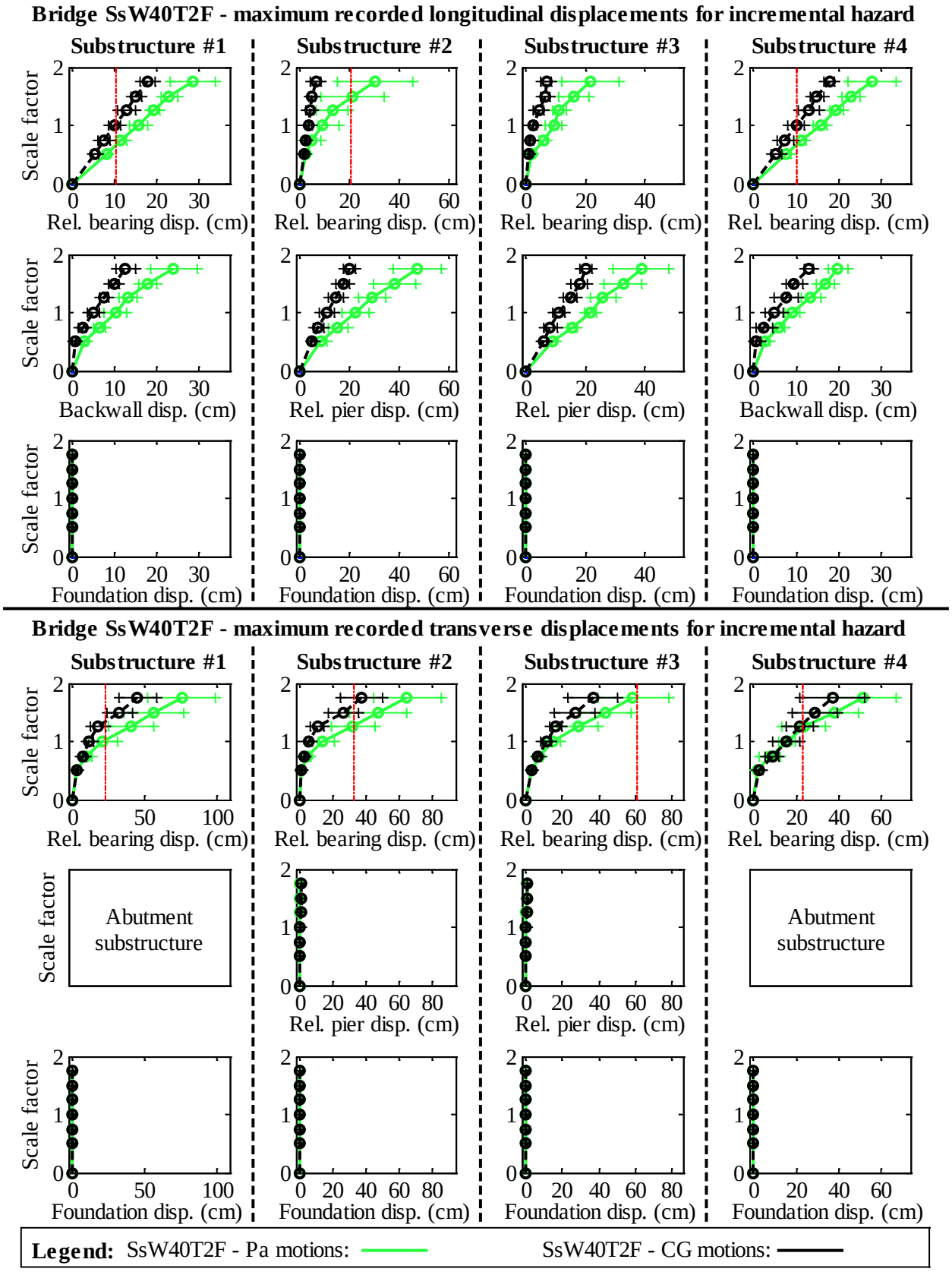

Figure C.99. Bridge SsW40T2F – displacement results.

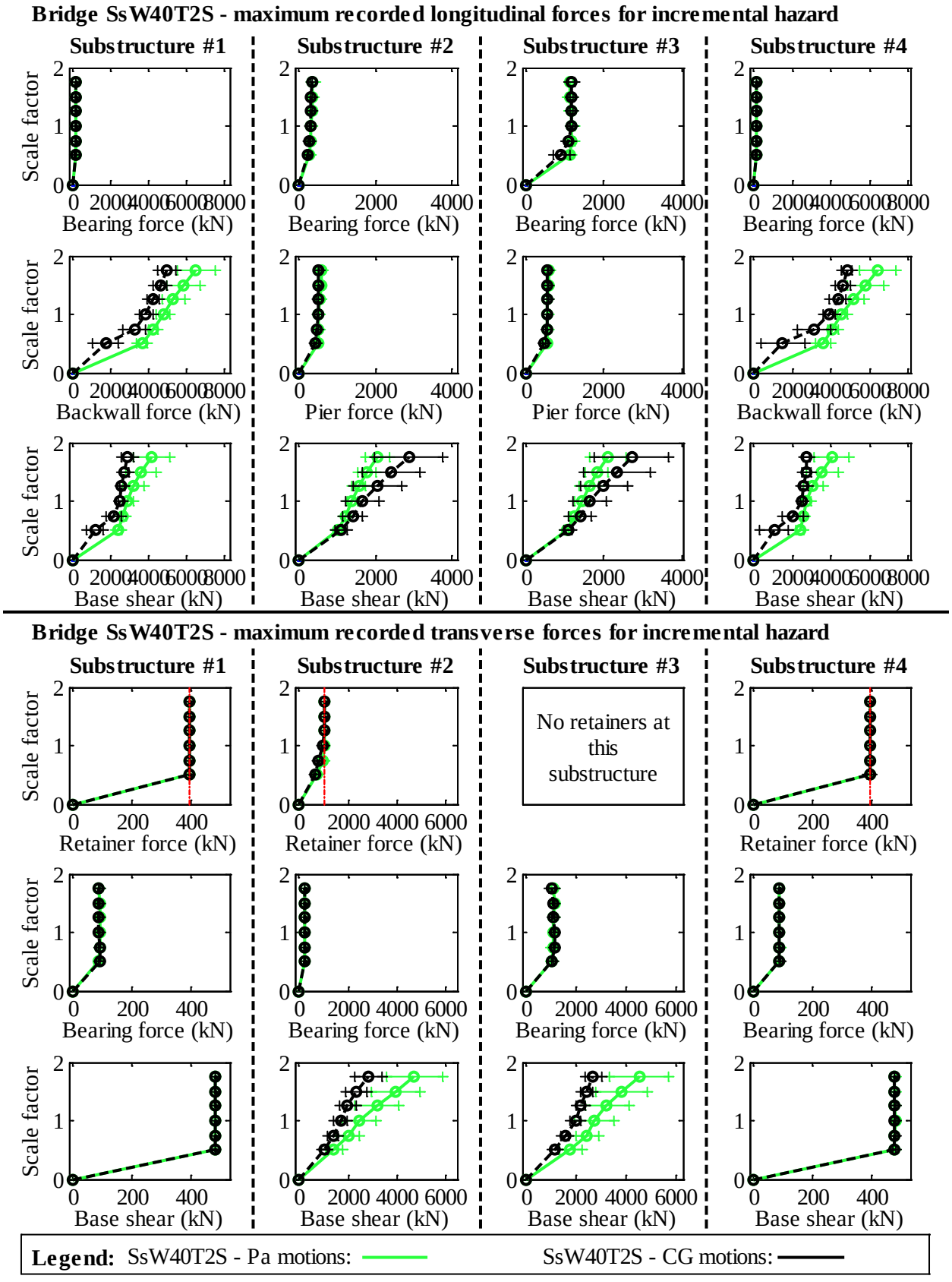

Figure C.100. Bridge SsW40T2S – force results.

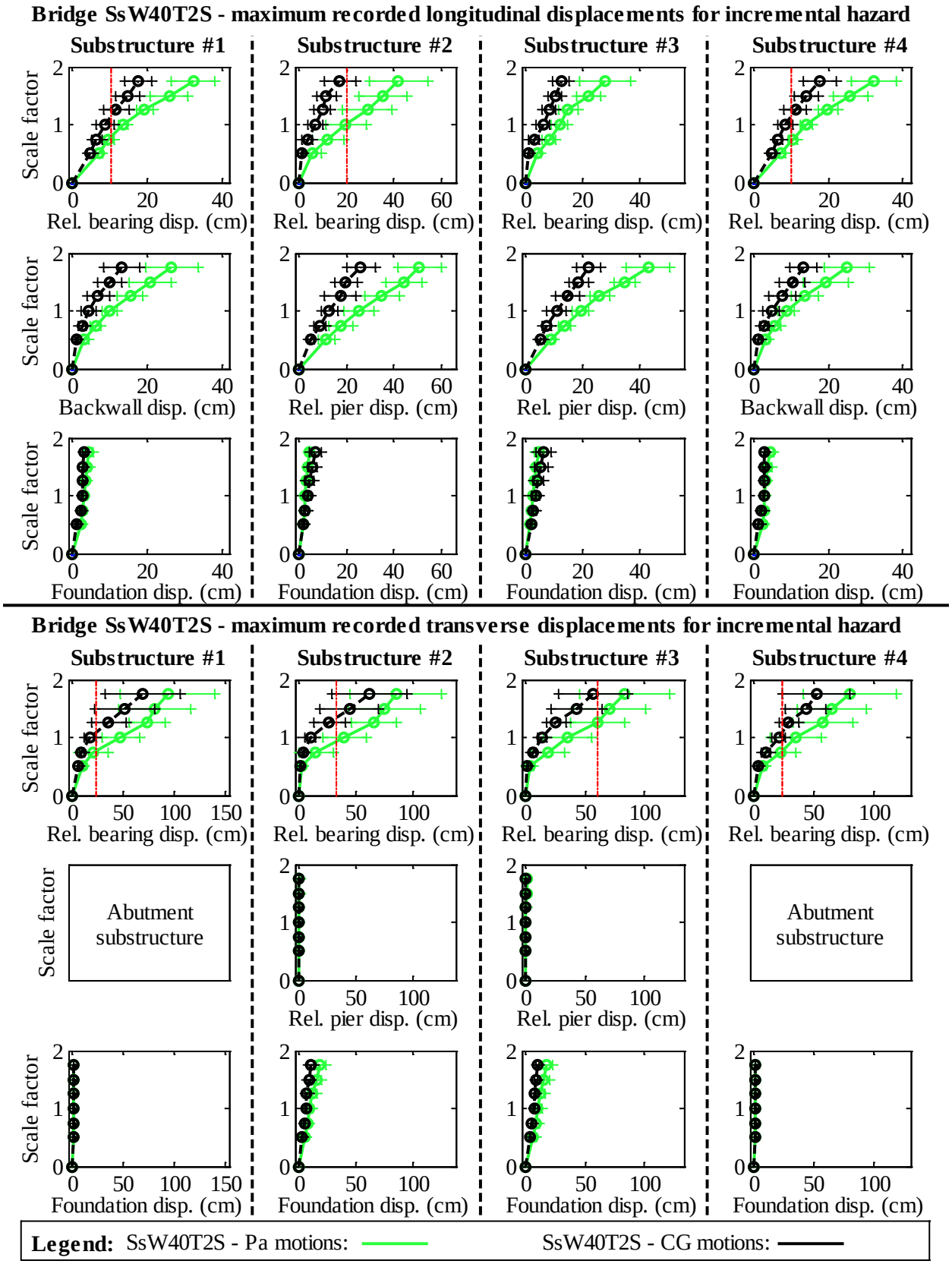

Figure C.101. Bridge SsW40T2S – displacement results.

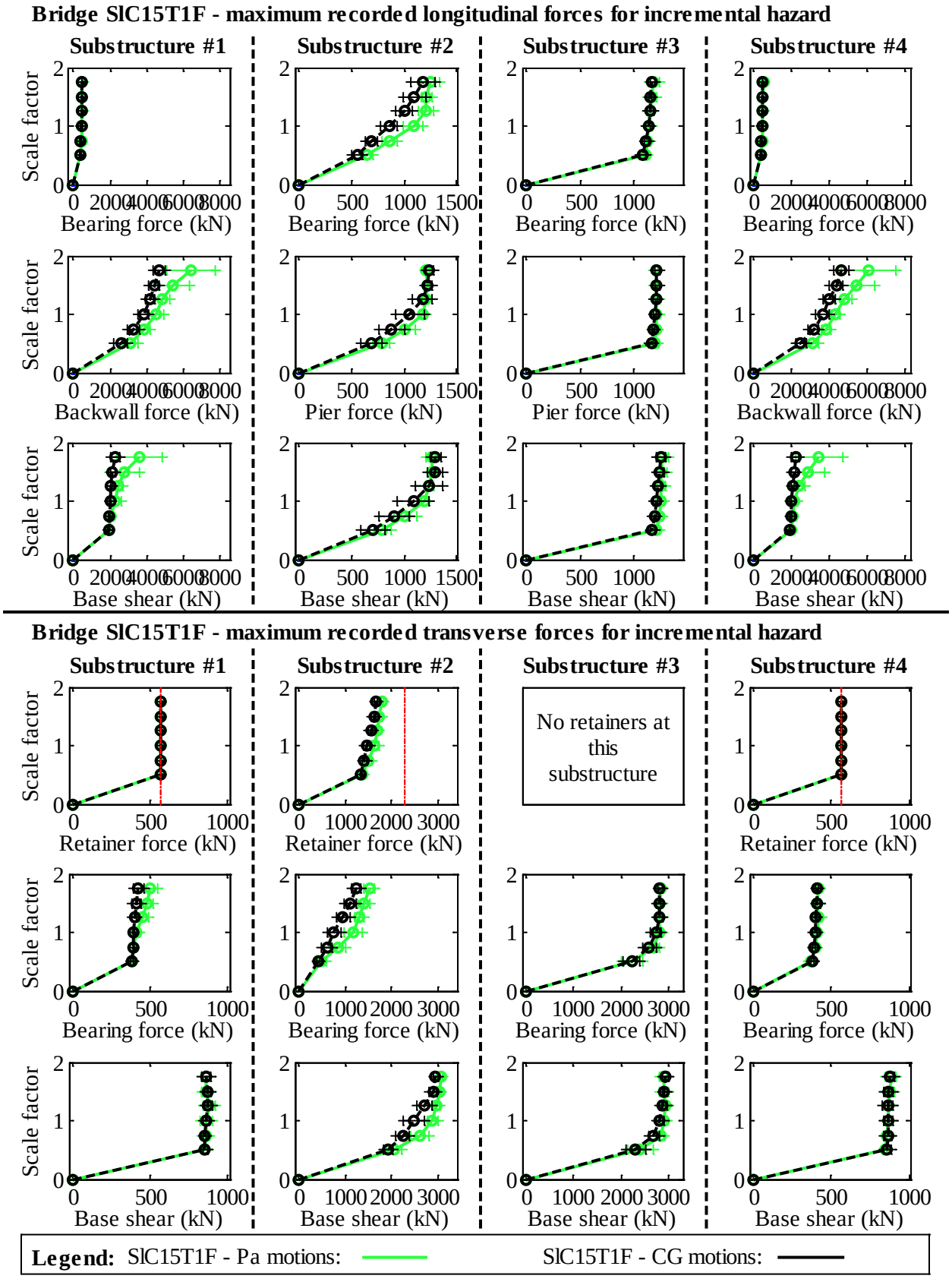

Figure C.102. Bridge SlC15T1F – force results.

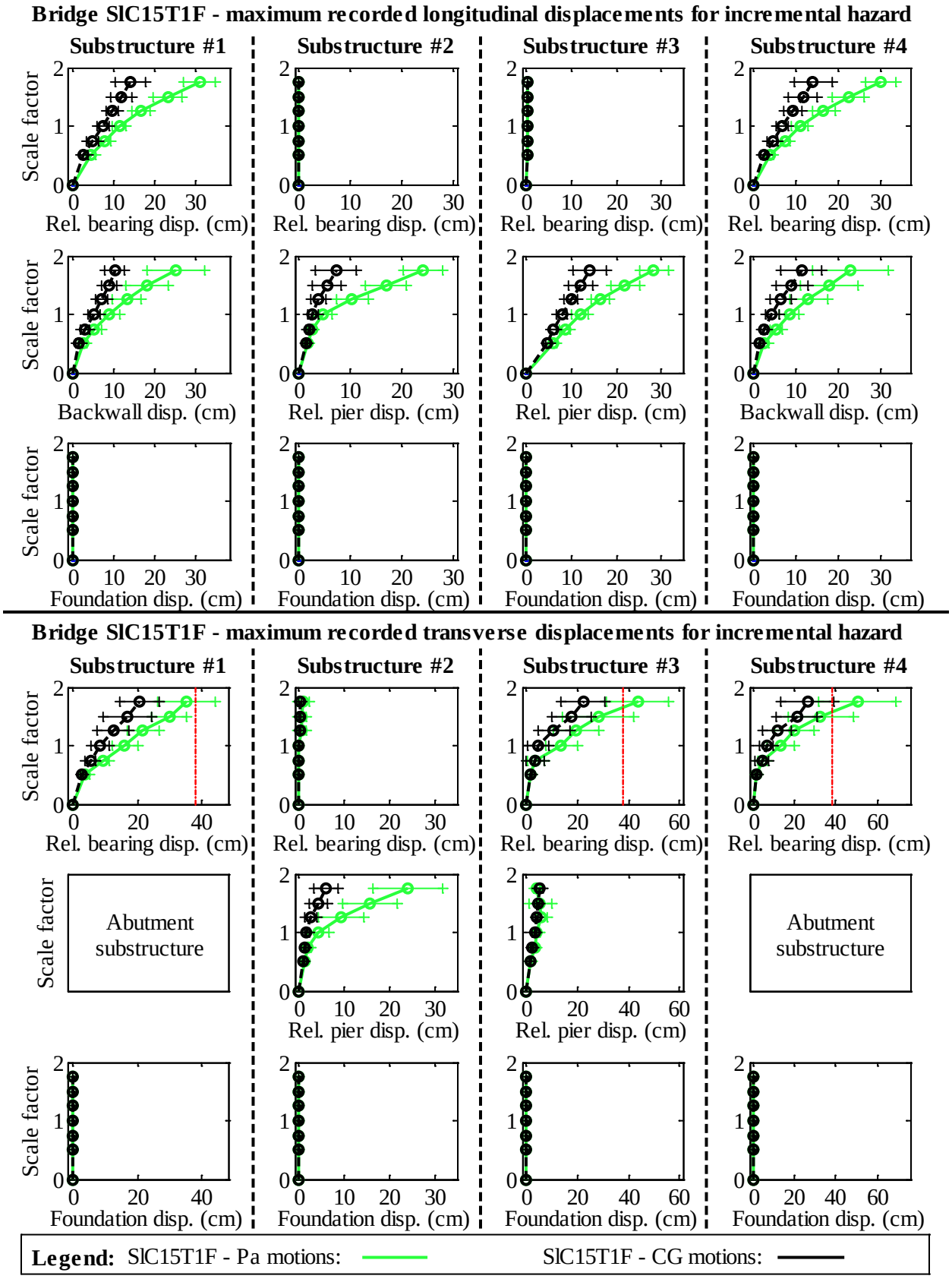

Figure C.103. Bridge SlC15T1F – displacement results.

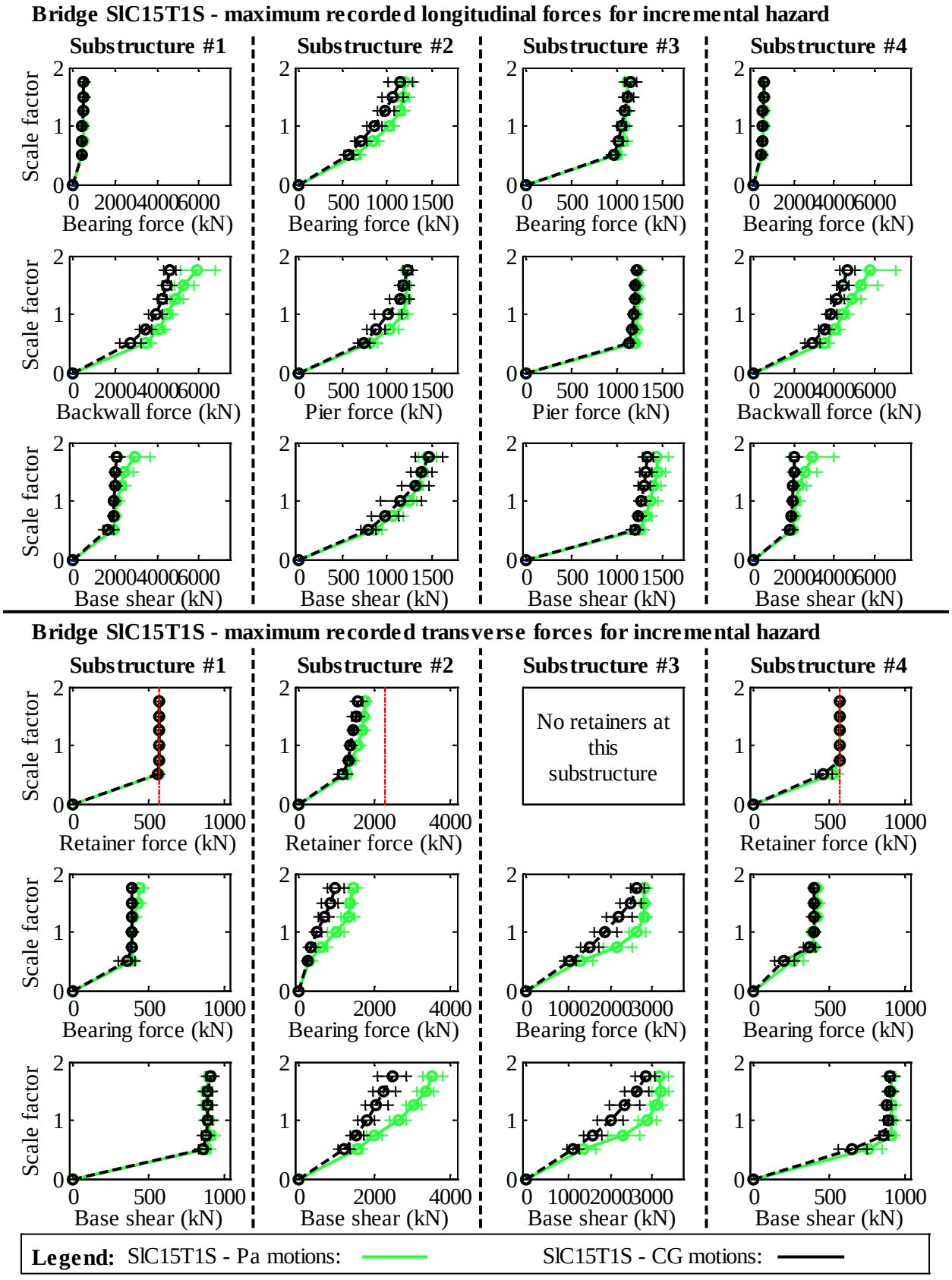

Figure C.104. Bridge SlC15T1S – force results.

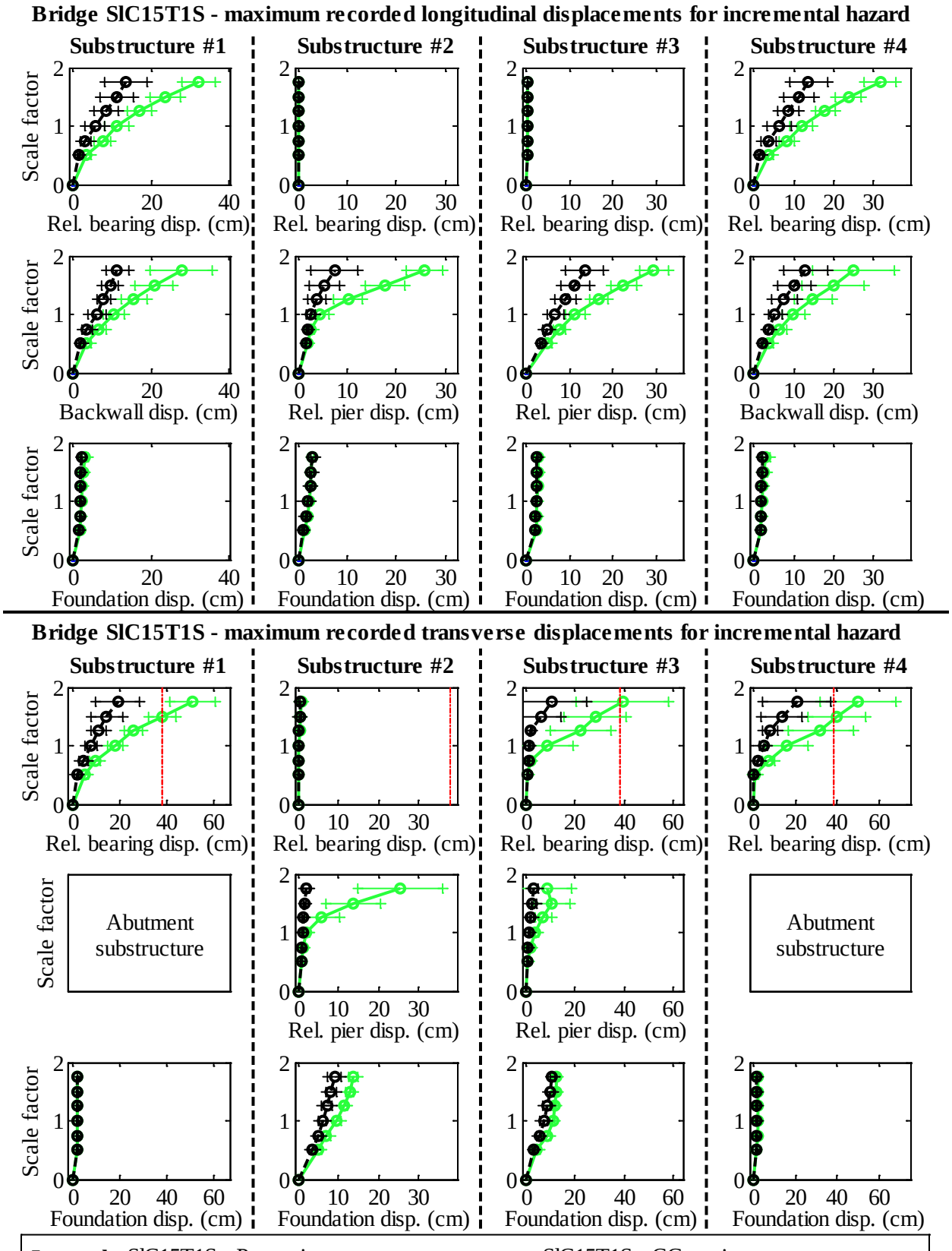

Figure C.105. Bridge SlC15T1S – displacement results.

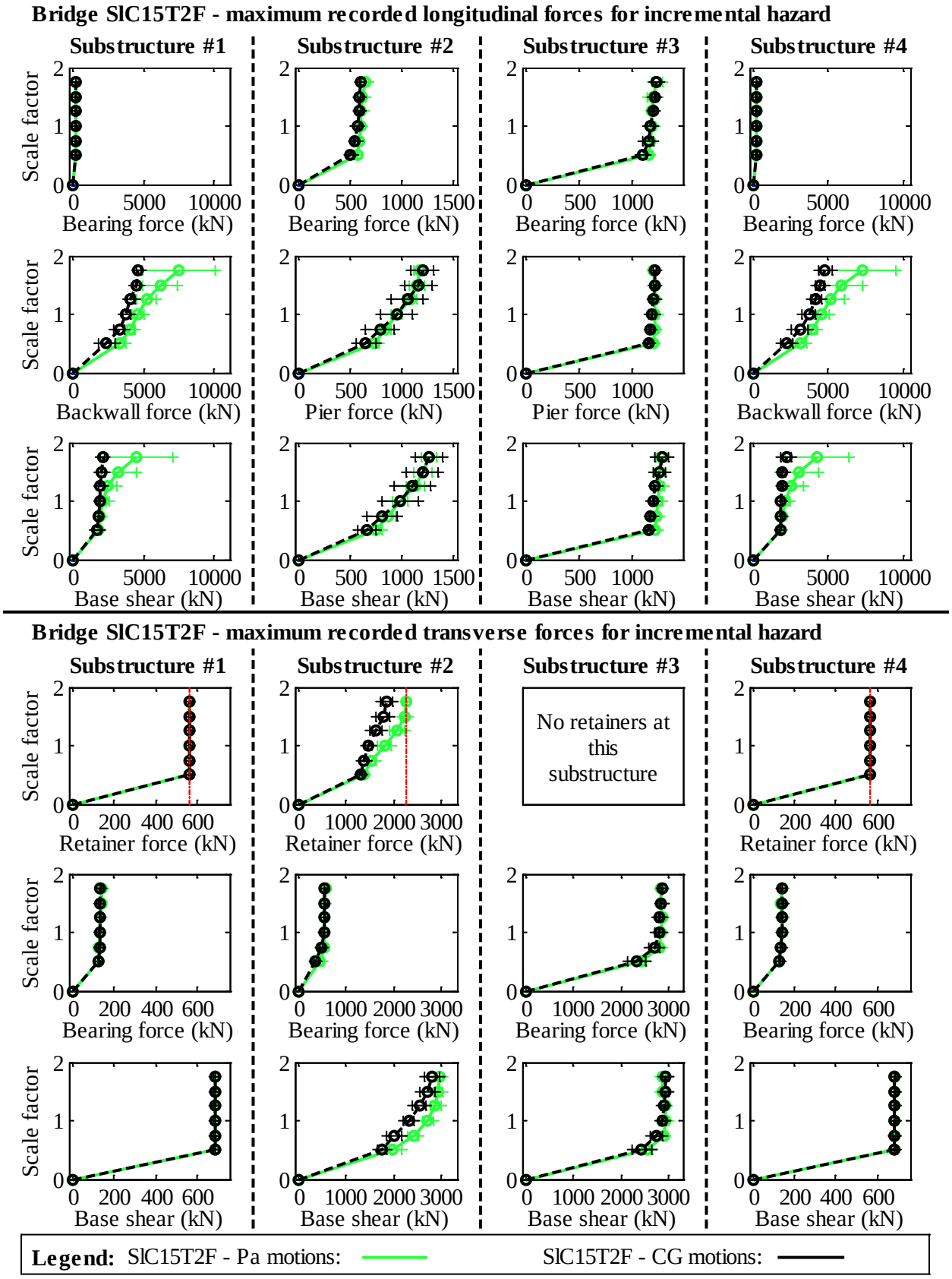

Figure C.106. Bridge SlC15T2F – force results.

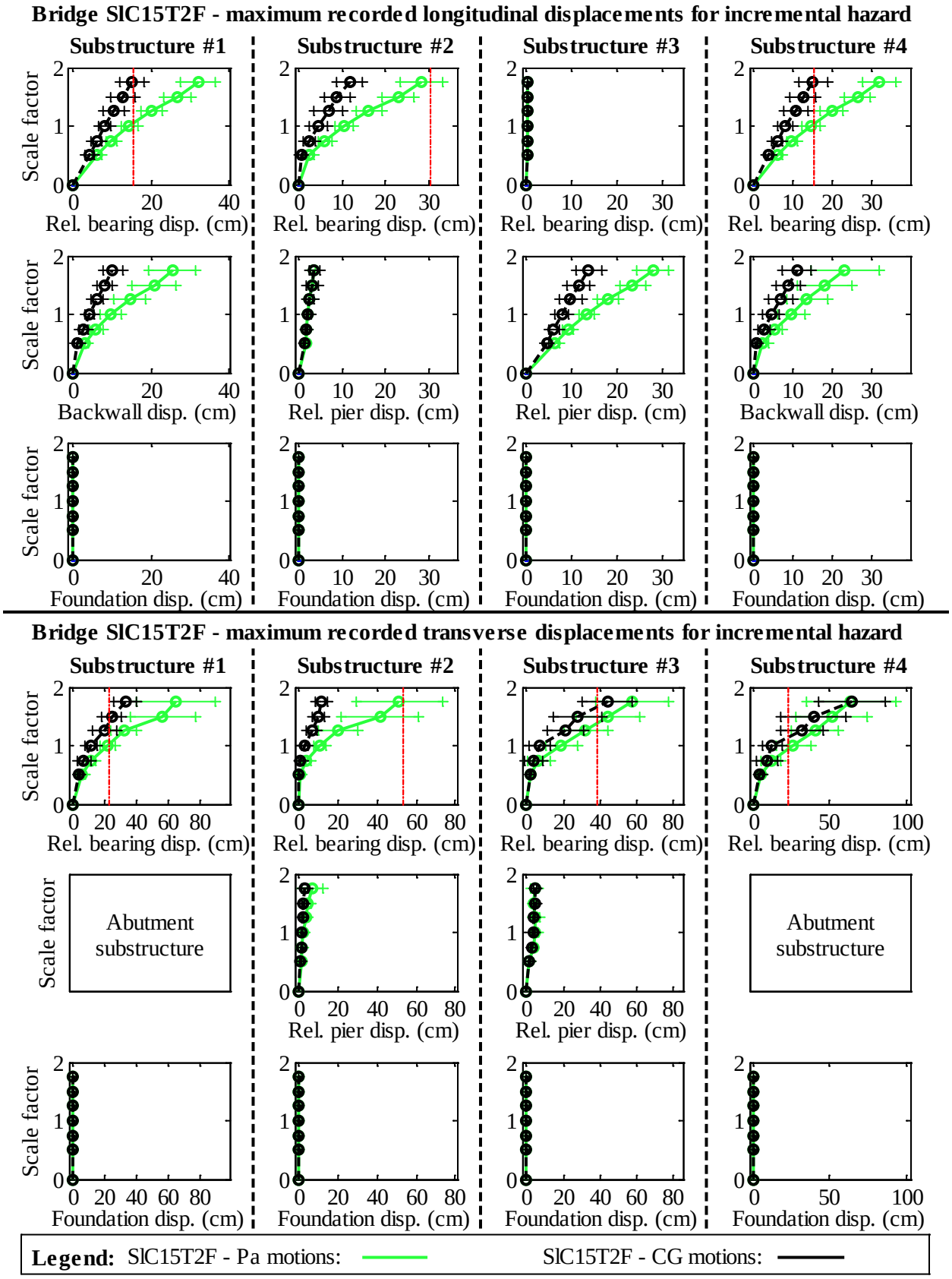

Figure C.107. Bridge SlC15T2F – displacement results.

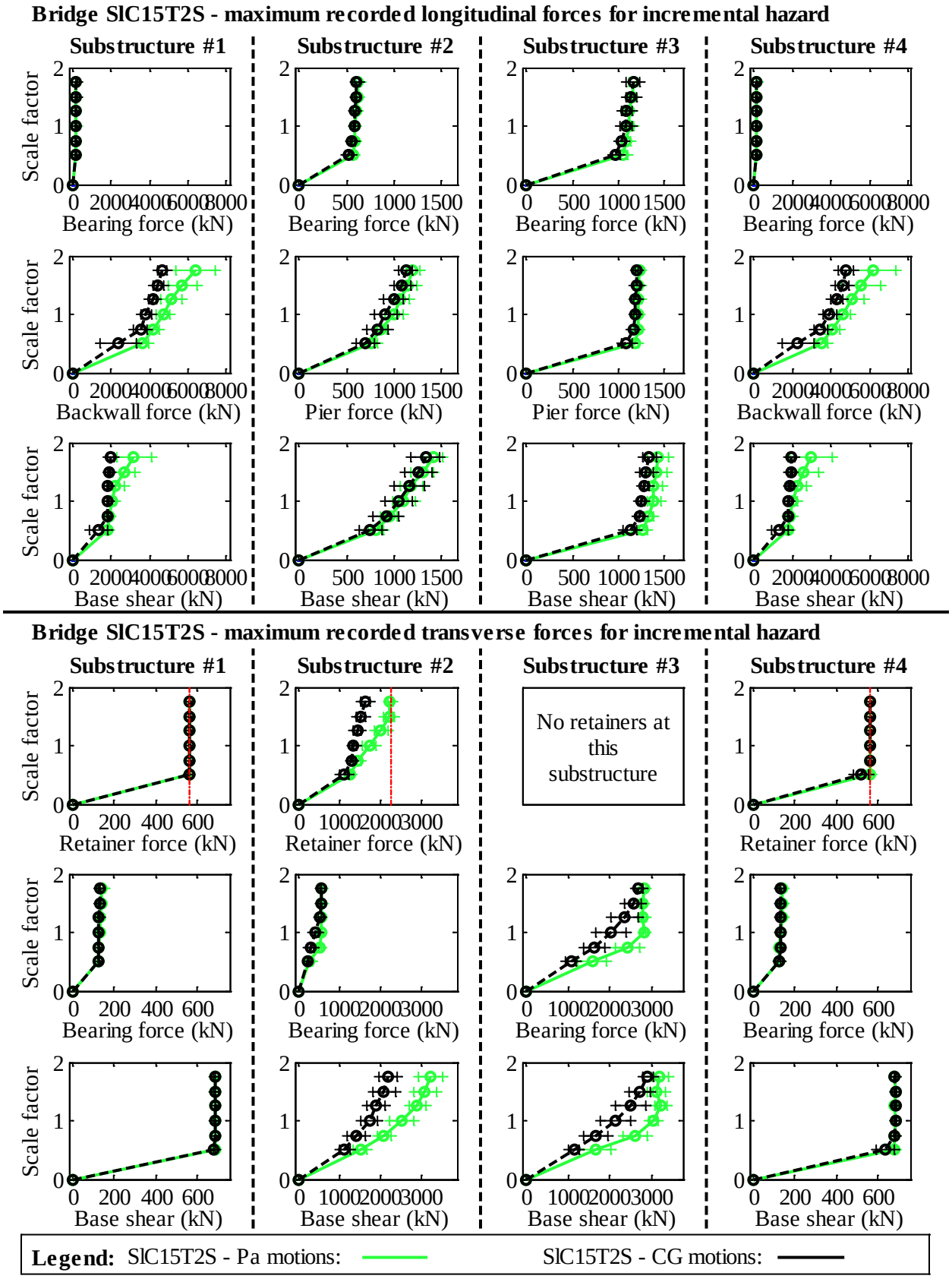

Figure C.108. Bridge SlC15T2S – force results.

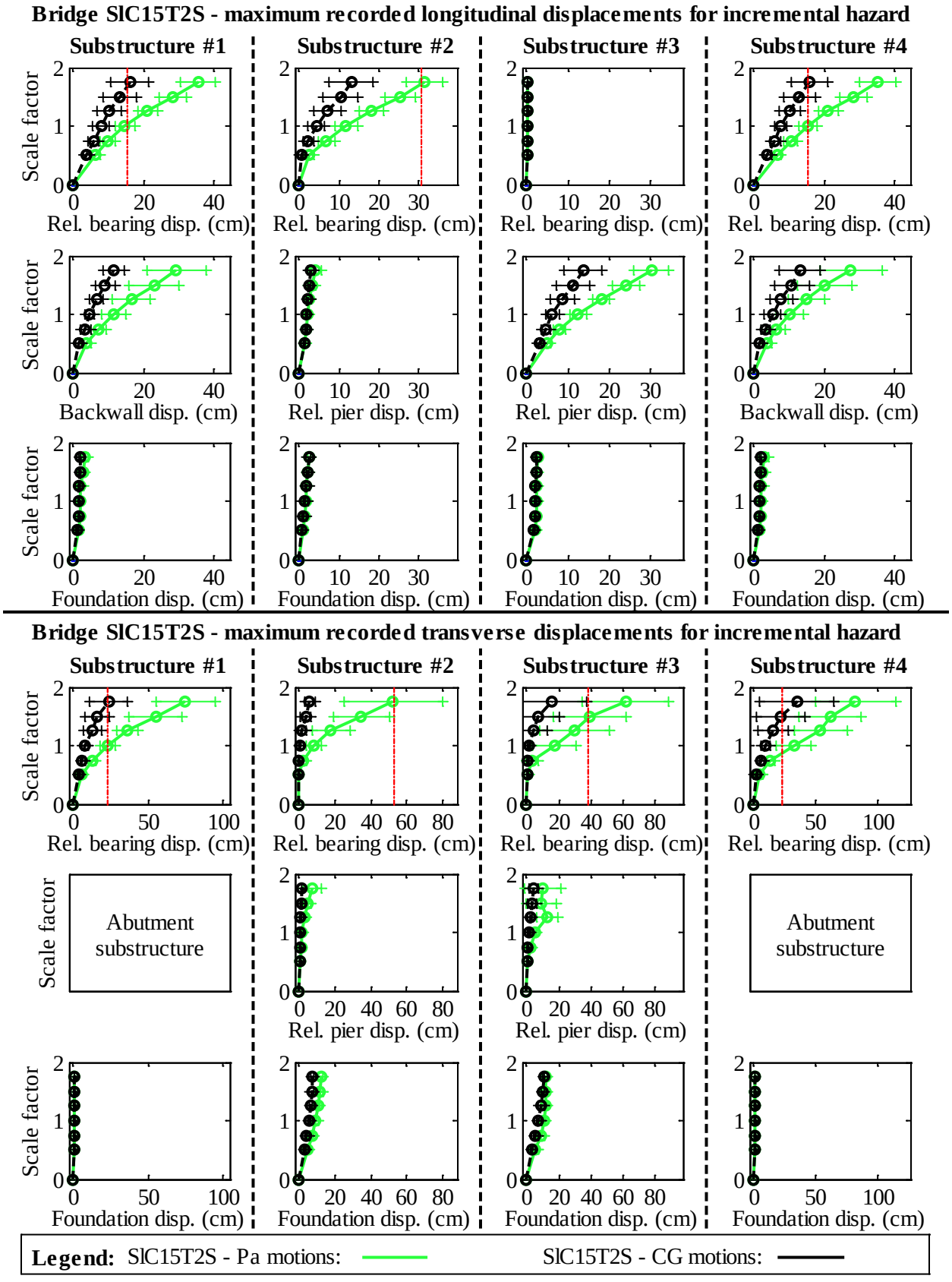

Figure C.109. Bridge SlC15T2S – displacement results.

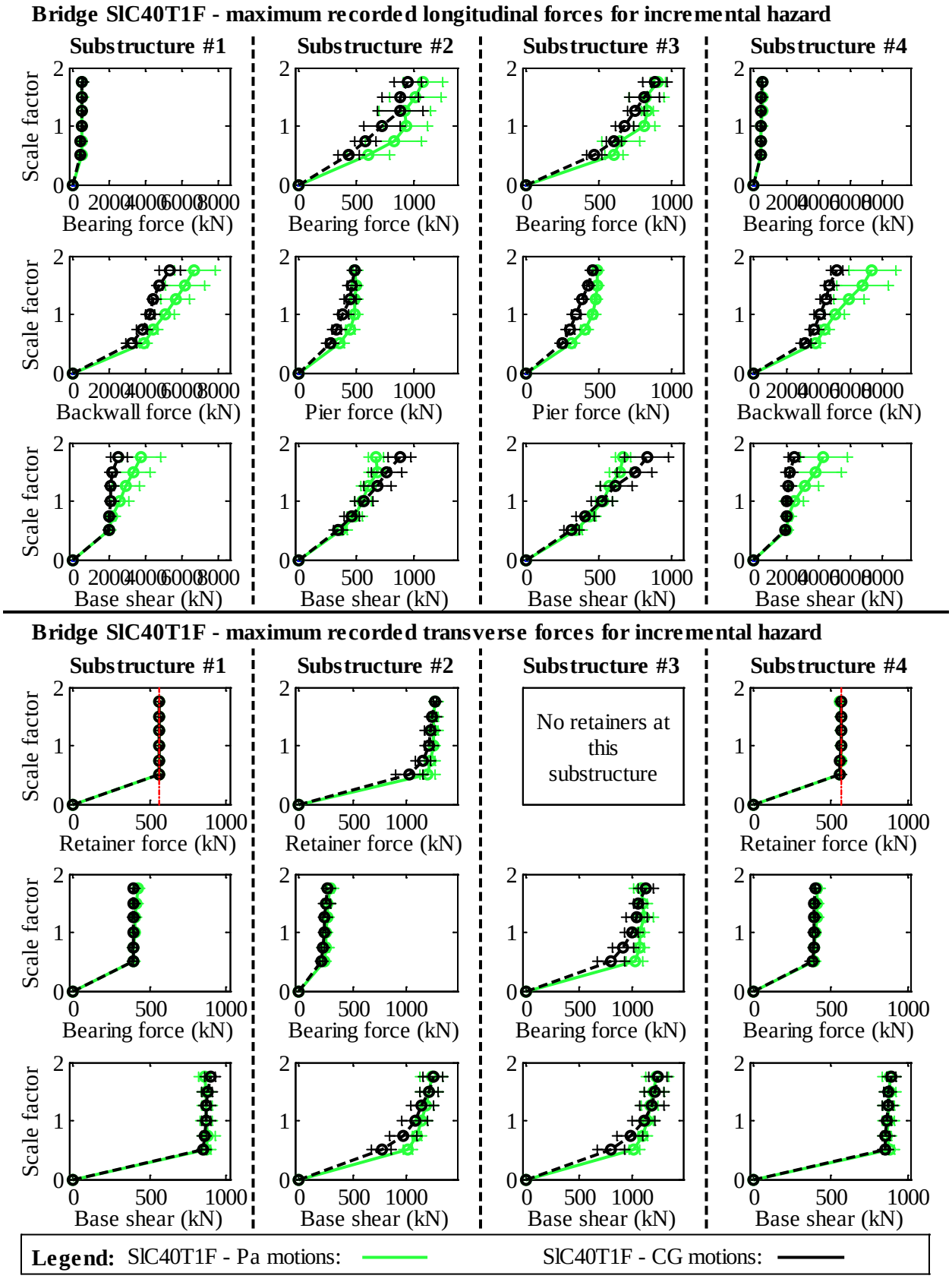

Figure C.110. Bridge SlC40T1F – force results.

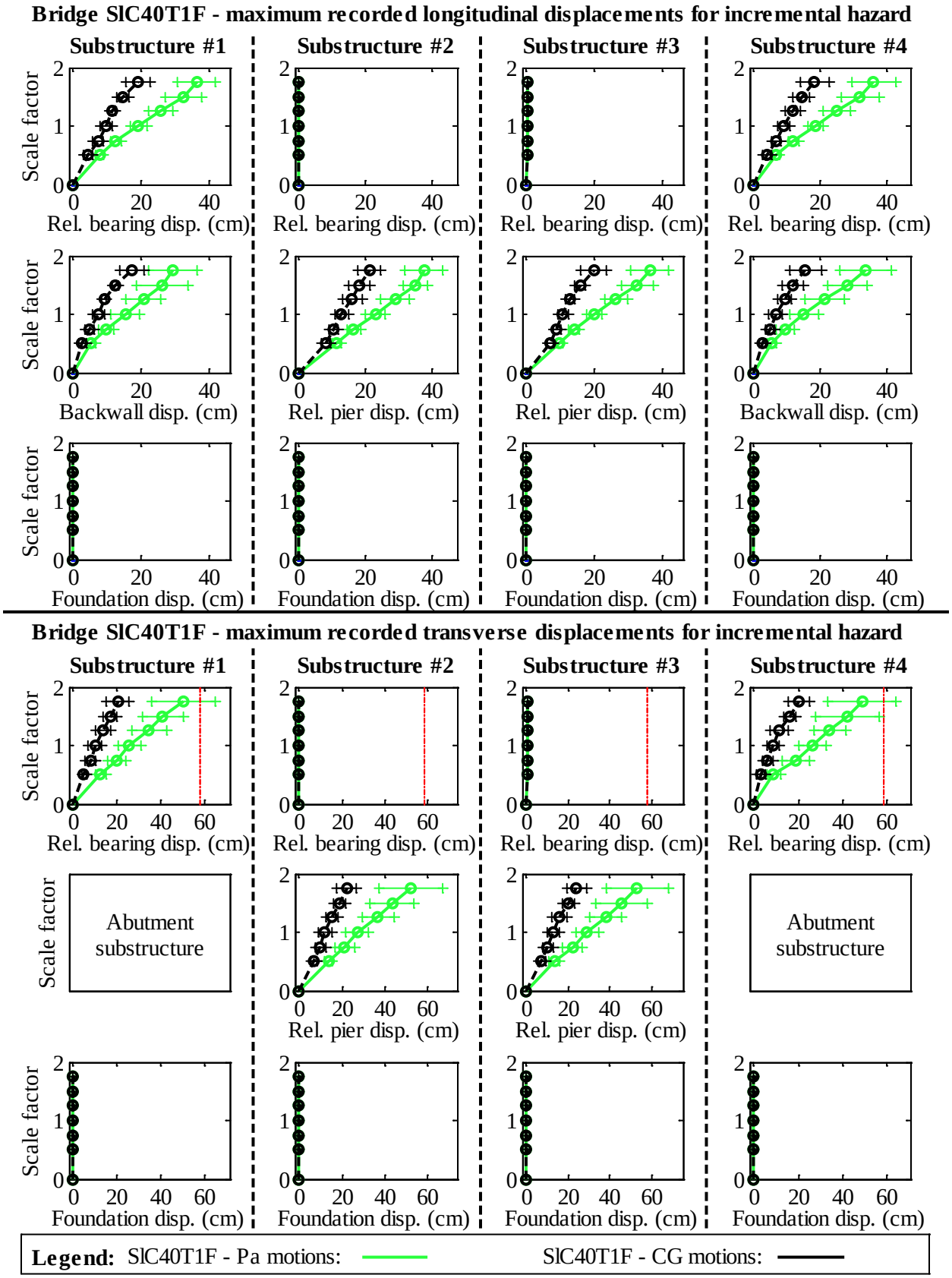

Figure C.111. Bridge SlC40T1F – displacement results.

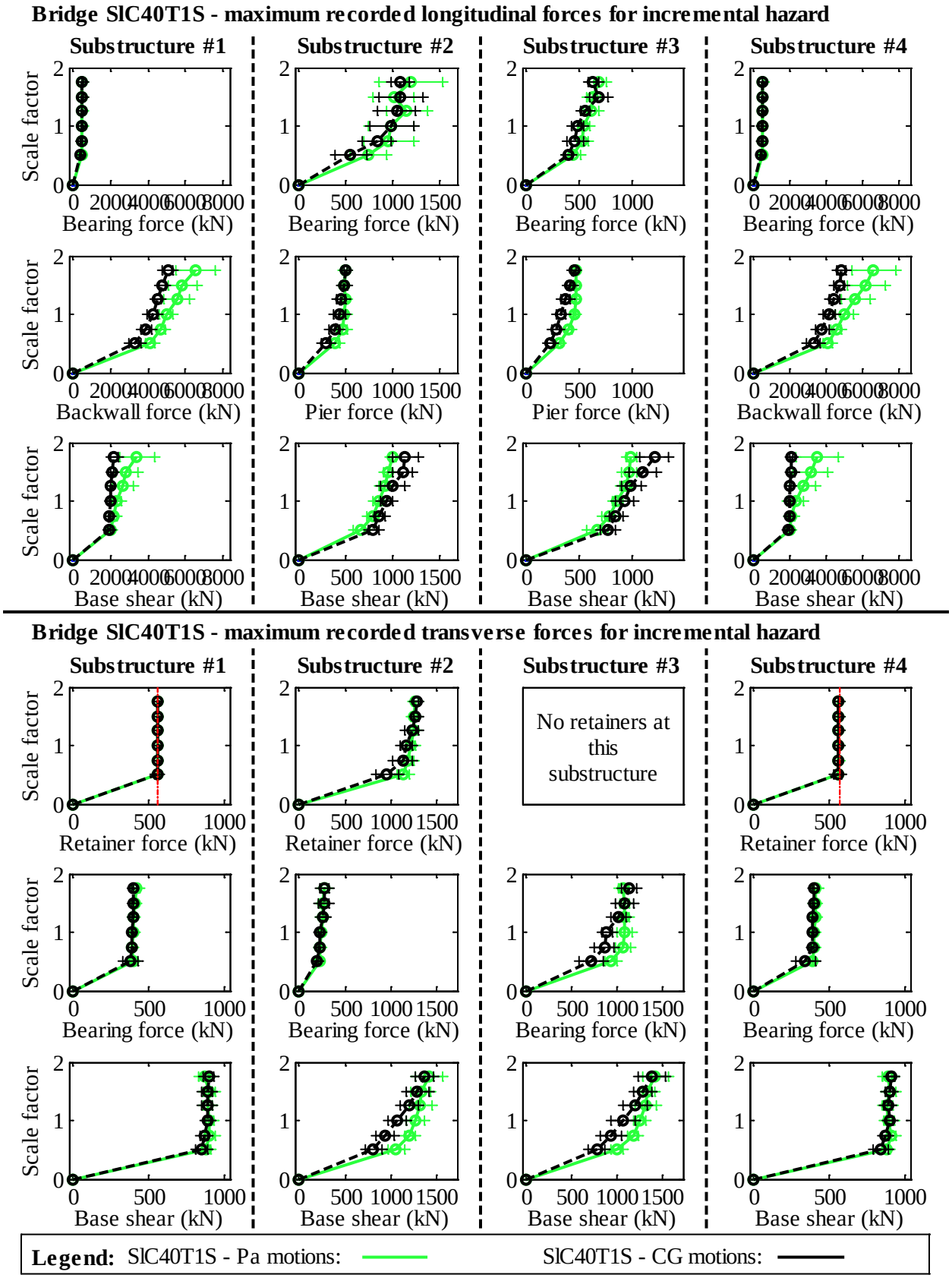

Figure C.112. Bridge SlC40T1S – force results.

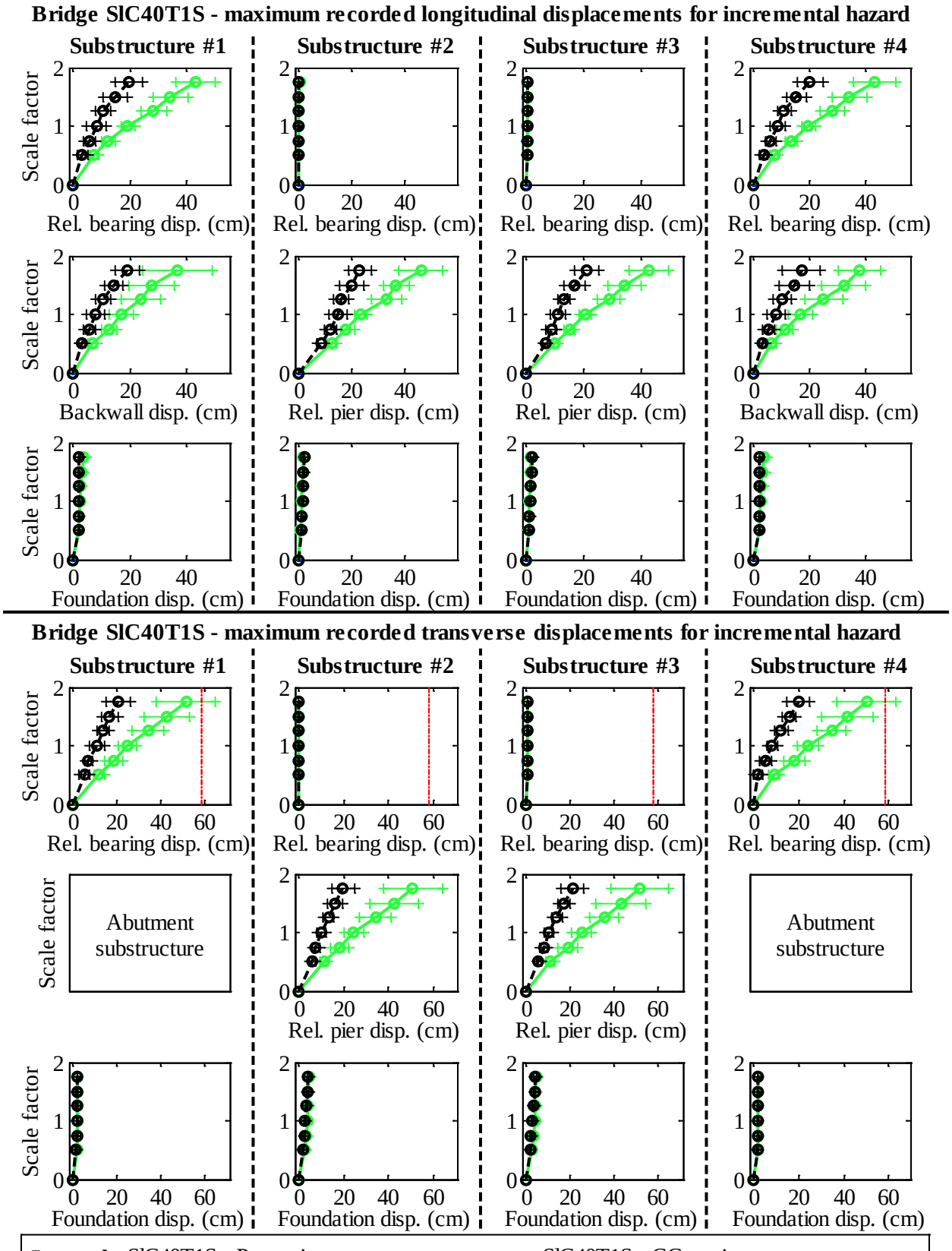

Figure C.113. Bridge SlC40T1S – displacement results.

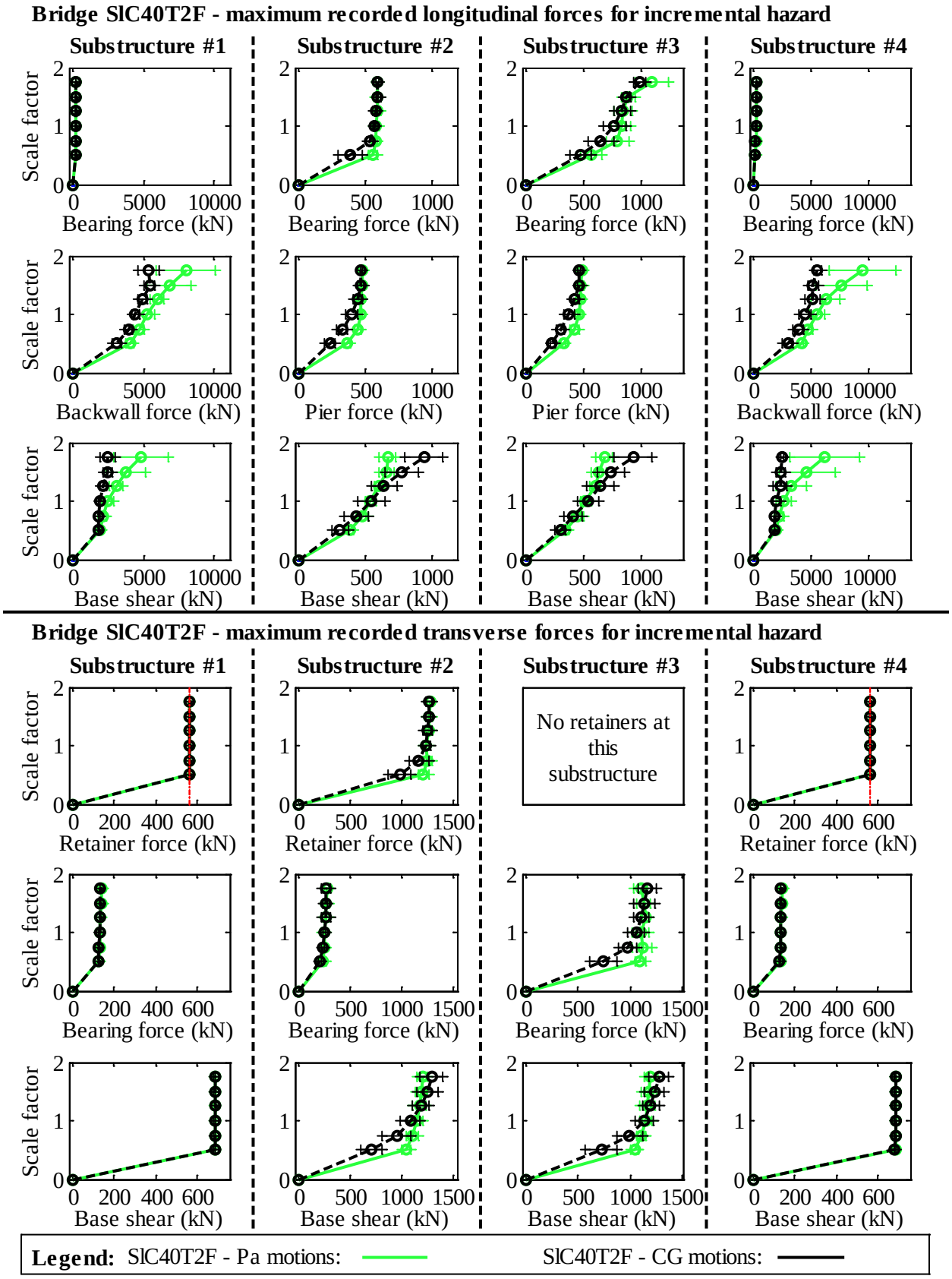

Figure C.114. Bridge SlC40T2F – force results.

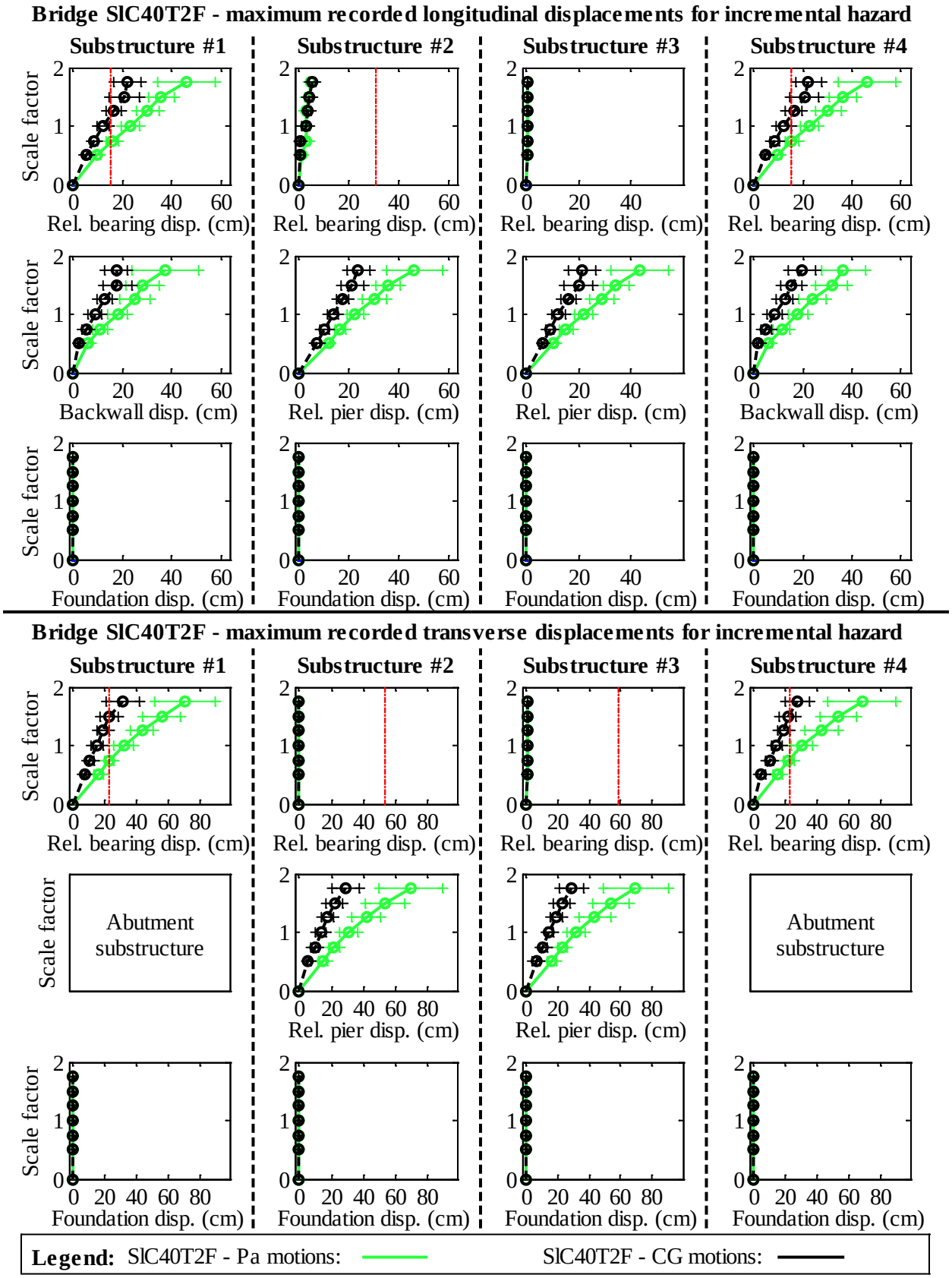

Figure C.115. Bridge SlC40T2F – displacement results.

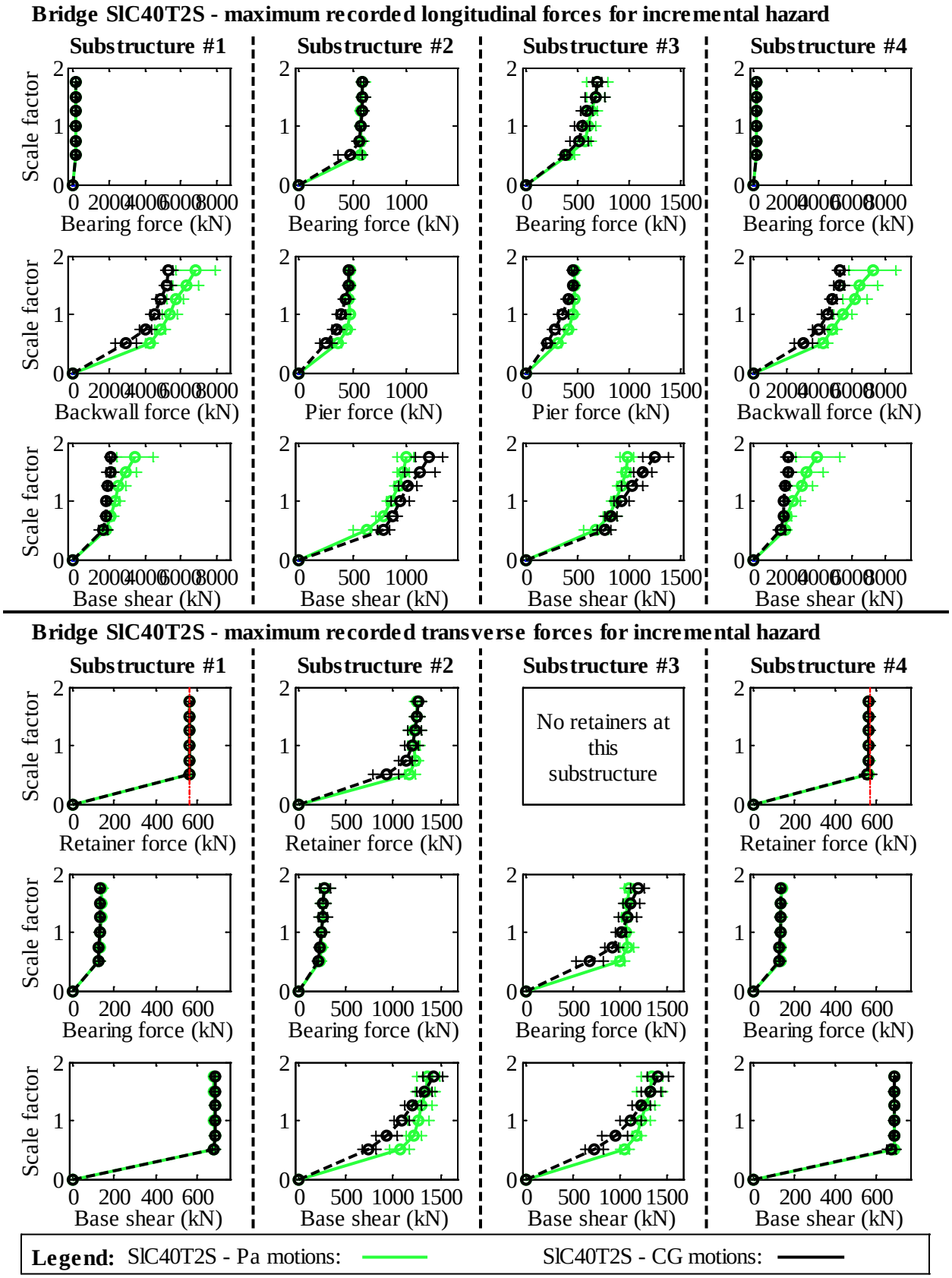

Figure C.116. Bridge SlC40T2S – force results.

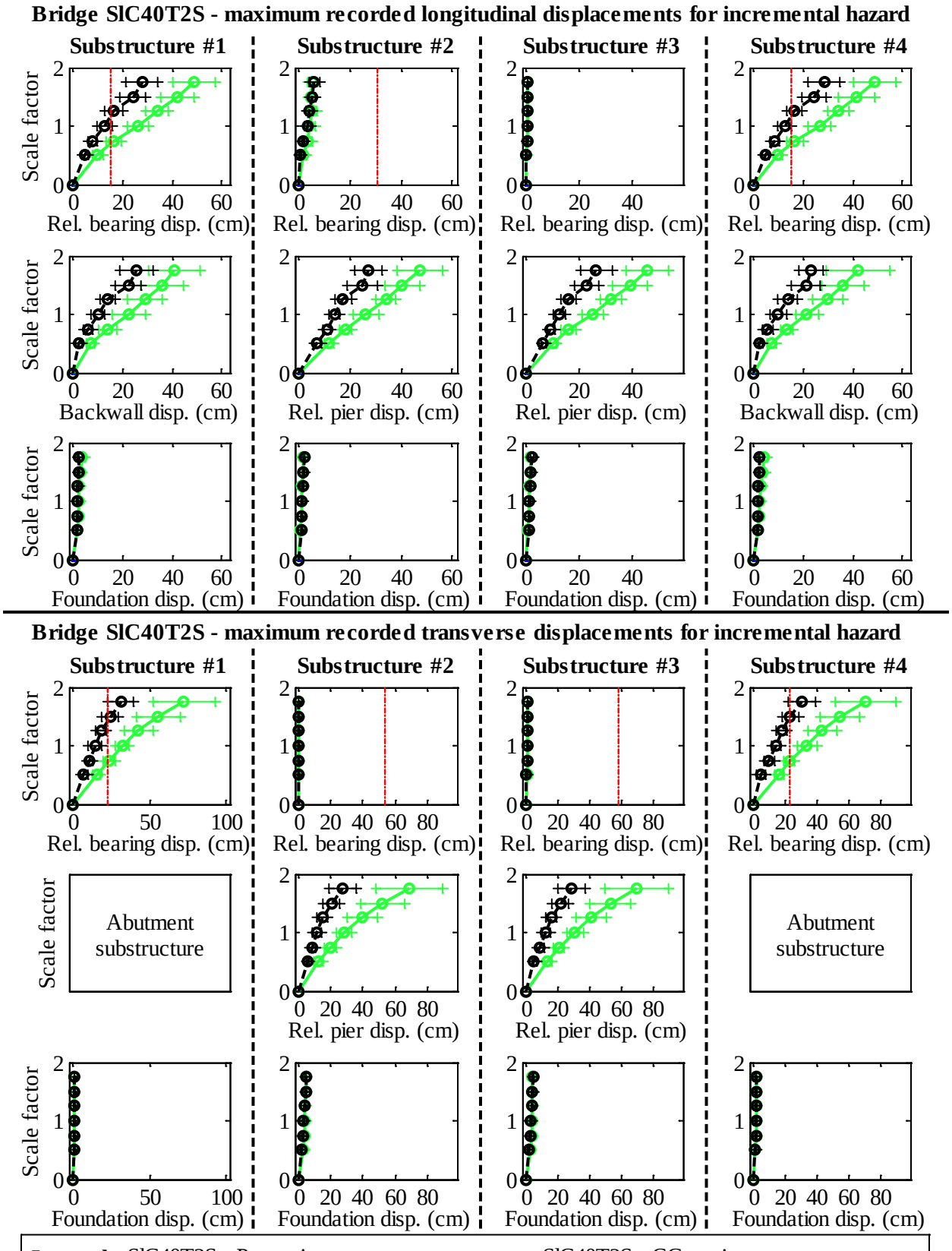

Figure C.117. Bridge SlC40T2S – displacement results.

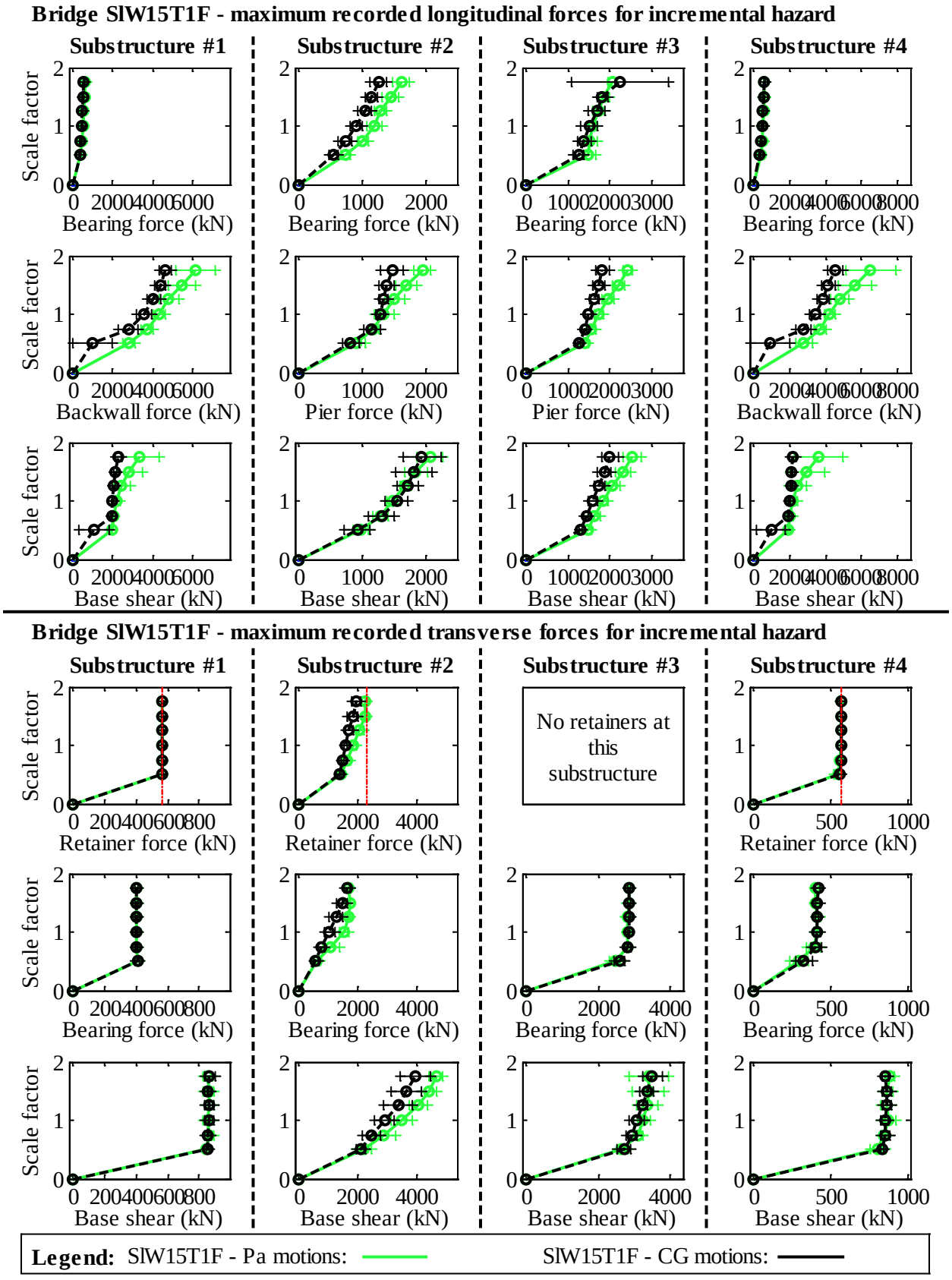

Figure C.118. Bridge SlW15T1F – force results.

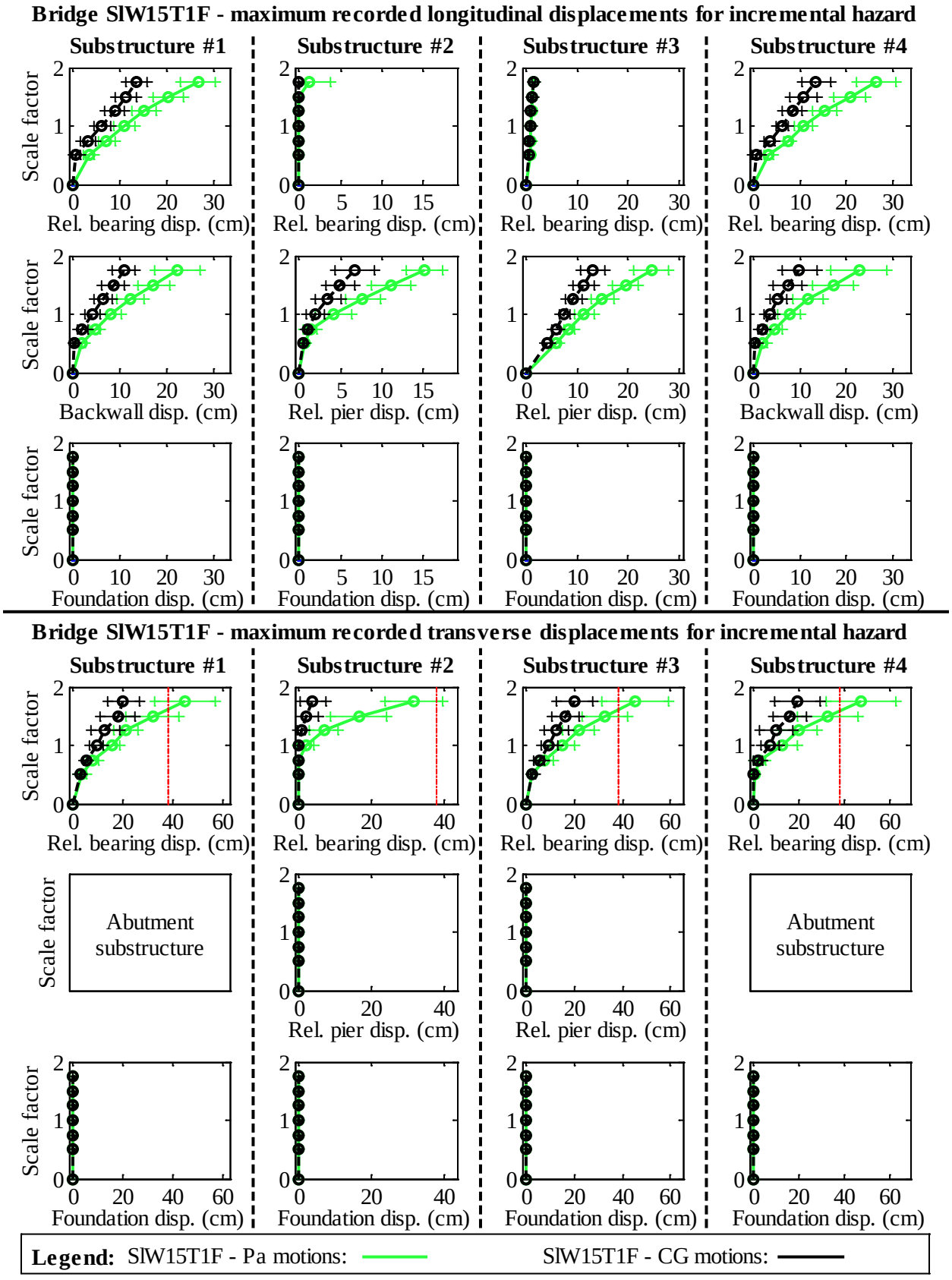

Figure C.119. Bridge SlW15T1F – displacement results.

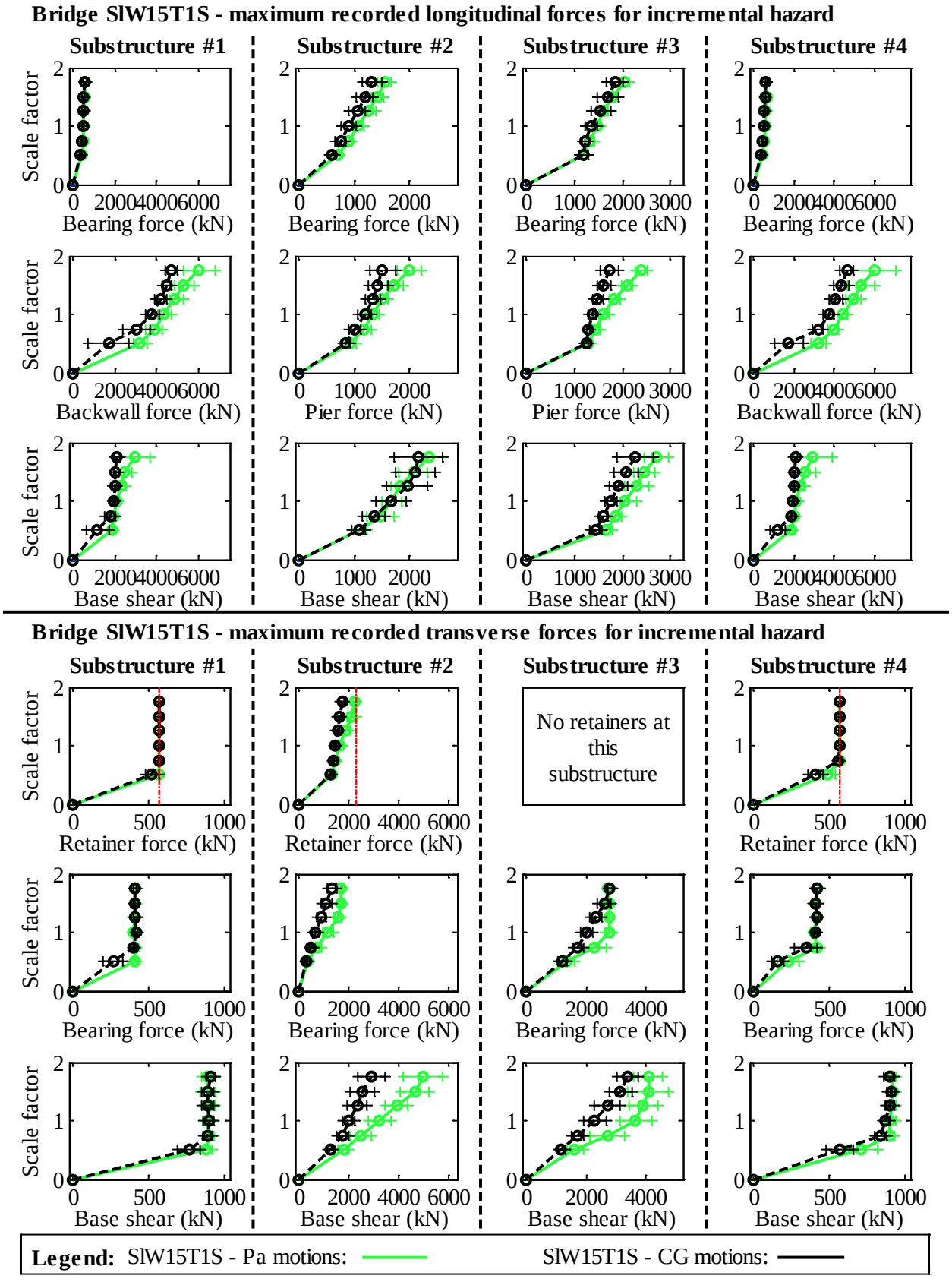

Figure C.120. Bridge SlW15T1S – force results.

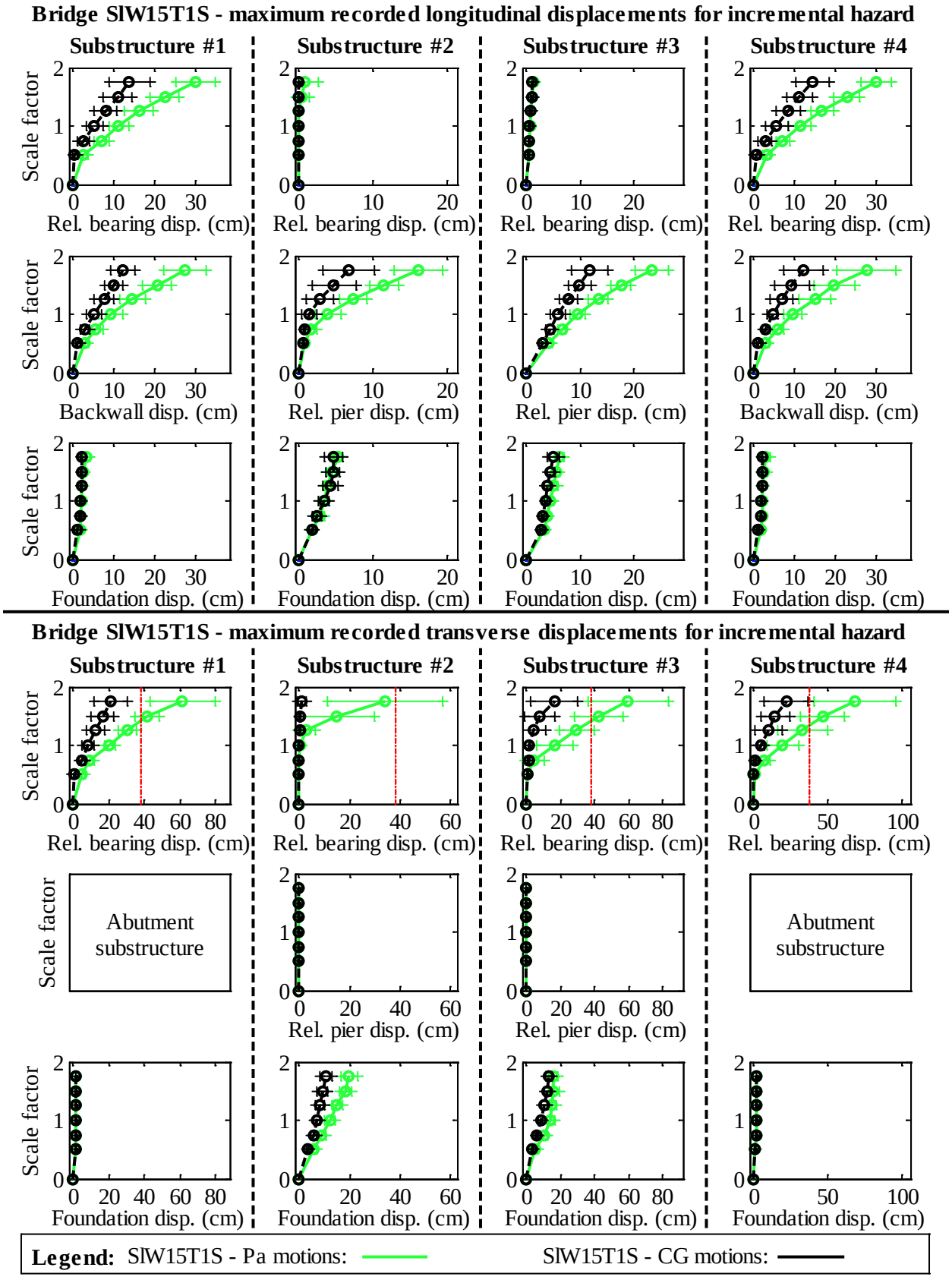

Figure C.121. Bridge SlW15T1S – displacement results.

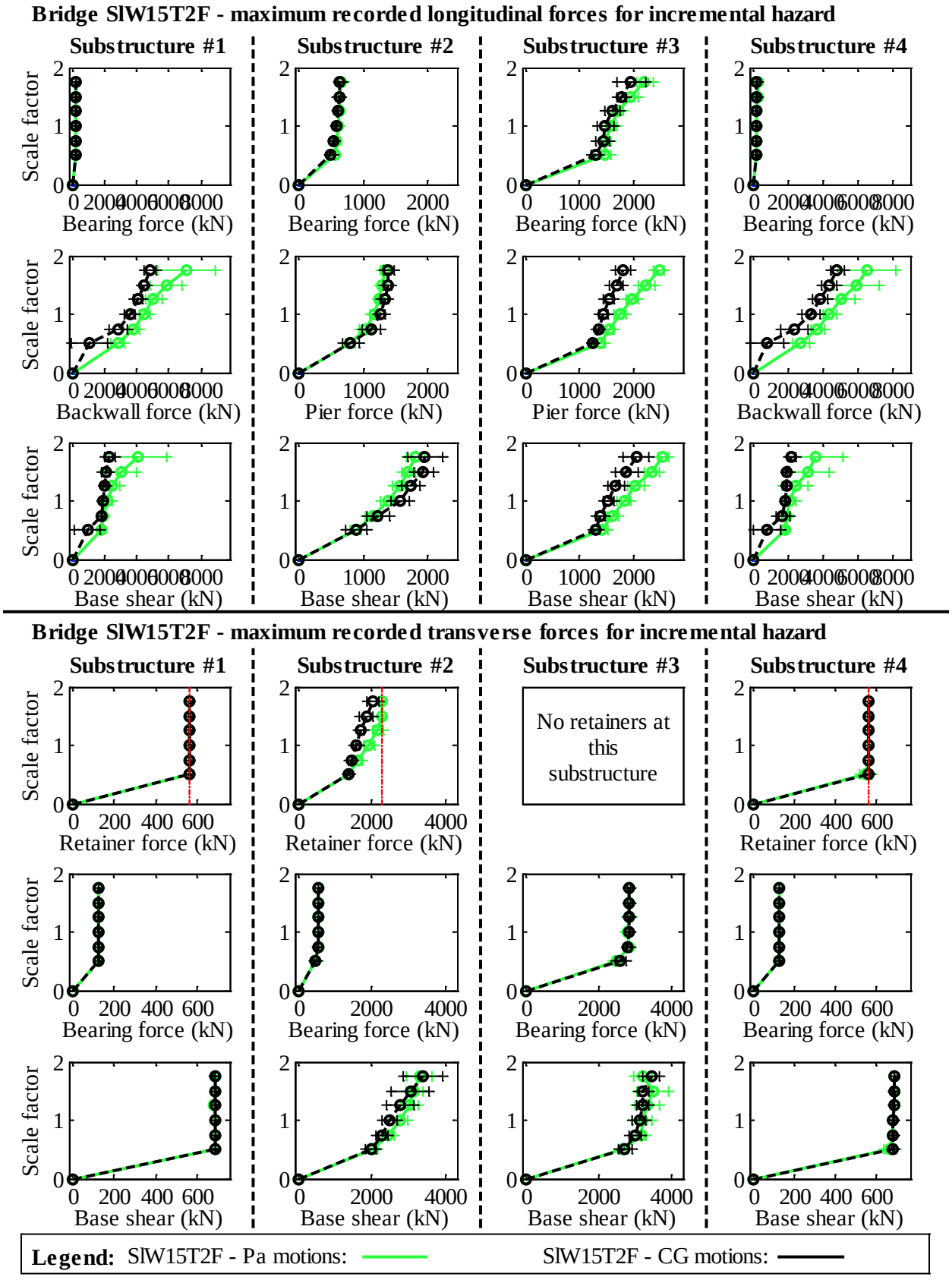

Figure C.122. Bridge SlW15T2F – force results.

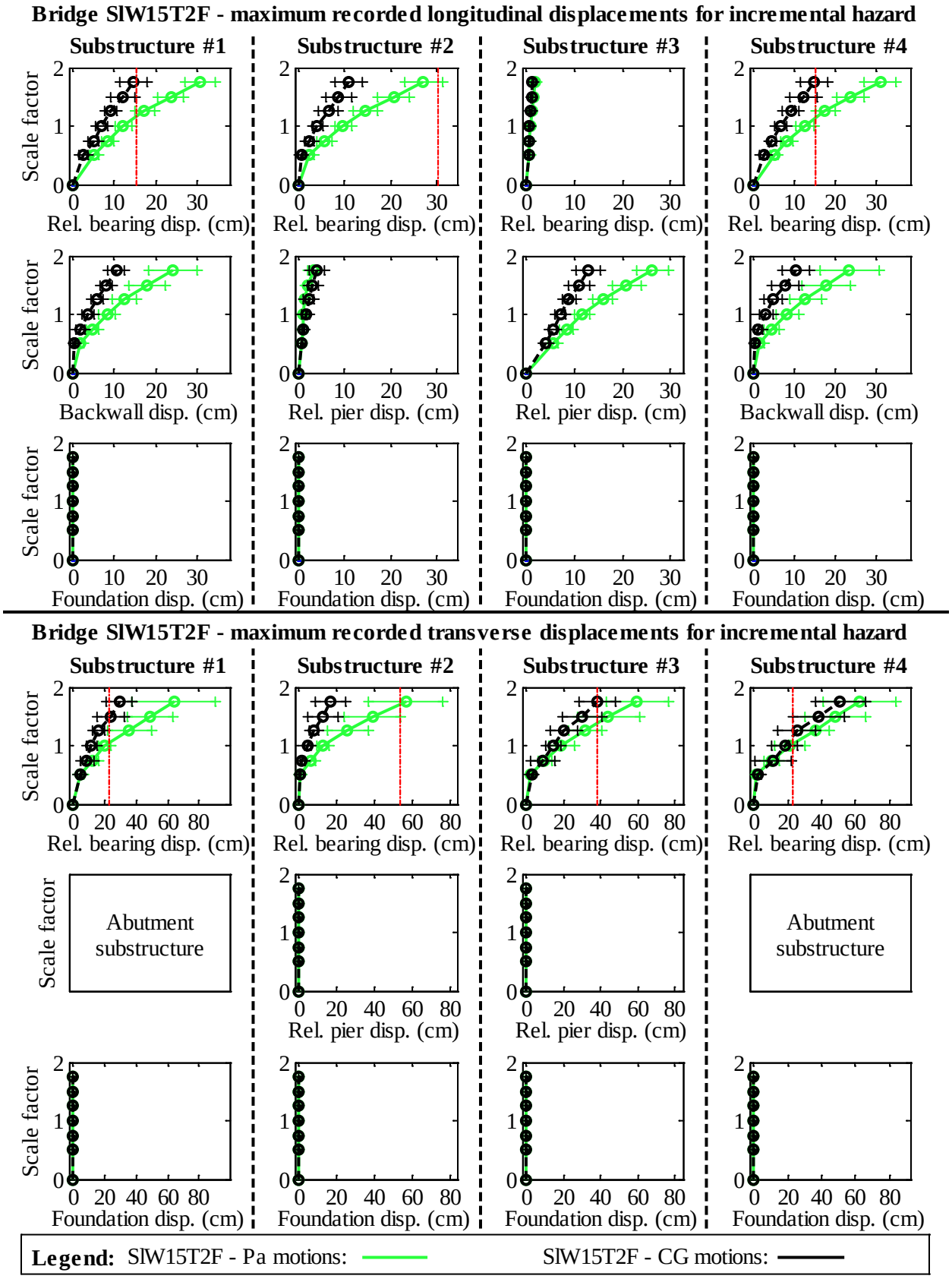

Figure C.123. Bridge SlW15T2F – displacement results.

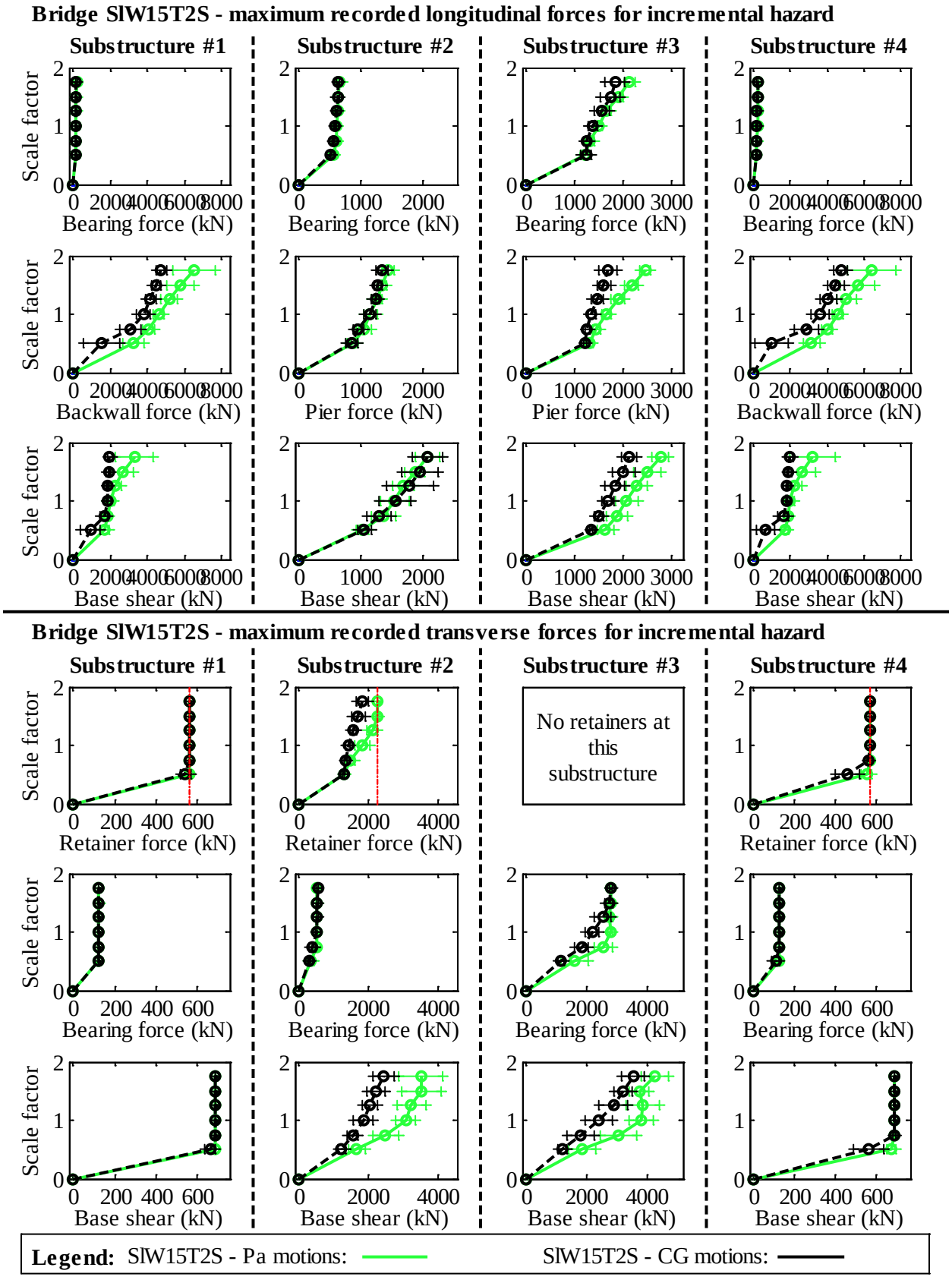

Figure C.124. Bridge SlW15T2S – force results.

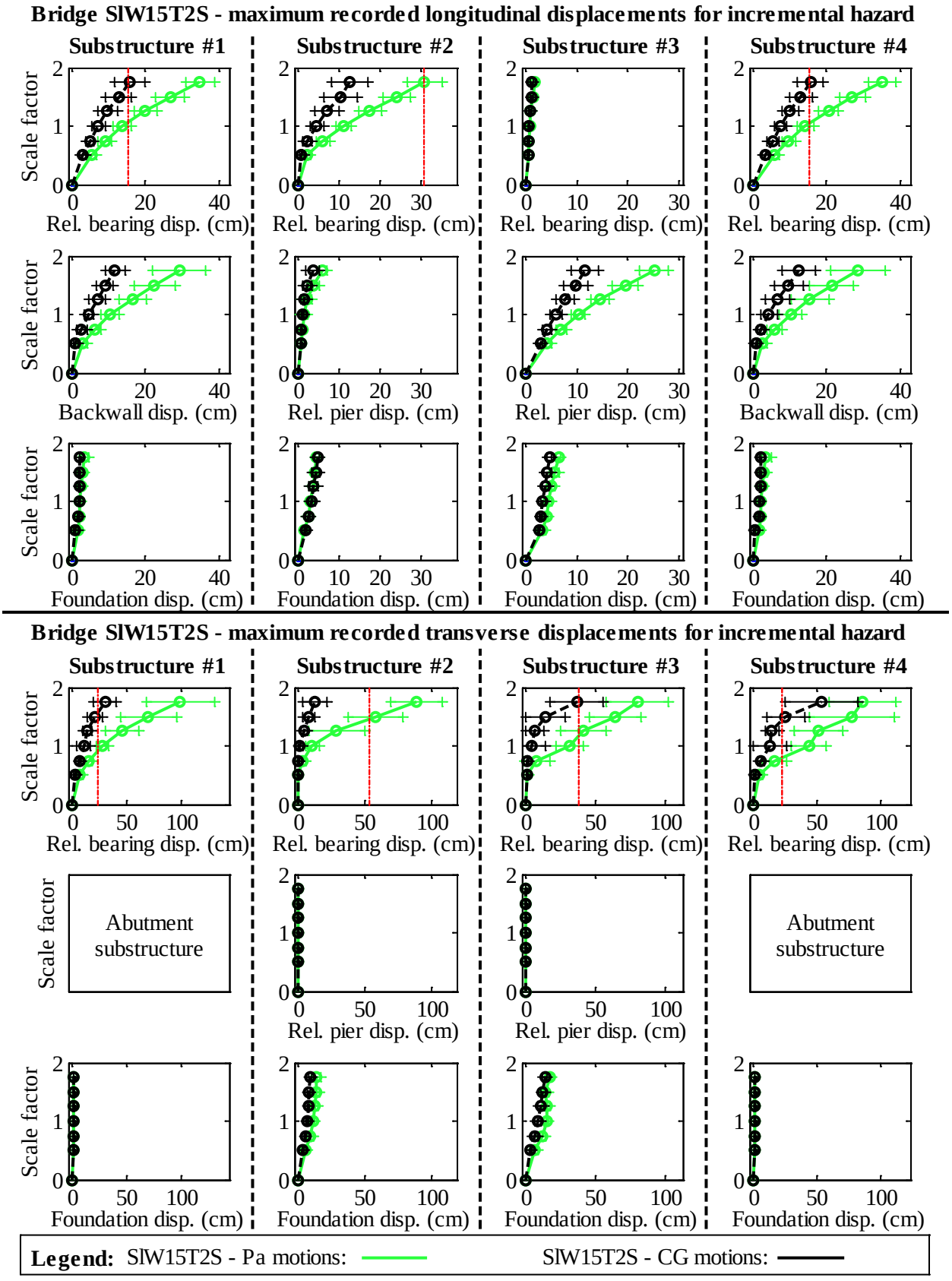

Figure C.125. Bridge SlW15T2S – displacement results.

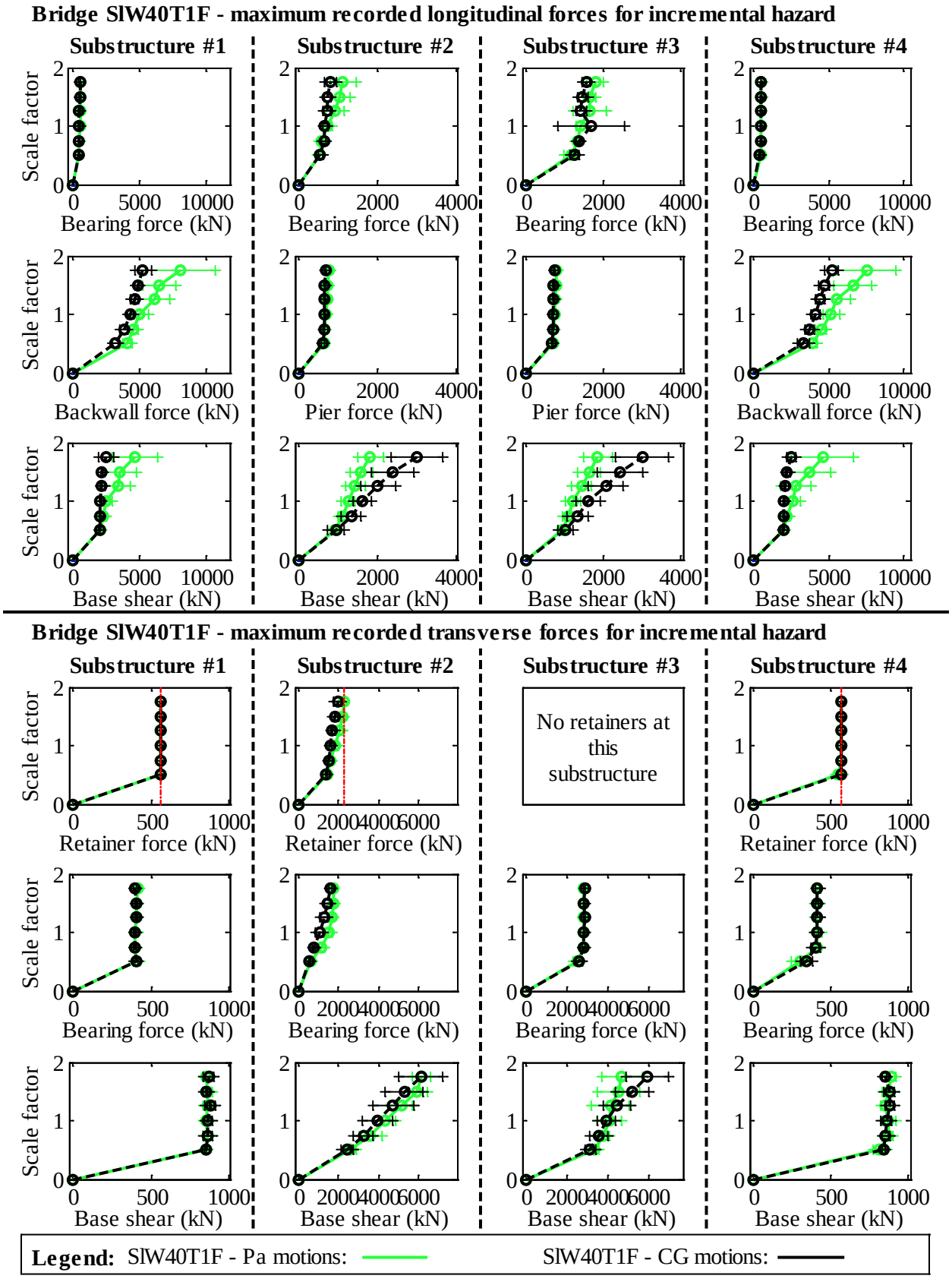

Figure C.126. Bridge SlW40T1F – force results.

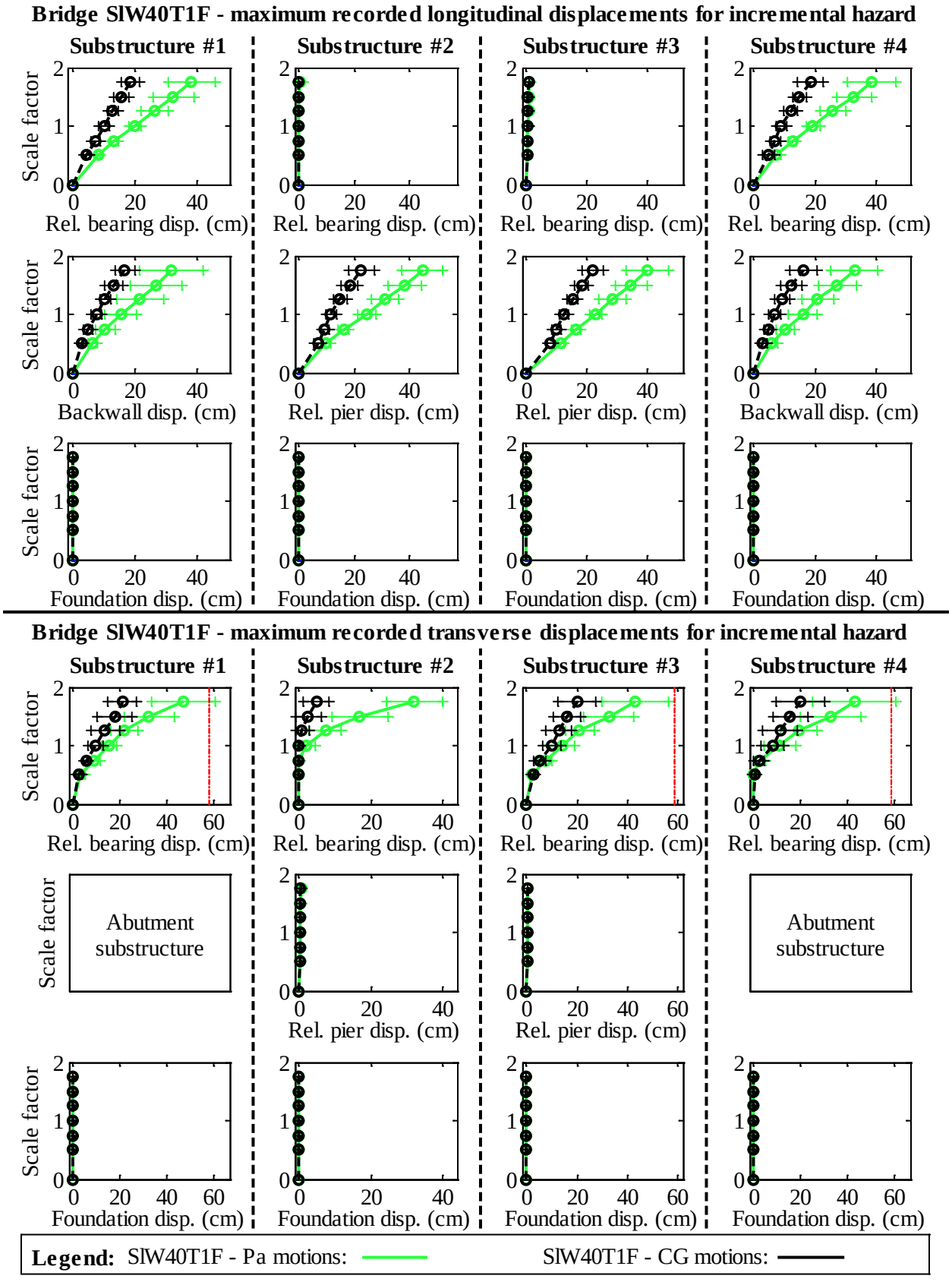

Figure C.127. Bridge SlW40T1F – displacement results.

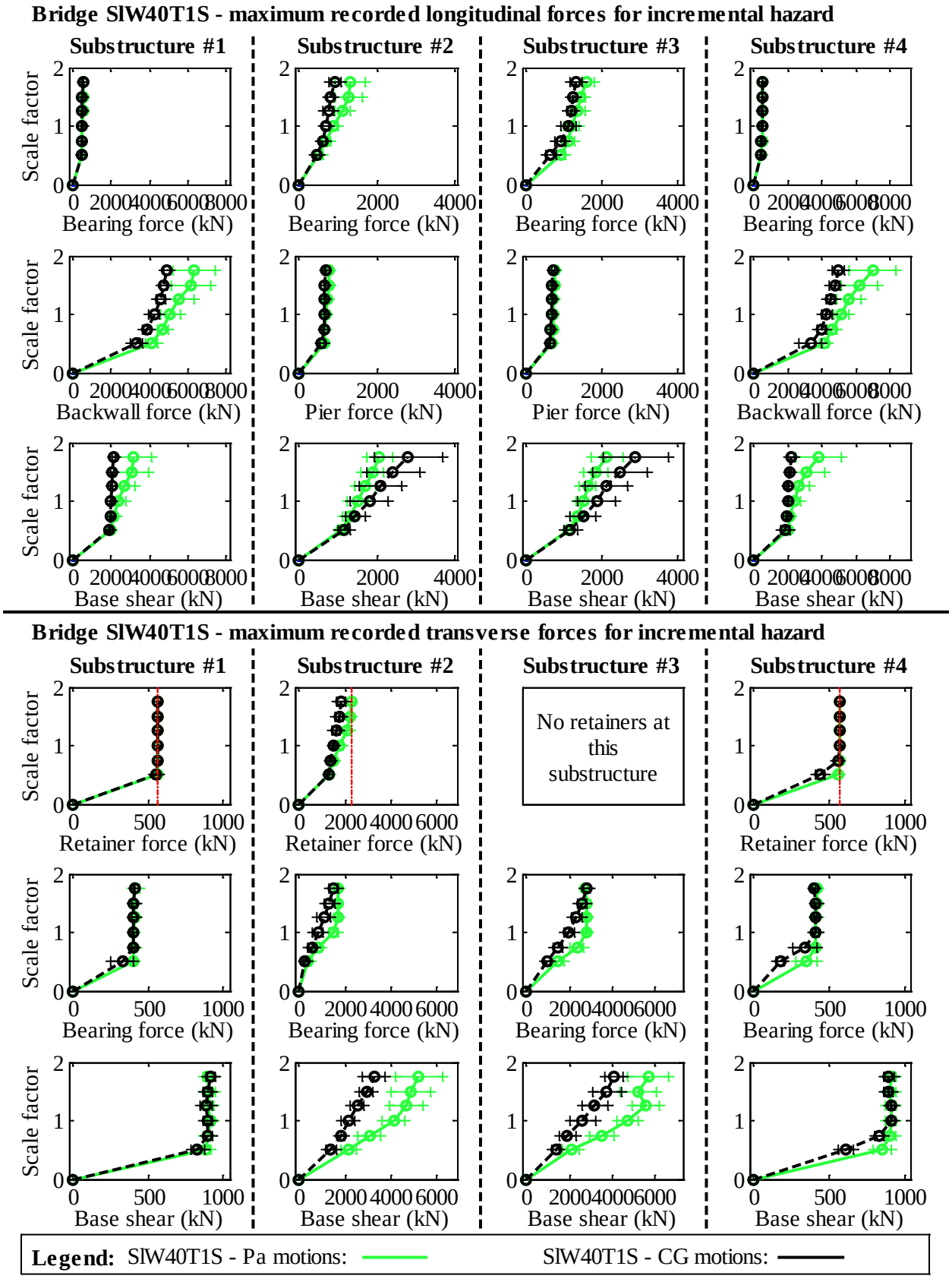

Figure C.128. Bridge SlW40T1S – force results.

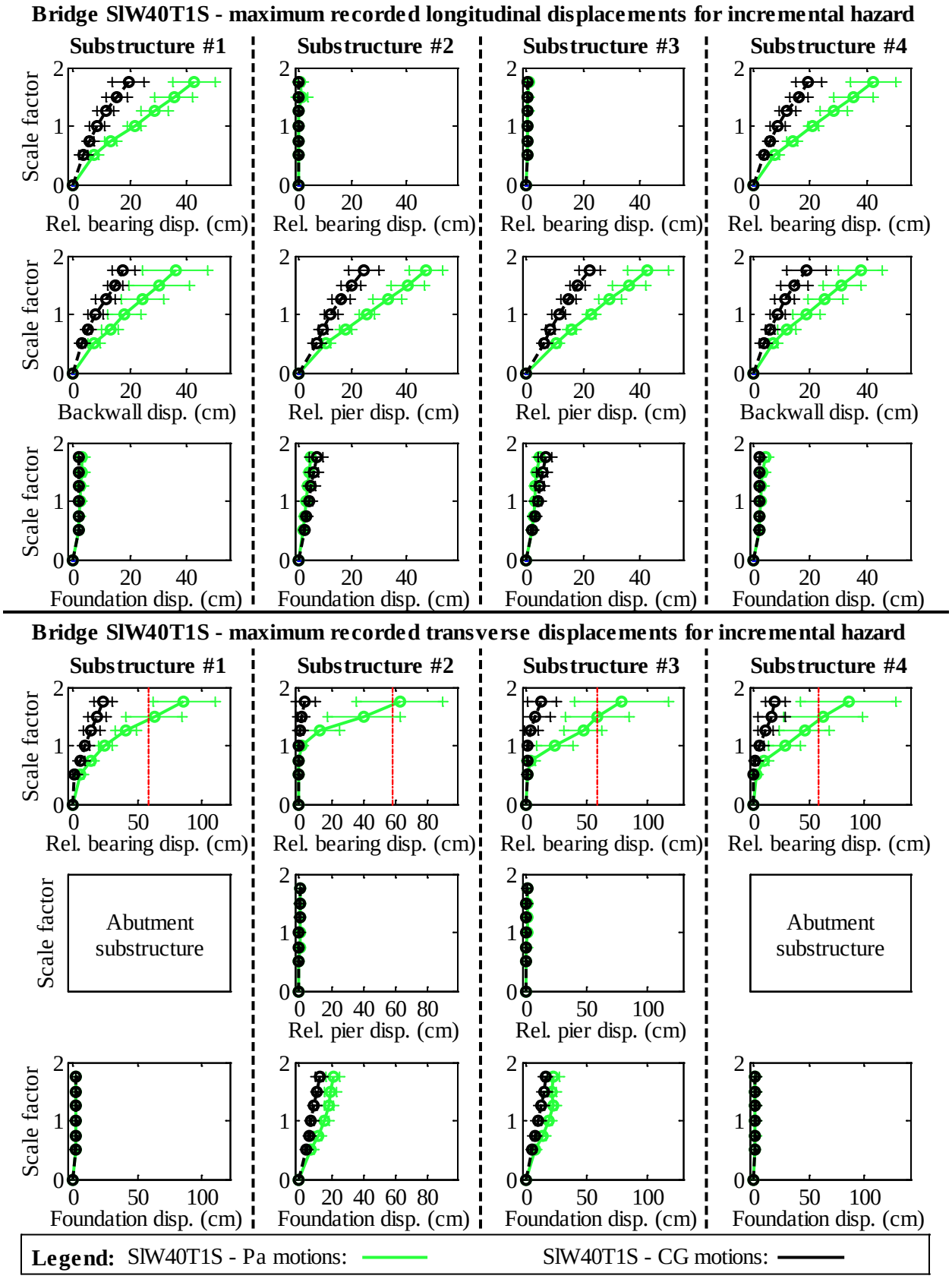

Figure C.129. Bridge SlW40T1S – displacement results.

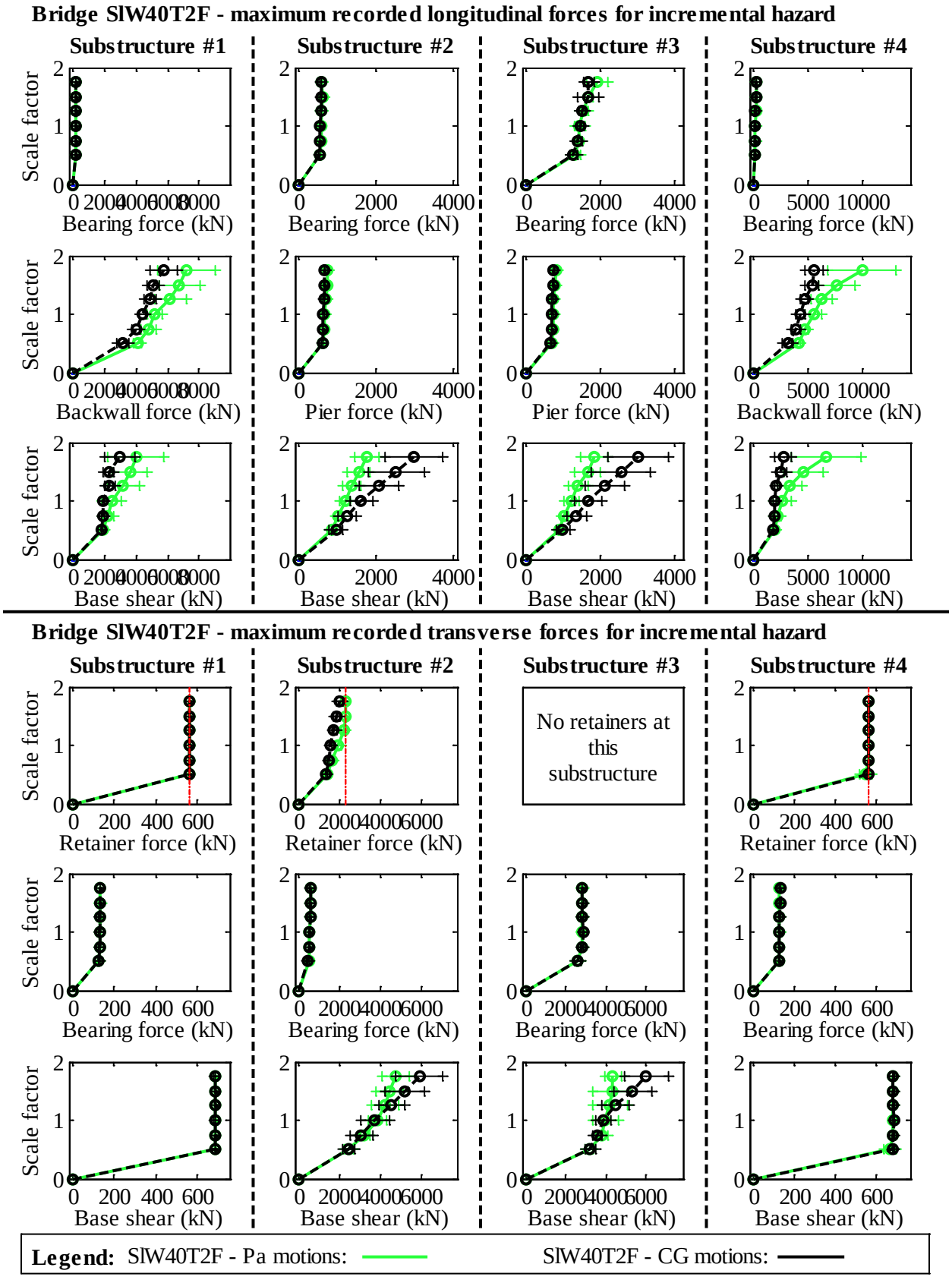

Figure C.130. Bridge SlW40T2F – force results.

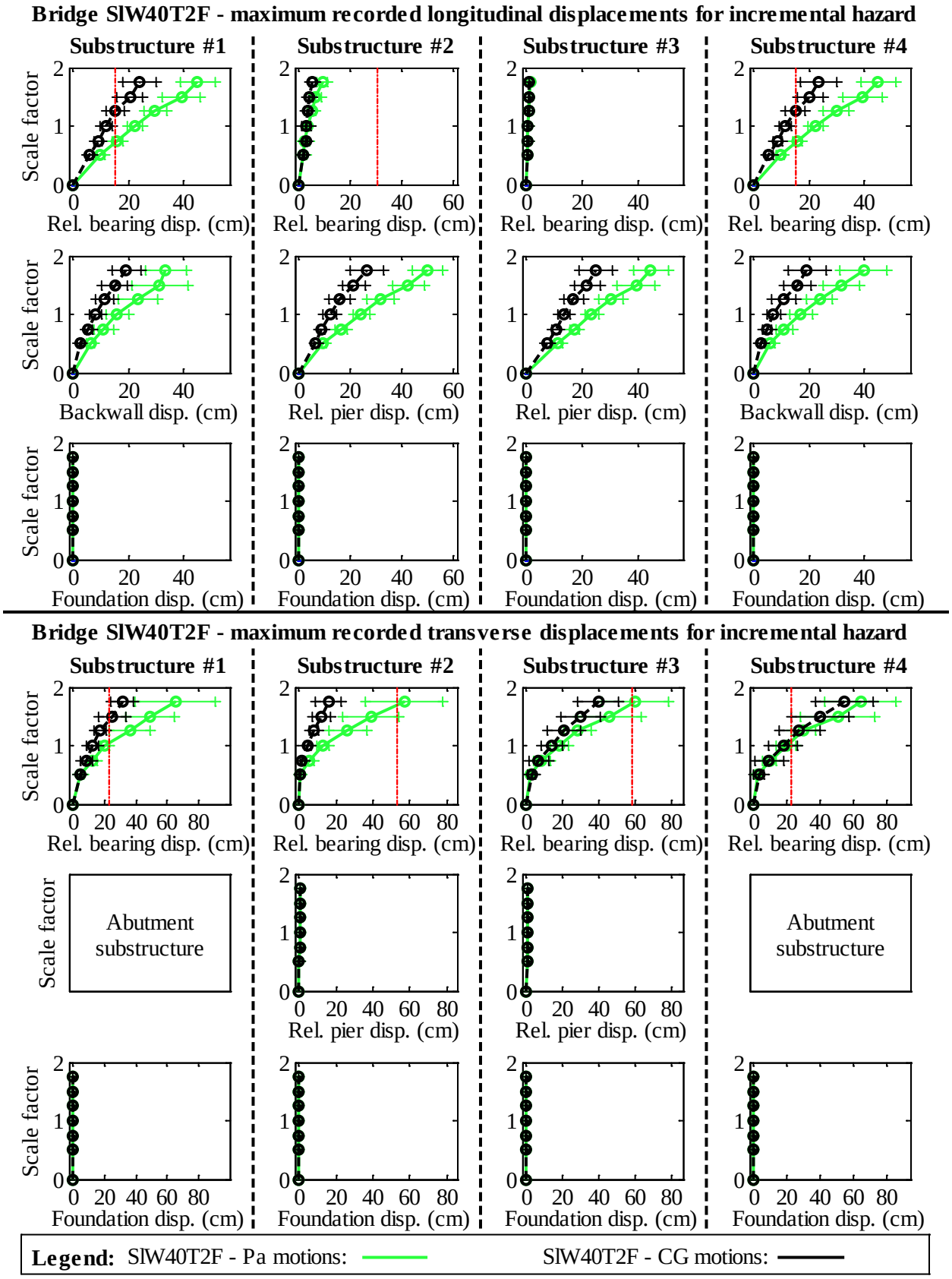

Figure C.131. Bridge SlW40T2F – displacement results.

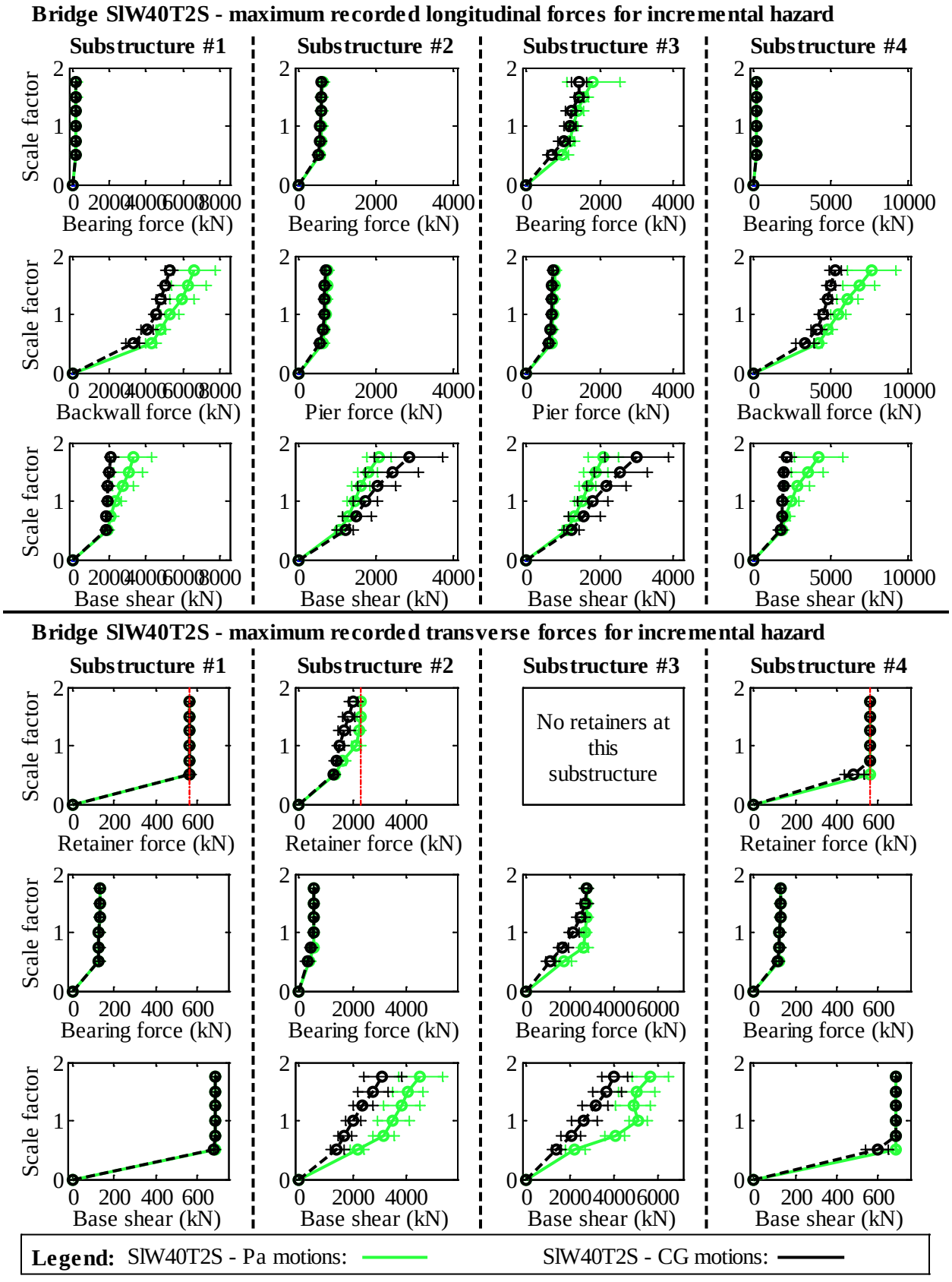

Figure C.132. Bridge SlW40T2S – force results.

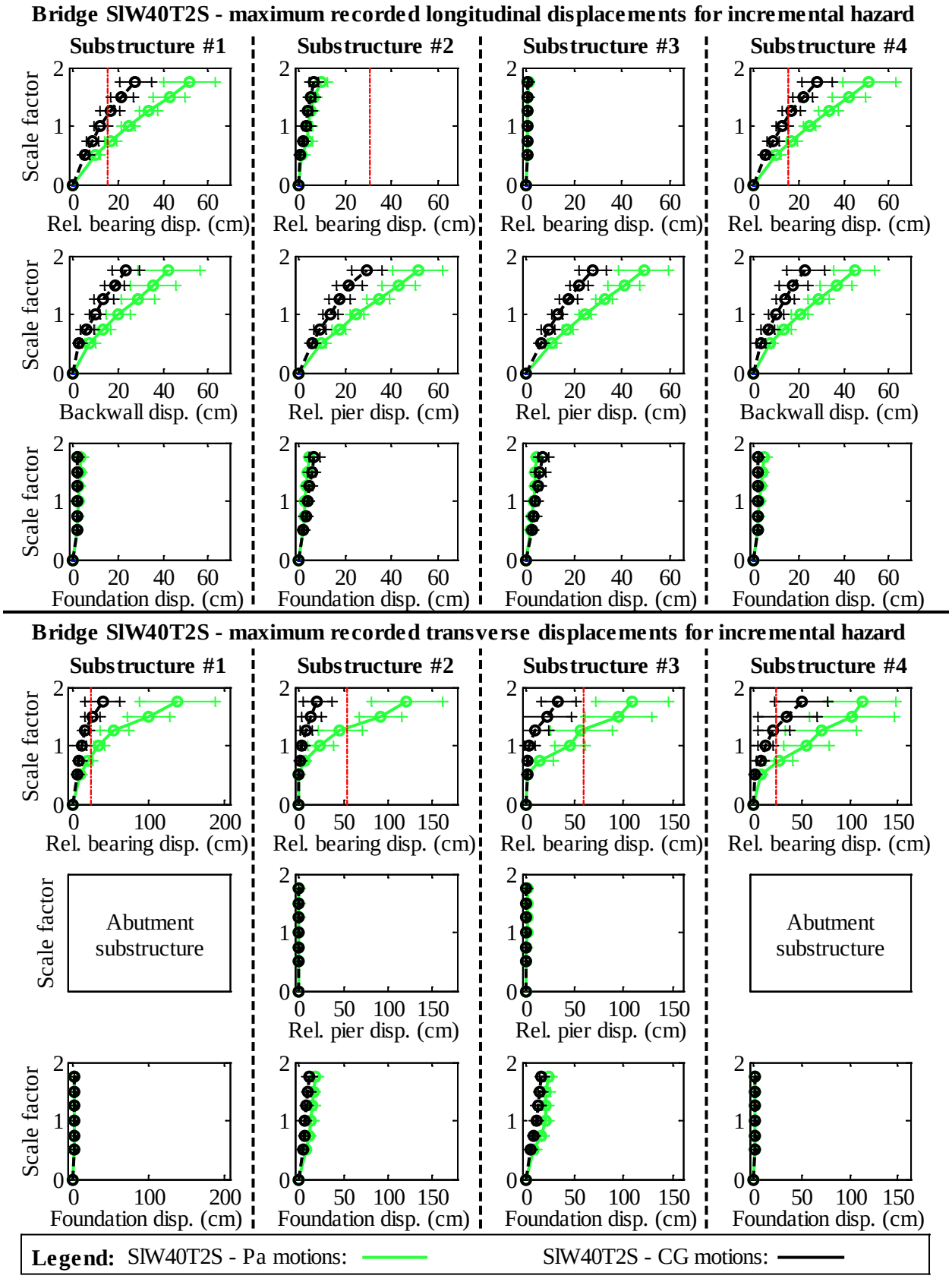

Figure C.133. Bridge SlW40T2S – displacement results.

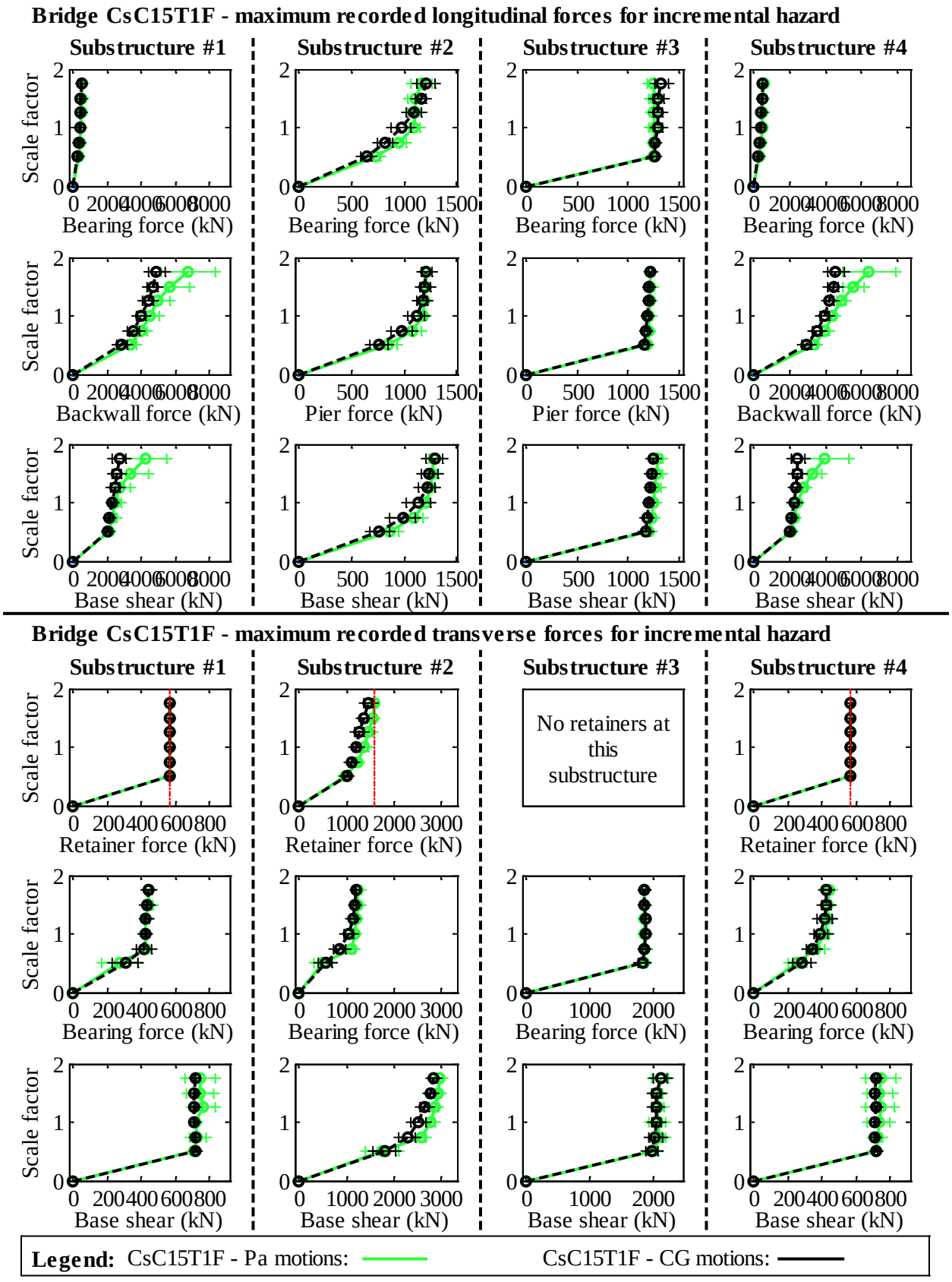

Figure C.134. Bridge CsC15T1F – force results.

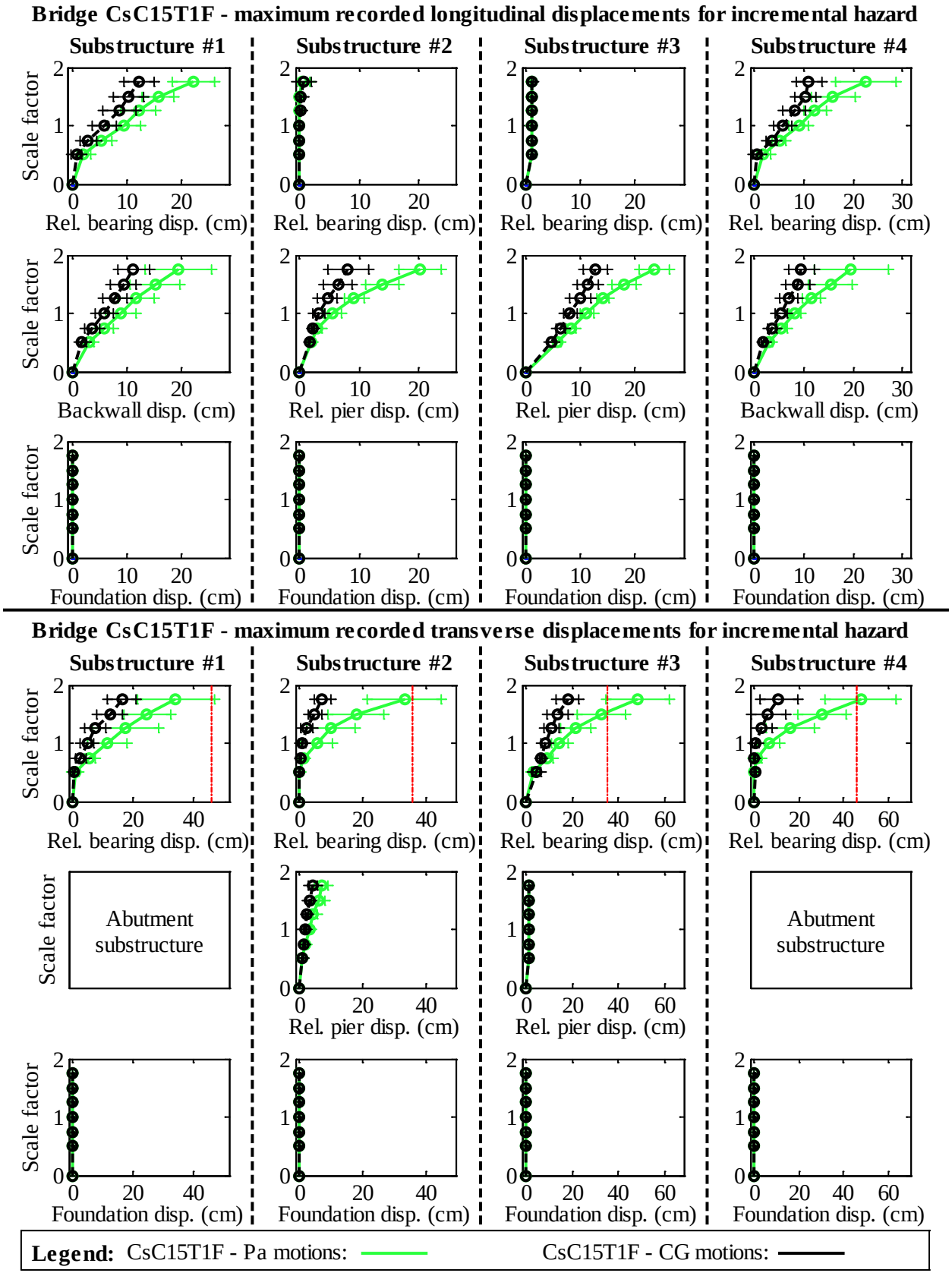

Figure C.135. Bridge CsC15T1F – displacement results.

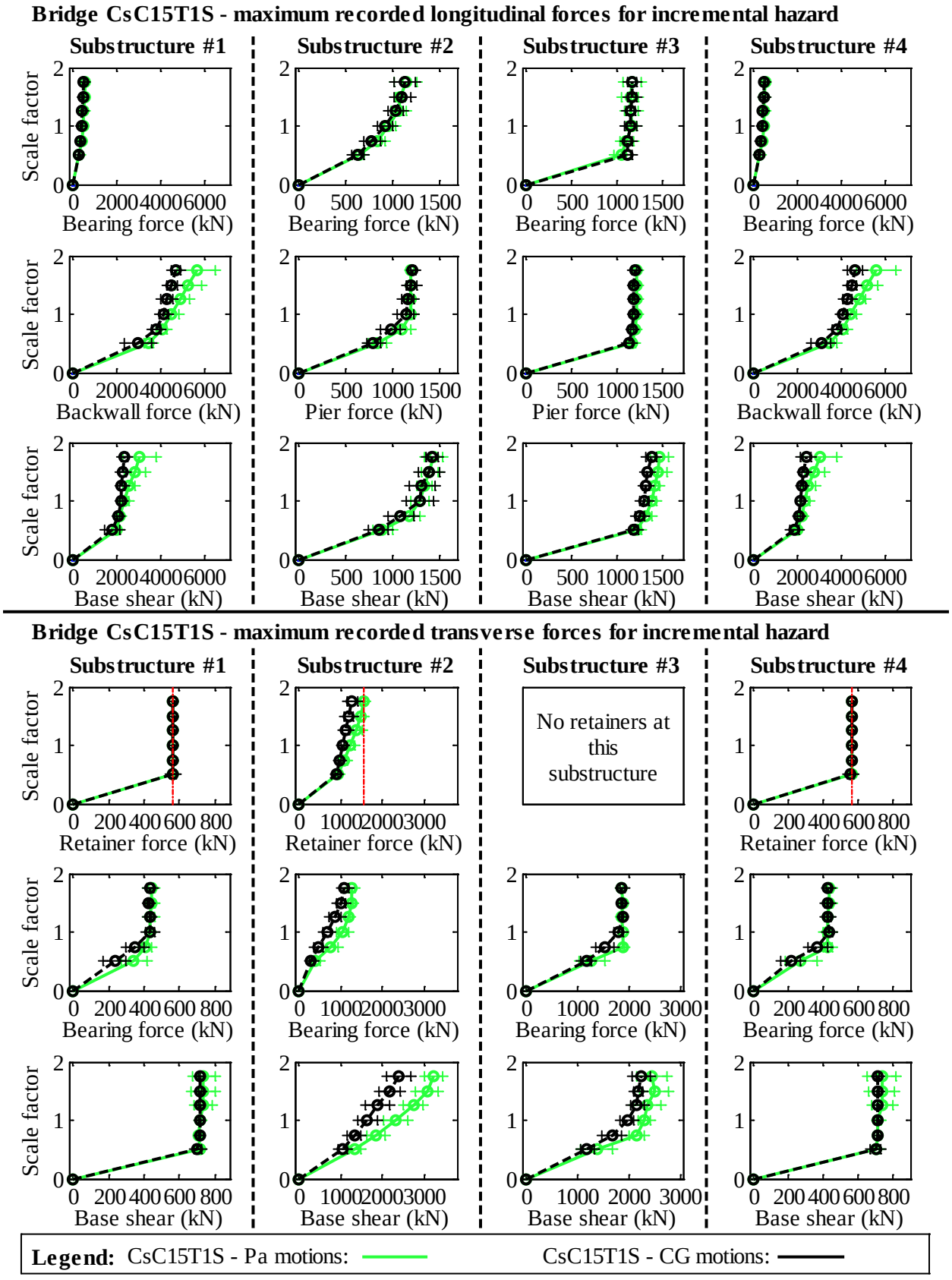

Figure C.136. Bridge CsC15T1S – force results.

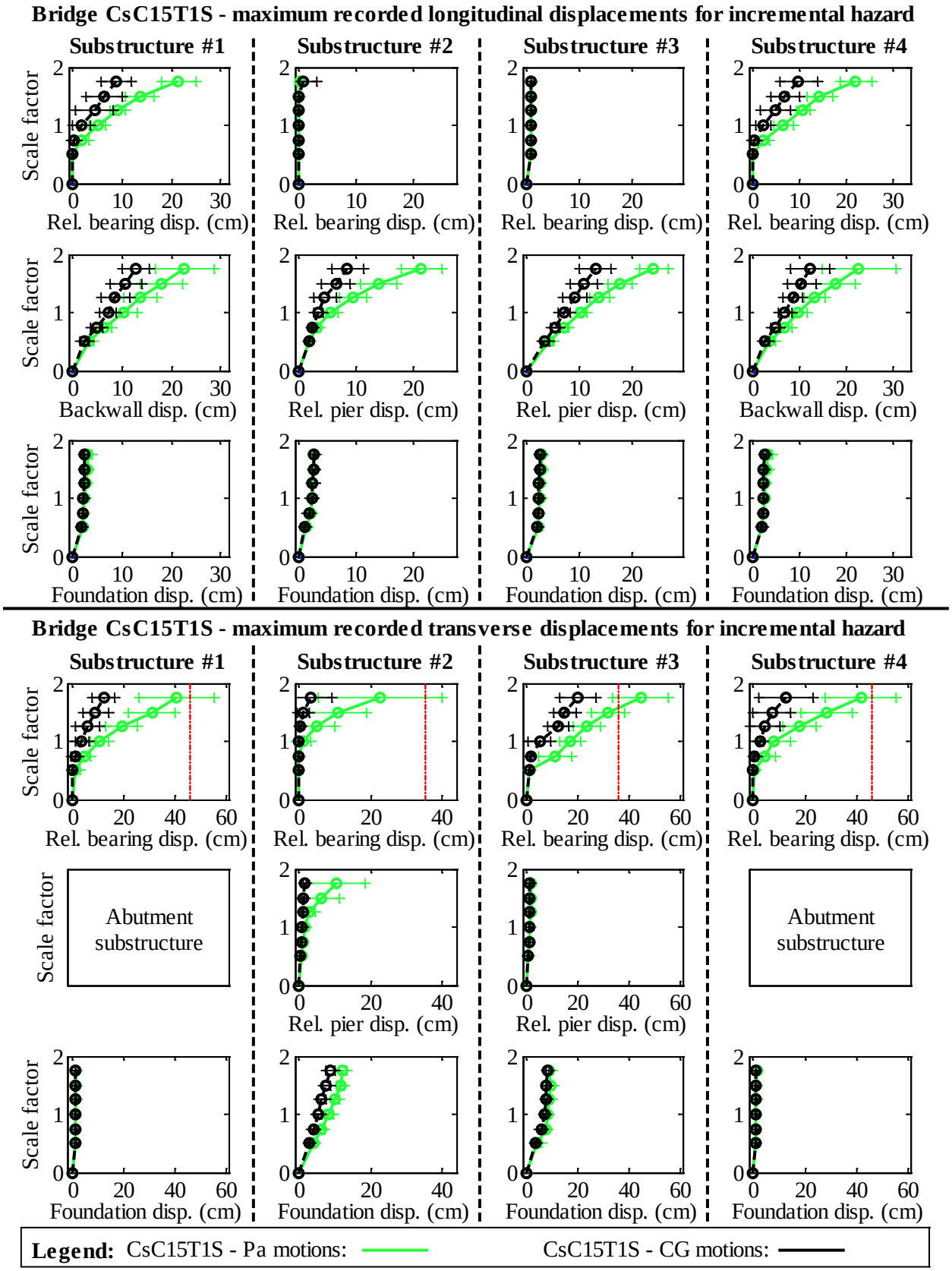

Figure C.137. Bridge CsC15T1S – displacement results.

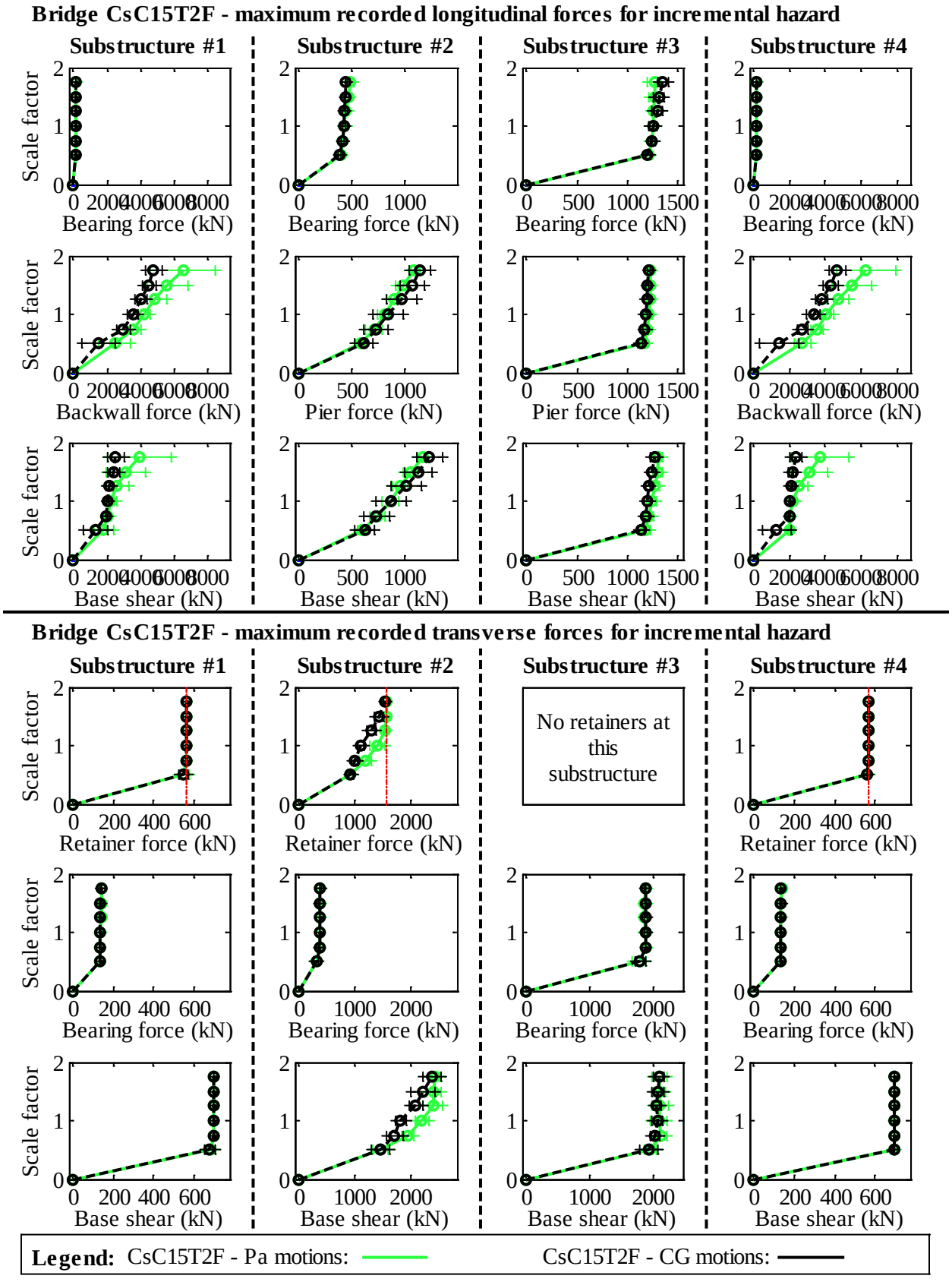

Figure C.138. Bridge CsC15T2F – force results.

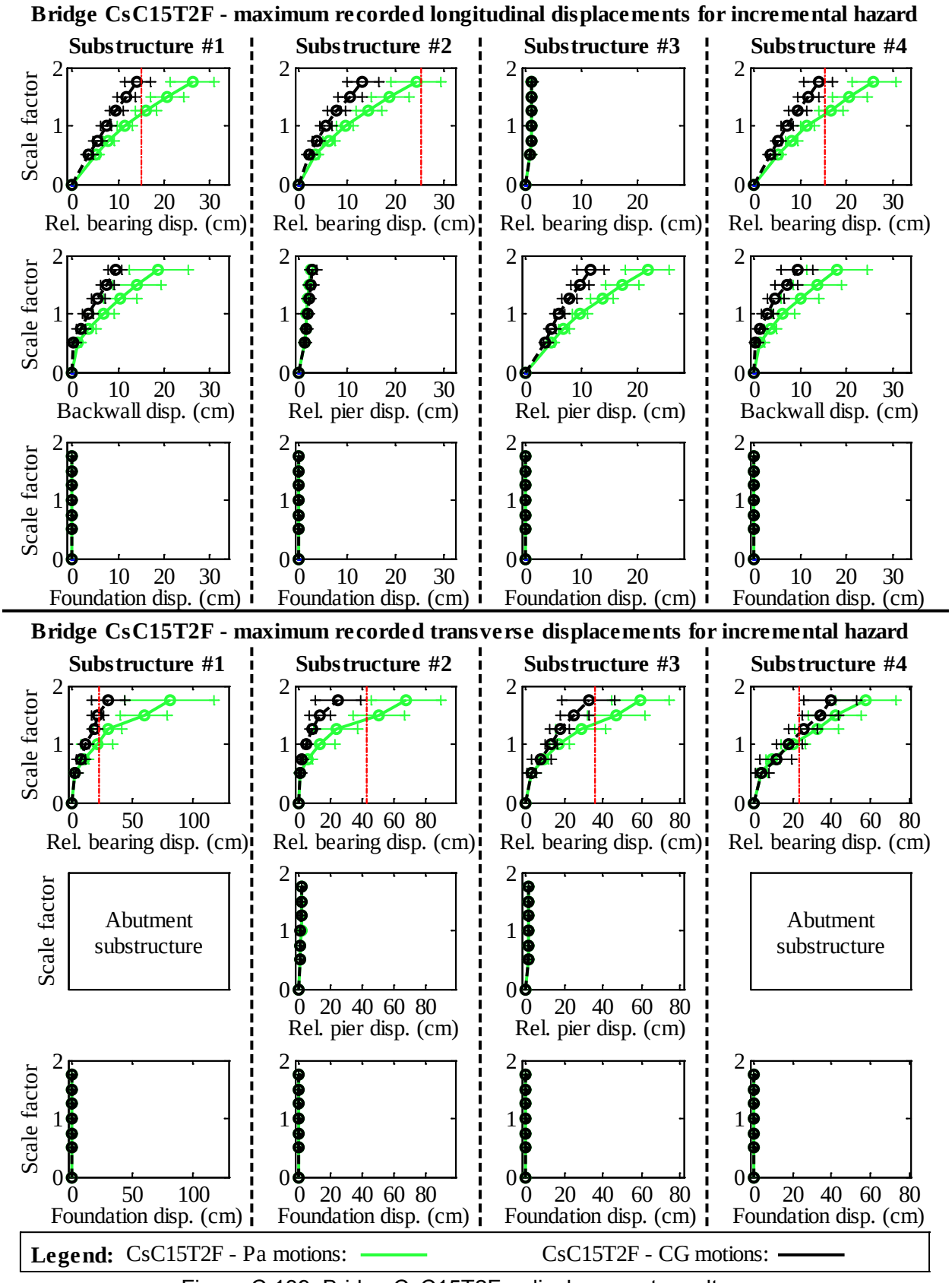

Figure C.139. Bridge CsC15T2F – displacement results.

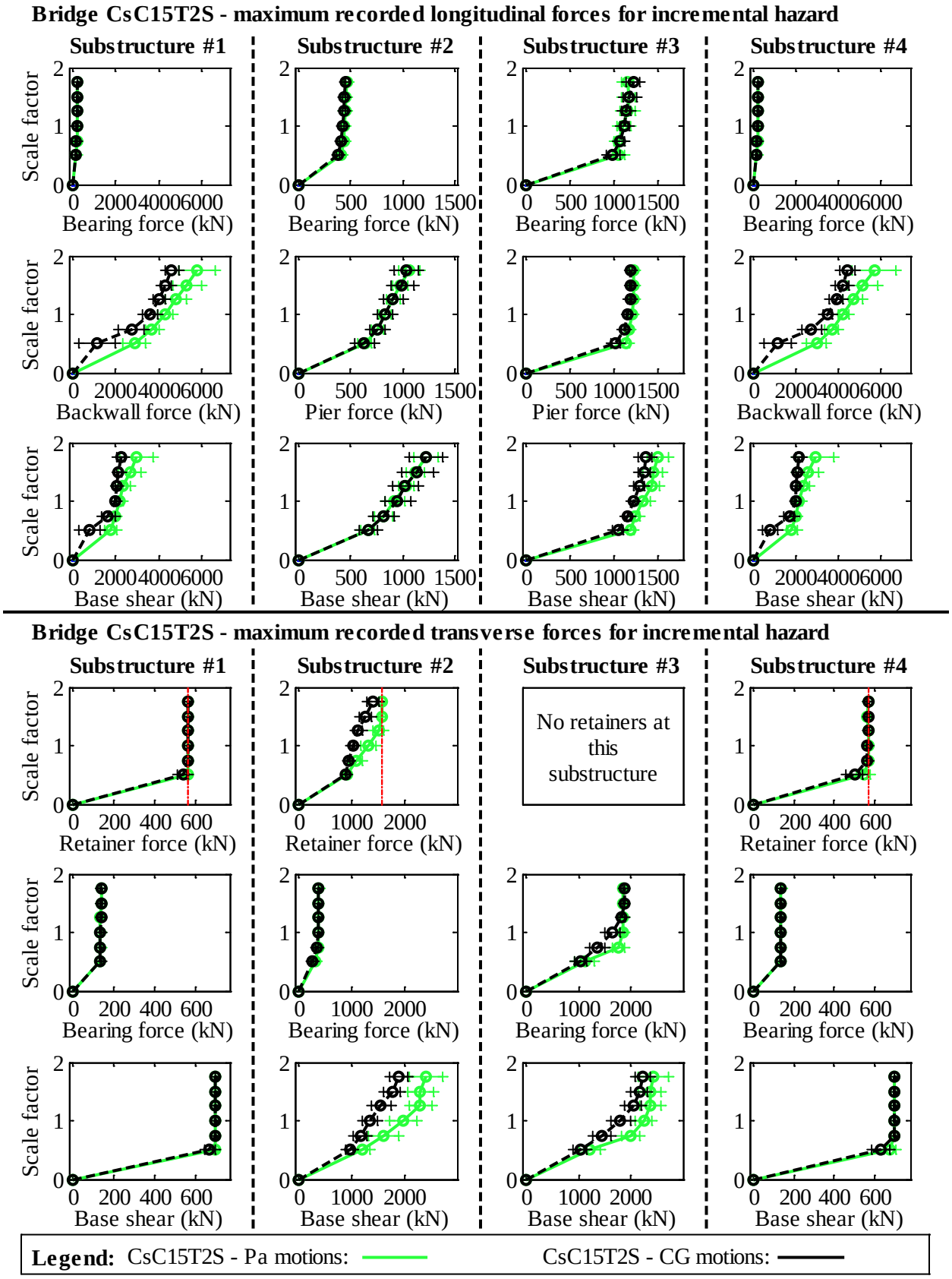

Figure C.140. Bridge CsC15T2S – force results.

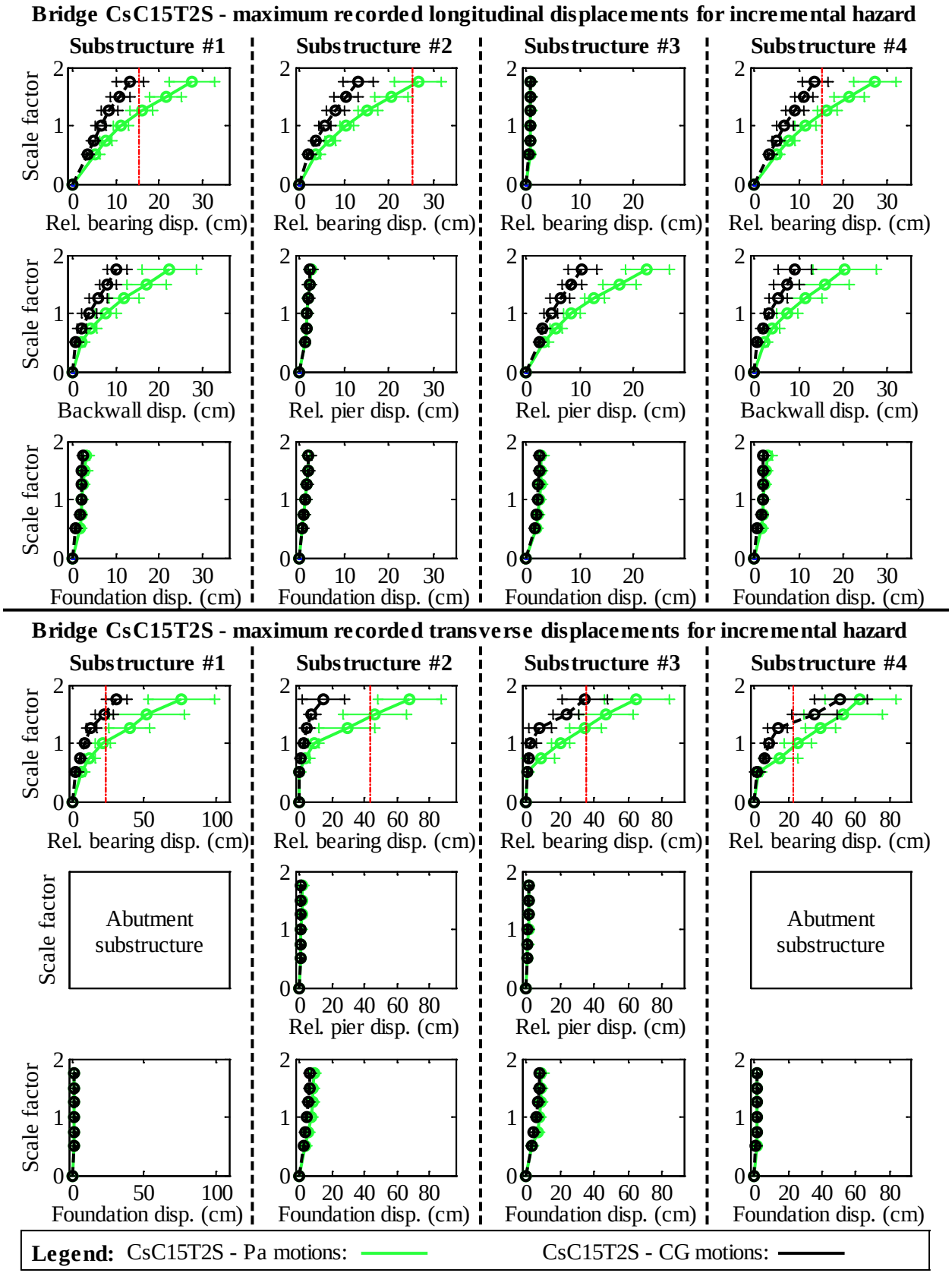

Figure C.141. Bridge CsC15T2S – displacement results.

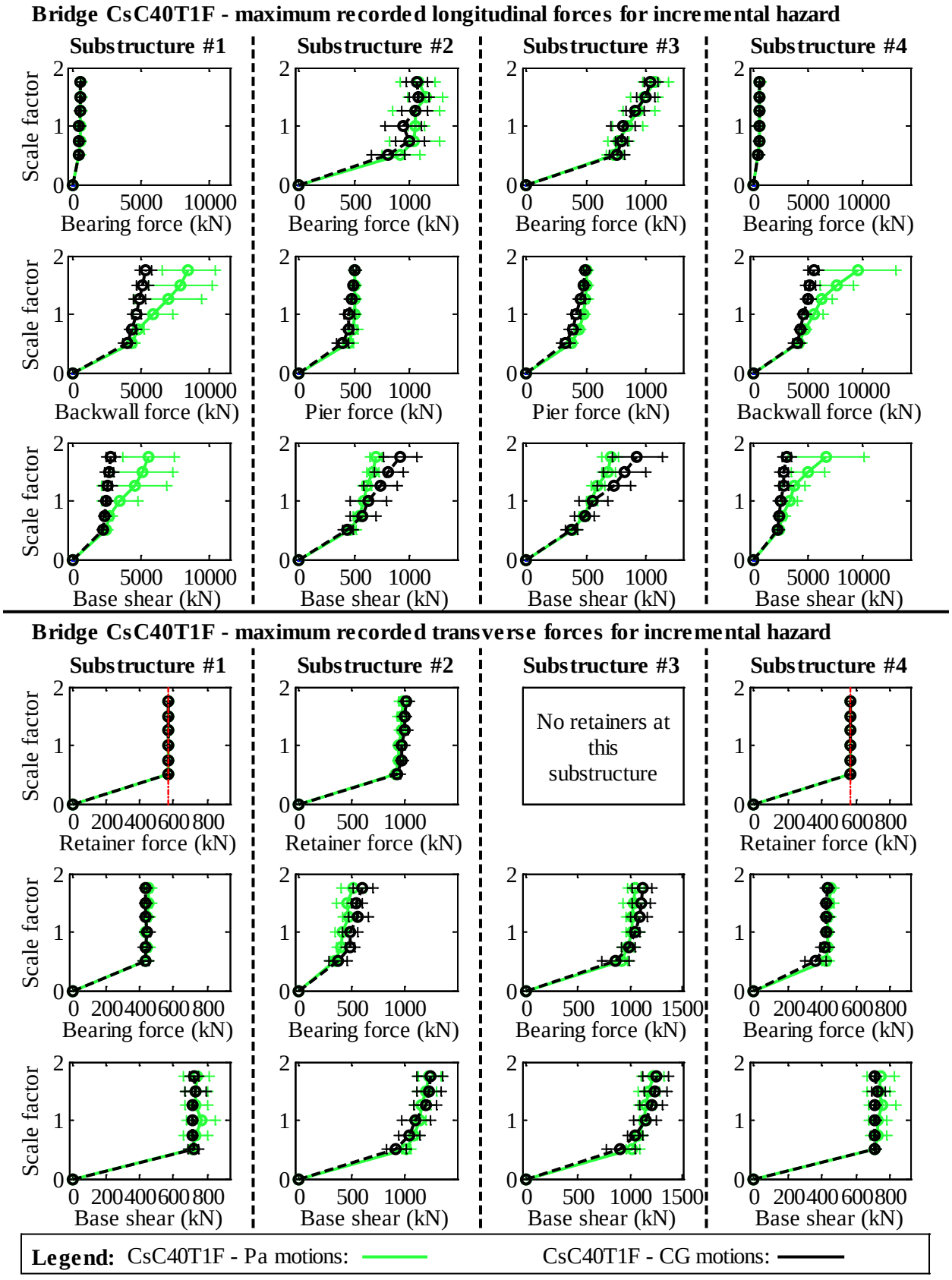

Figure C.142. Bridge CsC40T1F – force results.

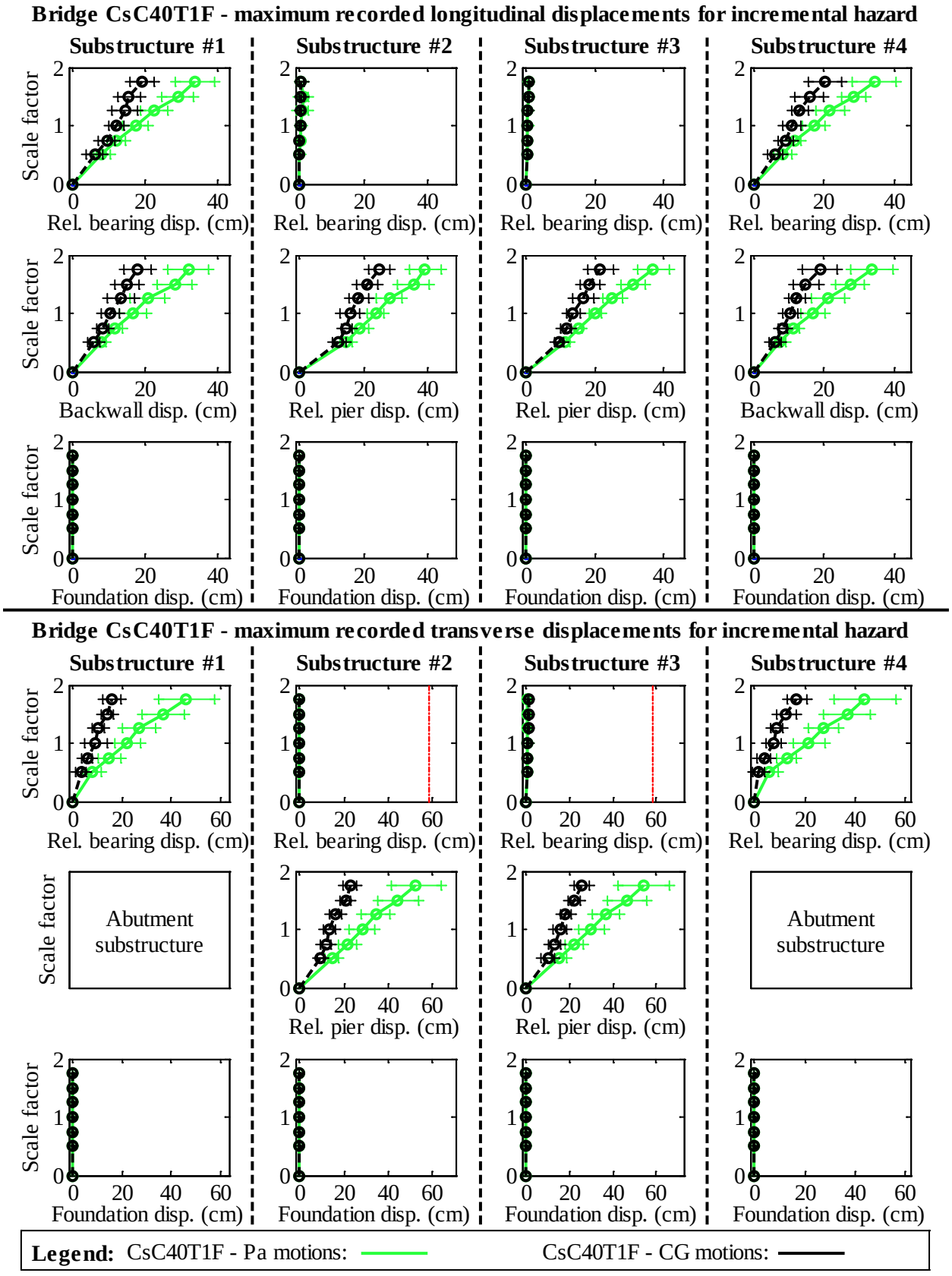

Figure C.143. Bridge CsC40T1F – displacement results.

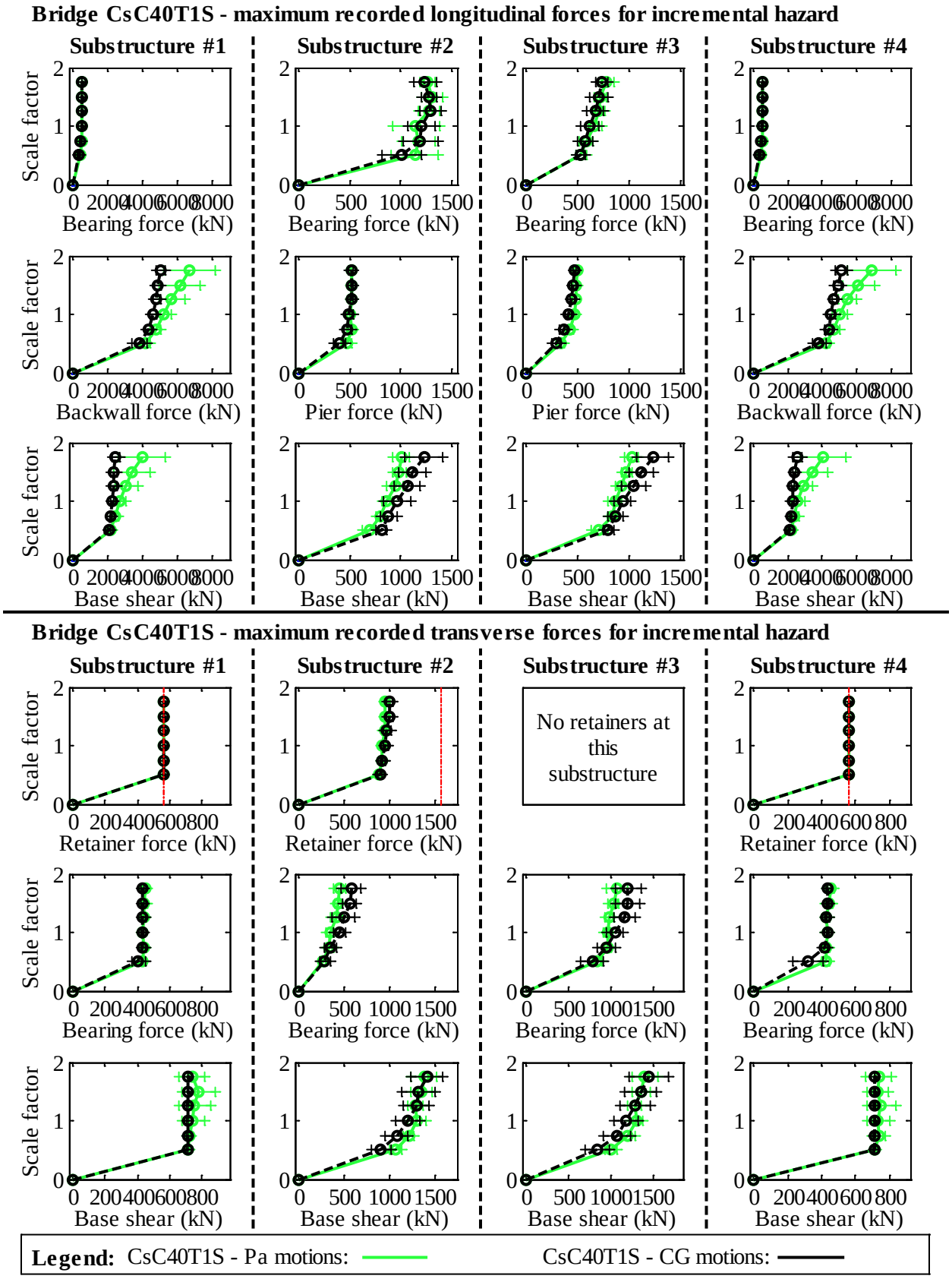

Figure C.144. Bridge CsC40T1S – force results.

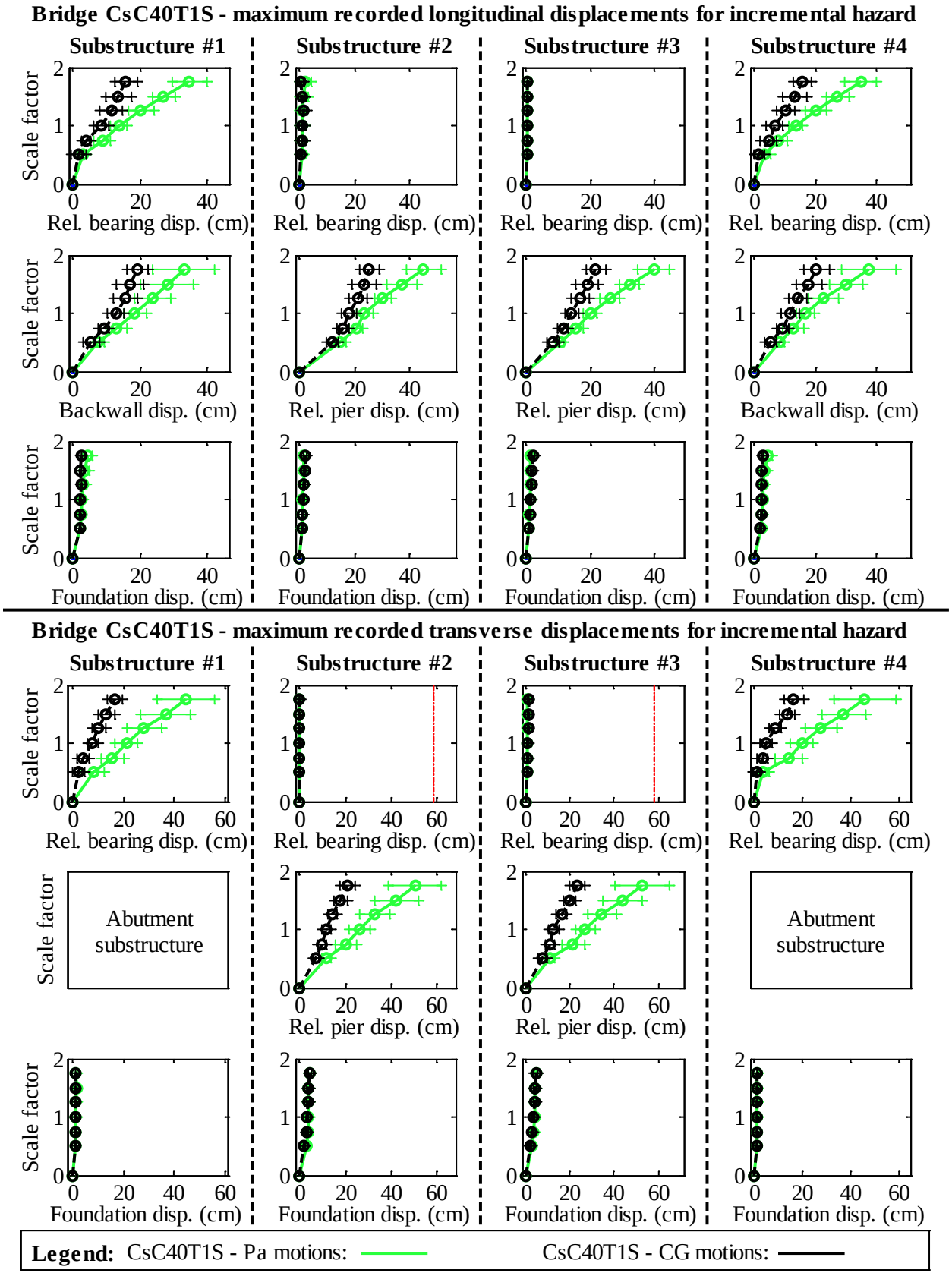

Figure C.145. Bridge CsC40T1S – displacement results.

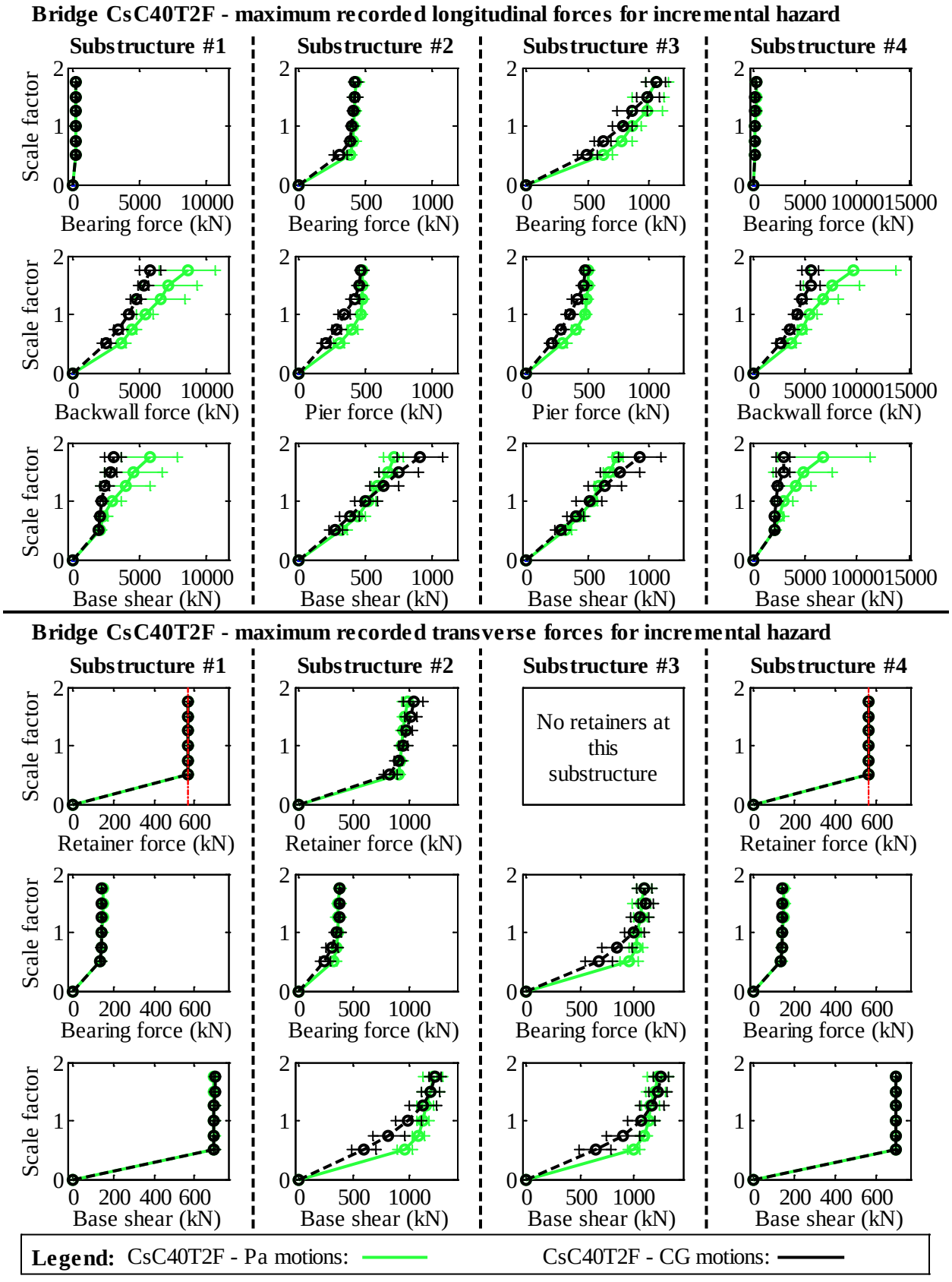

Figure C.146. Bridge CsC40T2F – force results.

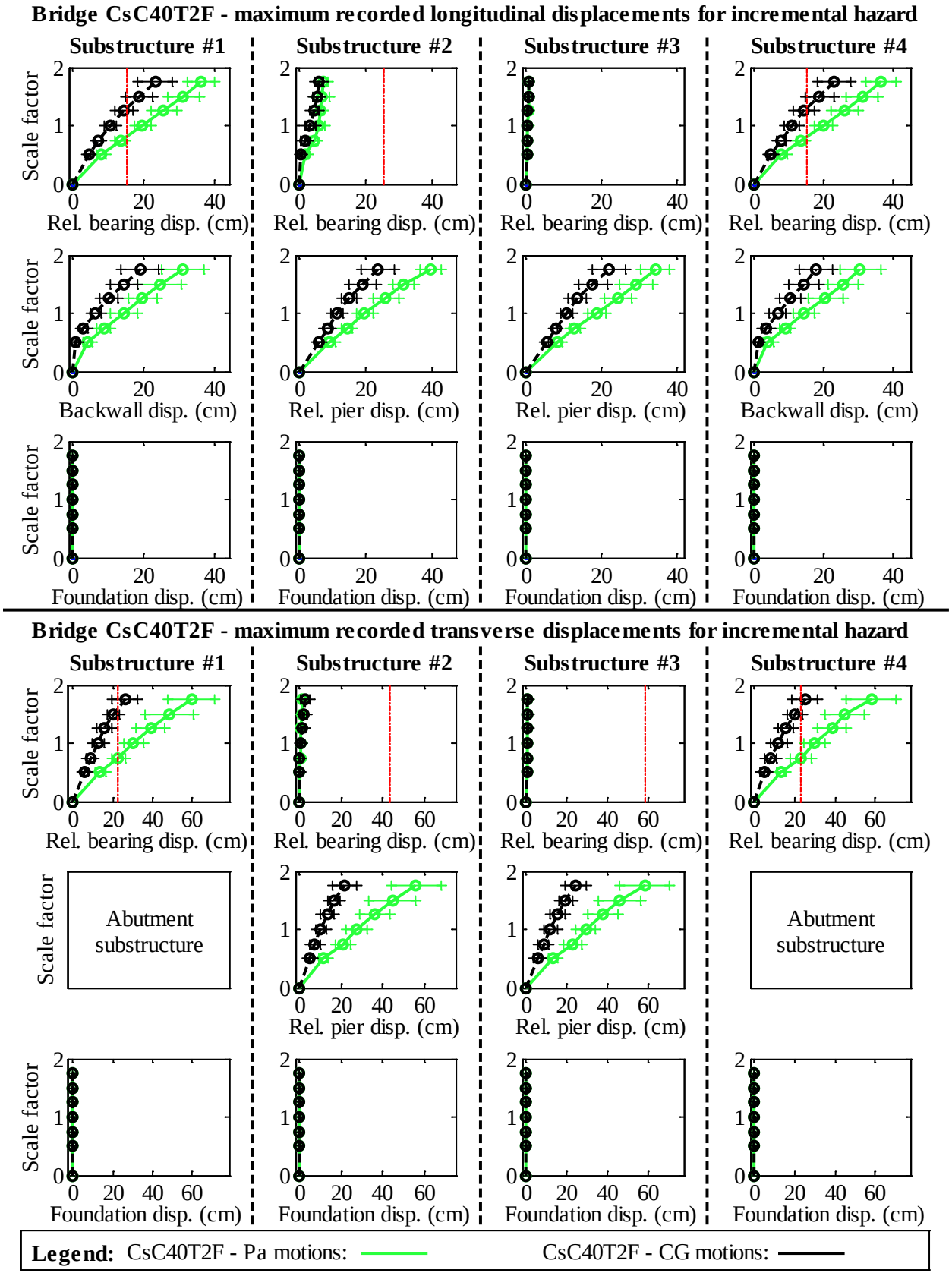

Figure C.147. Bridge CsC40T2F – displacement results.

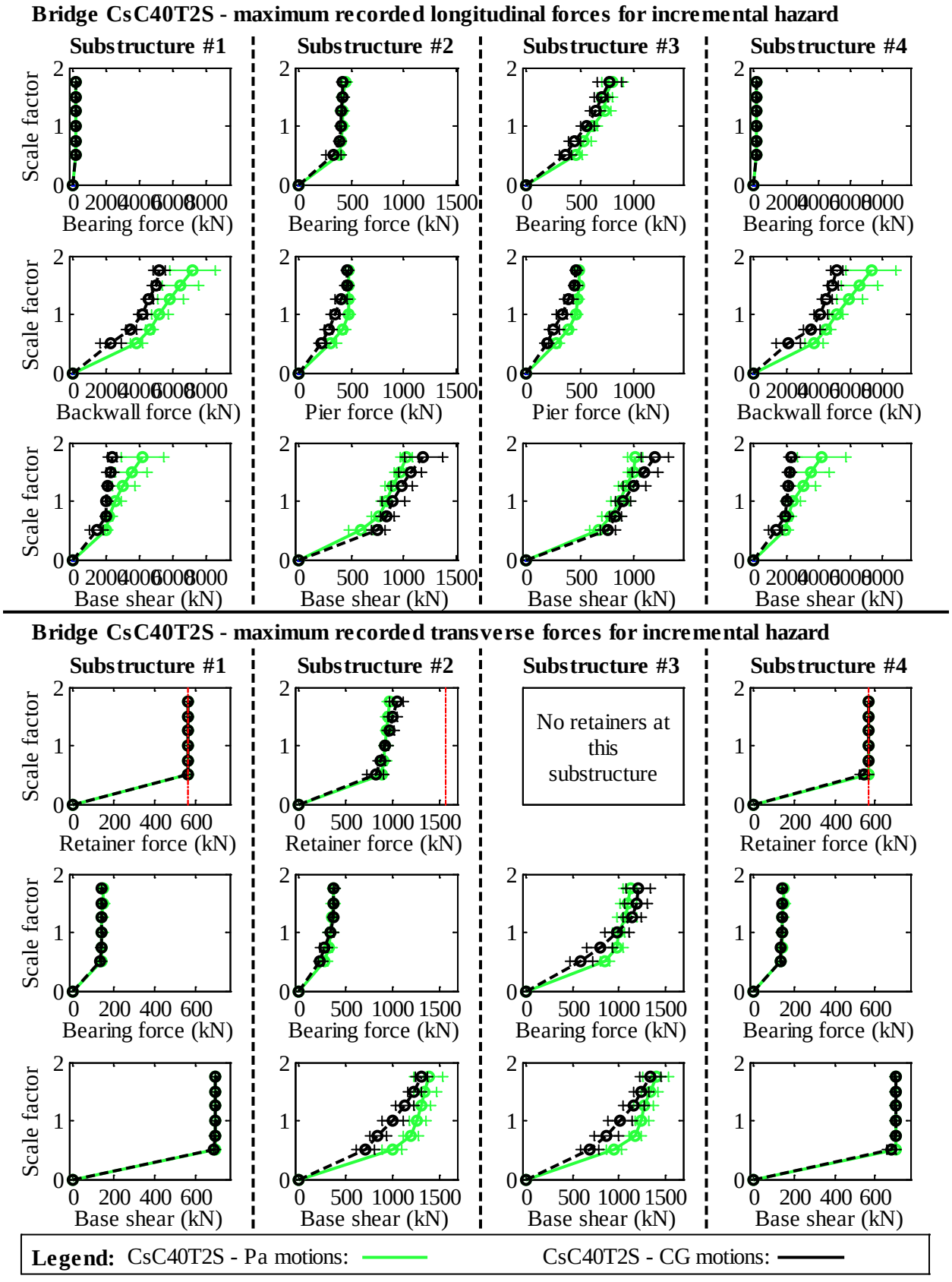

Figure C.148. Bridge CsC40T2S – force results.

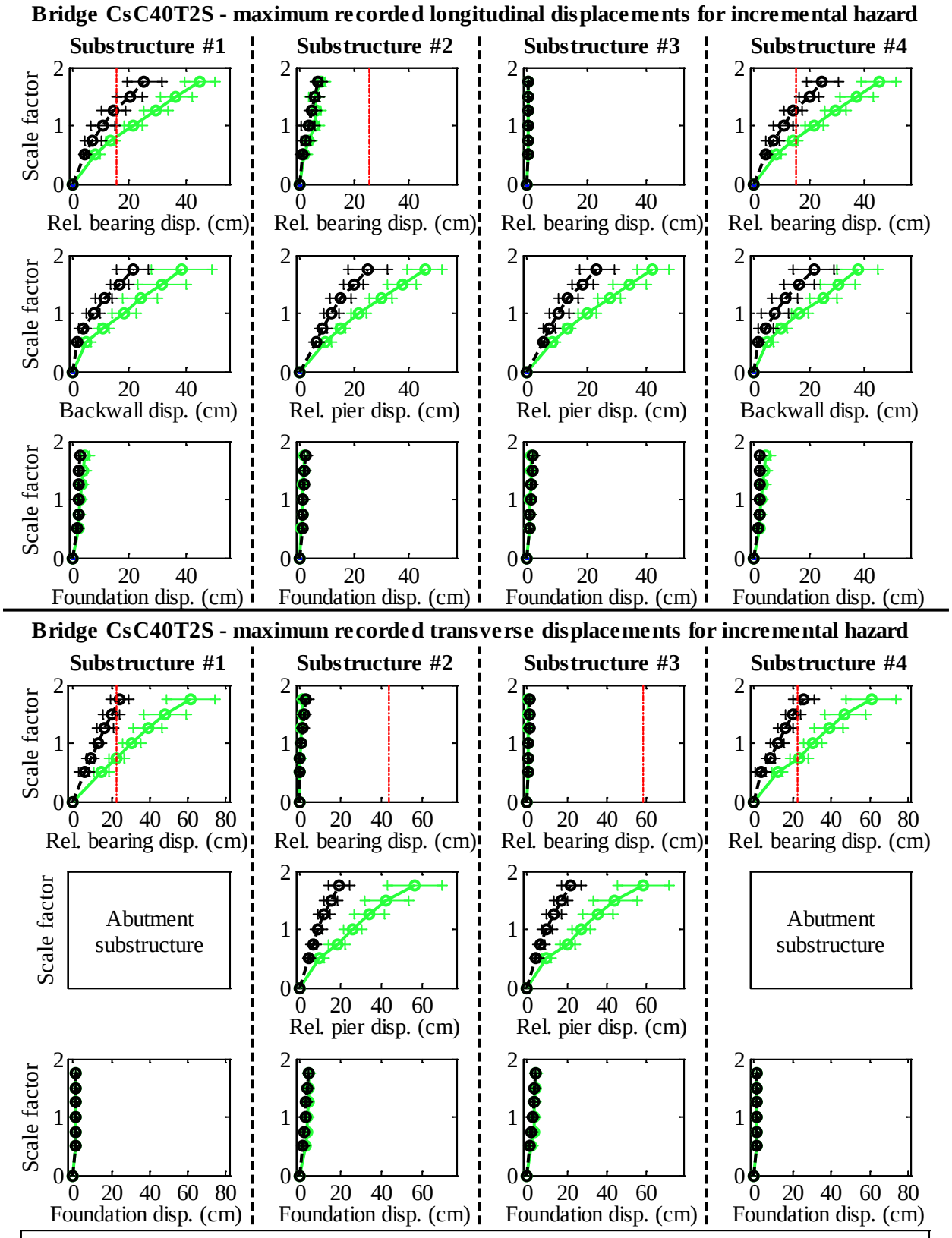

Figure C.149. Bridge CsC40T2S – displacement results.

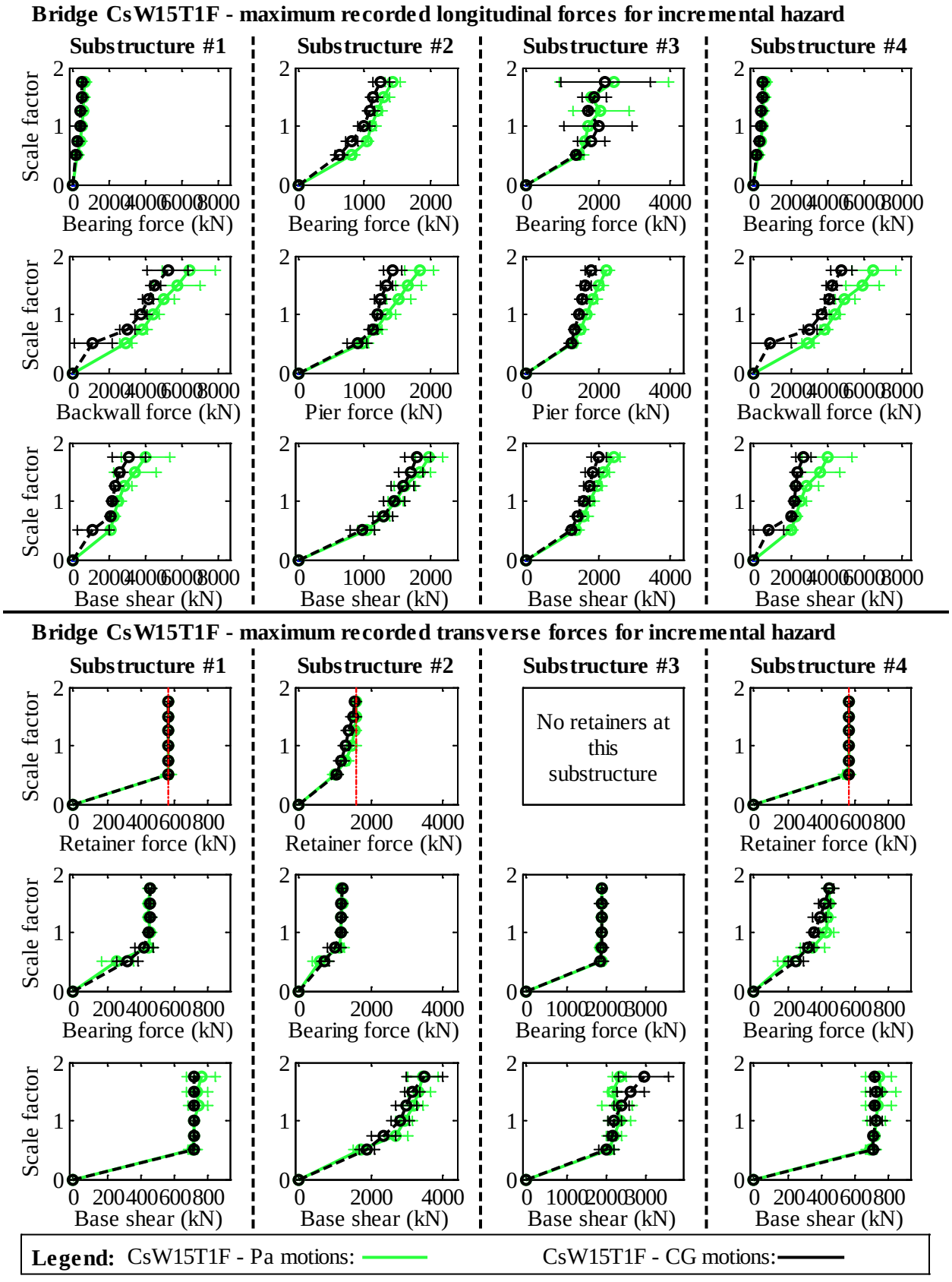

Figure C.150. Bridge CsW15T1F – force results.

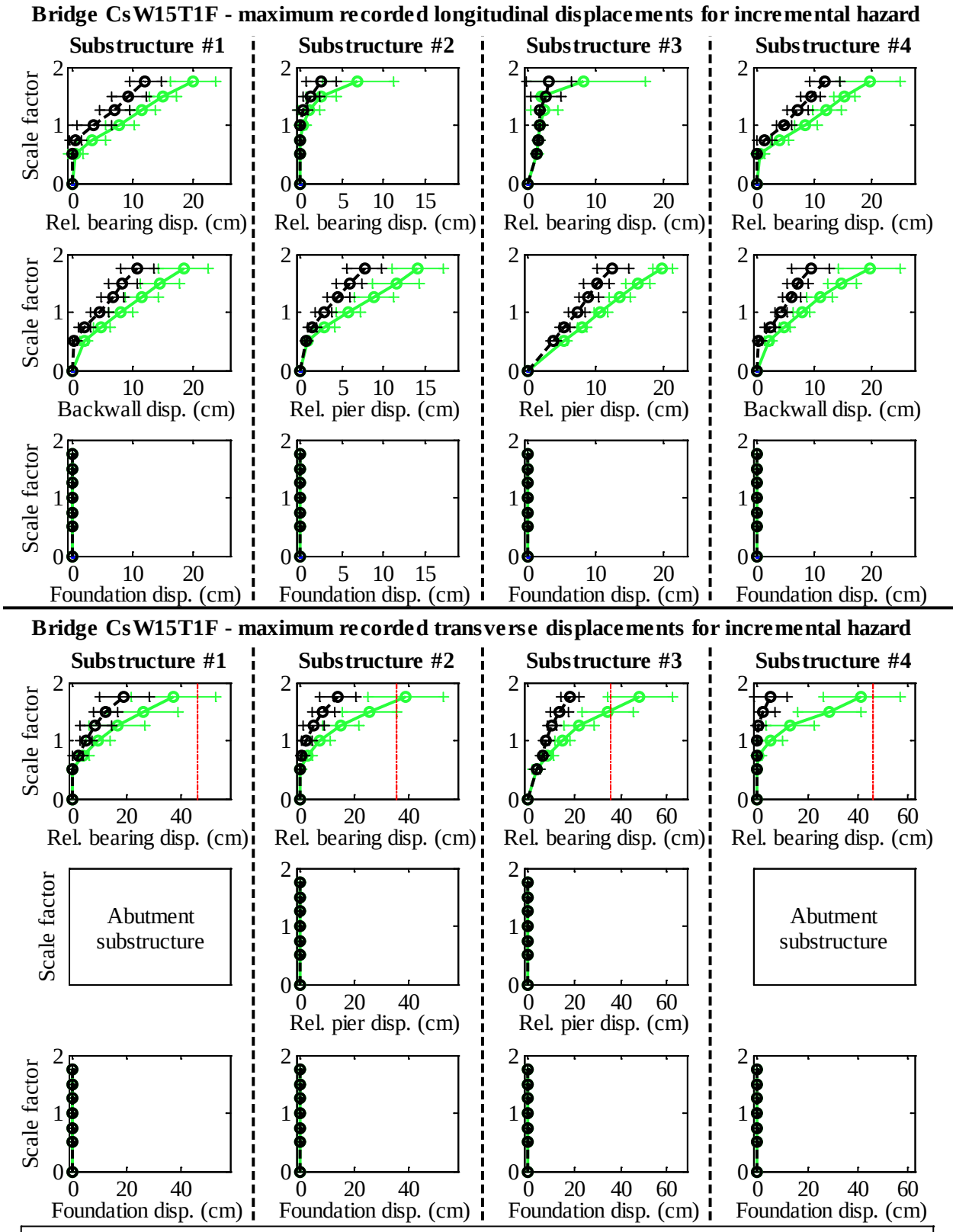

Figure C.151. Bridge CsW15T1F – displacement results.

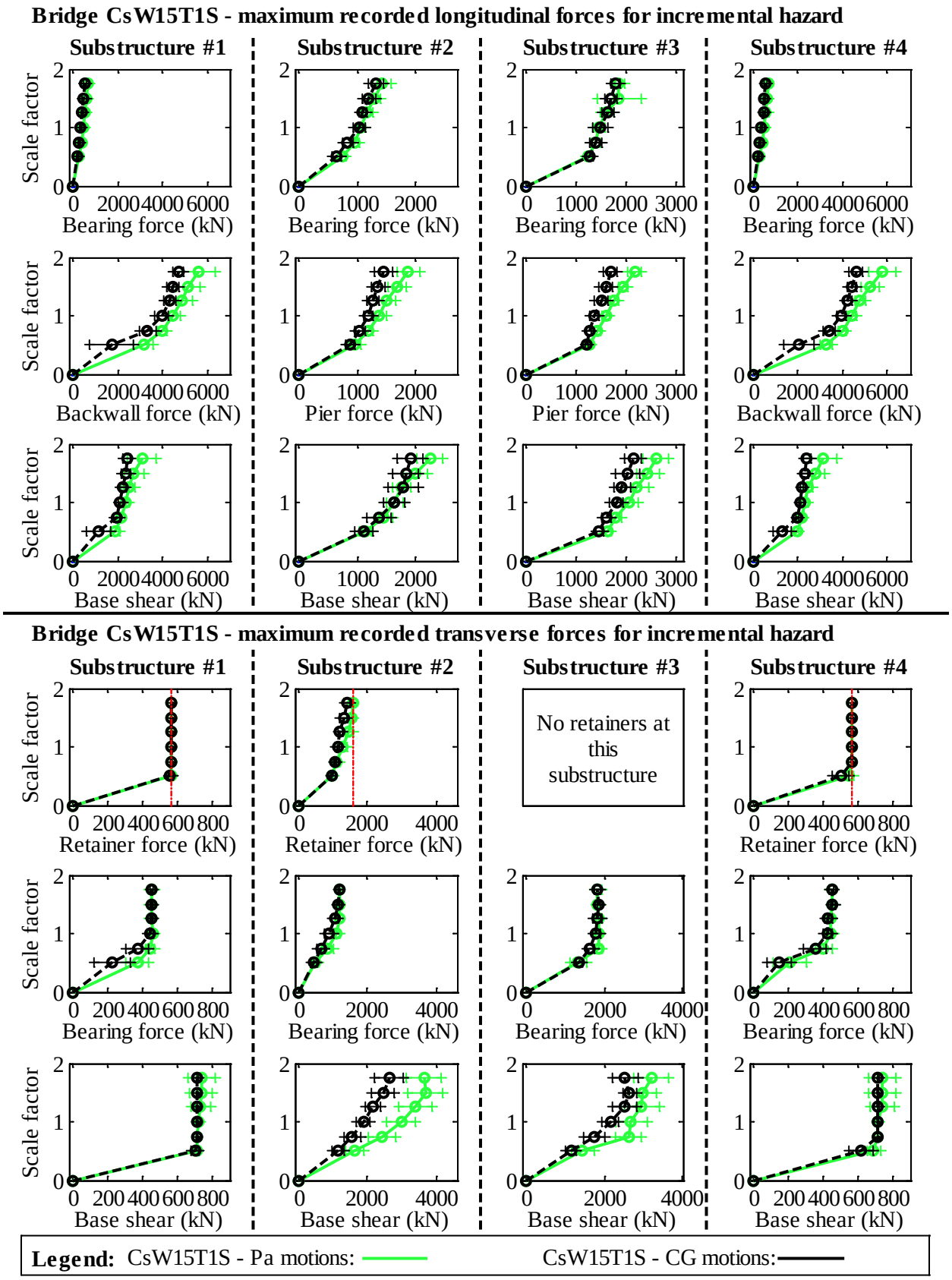

Figure C.152. Bridge CsW15T1S – force results.

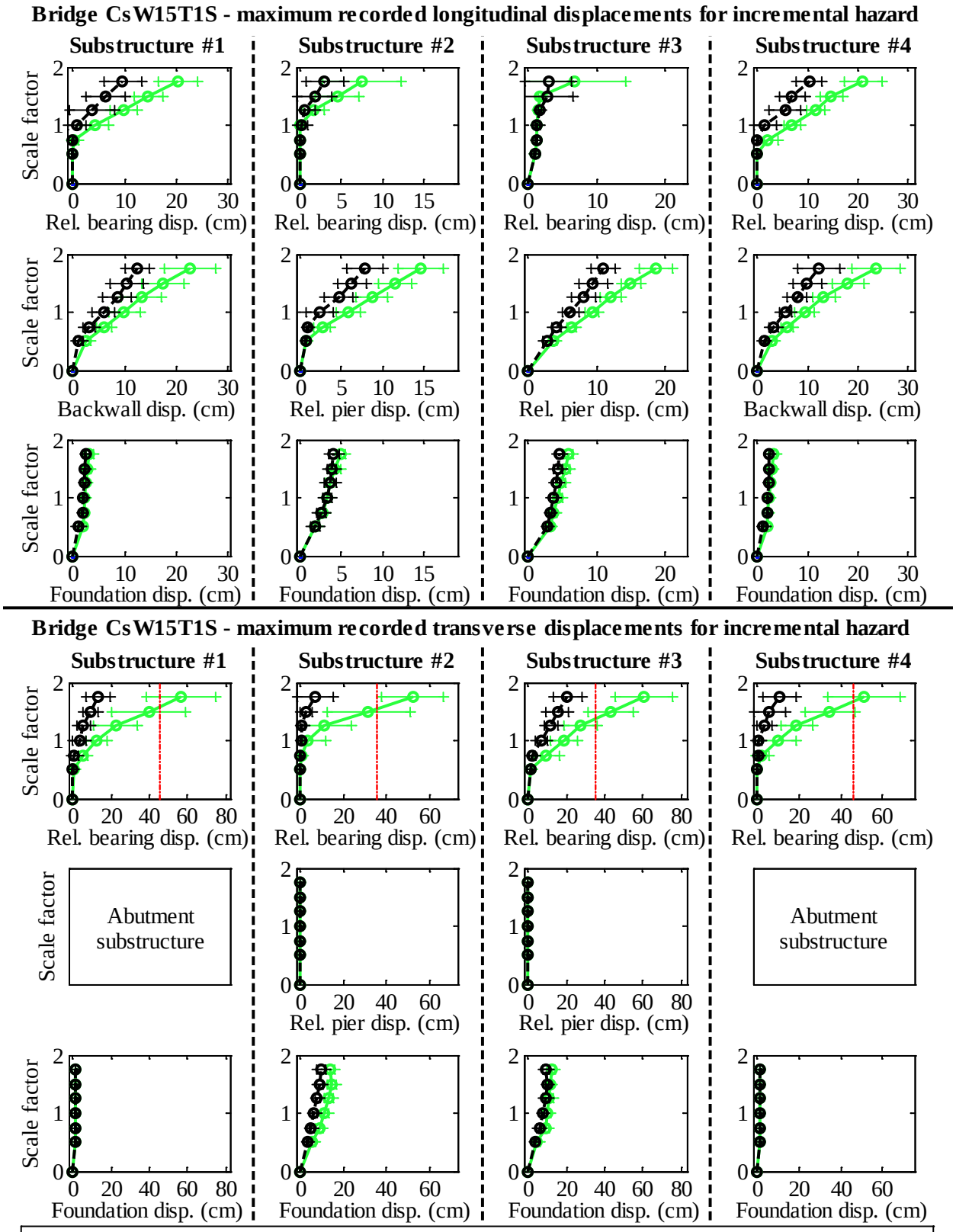

Figure C.153. Bridge CsW15T1S – displacement results.

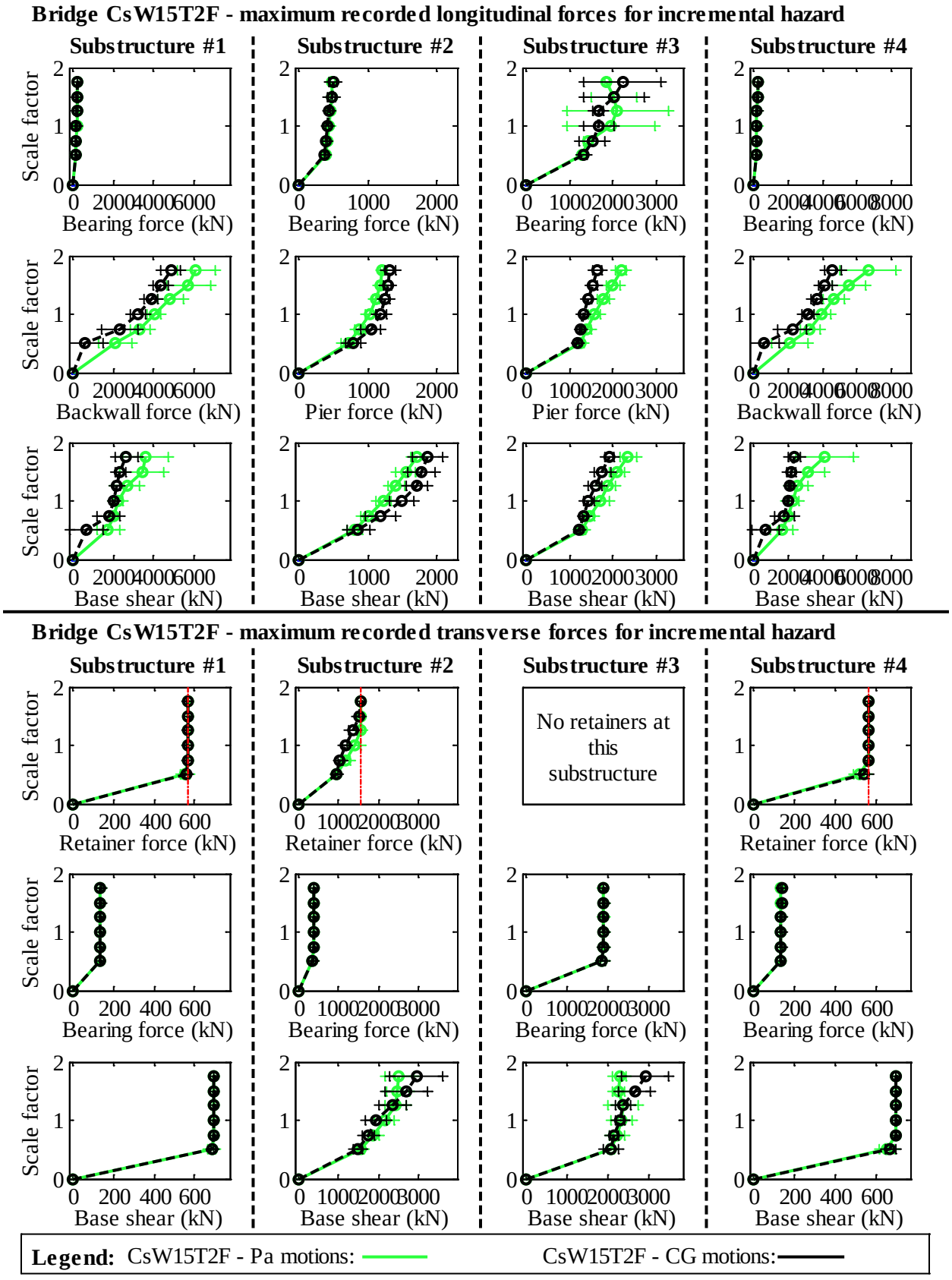

Figure C.154. Bridge CsW15T2F – force results.

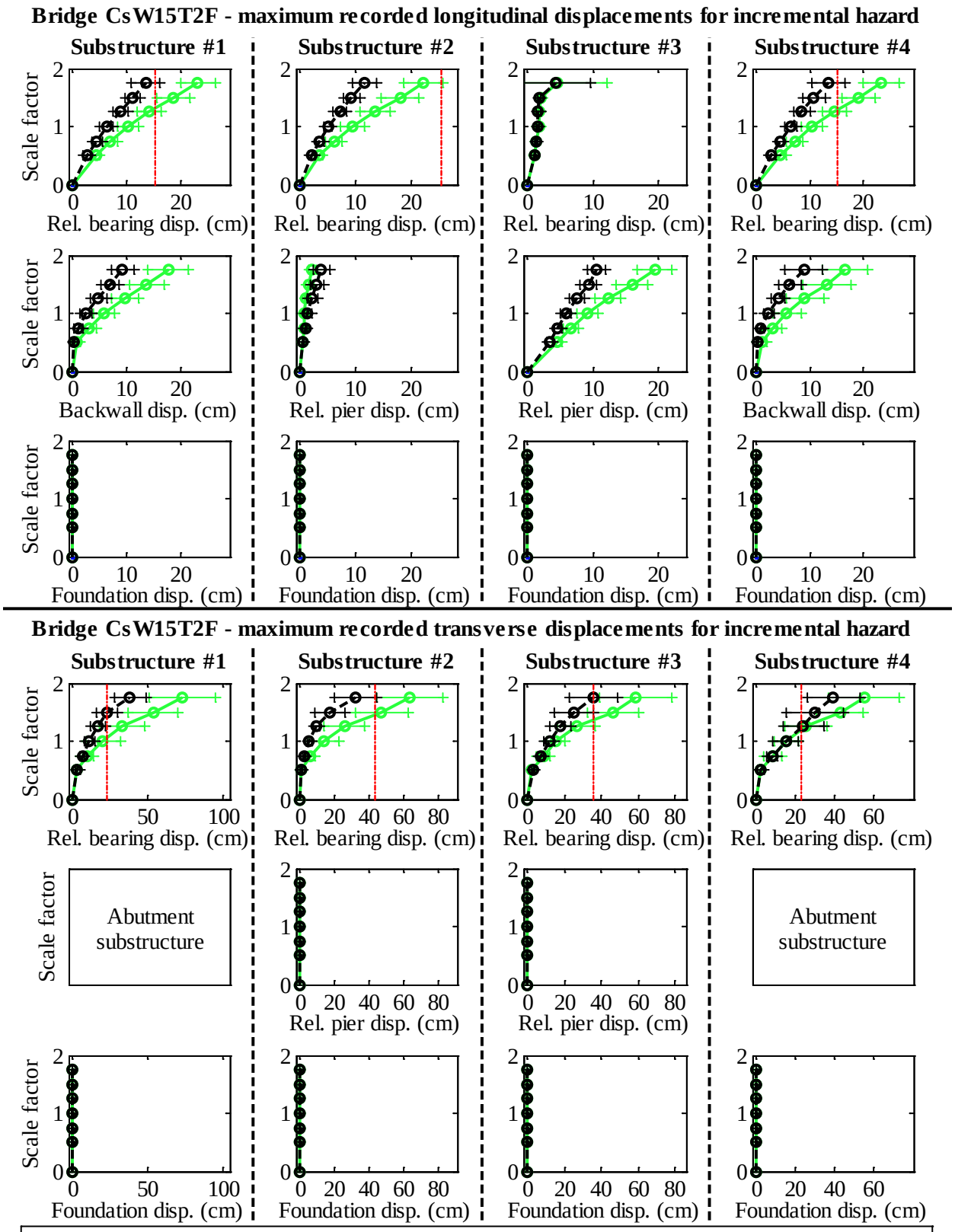

Figure C.155. Bridge CsW15T2F – displacement results.

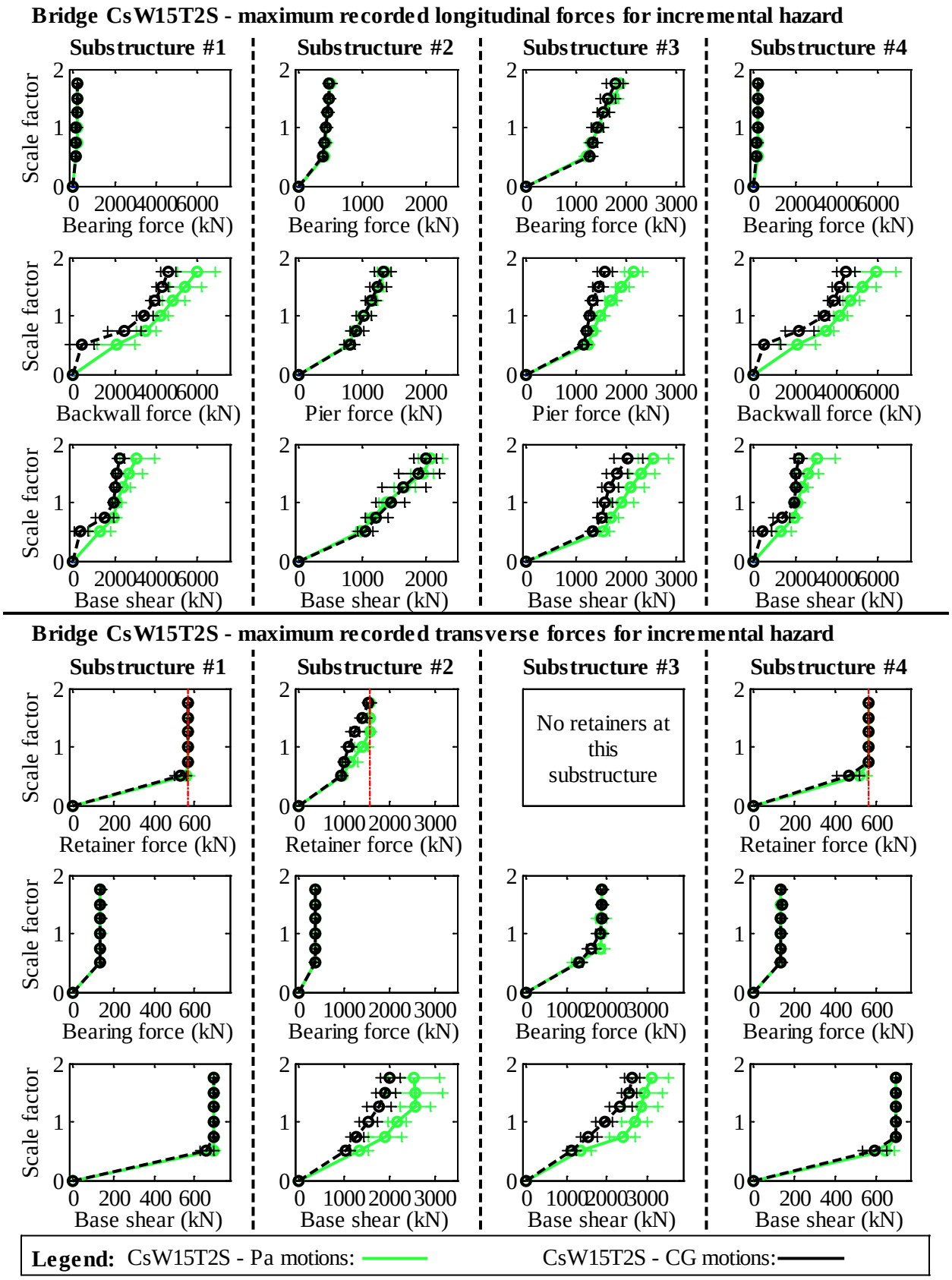

Figure C.156. Bridge CsW15T2S – force results.

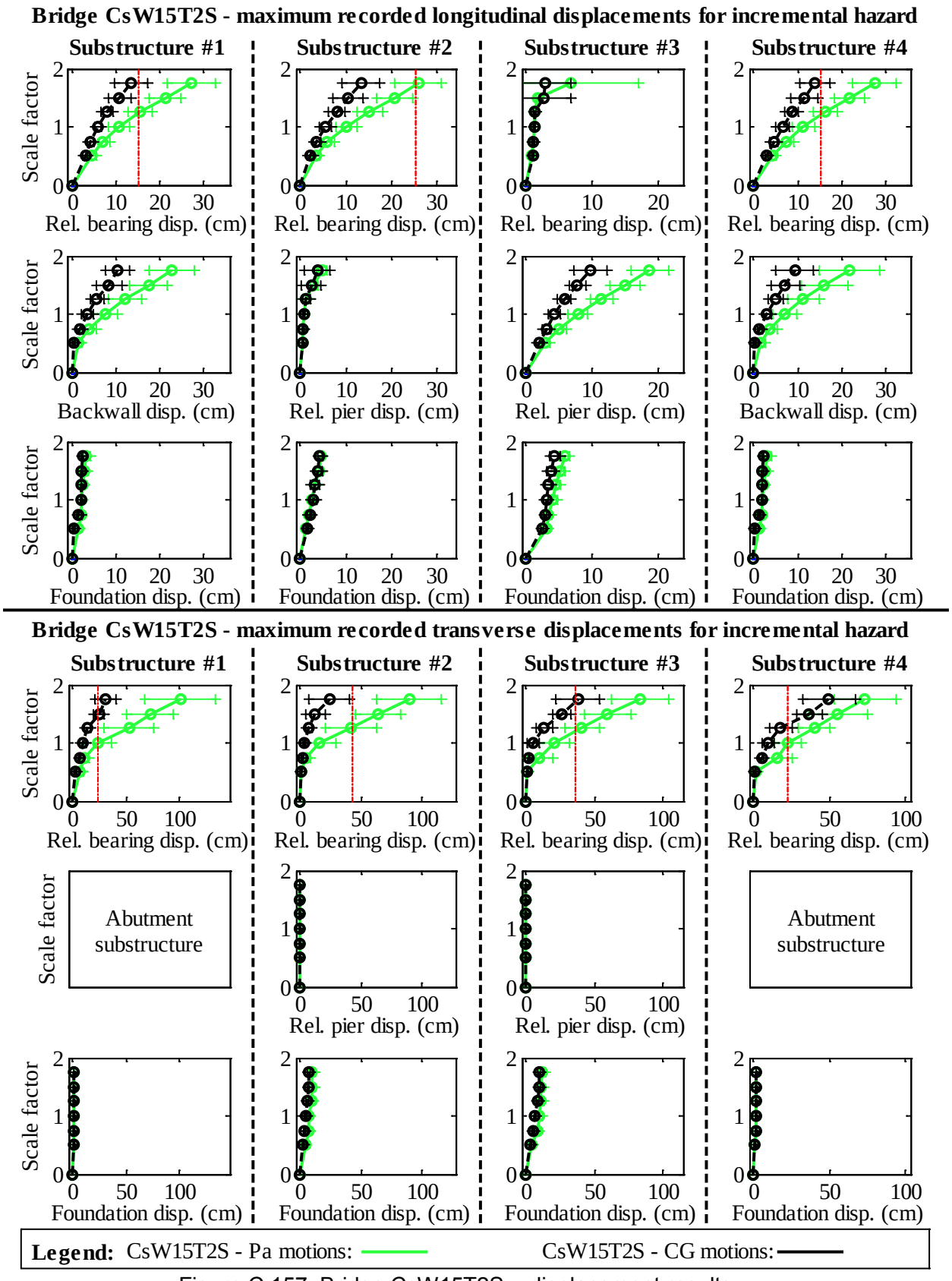

Figure C.157. Bridge CsW15T2S – displacement results.

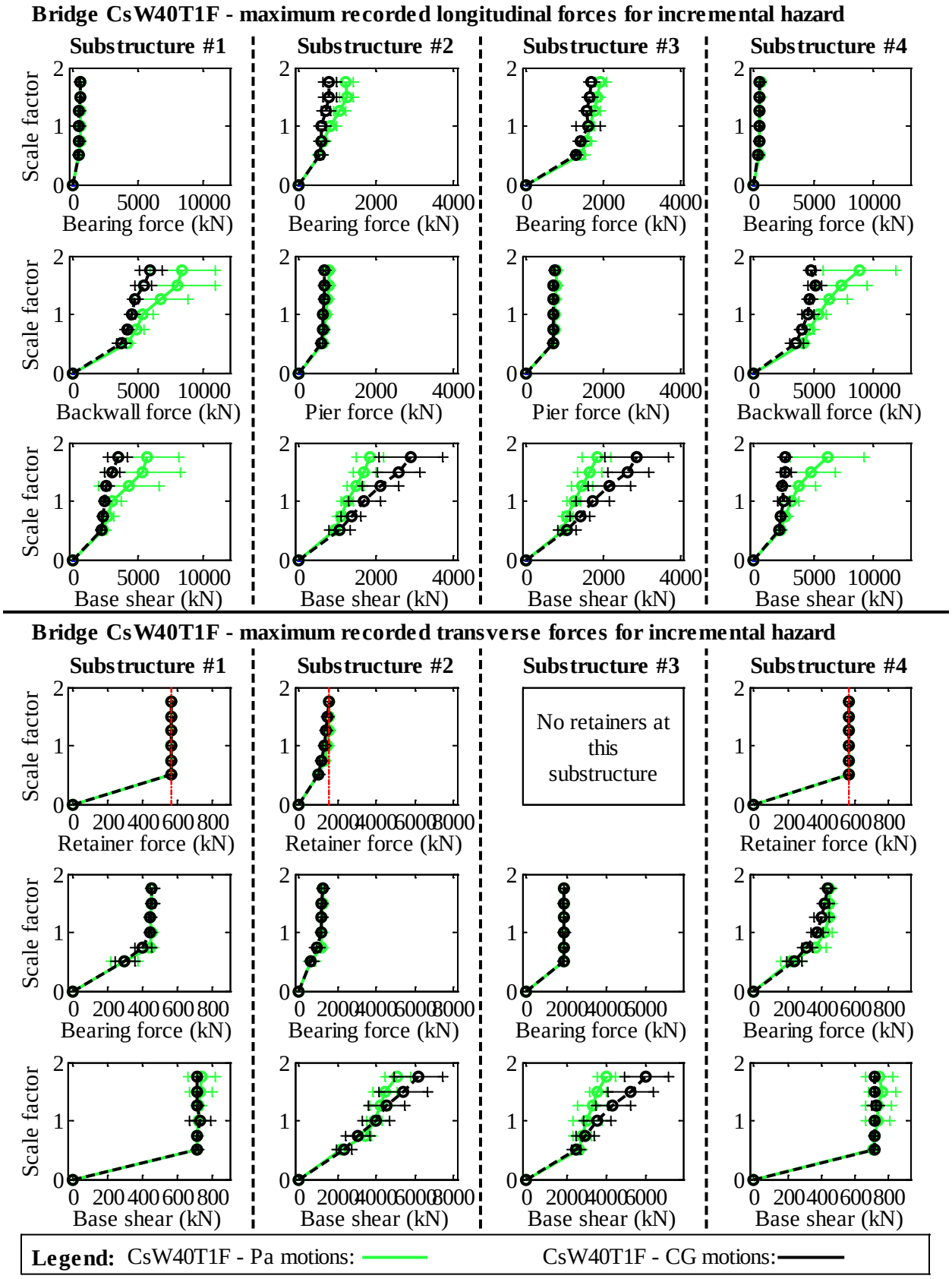

Figure C.158. Bridge CsW40T1F – force results.

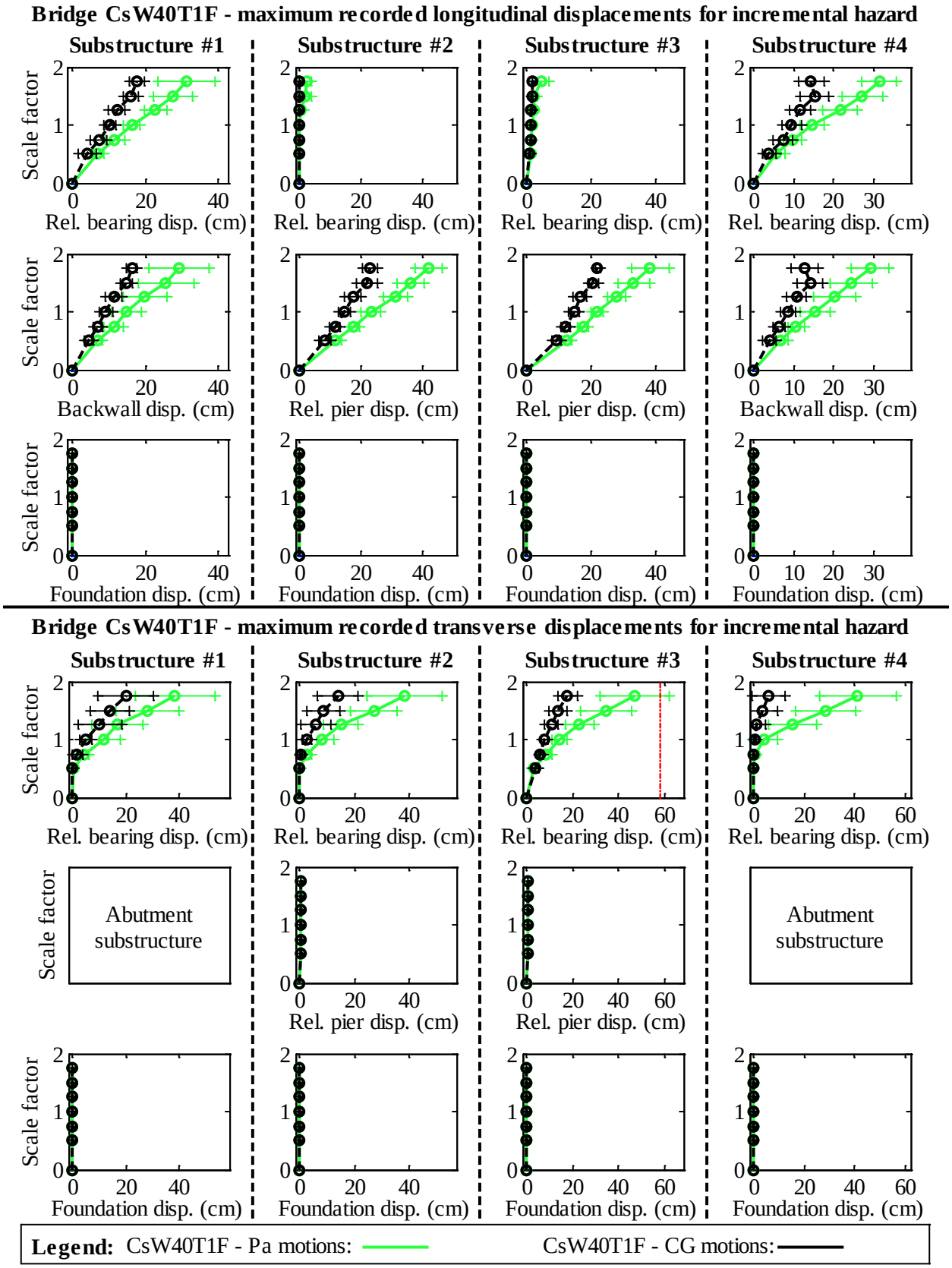

Figure C.159. Bridge CsW40T1F – displacement results.

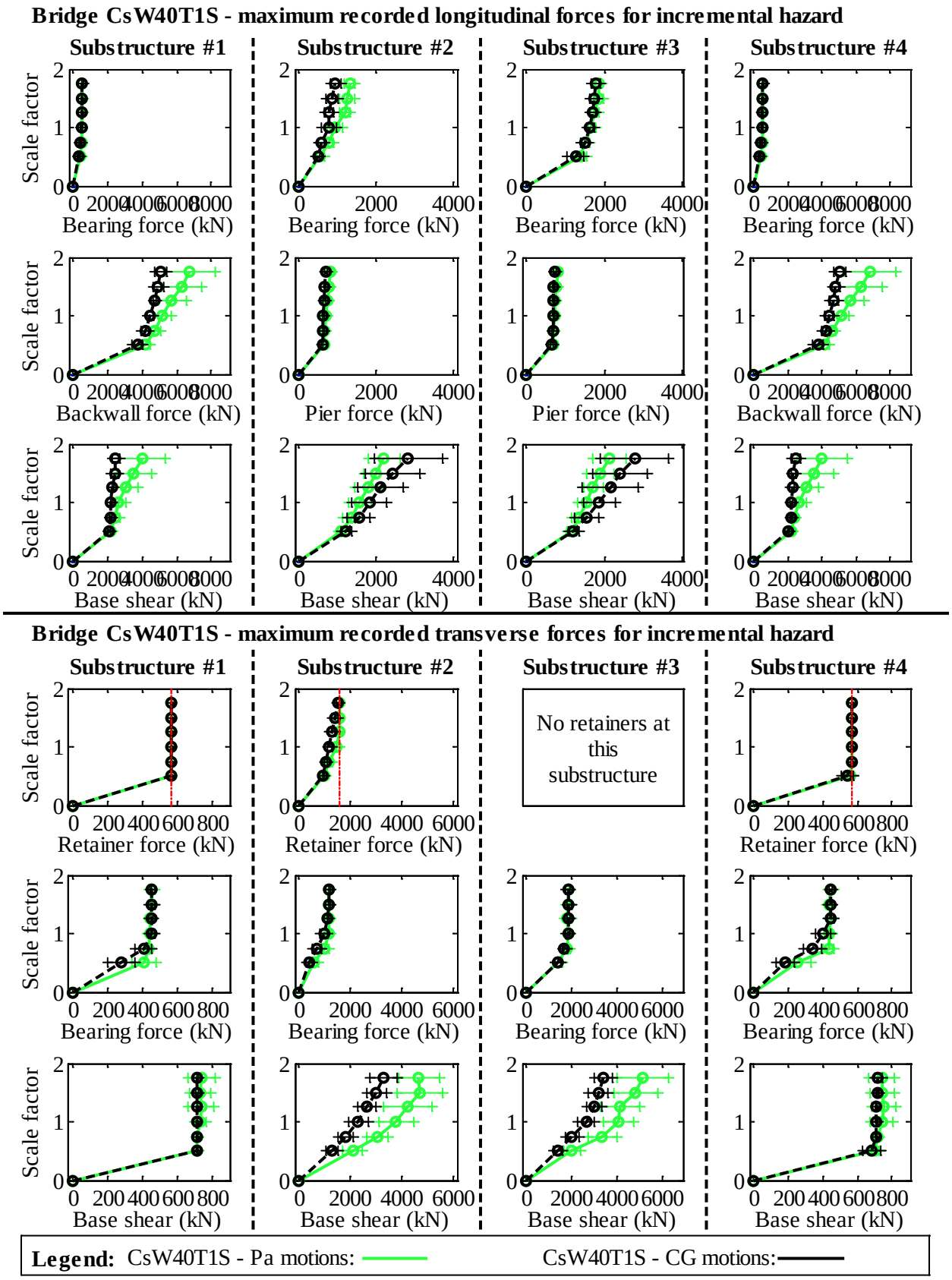

Figure C.160. Bridge CsW40T1S – force results.

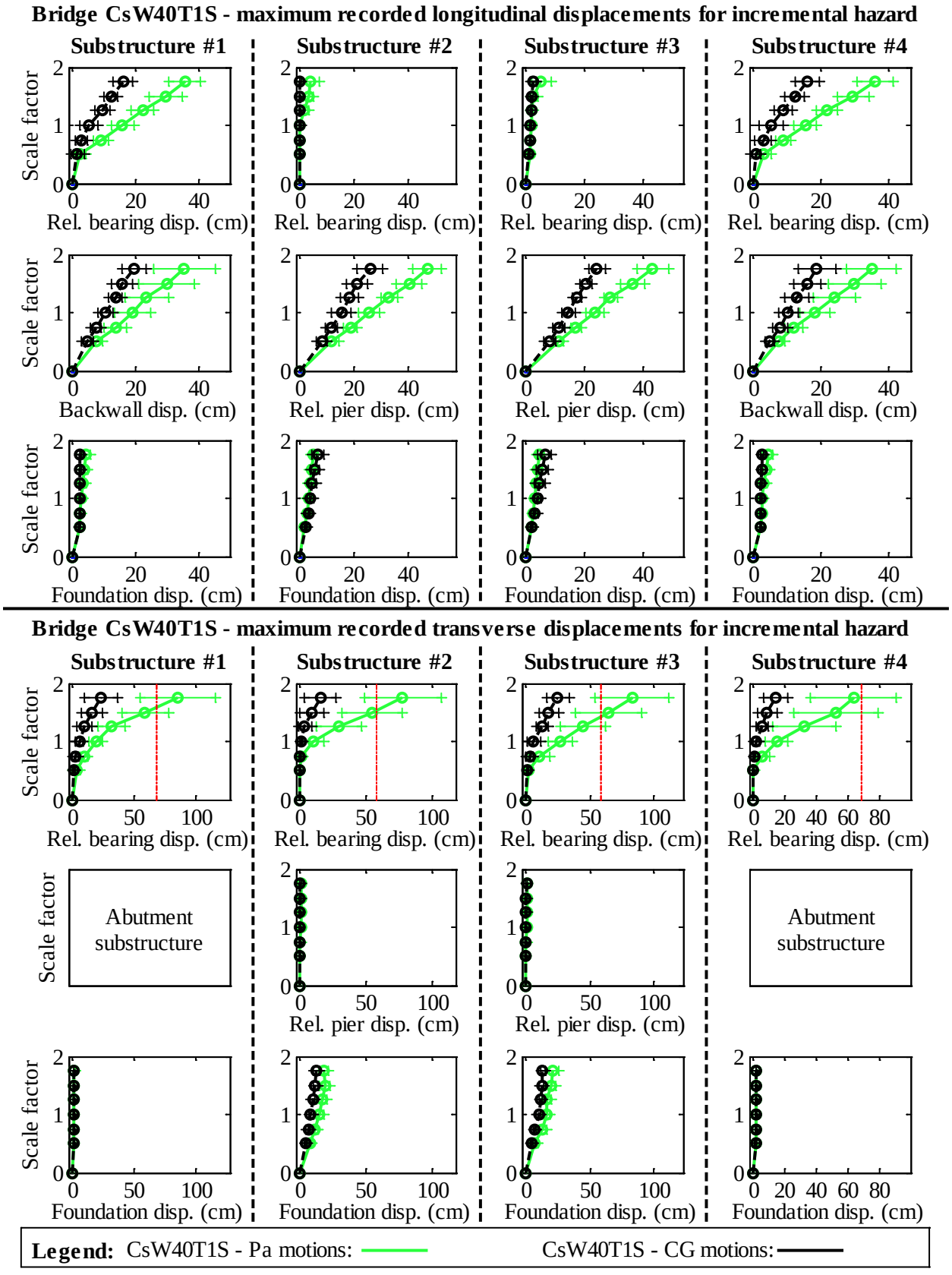

Figure C.161. Bridge CsW40T1S – displacement results.

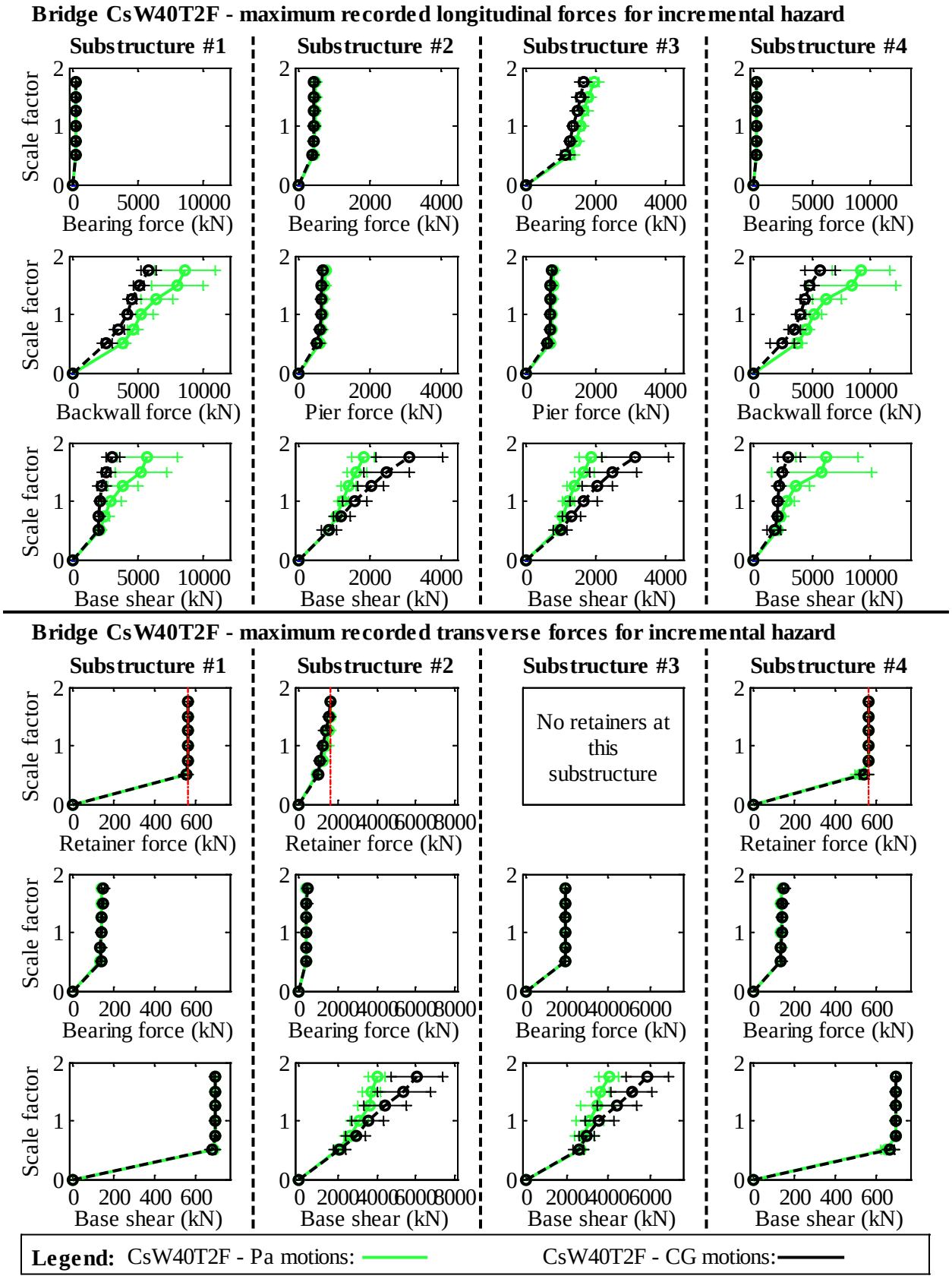

Figure C.162. Bridge CsW40T2F – force results.

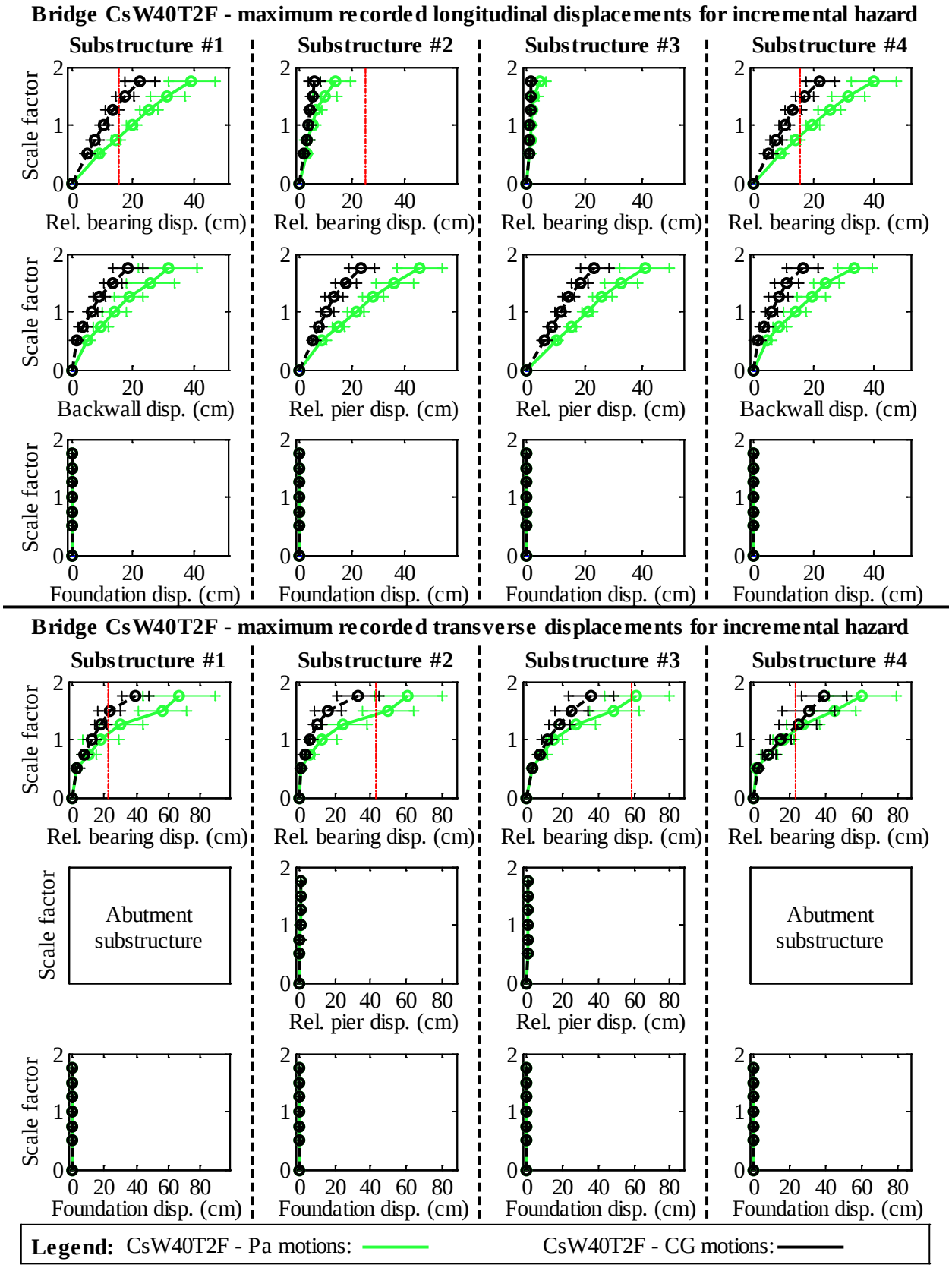

Figure C.163. Bridge CsW40T2F – displacement results.

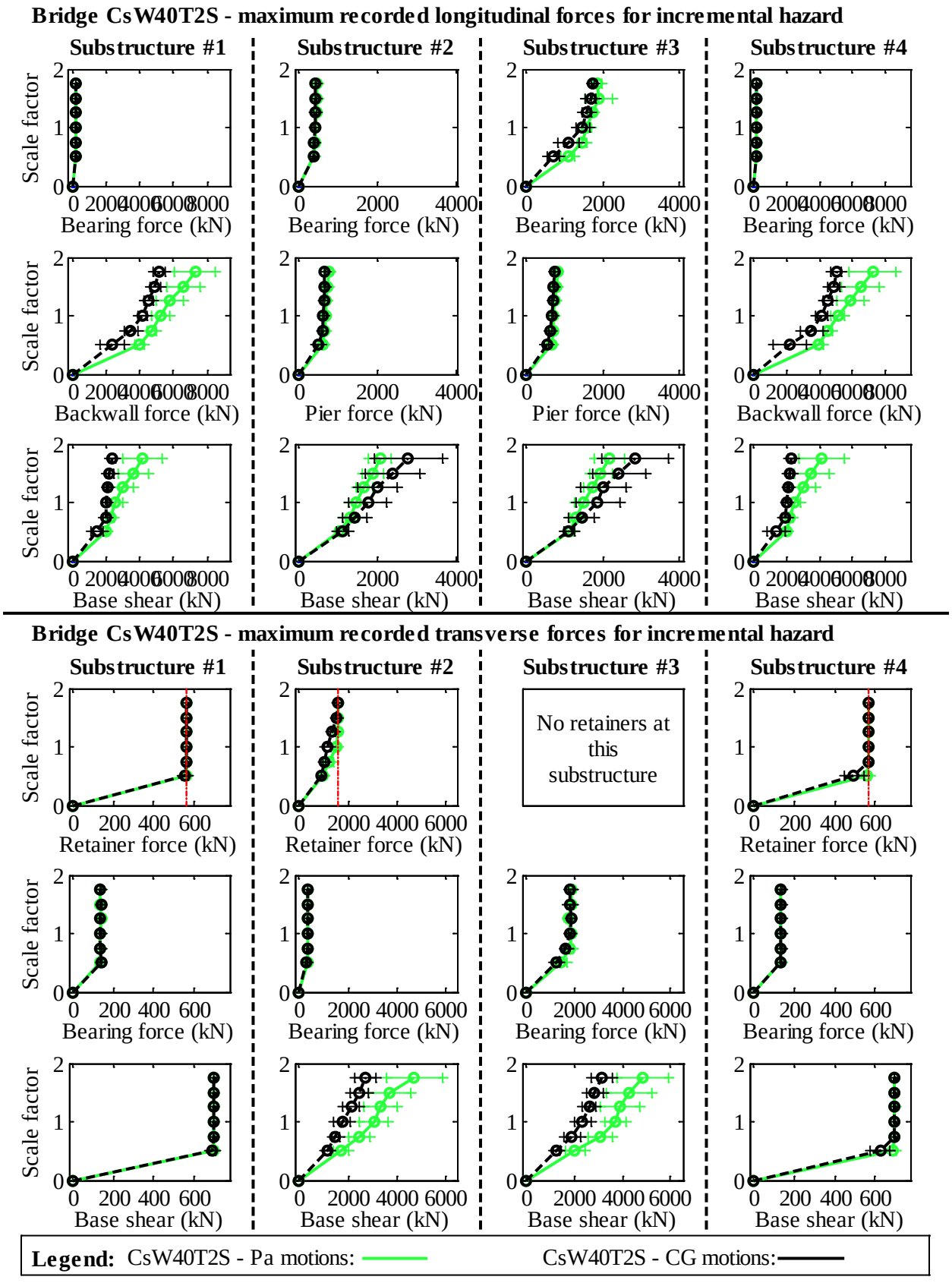

Figure C.164. Bridge CsW40T2S – force results.

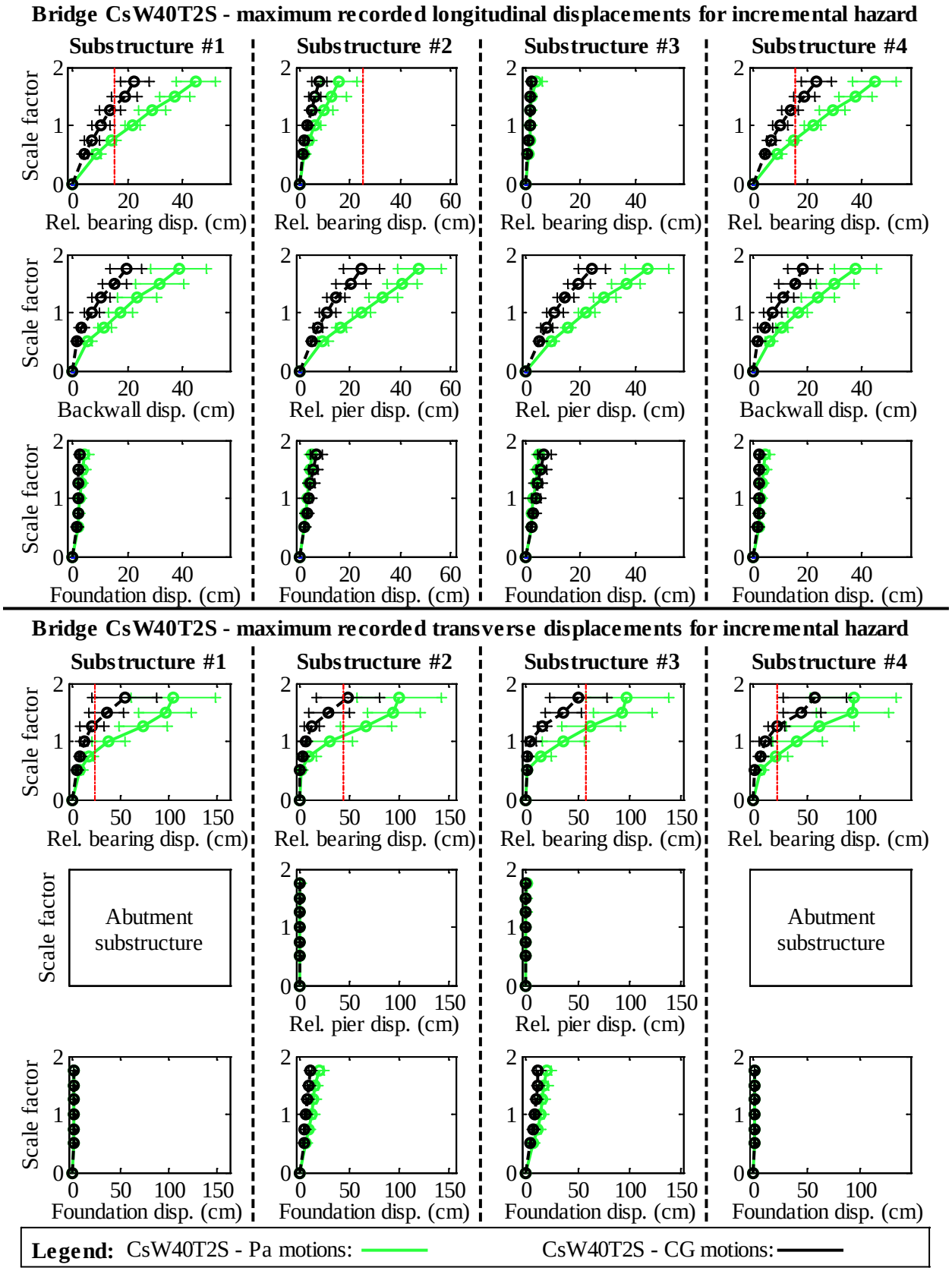

Figure C.165. Bridge CsW40T2S – displacement results.

APPENDIX D RETAINER DATA PROCESSING AND ALTERNATE DESIGN PROCEDURE

D.1 DEVELOPMENT OF RETAINER RESPONSE EQUATIONS

This appendix contains a broader discussion of how the retainer data was calculated from the data records obtained from experiments, and a more detailed discussion of the proposed alternate design methodology for retainers described in Chapter 5. The primary objective of the data processing for the retainers was to isolate the mechanical components of the anchor reaction at incipient fusing. To accomplish this goal, the unity check described in ACI 318 (2008), Appendix D, was invoked as the governing limit state. In ACI 318 (2008), the unity check is a fixed value (unity), but a variable, Φ, is substituted in Eq. D-1 to reflect the dependency of the equation on the assumed orientation of the toe reaction.

$$F = \left(\frac{F_{ANC,n}}{N_n}\right)^{V} + \left(\frac{F_{ANC,v}}{V_n}\right)^{V} \qquad \text{(Eq. D-1)}$$

Where:

F = Interaction check value

$F_{ANC,n}$ = Normal component of anchor load demand

$F_{ANC,v}$ = Shear component of anchor load demand

N_n = Nominal strength of anchor in pure tension

V_n = Nominal strength of anchor in pure shear

V = Exponent used when combining tension and shear for interaction check

Nominal strengths for threaded anchors, N_n and V_n, are evaluated consistently with procedures commonly employed in various material design specifications and AASHTO (2008). Equations may be presented differently depending on the reference, but the underlying approach is consistent. Tension strength is determined by multiplying ultimate tensile strength by the effective area of the anchor, and the value is reduced with a multiplier of 0.6 for shear strength.

$$N_n = F_u A_b \qquad \text{(Eq. D-2)}$$

$$V_n = 0.6 F_u A_b \qquad \text{(Eq. D-3)}$$

Where:

F_u = Ultimate tension strength (ksi)

A_b = Effective anchor cross-sectional area

The area, A_b, for threaded anchors is taken equal to the “stress area” presented in ASTM F 1554 (ASTM, 2007), which accounts for the reduction of area at threaded sections.

Data are acquired during each transverse bearing test for individual actuator loads, position of the bearing, and positions of the individual retainers. There is no direct measurement of loads acting on the retainers, and so the mechanical interaction of the bearing and retainers must be inferred from the available data. First, the reactions between the retainer and the bearing must be determined. A schematic view of the mechanical interaction between a Type I bearing and a retainer is shown in Figure D.1.

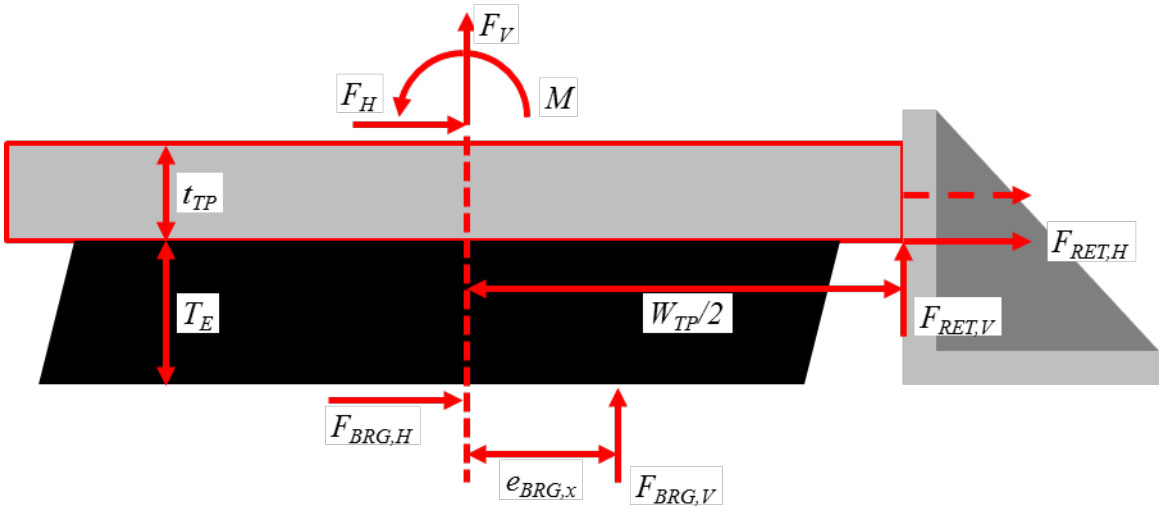

Figure D.166 Bearing and Retainer Reaction Interaction Schematic

In Figure D.1, signs have been assigned consistent with the indicated direction of the force vectors. The F_H, F_V, and M terms are determined from the recorded loads and current orientations at individual actuators. During post-processing of the data from a test, indices are identified in the recorded data corresponding to changes in mechanical response (e.g., engaging or disengaging contact between bearing and retainer). Typical variations in shear load and moment (determined independently for each direction of loading) are extracted from the data by compiling vectors of representative segments (those where the bearing elastomer is exhibiting a softened secondary slope) from the overall record and linearly interpolating first-order approximations of $dF_H / d\gamma_s$ and $dM / d\gamma_s$. Then, when contact between the bearing and retainer is identified in the record, the horizontal load in the bearing, $F_{BRG,H}$, is extrapolated from the load prior to contact, and the linear trend of the shear stiffness, i.e.,

$$F_{BRG,H-i} = F_{BRG,H-0} - \left(\frac{dF_H}{d\gamma_s}\right)\left(\gamma_{si} - \gamma_{s0}\right) \qquad \text{(Eq. D-4)}$$

Where:

$F_{BRG,H-i}$ = Current horizontal reaction at base of elastomer and index *i*, relative to 0

$F_{BRG,H-0}$ = Initial horizontal reaction at base of elastomer when bearing engages retainer (at index 0)

$\left(\frac{dF_H}{d\gamma_s}\right)$ = Linear trend of change in horizontal load with respect to shear strain in absence of retainer contact

γ_{si} = Current shear strain in elastomer at index *i*, relative to 0

γ_{s0} = Initial shear strain in elastomer when bearing engages retainer (at index 0)

The negative sign preceding the second term reflects that the base reaction will act in the opposite direction to the horizontal load applied to the top of the bearing from the loading frame actuators. The horizontal load acting on the top plate from the retainer, $F_{RET,H}$, can then be determined from the sum of horizontal forces, so that

$$F_{RET,H-i} = - F_{H-i} - F_{BRG,H-i} \qquad \text{(Eq. D-5)}$$

Where:

$F_{RET,H-i}$ = Current horizontal reaction from retainer onto bearing at index *i*, relative to 0

F_{H-i} = Current horizontal reaction at top of bearing and index *i*

$F_{BRG,H-i}$ = Current horizontal reaction at base of elastomer and index *i*

The bearing also develops a vertical reaction, $F_{RET,V}$, initially due to friction acting to restrain overturning of the retainer. Once the vertical face has slipped against the bearing top plate, the resulting geometry leads to an increased vertical load component. The vertical stiffnesses of the bearings in the testing program are high, on the order of 700 to 2000 kips/in. Changes in vertical position recorded during the tests were more likely to be the result of a slight slope of the concrete surface, either due to finishing, subsequent roughening, or a slight tilt of the concrete pad during installation. Consequently, determining a change in vertical load in the bearing associated with a change in vertical position was found to be unsatisfactory.

Instead, the vertical reaction at the retainer was inferred from the moment acting on the bearing. The moment developed at the top of the bearing in the absence of contact with a retainer is due to the combined effects of the shear reaction acting at the base of the elastomer, and the vertical reaction with a resultant acting at an offset from the center of the top plate, i.e.,

$$\Sigma M = 0 = M + F_{BRG,V} e_{BRG,x} + F_{BRG,H}\left(t_{TP} + T_E\right) \qquad \text{(Eq. D-6)}$$

Where:

M = Moment acting at top of bearing from loading frame

$F_{BRG,V}$ = Vertical resultant force acting at base of elastomer

$e_{BRG,x}$ = Eccentricity of vertical reaction relative to center of top plate

$F_{BRG,H}$ = Horizontal resultant force acting at base of elastomer

t_{TP} = Top plate thickness

T_E = Total thickness of elastomer

In Eq. D-6, the terms for the components of the moment developed in the bearing, M_{BRG}, are

$$M_{BRG} = F_{BRG,V} e_{BRG,x} + F_{BRG,H}\left(t_{TP} + T_E\right) \quad \text{(Eq. D-7)}$$

and the variation in bearing moment with respect to shear strain is

$$\frac{dM_{BRG}}{d\gamma_s} = -\frac{dM}{d\gamma_s} \quad \text{(Eq. D-8)}$$

When the bearing contacts the retainer, the bearing moment equilibrium expression becomees the following (instead of Eq. D-6):

$$\Sigma M = 0 = M_i + M_{BRG-0} - \left(\frac{dM}{d\gamma_s}\right)\left(\gamma_{si} - \gamma_{s0}\right) + F_{RET,H-i} t_{TP} + F_{RET,V-i}\left(DIR\right)\frac{W_{TP}}{2} \quad \text{(Eq. D-9)}$$

Where:

M_i = Current moment at top of bearing and index *i*, relative to 0

M_{BRG-0} = Initial moment developed in bearing when bearing engages retainer (at index 0)

$\left(\frac{dM}{d\gamma_s}\right)$ = Linear trend of change in moment with respect to shear strain in absence of retainer contact

$F_{RET,H-i}$ = Current horizontal reaction from retainer onto bearing at index *i*, relative to 0

$F_{RET,V-i}$ = Current vertical reaction from retainer onto bearing at index *i*, relative to 0

DIR = Directionality flag, $\begin{cases} +1: \textit{engaging east retainer} \\ -1: \textit{engaging west retainer} \end{cases}$

W_{TP} = Top plate plan dimension measured transverse to bridge span

The other terms are as indicated in Eq. D-4 and Eq. D-6. In Eq. D-9, the moment arm for the horizontal reaction from the retainer is taken as the full depth of the top plate. When the bearing initially contacts the retainer, there may be a short sliding segment where the horizontal reaction centroid is closer to the center of the top plate, as shown with a dashed arrow in Figure D.1. However, once the retainer slides sufficiently to engage the concrete anchor, the retainer will pivot at the toe, rotating and leaning forward, and the contact surface will be reduced to a knife-edge condition at the bottom edge of the top plate.

The local loads acting on the retainer can be investigated following the determination of reactions acting at the knife-edge condition between the bearing top plate and the retainer vertical face. As shown in Figure D.2, there are three locations where concentrated loads act on a retainer: at the contact between the top plate and the vertical face ($F_{RET,H}$ and $F_{RET,V}$), at the concrete anchor ($F_{ANC,H}$ and $F_{ANC,V}$), and at the toe ($F_{TOE,H}$ and $F_{TOE,V}$). Only two of these six unknowns are available, leaving four unknowns to be determined from the three static equilibrium conditions. To reduce the number of unknowns, the concrete reaction orientation, θ_{RXN}, was parameterized, leaving $F_{ANC,H}$, $F_{ANC,V}$, and F_{TOE} as unknowns.

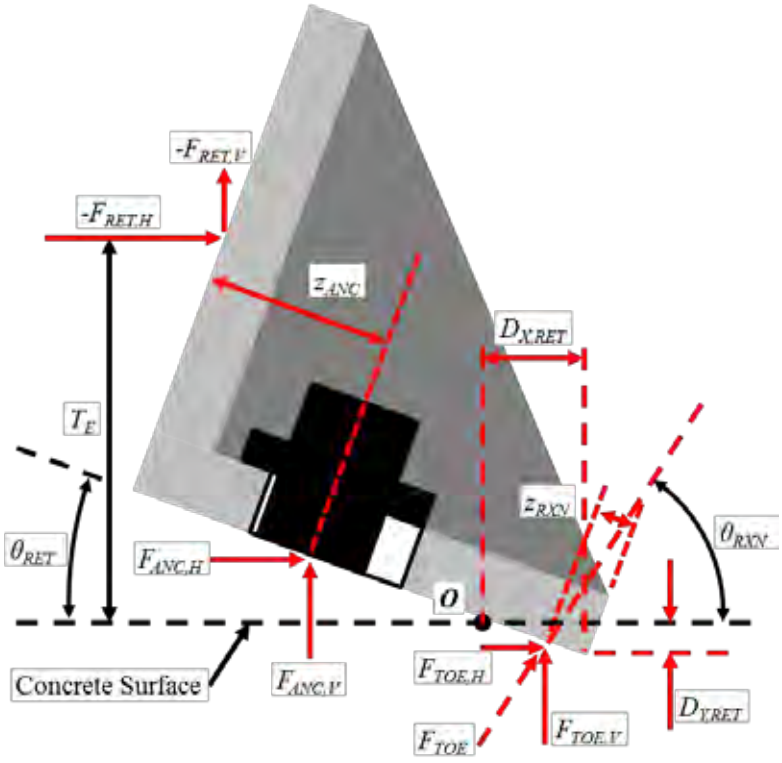

Figure D.167 Retainer Local Reaction Schematic

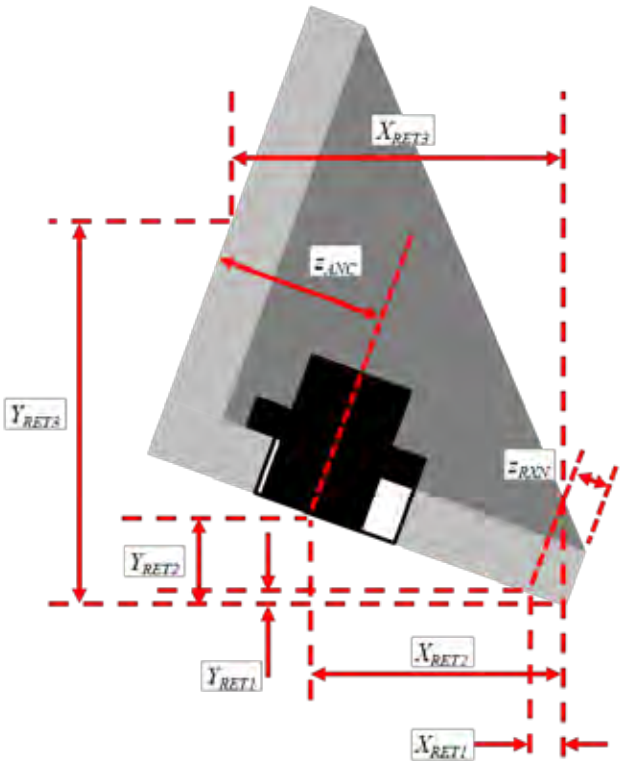

Figure D.168 Retainer Local Reaction Positions

The rigid body motion ($D_{X,RET}$, $D_{Y,RET}$, and θ_{RET}) of the retainer is evaluated from cable-extension potentiometer and LVDT data. Rigid body motions can then be incorporated into position calculations to describe where reactions act on the retainer relative to the toe, as shown in Figure D.3. Locations 0, 1, 2, and 3 correspond to the toe, the centroid of the toe reaction, the centroid of the anchor reaction, and the top plate contact location, respectively.

$$X_{RET1} = (-DIR)\, z_{RXN} \cos f_{RET} \quad \text{(Eq. D-10)}$$

$$Y_{RET1} = (-DIR)\, z_{RXN} \sin f_{RET} \quad \text{(Eq. D-11)}$$

$$X_{RET2} = (-DIR)(b_{RET} - z_{ANC}) \cos f_{RET} \quad \text{(Eq. D-12)}$$

$$Y_{RET2} = (-DIR)(b_{RET} - z_{ANC}) \sin f_{RET} \quad \text{(Eq. D-13)}$$

$$Y_{RET3} = T_E - D_{Y,RET} \quad \text{(Eq. D-14)}$$

$$X_{RET3} = (-DIR) b_{RET} \cos f_{RET} - \left(Y_{RET3} + (DIR) b_{RET} \sin f_{RET}\right) \tan f_{RET} \quad \text{(Eq. D-15)}$$

Where:

f_{RET} = Rotation of retainer from initial position, taken as positive counter-clockwise when viewed from the south (degrees)

$D_{Y,RET}$ = Vertical displacement of retainer, taken as positive when directed in the +Y (upward) direction (in.)

z_{RXN} = Distance from retainer toe to centroid of concrete reaction (always positive) (in.)

z_{ANC} = Distance from retainer heel to center of anchor (always positive), when retainer has been displaced sufficiently to bear against the face of the embedded concrete anchor (in.)

b_{RET} = Retainer width measured transverse to bridge span (in.)

The toe reactions are

$$F_{TOE,H} = F_{TOE} \cos f_{RXN} \quad \text{(Eq. D-16)}$$

$$F_{TOE,V} = F_{TOE} \sin f_{RXN} \quad \text{(Eq. D-17)}$$

The value for θ_{RXN} is parameterized through one quadrant, in the range of [90º, 180º] for the east retainer and [0º, 90º] for the west retainer. Summing moments at the "2" position to exclude both of the unknown anchor reaction components,

$$\begin{aligned} SM_2 = 0 = &\left(- F_{RET,V}\right)\left(- X_{RET2} + X_{RET3}\right) - \left(- F_{RET,H}\right)\left(- Y_{RET2} + Y_{RET3}\right) \\ &+ F_{TOE} \sin f_{RXN} \left(- X_{RET2} + X_{RET1}\right) \\ &- F_{TOE} \cos f_{RXN} \left(- Y_{RET2} + Y_{RET1}\right) \end{aligned} \quad \text{(Eq. D-18)}$$

And rearranging for the unknown reaction at the toe, F_{TOE},

$$F_{TOE} = \frac{F_{RET,V}\left(- X_{RET2} + X_{RET3}\right) - F_{RET,H}\left(- Y_{RET2} + Y_{RET3}\right)}{\sin f_{RXN}\left(- X_{RET2} + X_{RET1}\right) - \cos f_{RXN}\left(- Y_{RET2} + Y_{RET1}\right)} \quad \text{(Eq. D-19)}$$

Summing forces in the horizontal and vertical directions yields the anchor reaction components.

$$F_{ANC,H} = F_{RET,H} - F_{TOE} \cos f_{RXN} \quad \text{(Eq. D-20)}$$

$$F_{ANC,V} = F_{RET,V} - F_{TOE} \sin f_{RXN} \quad \text{(Eq. D-21)}$$

Lastly, the horizontal and vertical components can be transformed into tension and shear reactions on the anchors, $F_{ANC,n}$ and $F_{ANC,v}$, respectively.

$$F_{ANC,n} = F_{ANC,H} \sin f_{RET} - F_{ANC,V} \cos f_{RET} \quad \text{(Eq. D-22)}$$

$$F_{ANC,v} = (-DIR)\left(F_{ANC,V}\sin f_{RET} + F_{ANC,H}\cos f_{RET}\right) \quad \text{(Eq. D-23)}$$

These anchor reaction components can then be substituted into Eq. D-1 to indicate a mechanically probable toe reaction orientation and associated configuration of reaction components at both the toe and anchor when Φ is approximately equal to unity.

D.2 PROPOSED DESIGN PROCEDURE

D.2.1 Initialization

Several initial parameters must be established, based on project specifications, to initiate the alternate design procedure:

- required fuse capacity, V_{fuse}
- steel ultimate strength, F_u
- concrete limiting stress, $f_{c,lim}$
- elastomer shear modulus, G
- elastomer footprint area, A
- elastomer shear strain at retainer anchor rupture, γ

Other parameters must be selected from a reasonable range:

- exponent to use for unity check, ς
- ratio of vertical to horizontal load, μ
- inclination of toe reaction, θ_{RXN}
- rigid body rotation of retainer, θ_{RET}
- rigid body vertical translation of retainer, $D_{Y,RET}$
- width of compression strip at toe, z_{stress}

D.2.2 Calculations

For illustration, assume that V_{fuse} is 90 kips for a 13c bearing. Assume the anchor is F1554, Gr 55, with an ultimate strength, Fu, of 75 ksi. An anchor diameter may be selected according to

$$d_{ANC} = \sqrt{\frac{4V_{fuse}}{1.2F_u p}} \quad \text{(Eq. D-24)}$$

So that

$$d_{ANC} = \sqrt{\frac{4(90)}{1.2(75ksi)p}}$$

$$d_{ANC} = 1.128 \text{ ® } 1.25in$$

This anchor diameter corresponds to a distance from center of anchor hole to heel of retainer, z_{hole}, equal to 2.375 in. The position of the anchor relative to the heel, z_{anc}, is then

$$z_{ANC} = z_{hole} - \frac{d_{hole}}{2} + \frac{d_{ANC}}{2} \quad \text{(Eq. D-25)}$$

So that

$$z_{ANC} = 2.375\,in - \frac{1.5\,in}{2} + \frac{1.25\,in}{2}$$
$$z_{ANC} = 2.25\,in$$

The bearing contribution to shear resistance at incipient retainer anchor rupture is approximated as

$$F_{BRG,H} = GAg \quad \text{(Eq. D-26)}$$

So that

$$F_{BRG,H} = (0.12\,ksi)(13\,in * 20\,in)(0.5\,in/in)$$
$$F_{BRG,H} = 15.6\,kips$$

The required horizontal load acting on the retainer is then

$$F_{RET,H} = V_{fuse} - F_{BRG,H} \quad \text{(Eq. D-27)}$$

So that

$$F_{RET,H} = 90\,kips - 15.6\,kips$$
$$F_{RET,H} = 74.4\,kips$$

The strip width, z_{stress}, where the toe reacts against the concrete varied across the tests, but was generally in the range of 0.75 in. to 1.5 in (although the width may have approached 3 inches for the 8 in. wide alternate retainer tested with a 13c bearing). Assuming z_{stress} equal to 1 in. is a reasonable approximation. The stress distribution is assumed to be linear along z_{stress}, so the distance to the toe reaction centroid, z_{RXN}, is

$$z_{RXN} = \frac{z_{stress}}{3} \quad \text{(Eq. D-28)}$$

For simplicity, initially assume that the bearing rigid body motions (θ_{RET} and $D_{Y,RET}$) are negligible. Also, assume that the ratio of vertical to horizontal load acting on the retainer from the bearing is 0.5, so that

$$F_{RET,V} = \mu F_{RET,H}$$
$$F_{RET,V} = 0.5\left(74.4\,kips\right)$$
$$F_{RET,V} = 37.2\,kips \qquad \text{(Eq. D-29)}$$

The total elastomer thickness (T_E) for a 13c bearing is 3.875 in. Applying the equations given in Eq. D-10 through D-15 yields the following (note that a "west" retainer is assumed, so that $-DIR = 1$):

$$X_{RET1} = z_{RXN} = \frac{z_{stress}}{3} = \frac{1}{3}in.$$
$$Y_{RET1} = 0$$
$$X_{RET2} = b_{RET} - z_{ANC} = b_{RET} - 2.25\,in.$$
$$Y_{RET2} = 0$$
$$Y_{RET3} = T_E = 3.875\,in.$$
$$X_{RET3} = b_{RET}$$

The required concrete strength for class SI concrete is 3500 psi at 14 days, so concrete strength can reasonably be expected to exceed 4500 psi for structures months or years old. Accounting for the bearing condition of the toe on the concrete surface, an increase beyond the anticipated cylinder strength is also reasonable, so 5000 psi is proposed as a reasonably conservative estimate of the capacity of the concrete to resist the concentrated compression at a retainer toe. Therefore, taking the estimated concrete limiting stress, $f_{c,lim}$, as 5000 psi (5 ksi), and recalling the assumed z_{stress} value that was set as 1 in., the capacity of the concrete at the retainer toe in the vertical direction for a typical 8 in. wide retainer is

$$F_{TOE,V} = \left(f_{c,\lim}\right)\left(z_{stress}\right)\left(L_{RET}\right)$$
$$F_{TOE,V} = \left(5\,ksi\right)\left(1in\right)\left(8in\right)$$
$$F_{TOE,V} = 40\,kips \qquad \text{(Eq. D-30)}$$

Note that the μ value that was assumed for Eq. D-29 must be low enough so that $F_{RET,V}$ will not exceed $F_{TOE,V}$, or the calculations will predict a normal compression acting at the anchor. Using the dimensions and forces to sum moments at the anchor centroid as in Eq. D-18,

$$\Sigma M_2 = 0 = \left(F_{RET,V}\right)\left(X_{RET3} - X_{RET2}\right) - \left(F_{RET,H}\right)\left(Y_{RET3}\right) + F_{TOE,V}\left(X_{RET1} - X_{RET2}\right)$$

$$\Sigma M_2 = 0 = \left(F_{RET,H}\right)\left(T_E\right) - \left(m F_{RET,H}\right)\left(z_{ANC}\right) + F_{TOE,V}\left(z_{RXN} + z_{ANC} - b_{RET}\right)$$

$$b_{RET} = \frac{F_{RET,H}\left(T_E - m z_{ANC}\right)}{F_{TOE,V}} + z_{RXN} + z_{ANC}$$

$$b_{RET} = \frac{74.4\left(3.875 - 0.5*2.25\right)}{40} + \frac{1}{3} + 2.25$$

$$b_{RET} = 7.70 \text{ to } 7.75\,in$$

The inclination angle, θ_{RXN}, of the toe reaction relative to horizontal ranges between about 55 and 65 degrees. Assuming a value of 60 degrees, the horizontal component of the toe reaction is evaluated as

$$F_{TOE,H} = \frac{F_{TOE,V}}{\tan\left(q_{RXN}\right)} \qquad \text{(Eq. D-31)}$$

$$F_{TOE,H} = \frac{40\,kips}{\tan\left(60°\right)}$$

$$F_{TOE,H} = 23.1\,kips$$

Then, balancing force equilibrium in the horizontal and vertical directions,

$$\Sigma F_H = 0 = F_{TOE,H} + F_{ANC,H} - F_{RET,H} \qquad \text{(Eq. D-32)}$$

$$F_{ANC,V} = F_{TOE,V} - F_{RET,V}$$

$$F_{ANC,V} = 40 - 37.2$$

$$F_{ANC,V} = 2.8\,kips$$

$$\Sigma F_V = 0 = F_{TOE,V} - F_{ANC,V} - F_{RET,V} \qquad \text{(Eq. D-33)}$$

$$F_{ANC,H} = F_{RET,H} - F_{TOE,H}$$

$$F_{ANC,H} = 74.4 - 23.1$$

$$F_{ANC,H} = 51.3\,kips$$

To find the nominal capacity of the anchor in tension,

$$T_n = \frac{F_u \pi d_{ANC}^2 * 0.8}{4} \qquad \text{(Eq. D-34)}$$

$$T_n = \frac{(75\,ksi)\pi(1.25\,in)^2}{4}$$

$$T_n = (75\,ksi)(0.982\,in^2)$$

$$T_n = 73.6\,kips$$

Alternatively, the stress area from ASTM F 1554 may be used instead of the nominal circular cross-sectional area scaled by 0.8.

$$T_n = (75\,ksi)(stress\,area)$$

$$T_n = (75\,ksi)(0.969\,in^2)$$

$$T_n = 72.7\,kips$$

The shear capacity is approximately 60% of the tension capacity.

$$V_n = 0.6T_n \qquad \text{(Eq. D-35)}$$

$$V_n = 0.6 * 72.7\,kips$$

$$V_n = 43.6\,kips$$

The interaction check is performed by combining ratios of demand to capacity for tension and shear, with each ratio raised to a power, ζ. The value targeted by the ACI 318 trilinear envelope is a ζ value of 5/3. Performing the calculation for this scenario,

$$F = \left(\frac{F_{ANC,V}}{T_n}\right)^{V} + \left(\frac{F_{ANC,H}}{V_n}\right)^{V} \qquad \text{(Eq. D-36)}$$

$$F = \left(\frac{2.8}{72.7}\right)^{\frac{5}{3}} + \left(\frac{51.3}{43.6}\right)^{\frac{5}{3}}$$

$$F = 1.32$$

An interaction check exceeding unity indicates that the anchor is likely to rupture prior to the bearing assembly reaching the target fuse capacity. If the anchor diameter is increased from 1.25 in. to 1.5 in., the stress area increases to 1.405, and the interaction check reduces to 0.71. To estimate a maximum capacity, rigid body rotation should be incorporated in addition to exchanging the lower bound of ultimate strength for an upper bound, as permitted by the material specification (95 ksi in this example for ASTM F 1554 Gr 55 steel). As the retainer rotates, the transformed vertical and horizontal reactions will

become more characterized by tension and less characterized by shear, which will manifest as a reduced interaction utility. As an example, if the width of the retainer is increased to 8 in., the applied load (74.4 kips) could be increased by 57% prior to anchor failure, assuming 95 ksi ultimate strength for the steel, a rigid body rotation of 10 degrees, and a vertical rigid body translation of -0.3 in. Increasing the load by 57% would not breach the interaction check in these conditions, but the concrete average stress would increase to about 8 ksi. To keep the concrete stress below 6 ksi (a more liberal allowance than the 5 ksi used previously), the load could only be increased by about 17%. Ideally, the retainer width would be sufficiently large that the concrete stress limit would not control, even when the parameters generate the maximum strength that can reasonably be expected, consistent with design specifications.


Illinois Department
of Transportation


ILLINOIS
UNIVERSITY OF ILLINOIS AT URBANA-CHAMPAIGN